Dissertation

submitted to the Combined Faculties of the Natural Sciences and Mathematics

of the Ruperto-Carola-University of Heidelberg, Germany

for the degree of

Doctor of Natural Sciences

Put forward by

Freya Hemsing, M. Sc.

Born in Würselen

Oral examination: 12.12.2017

Cold-Water Corals as Archives for Ocean Dynamics, Environmental Conditions and Glacial Reef Accumulation

Referees:

Prof. Dr. Norbert Frank

Dr. Monica Dunford

Cold-Water Corals as Archives for Ocean Dynamics, Environmental Conditions and Glacial Reef Accumulation

Paleoceanographic reconstructions are fundamental for our understanding of past climate variabilities and have mainly focused on changes of circulation and environmental conditions in the surface or deep ocean. The thermocline (100 – 1000 m), acting as a link and buffer between the well-mixed warm surface and the slow and cold deep water, has been largely overlooked. In this study two cold-water coral (CWC) bearing cores from two depths in the thermocline of the southern Gulf of Cádiz (sGoC) were analysed in a mutli-proxy approach. U-series dated glacial CWCs were analysed for recorded Li/Mg temperatures, water mass ^{14}C reservoir ages and radiogenic Nd isotope signatures (εNd). For the first time, a CWC εNd record was extended by two independent co-located hemipelagic sediment records. A seesaw pattern for the glacial sGoC intermediate waters alternating between predominant Eastern North Atlantic Central Water (ENACW) and Eastern Antarctic Intermediate Water (EAAIW) is proposed. Glacial ENACW and EAAIW both exhibited polar temperatures ($\sim 0°C$) and more radiogenic εNd signatures ($\sim$ -9) than nowadays and were distinguishable by their reservoir ages, with better ventilated glacial ENACW than EAAIW. A compilation of existing CWC mound aggregation records allowed for a first estimate of initial CWC settlement in the ocean around 3.4 Ma ago, coinciding with the mid-Pliocene warm period and the onset of Northern Hemisphere glaciation. Additionally, Ba isotopes ($\delta^{138/134}$Ba) recently introduced for seawater, was calibrated for the use in CWCs. This lays the foundation for the missing nutrient or surface biological productivity proxy in fossil CWCs.

Kaltwasserkorallen als Archiv für Ozeandynamik, marine Umweltbedingungen und glaziale Riffakkumulation

Paläoozeanographische Studien sind für unser Verständins der Klimavariabilität in der Vergangenheit von zentraler Bedeutung. Ihr Fokus lag bisher hauptsächlich auf Veränderungen von Zirkulationsmustern und Umweltbedingen im Oberflächen- und Tiefenwasser des Ozeans. Die Thermokline (100 – 1000 m), die die warme gut durchmischte Oberfläche mit dem kalten und langsam strömendem Tiefenwasser verbindet und gleichzeitig als Puffer agiert, wurde weitestgehend ignoriert. In dieser Studie wurden zwei Sedimentkerne mit Kaltwasserkorallen (CWC) aus zwei Tiefen in der Thermokline im südlichen Golf von Cádiz (sGoC) mithilfe eines Multi-Proxy Ansatzes analysiert. Für die U-Reihen datierten CWCs wurden Li/Mg-Temperaturen, Wassermassen-Reservoiralter und die radiogene Isotopenzusammensetzung von Nd (εNd) rekonstruiert. Zusätzlich wurde zum ersten Mal ein εNd Datensatz aus CWCs mit zwei benachbarten hemi-pelagischen Sedimentkernen ergänzt und verglichen. Die erhaltenden Ergebnisse legen einen "Seesaw"-Mechanismus nahe, in dem die glazialen Zwischenwasser im sGoC abwechselnd von östlichen Nordatlantischem Zentralwasser (ENACW) und östlichen Antarktischem Zwischenwasser (EAAIW) dominiert wurden. Das glaziale ENACW und EAAIW waren durch polare Temperaturen ($\sim 0°C$) und radiogenere εNd-Werte ($\sim$ -9) als heutzutage charakterisiert und konnten anhand ihres ^{14}C-Reservoiralters unterschieden werden, wobei ENACW besser 'belüftet' war als EAAIW. Durch die Zusammenstellung existierender Studien über Korallenhügelaggregation konnte der Zeitraum der erstmaligen Korallenansiedlung auf 3.4 Ma vor heute geschätzt werden, was mit der Erwärmung im mittleren Pliozän und dem Anfang der Vereisung in der Nordhemisphäre zusammenfällt. Außerdem wurde das kürzlich in Meerwasser eingeführte Ba-Isotopenverhältnis ($\delta^{138/134}$Ba) für die Verwendung in CWCs kalibriert. Dies legt den Grundstein für einen bis heute fehlenden Nährstoff- oder Oberflächenproduktivitätsproxy, der in fossilen CWCs benutzt werden kann.

Contents

Based on publications from the last century, the only results that we should expect in the future are more surprises.

L. Robinson & M. Siddall

1 Motivation

Our ability to resolve current and past variability of the Earth's climate greatly relies on our understanding of the circulation patterns and geochemical processes in the ocean. Interacting with all other Earth compartments, the atmosphere, cryosphere and biosphere, the ocean occupies a key role in the modulation and control of the global climate. This includes the transport and storage of heat, carbon and nutrients (Robinson and Siddall, 2012). The present oceanic current systems, environmental conditions and geochemical processes are measured directly in the scope of global scientific programs such as ARGO (Roemmich et al., 2001) or GEOTRACES (SCOR Working Group, 2007) and simulated in models of different complexity (Jansen, 2017; Flato et al., 2013; Stocker and Johnsen, 2003). In contrast to the relatively short time scales (hours to decades) mostly relevant in the atmosphere, oceanic processes predominantly occur on time scales from merely a few decades to millions of years. Therefore, to reliably constrain conceptual and computational models for present and past oceanic changes, a further look back in the past, using geologic records, is needed.

Over the past few decades the development of new and re-evaluation of established proxy-archive systems that record the variability in oceanic circulations, environmental conditions and geochemical processes has been a key effort in paleoceanography (Robinson and Siddall, 2012; Henderson, 2002). The most widely used archive is abyssal pelagic sediment, from which different fractions can be used to reconstruct deep ocean parameters (e.g. benthic foraminifera, Fe-Mn coating) and surface ocean properties (planctonic foraminifera) (Skinner et al., 2017; Waelbroeck et al., 2009; Rutberg et al., 2000; Adkins and Boyle, 1997). Therefore, most paleoceanographic studies and models for past ocean circulation are constrained by surface and deep water mass parameters. Periods such as the Last Glacial Maximum are connected to a reorganisation of the ocean's deep overturning circulation (Adkins, 2013). This also applies to Heinrich stadials and Dansgard-Oeschger cycles, reoccurring short-term events of rapid cooling and warming on decadal to millennial time scales during the last glacial (Adkins, 2013). However, the exact processes involved in the oceanic reorganisation are still not well understood. It is possible that the thermocline (70 – 1000 m), buffering and linking the well mixed warm surface waters with the slow and cold deep water masses, had a significant impact which has been largely overlooked. For a long time, this was mainly due to a lack of a suitable archive, but in the last 20 years cold-water corals, that mainly grow in thermocline depths between 50 and 1000 m, have come into focus of paleoceanography (Roberts et al., 2009). Cold-water corals can be precisely dated by U-series dating and resolve time scales of years to decades. However, even records of coral-bearing cores retrieved from coral mounds are often discontinuous (Wienberg and Titschack, in press; Robinson et al., 2014). In contrast, sediment records are generally continuous but typically exhibit lower resolutions of centennial to millennial time scales and have to be dated relatively by stable isotope stratigraphy and radiocarbon dating (Imbrie et al., 1984).

The analysis of a single proxy-archive system in one location only provides limited information. This can be overcome by analysing the same proxy-archive system in different regions of the ocean or by applying a multi-proxy approach at one site. In this thesis, a multi-proxy multi-

archive approach is applied to reconstruct thermocline changes in the southern Gulf of Cádiz over the last 65 ka (Part I). In this region, water masses that originate from the Mediterranean Sea, the North Atlantic and the South Atlantic compete with each other in intermediate depths (Louarn and Morin, 2011). Several studies have shown that the strength and penetration of southern and northern sourced waters was significantly different during the LGM and stadials or interstadials (Böhm et al., 2015; Adkins, 2013; Pahnke et al., 2008). Additionally, a link between the strength of Mediterrean Outflow Water and these periods has been proposed (Bahr et al., 2015; Voelker et al., 2006). This site is thus particularly well suited to investigate thermocline dynamics in records that cover periods of changing oceanic conditions.

Two coral-bearing cores were retrieved on two cold-water coral mounds from adjacent coral provinces in the southern Gulf of Cádiz with different water depths (550 & 950 m) in the thermocline, hence resolving vertical variations in the water column. The frame-work forming corals were U-series dated (Chap. 4) and analysed for Li/Mg temperatures (Montagna et al., 2014) which provided insight into the glacial thermocline temperature evolution on both long (tens of thousands of years) and short time scales (centennial) (Chap. 5). Two different proxies were used to discern changes in water mass provenance and hence circulation patterns. U-series ages were combined with ^{14}C dates to reconstruct water mass reservoir ages (Adkins et al., 1998) (Chap. 7). Radiogenic Nd isotopes (εNd; (Piepgras et al., 1979)) were applied on both coral-bearing cores and two additional hemipelagic sediment cores from the same region (640 & 860 m) (Chap. 6). The sediment records allowed to fill gaps in the coralline records of the last glacial, providing a near continuous εNd record between 40 ka and today. This direct combination of two independent archives is unique and allowed to discern the influence of different time scales resolved in corals and sediment on the timing and amplitude of the recorded signals.

In addition to the paleoceanographic information obtained from these proxies in individual corals, the mound aggregation rates recorded in the coral-bearing cores can be used to gain insight into general mound evolution patterns (Chap. 4). Several studies have suggested that a space-time evolution linked to long-term climate and oceanic changes is observed for the aggregation of flourishing cold-water coral mound aggregation (e.g. Frank et al., 2011). Here, a compilation of published studies on mound aggregation, including the glacial mound evolution recorded in the two coral-bearing cores of this study, will be analysed for possible common time scales in cold-water coral mounds found throughout the Atlantic and the Mediterranean Sea.

The ensemble of proxies in cold-water corals used in this thesis does not consider a main factor limiting and favouring coral growth: the supply of food. However, currently no proxy for nutrients or the closely linked surface biological productivity has been established for the archive cold-water coral. For example, the element ratios P/Ca or Cd/Ca had to be discarded as both are influenced greatly by biological processes in the coral, so-called vital effects. Although not a nutrient itself, the oceanic distribution of Ba is closely correlated to the nutrient distribution (Wolgemuth and Broecker, 1970; Chow and Goldberg, 1960), which gave rise to the idea that it can be used to trace nutrients and/or surface biological productivity. Recent studies have highlighted the potential of Ba isotopes in seawater ($\delta^{138/134}$Ba) to trace changes in the biological pump, nutrient supply, and riverine or hydrothermal inputs (Hsieh and Henderson, 2017; Cao et al., 2016; Horner et al., 2015). Therefore, in the last part of my thesis, I investigated if cold-water corals are a suitable archive for seawater $\delta^{138/134}$Ba, or if vital effects rule out the application of this novel tracer in cold-water corals (Part II). A successful calibration could provide the currently missing paleoceanographic proxy for nutrients or surface biological productivity in cold-water corals.

2 Background

2.1 Oceans and climate

Covering about 71% of the Earth's surface, the oceans are the largest reservoir and transport medium for heat or chemical substances like CO_2 and other greenhouse gases on our planet. The exchange of heat and gases with the atmosphere and the storage in the deep ocean, have a huge impact on the Earth's climate (Broecker, 1991). Many atmospheric climate variations recorded in $\delta^{18}O$ records from polar ice cores (Fig. 2.2; (Andersen et al., 2004)) were linked to changes of the global ocean circulation patterns (Thermohaline Circulation (THC) in Fig. 2.1(b); (Rahmstorf, 2006; Broecker, 1991)). This view on the circulation cycle is mainly based on warm surface and cold deep water mass currents forced by temperature and salinity differences due to evaporation and wind. A distinct feature of the THC and the Atlantic circulation cell in particular (*Atlantic Meridional Overturning Circulation*, AMOC) is given by the well-defined deep water formation zones such as the North Atlantic (*North Atlantic Deep Water*, NADW), in which cold saline surface water sinks into the abyss (Fig. 2.1(b)) directly linking the two water masses. A similar approach of focussing merely on the surface waters and the deep ocean is often successfully used to describe geochemical processes in the ocean. As Wally Broecker put it: '*For our rather elementary look at the ocean, we will divide it into just two such reservoirs - the warm waters and the cold waters. The zone separating these two major water types (the oceanic ther-*

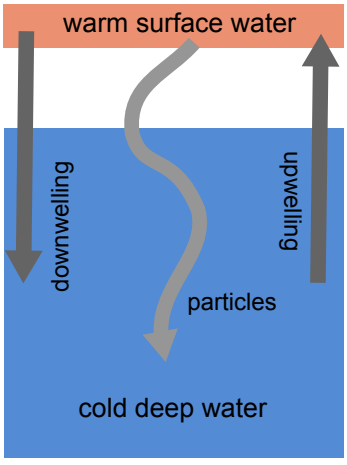

(a) Simplified two-box model often used to describe geochemical processes
after Broecker and Peng, 1982

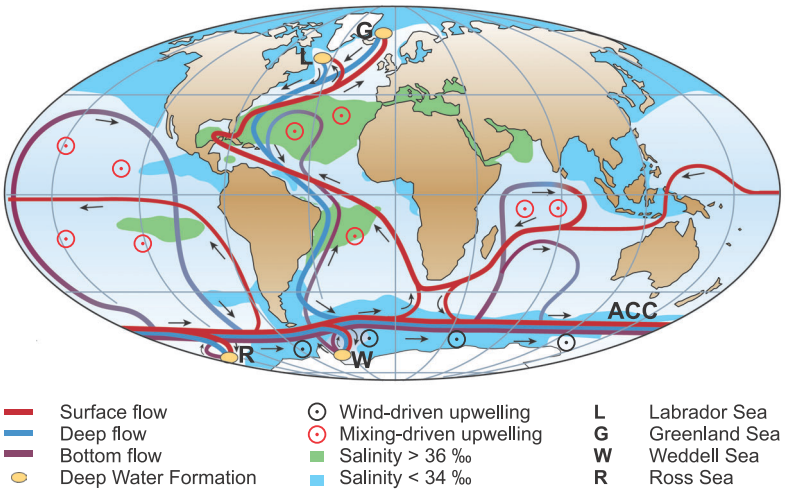

(b) THC: in contrast to the well-defined deep water formation zones, upwelling areas are spatially unconfined.
Figure taken from Rahmstorf, 2006

Figure 2.1: Schematic description of the global ocean circulation

mocline) lies between 70 meters (the average thickness of the wind stirred surface mixed layer) and 1000 meters (the beginning of the deep water regime)' (Fig. 2.1(a); (Broecker and Peng, 1982)). At the same time that Broecker highlights the importance of the thermocline as both the link and buffer between the highly dynamic surface waters and the slower changing deep ocean, he decides to neglect changes of circulation patterns and geochemical processes of this intermediate water mass, which could clearly have an impact on the other two regimes. However, various studies on acoustically tracked floats revealed the implications that intermediate circulation patterns can have on the deep and surface ocean in the North Atlantic (Bower et al., 2009; Lozier and Stewart, 2008; Bower et al., 2002).

δ^{18}O analysis on benthic foraminifera from deep-sea sediment cores established the close correlation between oceanic and ice core records (Imbrie et al., 1984). Long-term patterns following the Milankovitch cycles could be identified in the marine records defining the Marine Isotope Stages (MIS) with odd numbers representing interglacial and even numbers glacial periods.

A closer look at the last ~60 ka (MIS 3 – 1), on which I focus in this thesis, reveals several climate patterns linked to changes in oceanic circulation. The last glacial had its maximum global ice volume 26.5 to 19 ka BP ((Clark et al., 2009); BP: '*before present*', corresponds to before 1950), called the Last Glacial Maximum (LGM) and corresponding to MIS 2. Is was followed by the deglaciation, also named Termination I, shortly interrupted by a punctuated cooling leading to a near reversion to glacial conditions at around 12.5 ka (*Younger Dryas*, YD; (Dansgaard et al., 1993)) (Fig. 2.2; (Andersen et al., 2004)). With the subsequent abrupt warming, deglaciation ended (11.7 ka BP) and the warm Holocene (MIS 1) began (Walker et al., 2009) and still prevails until today. Compared to the modern ocean, proxy data suggests a more shallow NADW formation for the last glacial including the LGM. In contrast to a vigorous NADW circulation during the last glacial, the LGM is generally thought to have been accompanied by a decreased NADW formation (Böhm et al., 2015; McManus et al., 2004).

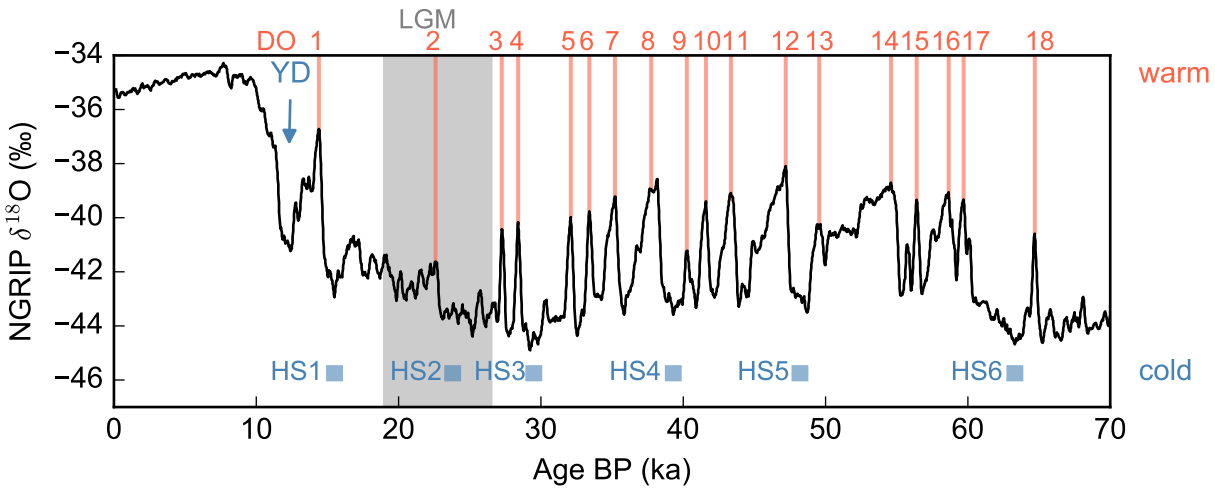

Figure 2.2: Climate variability recorded as δ^{18}O in the Arctic ice core NGRIP
Distinct periods of climate variations are indicated by blue rectangles for Heinrich stadials (HS 1 – 6), blue arrow for Younger Dryas (YD), orange bars for Dansgaard-Oeschger cycles (DO 1 – 18) and the grey shaded area representing the Last Glacial Maxium (LGM) (Clark et al., 2009; Andersen et al., 2004; Hemming, 2004; Dansgaard et al., 1993)

This long-term climate development over time scales of thousands to hundreds of thousands of years is overlain by two types of distinct short-term changes. Heinrich stadials (HS 1 – H6 in Fig. 2.2), extremely cold periods in the Northern Hemisphere, are triggered by H-Events, freshwater and massive iceberg discharges from the Laurentide ice sheet (Hemming, 2004; Heinrich, 1988). The change in North Atlantic freshwater budget is thought to have weakened or even halted the NADW formation, leading to a reduced heat transport to the North. These periods are known to have lasted for merely $\sim$500 a (Hemming, 2004; Heinrich, 1988). Dansgaard-Oeschger cycles (DO 1– 18 in Fig. 2.2) are rapid warming episodes on decadal time scales followed by gradual cooling and characterise MIS 3 (26 – 59 ka) in particular (Rahmstorf, 2003; Dansgaard et al., 1993; Johnsen et al., 1992). As HS precede some DO-Events, possible links are in constant discussion (e.g. Zhang et al., 2014). But oceanic changes during DOs are still unclear, hampering potential explanations for these links. Additionally, proxy analyses reconstructing oceanic changes (see next section) coinciding with these rapid climate variations as well as with long-term glacial-interglacial cycles have focused on abyssal and surface ocean archives. Thermocline analyses were often disregarded. However, various models of past oceanic circulation have long since revealed the important role of the thermocline in our understanding of global climate and oceanic changes (Stocker and Johnsen, 2003; Schiller et al., 1997; Stocker et al., 1992). These bipolar seesaw models predicted an Atlantic thermocline temperature drop of up to -10 °C in the mid-latitudes of the Northern Hemisphere during times of abrupt and extreme atmospheric cooling, presumed to coincide with a shut down of the THC (Fig. 2.3).

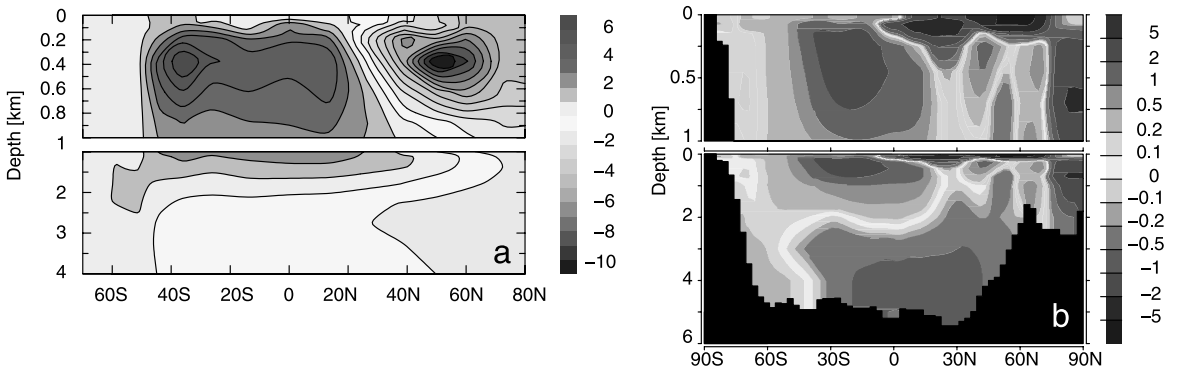

Figure 2.3: AMOC: active vs. shut-down results from bipolar seesaw models
Latitude-depth plots of the Atlantic temperature anomaly between off and on mode (off-on) Temperature differences exhibit a bipolar pattern with cold anomalies in the North Atlantic and warm anomalies south of 10 – 20°N.
Figure taken from Stocker and Johnsen, 2003 who combined (a) from Stocker et al., 1992 and (b) from Schiller et al., 1997

For a long time the neglect of intermediate processes was mainly due to a lack of good archives for thermocline circulation and geochemical processes. Therefore, no proxy analysis has yet reconstructed thermocline temperature patterns for the last glacial and the LGM, DO cycles and HS in particular.

2.1.1 Reconstructing past ocean circulations and geochemical processes

Past oceanic circulations and geochemical processes cannot be measured directly. However, seawater properties like temperature, salinity, water mass origin, local or regional flow strength and reservoir ages (time since a water mass was last in contact with the atmosphere) alter chemical and biological characteristics in marine archives. These characteristics, so-called proxies, can be measured. However, before a proxy can be used to reconstruct certain seawater characteristics, the exact processes controlling the proxy in question need to be well understood and re-evaluated regularly. Henderson, 2002 said '*All proxies respond to more than one variable, some of which can be overlooked*', stressing the continuing need to test both new and established proxies for their reliability.

The most widely used marine archive is abyssal pelagic sediment. Marine sediment consists of different phases, like calcite shells from foraminifera, dinoflagellates or other calcite forming organisms, continental particles of different grain size, ferromanganese coatings around these etc. Numerous proxies for seawater temperature (e.g. Mg/Ca in foraminifera, or species specific foraminifera assemblages; (Penaud et al., 2011; Lear et al., 2000)), nutrients or surface biological productivity (e.g. Ba/Ca, Cd/Ca foraminifera abundance; (Keigwin and Boyle, 1989; Lea et al., 1989)), water mass changes (εNd, δ^{13}C; (Frank, 2002; Piepgras et al., 1979)); ^{14}C reservoir age reconstructions on benthic and planctonic foraminifera Skinner et al., 2017; Adkins and Boyle, 1997; Broecker et al., 1990a) have successfully been introduced. However, the use of sediment cores is limited by several factors: 1) On steep slopes and in regions with strong currents only very little to no sediment deposition takes place. Therefore, the archive pelagic sediment is often missing (Wefer et al., 1999). 2) If there is deposition in regions with strong currents it is hard to tell where the sediment in question originated or if it was reworked, hampering interpretations (Frank et al., 1999; Rosenthal et al., 1995). 3) Locations with low sedimentation rates result in low time resolution records. 4) Mixing processes like bioturbation average out variations of the seawater, weakening or even eliminating their distinct signal. Typical mixing scale lengths are roughly 5 – 10 cm (Wefer et al., 1999; Manighetti et al., 1995). This prevents high-resolution records that resolve centennial or even decadal dynamics, even in areas with high sedimentation rates. 5) Sediment cores cannot be dated directly. Age-models are usually obtained by stable isotope reconstructions on foraminifera (δ^{18}O and δ^{13}C) that are correlated to ice core records (e.g. Paillard et al., 1996; Martinson et al., 1987; Prell et al., 1986; Imbrie et al., 1984). This always leaves the possibility of misinterpreting so-called age-depth tie points which alters the age-model of the sediment core in question. Precise radiocarbon-dating on planctonic foraminifera shells is possible. Therefore, usually a few dates are measured as tie points to check the age model obtained from the δ^{18}O analysis (e.g. Penaud et al., 2010). However, knowledge on the local marine reservoir effect and its variability through time (Waelbroeck et al., 2001, Chap. 2.5.2) is required for this method.

In contrast to sediment cores, cold-water corals (CWC) have only come into focus as marine archives in the last 20 years. CWCs can be seen as both a proxy and an archive. Their timing of occurrences (proxy) as well as variables like elemental or isotopic ratios incorporated into their skeletons (archive) are linked to environmental conditions and can hence be used for paleoceanographic reconstructions. One of the main advantages of CWCs is the ability to precisely date them by U-series (U/Th) and ^{14}C-dating. In combination with their growth rates between 0.5 and 26 mm/a, this allows for high-resolution paleoceanographic reconstructions

up to decadal time scales (e.g. Wienberg and Titschack, in press; Robinson et al., 2014). Depending on the species and size of the coral, even seasonal reconstructions on growth rings are possible (Montero-Serrano et al., 2011). Furthermore, CWCs grow in thermocline water depths (Chap. 2.2) presenting a valuable archive for regions of the water column not covered by traditional archives like abyssal sediment cores and planctonic foraminifera found in these (e.g. Dubois-Dauphin et al., 2016). However, CWCs do not grow everywhere and even in a region of CWC abundance typical records are discontinuous (e.g. Kano et al., 2007). Therefore, to obtain a full picture of the changing geochemical processes and ocean circulations it is beneficial to combine several archives and proxies.
This project thus focusses on thermocline CWCs combined with pelagic sediment cores used to fill the gaps in the coral record. To gain a more complete picture of oceanic changes and environmental conditions a multi-proxy approach, i.e. analysis of a number of elements and isotopic ratios, is applied.
The introduction of the relevant background given in this chapter will focus on CWCs and their most important characteristics. I will give an outline on the established temperature proxy Li/Mg concentration ratio in aragonitic CWCs and the two water mass tracers εNd (CWC and sediment) and ^{14}C reservoir age (CWC). Finally, I will motivate the need for the search of nutrient or biological productivity proxies. Background information given on sediment as an archive will cover the essentials, in particular concerning εNd, the proxy used on bulk sediment.

2.2 Cold-water corals

Coral reefs are typically associated with snorkelling or diving through beautiful colourful shallow tropical reefs populated by a vast number of multicoloured fish, like the Great Barrier Reef[1]. However, corals are not restricted to these shallow warm regions. The first known mentioning of 'deep-sea' or 'cold-water' corals living below the photic zone was in the mid-eighteenth century (Roberts et al., 2009). In fact, over 65% of all coral species live in water depths deeper than 50 m. However, until the 1970s, it has been nearly impossible to retrieve deep-sea corals systematically (Roberts et al., 2009). In the last 20 years, a vast variety of technologies has been developed that enable us to study coral ecosystems in the deep ocean as well as collect corals for laboratory analyses. Consequently, the interest in deep-sea corals has continuously increased. The global deep-sea coral distribution has been explored in more and more detail and has, in fact, only recently been updated (Fig. 2.4; (Freiwald et al., 2017)). A literature search by Roberts et al., 2009 on 'deep-sea coral' until 1996 showed '*less than 300 publications whereas the same search terms for the following 10 years revealed nearly 700*'. Repeating this with literature published until 1 August 2017 returned nearly 3500 publications, or even 4680 results when searching for 'cold-water coral'. There are several reasons for the huge scientific interest in deep-sea corals, one of them is their potential as a paleoceanographic archive.

But what exactly are cold-water corals?
Cairns, 2007 defined corals as *'Animals in the cnidarian classes Anthozoa and Hydrozoa that produce either calcium carbonate (aragonitic or calcitic) secretions resulting in a continuous skeleton or as numerous, microscopic individualised sclerites, or that have a black, horn-like, proteinaceous axis.'* This broad definition includes seven coral taxa (Tab.2.1) and outlines only

[1] Actually, in my generation the movie 'Finding Nemo' is one of the first things that comes to mind.

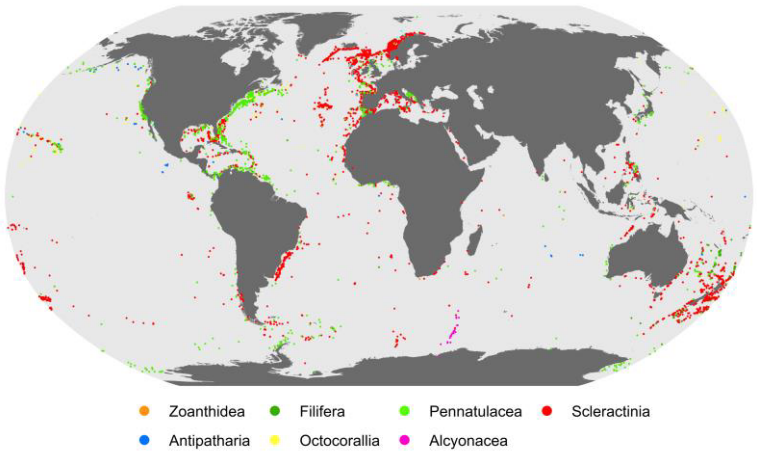

Figure 2.4: Global distribution of cold-water corals. Corals analysed in this project are all of the order 'Scleractinia'
Figure taken from Freiwald et al., 2017

a few morphological differences of corals. Corals investigated in this thesis all descend from the order 'Scleractinia', which have aragonite skeletons. Numerous paleoceanographic studies have already worked with these taxa (e.g. Struve et al., 2017; Robinson et al., 2014; Cheng et al., 2000; Adkins et al., 1998; Mangini et al., 1998.
The two terms 'deep-sea coral' and 'cold-water coral' are used similarly. This usage usually reflects the difference to 'surface / warm-water corals' of which many are so-called 'zooxanthellate', hence live in symbioses with photosynthesising algae (Falkowski et al., 1984; Porter et al., 1984). As roughly 90% of 'azooxanthellate' live in deep waters they are often referred to as deep-sea or cold-water corals (Roberts et al., 2009), but occur in both **cold** deep and surface waters. Therefore, in this thesis, I will use the term 'cold-water coral' (CWC) for azooxanthellate scleractinians.
A schematic illustration of a scleractinian coral polyp is shown in Figure 2.5. In the centre of each coral polyp is the mouth, which is surrounded by a ring of tentacles that form the so-called 'oral disc' (Roberts et al., 2009). Below are the gastrovascular (centre) and the rest of the polyp. The polyp is divided into longitudinal compartments passing into the tentacles. These compartments are divided by the mesentery pairs (thin sheets of tissue), which carry digestive cells, sperm and eggs. During the coral growth usually first six mesentery pairs are formed and subsequently new pairs in between the existing pairs. By incorporation of dissolved bi-carbonate from ambient seawater, inside each mesentery pair part of the calcium carbonate ($CaCO_3$) skeleton is formed (septa). The septa are joined at the outer wall (theca). The calcium carbonate skeleton is often formed in its crystalline form aragonite. This aragonitic skeleton can be used as an archive for paleoceanographic reconstructions.
CWCs occur as individuals, as isolated colonies, in small reefs (a few metres wide), and in the form of large reefs or even gigantic carbonate mounds reaching heights of up to 300 m and horizontal expansions of several kilometres (Roberts et al., 2009). Reef/mounds can span thousands to millions of years (Roberts, 2006; Freiwald et al., 2004). The taxa analysed in this thesis are both solitary and colonial / framework-forming corals. Of the six investigated solitary taxa

Table 2.1: The seven taxa of corals (highlighted in bold font) with common names
Also included are classifications of the eight scleractinian genera used in this thesis. Suborders and families of Scleractinia were reduced to the one relevant for this thesis (Cairns, 2007).

Class	Subclass	Order	Suborder	Family	Genus	Common names
Anthozoa	Hexacorallia	**Scleractinia**	Caryophylliina	Caryophylliidae	*Caryophyllia* *Dasmosmilia* *Desmophyllum* *Lophelia*	Hard corals, stony corals, true corals, cup corals, star corals
				Flabellidae	*Flabellum* *Javania*	
			Fungiina	Oculinidae	*Madrepora*	
			Dendrophylliina	Dendrophylliidae	*Balanophyllia*	
		Zoanthidea				Gold corals
		Antipatharia				Black corals, whip corals, wire corals, thorny corals
	Octocorallia					Soft corals, gorgonians, sea fans, etc.
Hydrozoa	Hydroidolina	Anthoathecata	Filifera	**Stylasteridae** **Hydractiniidae**		'Hydrocorals', lace corals Longhorn hydrozoans
			Capitata	**Milleporidae**		'Hydrocorals', fire corals, millepores

Desmophyllum dianthus (D.dianthus) is perhaps the most widely studied species. The other five taxa are of genus *Caryophyllia sp., Flabellum sp., Javania sp., Dasmosmillia sp.*, and *Balanophyllia sp.*. Of all CWC species less than ten are known to build substantial reef frameworks (Wienberg and Titschack, in press; Roberts, 2006; Freiwald et al., 2004). The two most abundant of all reported framework-forming taxa are the species *Lophelia pertusa (L.pertusa)* and *Madrepora oculata (M.oculata)*, also the framework-forming species investigated in this thesis.

2.2.1 Environmental controls on cold-water coral growth

CWCs are found throughout the entire global ocean (Fig. 2.4). They are generally restricted to seawater temperatures between 4°C and 12°C, conditions usually found in 50 to 1000 m water depth in high latitudes and abyssal depths (up to 4000 m) in low latitudes (Cairns, 2007; Roberts, 2006). In addition to temperature, salinity, the seawater oxygen concentration, the food supply, carbonate chemistry, the substrate on which they grow, and the connectivity for larvae govern the occurrence of CWCs (Flögel et al., 2014; Henry et al., 2014; Davies and Guinotte, 2011; Davies et al., 2009; Roberts et al., 2009; Davies et al., 2008; Cairns, 2007; Mortensen et al., 2001. As they fundamentally influence the food supply, hydrographic and topographic variables like the current speed and the slope of the substrate are important factors. Possible transport processes of organic matter to corals in intermediate depths are associated with rapid downwelling and cascading (Taviani et al., 2016; Davies et al., 2009). Additionally, the food supply from the surface waters to the deeper ocean can be enhanced through geostrophic currents and the combination of topographic and tidal waves or eddies (Navas et al., 2014; White et al., 2005; Genin et al., 1986).

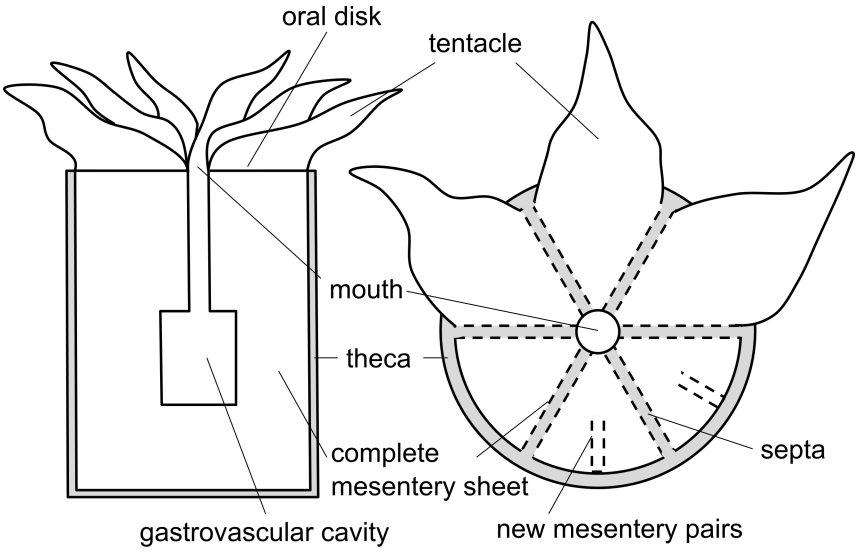

Figure 2.5: Schematic illustration of a scleractinian coral polyp lateral and top down
Grey colours show calcium carbonate skeleton consisting of the theca (outer wall) and the septa (between mesentary pairs).
Figure from Spooner, 2016 after Roberts et al., 2009

Mienis et al., 2007 reported that another pathway for lateral food supply are intermediate and bottom nepheloid layers. These are layers above the ocean floor that contain significant amounts of suspended sediment and hence an enrichment in food particles. Therefore, CWC preferentially grow along steep slopes of seamounts, ridges, canyons or mud volcanoes (Wienberg and Titschack, in press). In addition to the associated food supply, steep slopes and strong currents prevent burial from sediment (White, 2007; Dorschel et al., 2005).
As mentioned before, some CWC species form extensive three-dimensional reefs. These are of particular interest, as they provide high-resolution records of long-term CWC growth patterns and changes in oceanic dynamics or geochemical processes associated with climate variability (e.g. Wienberg and Titschack, in press; Roberts, 2006). Furthermore, particularly during periods of strong bottom currents leading to nondeposition and erosion in adjacent areas, CWC structures are still able to grow and entrap enough sediment to build CWC mounds providing an otherwise non-existing paleocanographic archive (Thierens et al., 2013; Titschack et al., 2009). However, studies have revealed that the formation of coral mounds depends on the interaction between both coral growth and sediment deposition (Wienberg and Titschack, in press) and that their aggregation is discontinuous (Stalder et al., 2015; López Correa et al., 2012; Eisele et al., 2008). The development of CWC mounds can be described by a reoccurring pattern (Fig. 2.6, Roberts et al., 2009; Roberts, 2006). After the initial coral lavae settlement on a suitable substrate, ongoing favourable conditions allow for a continued CWCs growth (Fig. 2.6 (A) and (B)). Corals may be (bio)-eroded to dead coral rubble (mid circle in Fig. 2.6) forming new substrate for living corals and/or stabilising the reef structure. Hence, new corals either grow on coral rubble or the dead framework from corals below. Additionally, during coral growth mobile sediment is entrapped in the reef structure, providing stability (Fig. 2.6 (C); (Titschack et al., 2015; Titschack et al., 2009; Dorschel et al., 2005)). A continuing period of favourable environmental conditions for coral growth in combination with a balancing sediment input, can lead to ‘coral

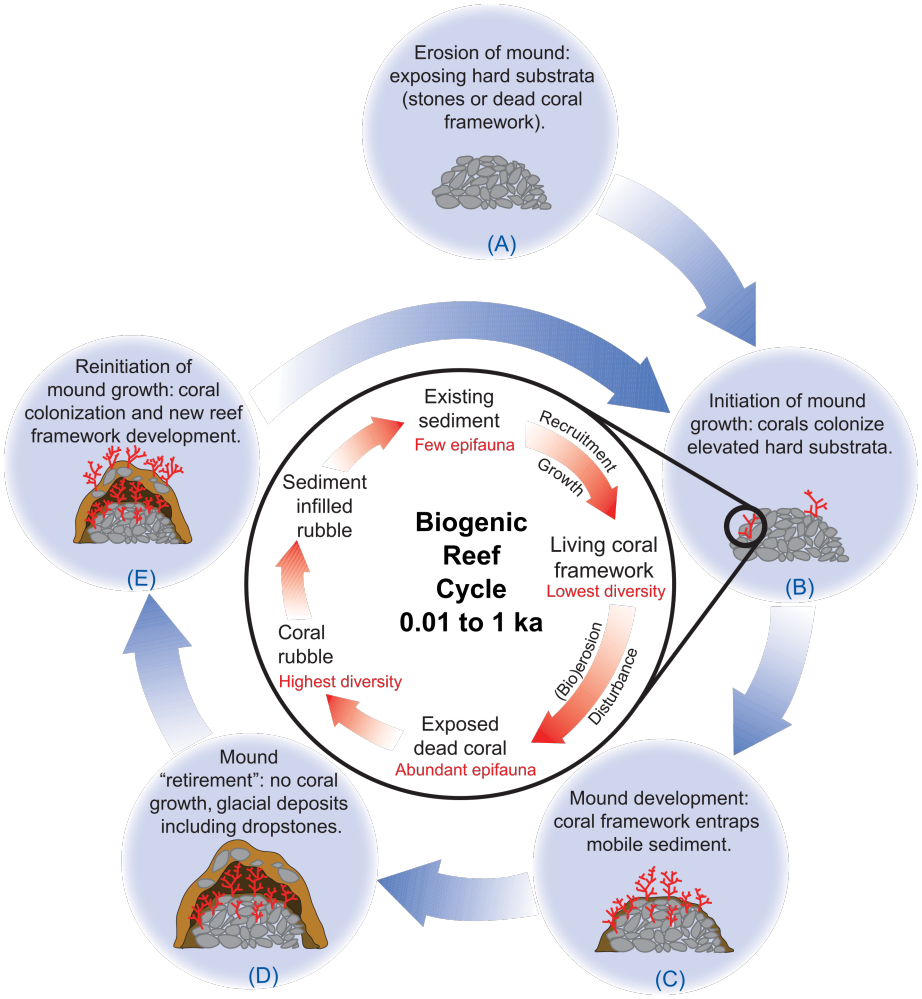

Figure 2.6: Schematic illustration of the CWC mound cycle
Outer circle: stages of a CWC mound aggregation starting at initiation, development, retirement and recolonisation.
Inner circle: small scale reef microhabitats, succession and faunal diversity.
Figure taken from Roberts, 2006

sediments' of several meters. Once conditions change, the CWCs stop growing (Fig. 2.6 D) and the reef structure can either be buried or (bio-)erode. When drilling through a carbonate mound periods of pure sedimentation, so-called hiatus, are easily recognised by sections lacking corals and exhibiting possible features like dropstones. As soon as local conditions change back to conditions favourable for reef-forming species, corals start growing on top of the old structure (Fig. 2.6 (E) and (C)). Following this cycle, CWC mounds are generally distinguished between 'active' and 'inactive'. It needs to be noted that this differentiation does not imply that during an active stadium no dead patches can be found on a mound, but that the general state of the mound is described (respectively for the inactive state).

2.2.2 Cold-water coral distribution through time

Numerous studies have shown that the presently changing climate conditions influence the distribution of living corals (e.g. Stramma et al., 2008; Feely et al., 2004). This was also the case in the past for both solitary and framework-forming CWCs.
Solitary CWCs investigated originate from the Drake Passage (Margolin et al., 2014; Burke et al., 2010) south of Tasmania (Thiagarajan et al., 2013), the eastern Atlantic (Eltgroth et al., 2006), the Northwest Atlantic (Thiagarajan et al., 2013; Robinson et al., 2007), the Mediterranean (McCulloch et al., 2010) and the Galapagos Islands (McIntyre et al., 2011).
The Drake Passage is a good example for CWC population movement closely linked to climate changes. It was shown that during the last deglaciation the population of *D. dianthus* probably moved from living south of the Polar Front to north of the Polar Front (Margolin et al., 2014; Burke et al., 2010). In contrast, *Caryophyllia sp.* could not be found at all until deglaciation, but started thriving south of the Polar Front during the same time *D. dianthus* moved northwards. This growth pattern of *Caryophyllia sp.* living south and *D. dianthus* living north of the Polar Front still seems to be valid in present conditions. This change in CWC distribution was linked to varying oxygen concentration (Margolin et al., 2014). Another interesting feature can be observed at the Galapagos Islands. CWCs analysed were either modern or dated to ages of 30 ka and older (McIntyre et al., 2011). Hence, an on- and offset of coral growth in one region can be observed, similar to CWC mound patterns described in chapter 2.2.1.
Following the CWC mound aggregation cycle, the distribution of living framework-forming CWCs also changes with time following variations in the climate system. Studies on frame-work forming CWCs investigated corals from the Northeast Atlantic (e.g. López Correa et al., 2012; Kano et al., 2007; Rüggeberg et al., 2007; Dorschel et al., 2005; Frank et al., 2004; De Mol et al., 2002; Mortensen et al., 2001), the Mediterranean (Fink et al., 2013; McCulloch et al., 2010), the Northwest Atlantic (*Solenosmilia variabilis*; (Robinson et al., 2007)), off Florida (van de Flierdt et al., 2010) and off the Brazilian margin (*L. pertusa* and *S. variabilis*; (Mangini et al., 2010)). Recently active CWC mounds (mainly *L. pertusa*) have been found in the Gulf of Mexico (Matos et al., 2017; Hebbeln et al., 2014), more southern Moroccon margin (Glogowski et al., 2015) and at the Angolan margin (Beisel, 2017; Roesch, 2017; Hebbeln et al., 2016b; Wefing, 2016).
A lot of the research has focused on the Northeast Atlantic, in particular on Porcupine Seabight and Rockall Bank along the Irish and UK margins (e.g. Kano et al., 2007; Rüggeberg et al., 2007; Dorschel et al., 2005; Frank et al., 2004; De Mol et al., 2002) that exhibit more than 1000 thriving CWC mounds (Roberts, 2006). Another region with flourishing CWC reef growth is the Norwegian shelf (e.g. López Correa et al., 2012; Mortensen et al., 2001). While Porcupine Seabight and Rockall Bank are largely colonised by *L. pertusa* and *M. oculata*, the Norwegian shelf is dominated by solely *L. pertusa*, not implying the total absence of other species. In fact, in both regions other species of both solitary and framework forming CWCs were reported (e.g. Mortensen et al., 2001). In contrast to these two regions of thriving CWC communities, CWC mounds along the Moroccan margin and off Mauritania are covered by dead *L. pertusa* and *M. coulata*, with a few scattered patches of living colonies (diameter $\approx 10-20$ cm) on the Mauritanian mounds (Eisele et al., 2011; Wienberg et al., 2010; Wienberg et al., 2009; Colman et al., 2005). Dates obtained from the fossil corals suggest that CWC mound aggregation was observed during glacial periods. Combining the findings of presently flourishing northern regions limited up to 70°N with the suggested CWC mound aggregation limit during glacial periods of 50°N Frank et al., 2011 suggested an 'orbitally-paced north-south oscillation'. This north-south oscillation was linked to possible different paths of cold nutrient-rich intermediate waters and surface

productivity.
CWCs from Scary Mound at the Angolan Margin, exhibit mound aggregation during both interglacial and glacial periods. This makes Scary Mound the second coralline ecosystem that covers the last glacial, the deglaciation and the warm Holocene. First observations of CWC growth during both major climate stages from the Brazilian margin cover ages between 30 and 8 ka BP (Mangini et al., 2010), while CWCs from Scary Mound still flourish today (Beisel, 2017; Roesch, 2017; Hebbeln et al., 2016b; Wefing, 2016).

2.2.3 Growth rates

It is important to accurately resolve the linear growth rates of CWCs, in particular for high resolution records on one coral. The frame-work building species *L. pertusa* exhibits growth rates of 5 – 26 mm/a (Orejas et al., 2008; Gass and Roberts, 2006; Mortensen, 2001; Mortensen et al., 1998) covering a wider range than *M. oculata* (3 – 18 mm/a) (Sabatier et al., 2012; Orejas et al., 2008). However, this result might just be due to the larger number of *L. pertusa* analysed. In contrast, the slower growing framework-forming species *Enallopsammia rostrata* has linear growth rates of 10 – 70 µm/a (Houlbrèque et al., 2010; Adkins et al., 2004). The only solitary scleractinian CWC species investigated for its growth rate is *D. dianthus*. ^{210}Pb, ^{14}C and U-series dating based studies revealed growth rates between 0.5 and 3.1 mm/a (Adkins et al., 2004; Risk et al., 2002; Cheng et al., 2000). Life spans of *L. pertusa* and *D. dianthus* are reported to be on the order of 100 to 200 years (Robinson et al., 2014; Adkins et al., 2004). Hence, by subsampling on a single coral centennial or even decadal records can be obtained (Border, 2016). As explained in chapter 2.1.1 this extremely high temporal resolution is unique in the mid-depth and deep ocean as sediment is subject to bioturbation and other mixing mechanisms corals are not affected by.
CWC reef aggregation is usually considerably slower than the growth of an individual coral, but can reach almost comparable rates. A summary of published reef records showed aggregation rates spanning from 1 cm/ka to 1500 cm/ka (Wienberg and Titschack, in press). It has to be noted that the extremely fast aggregation of 1500 cm/ka is the exception, with most recorded aggregation rates varying between 10 and 100 cm/ka. CWC mound aggregation rates will be discussed in detail in chapter 4.

2.2.4 Vital effects

Inorganic calcium carbonate precipitates from solution into crystallised $CaCO_3$ in thermodynamic equilibrium. However, similar to many other marine biological organisms, CWCs alter the chemistry of calcifying fluids during the precipitation of their aragonite skeletons (Roberts, 2006). Therefore, the chemical composition of CWC skeletons depends on both environmental conditions and internal biological reaction pathways. These internal biological processes are called 'vital effects' and can vary from species to species as well as for the element or isotopic system considered. For example, the two classical temperature proxies stable oxygen isotopes (δ^{18}O) and Mg/Ca ratio are extensively and successfully used in other marine carbonate archives like foraminifera and tropical corals. However, due to the higher complexity of the reaction pathways, in CWCs the environmental controls are dominated by the vital effects (e.g. Rollion-Bard et al., 2010; Gagnon et al., 2007; Cohen et al., 2006; Adkins et al., 2003; Smith et al., 2002; Weber, 1973). Therefore, vital effects make the search for reliable paleoceanographic proxies

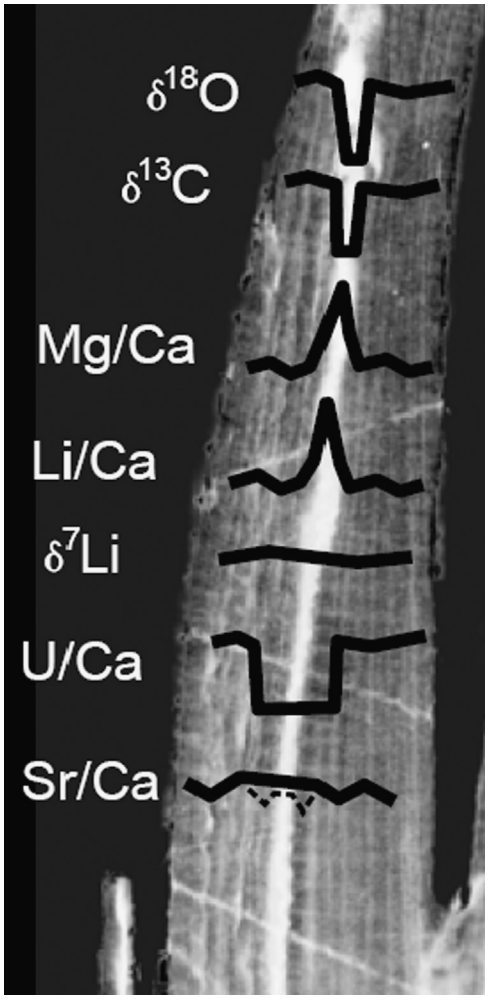

Figure 2.7: Microscale elemental and stable isotope variations inside a CWC skeleton
A negative transmitted light photomicrograph of a transversely-sectioned septa from a *D. dianthus* is overlain by schematic compositional profiles of element/Ca ratios and stable isotopes. Figure taken from Robinson et al., 2014

considerably more challenging. However, they also present a valuable tool to improve our understanding of the coralline biomineralisation processes. For example, microscale analysis of the aragonitic skeleton revealed clear geochemical patterns within one coral (*D. dianthus*; Fig.2.7). Inside the fast growing small bands, the 'centers of calicification' (COC), the two elements Mg and Li are clearly enriched (Montagna et al., 2014; Case et al., 2010; Gagnon et al., 2007), while U/Ca ratios are considerably smaller (Robinson et al., 2006; Sinclair et al., 2006) than in the fibrous aragonitic parts subsequently overgrowing the COCs. δ^{18}O and δ^{13}C signatures of COCs are generally lower than in the rest of the skeleton (Adkins et al., 2003). Presently, the processes underlying this pattern are not yet well understood. However, the features observed have already proven to be a useful tool in verifying proposed biomineralisation models and finding alternative proxies for environmental conditions (e.g. Li/Mg in CWCs as a temperature proxy; Chap. 2.4 and Chap. 5).

2.3 U-series dating of cold-water corals

One of the main advantages of CWCs as paleoceanographic archives is our ability to precisely date them by U-series (U/Th) and ^{14}C-dating. As in this thesis ^{14}C-dating is not used for dating purposes alone, but also to investigate water mass circulation patterns, it is explained later in chapter 2.5.2. The elucidations here are based on Ivanovich, 1994.
U-series dating is a geochronological tool used to reconstruct past Earth history back as far as 800 ka BP. It is based on the radioactive decay series of ^{238}U into ^{230}Th.

$$\boxed{^{238}\mathrm{U}} \xrightarrow[4.5\times10^{9}\,\mathrm{a}]{\alpha} \boxed{^{234}\mathrm{Th}} \xrightarrow[24\,\mathrm{a}]{\beta} \boxed{^{234}\mathrm{Pa}} \xrightarrow[7\,\mathrm{h}]{\beta} \boxed{^{234}\mathrm{U}} \xrightarrow[245\times10^{3}\,\mathrm{a}]{\alpha} \boxed{^{230}\mathrm{Th}} \xrightarrow[7.52\times10^{4}\,\mathrm{a}]{\alpha} \boxed{^{226}\mathrm{Ra}}\ldots \tag{2.1}$$

Due to the short half-lives of ^{234}Th and ^{234}Pa, only analyses of the time-dependent activity ratios of (^{230}Th/^{238}U), (^{234}U/^{238}U) and (^{232}Th/^{238}U) are needed to obtain the age of the sample using the 'marine age equation'

$$\left(\frac{^{230}\mathrm{Th}}{^{238}\mathrm{U}}\right)_{\mathrm{t}} = 1 + \left[\left(\frac{^{230}\mathrm{Th}}{^{238}\mathrm{U}}\right)_{\mathrm{i}} - 1\right] e^{-\lambda_{230}} + \left[\left(\frac{^{234}\mathrm{U}}{^{238}\mathrm{U}}\right) - 1\right] \frac{\lambda_{230}}{\lambda_{230} - \lambda_{234}} \left(1 - e^{-(\lambda_{230}-\lambda_{234})t}\right) \tag{2.2}$$

with parentheses denoting activity ratios. λ_{i} are the decay constants of the respective isotope, $\left(^{230}\mathrm{Th}/^{238}\mathrm{U}\right)_{\mathrm{i}}$ is the initial activity ratio in the carbonate and t is the sample age. In literature $\left(^{234}\mathrm{U}/^{238}\mathrm{U}\right)$ is commonly expressed in δ notation:

$$\delta^{234}\mathrm{U} = \left(\left(^{234}\mathrm{U}/^{234}\mathrm{U}\right)_{\mathrm{meas}} - 1\right) \times 1000 \tag{2.3}$$

Therefore, the activity ratio of $\left(^{234}\mathrm{U}/^{238}\mathrm{U}\right)$ at time t is

$$\delta^{234}\mathrm{U_t} = \delta^{234}\mathrm{U_i} \times e^{-\lambda_{234}\times \mathrm{t}} \tag{2.4}$$

Using EQ. 2.2 and EQ. 2.4 and assuming $\left(^{230}\mathrm{Th}/^{238}\mathrm{U}\right)_{\mathrm{i}} = 0$, the so-called 'seawater evolution curve' of ^{230}Th/^{238}U in terms of δ^{234}U can be formulated as

$$\frac{^{230}\mathrm{Th}}{^{238}\mathrm{U}} = 1 - e^{\frac{\lambda_{230}}{\lambda_{234}} \times ln\left(\frac{\delta^{234}\mathrm{U}}{\delta^{234}\mathrm{U_i}}\right)} + \frac{\lambda_{230}}{\lambda_{230} - \lambda_{234}} \times \frac{\delta^{234}\mathrm{U}}{1000} \times \left(1 - e^{\frac{\lambda_{230}-\lambda_{234}}{\lambda_{234}} \times ln\left(\frac{\delta^{234}\mathrm{U}}{\delta^{234}\mathrm{U_i}}\right)}\right) \tag{2.5}$$

The residence time of ^{238}U (400 ka) in the ocean is considerably larger than the global mixing time ($\sim$ 1000 a) leading to a homogeneous distribution. As can be seen in EQ. 2.1, the decay of ^{238}U constantly produces ^{230}Th, which exhibits a residence time of only 40 a. As in the global ocean ^{230}Th is insoluble and relatively reactive, ^{230}Th is removed from the water column through adsorption to other particles and reverse scavenging processes. Hence, in seawater U and Th are in an activity disequilibrium, setting the basis for U-series dating of marine archives such as CWCs.
During the $CaCO_3$ precipitation forming the aragonitic coral skeletons (Chap. 2.2, 2.2.4), ^{238}U can occasionally replace Ca in the crystal lattice. U concentrations in CWCs, related to the calcification temperature and previously mentioned vital effects, are typically between 2 and 5 ppm. Once the CWC stops growing, the incorporation of U stops and it decays into ^{230}Th.
Despite the short oceanic residence time of ^{230}Th it is possible that non-radiogenic ^{230}Th is in-

corporated into the coral. Additionally, most $^{230}Th_i$ contamination results from ferromanganese coatings that sometimes form around the coral skeleton and exhibit high $^{230}Th_i$ concentrations. These are removed by the cleaning procedure of the corals. To correct for any remaining initial $^{230}Th_i$, the most abundant thorium isotope, ^{232}Th, is used (Frank et al., 2004; Cheng et al., 2000; Lomitschka and Mangini, 1999).

$$\left(\frac{^{230}Th}{^{238}U}\right)_i = \left(\frac{^{232}Th}{^{238}U}\right) \times \left(\frac{^{230}Th}{^{232}Th}\right)_i \tag{2.6}$$

Both half-lives of ^{232}Th and ^{238}U exceed the CWC age by several orders of magnitude. Therefore, their activity ratio can be assumed to have been constant since the coral's death. No Th fractionation occurs from seawater into coralline aragonite, hence, seawater $^{230}Th/^{232}Th$ measurements ranging between 0 and 30 in water depths from 0 – 400 m can be used to estimate the activity ratio of ^{232}Th and ^{238}U in CWC skeletons (Cheng et al., 2000).
Finally, it is critical that since its death the CWC has remained a closed system, i.e. changes in the U-series isotopes are only due to their radioactive decay (Edwards et al., 2003). Open system behaviour can be a result of diagenesis, the process of physical and chemical weathering of fossil CWC skeletons, that changes the U-series isotopic composition and hence the age determined. Consequential dissolution and/or recrystallisation are only two examples causing an open-system (e.g. Allison et al., 2007). To identify open system behaviour, it is possible to compare with other chronometers or to check whether $^{230}Th/^{238}U$ and $\delta^{234}U$ follow the seawater evolution curve (EQ. 2.5). The present-day $\delta^{234}U_{SW,\,i}$ for seawater is 146.8 ‰(Andersen et al., 2010). However, there is an ongoing discussion about the constancy of oceanic $\delta^{234}U_i$ over glacial-interglacial time scales (Thompson et al., 2011; Esat and Yokoyama, 2010; Robinson et al., 2004; Henderson, 2002; Henderson et al., 1993). CWCs represent a valuable archive to asses this question in the future. Chen et al., 2016 recently reported an overshoot of southern Atlantic seawater values by 3 ‰ during early deglaciation. Future studies will have to further analyse the seawater $\delta^{234}U_{SW,\,i}$. Here, we consider the known changes of $\delta^{234}U_{SW,\,i}$ when evaluating the quality of obtained U series ages.

2.4 Temperature reconstructions

Since CWCs came into focus of paleoceanography, it has been a priority to find a reliable proxy for ambient seawater temperature. However, as mentioned in chapter 2.2.4 temperature proxies that reliably work in other marine archives are altered in CWCs (e.g. $\delta^{18}O$ and Mg/Ca in foraminifera and tropical corals; (Rollion-Bard et al., 2010; Gagnon et al., 2007; Cohen et al., 2006; Adkins et al., 2003; Smith et al., 2002; Weber, 1973)). A wide range of elemental Ca ratios (x/Ca) in corals have been investigated for their temperature dependency (Sinclair et al., 2006; Mitsuguchi et al., 1996; Min et al., 1995; Shen and Dunbar, 1995; Beck et al., 1992; Smith et al., 1979) but most have been found to be affected by additional factors. Although Sr/Ca ratios in tropical corals robustly record ambient seawater temperatures (Gagan et al., 1998; Beck et al., 1992), concerns have been raised about possible global oceanic Sr/Ca changes between glacial and interglacial periods (Stoll et al., 1999). Additionally, it has been shown that within one coralline skeleton differences in $\delta^{18}O$ or x/Ca ratios up to several orders of magnitude can be observed (Montagna et al., 2014; Case et al., 2010; Gagnon et al., 2007; Adkins et al., 2003). These inner-skeleton microscale variations are attributed to varying physiological controls on

growth rates.
Recently, carbonate clumped isotopes Δ_{47} have been introduced as a promising new thermometer in CWCs (Spooner et al., 2016; Thiagarajan et al., 2014; Thiagarajan et al., 2011; Ghosh et al., 2006). However, it was shown that some CWC genera tend to overestimate Δ_{47} by up to 0.05 ‰ corresponding to a temperature underestimation by up to 9 °C (Spooner et al., 2016). Hence, the vital effects affecting coralline Δ_{47} are supposedly common to both warm- and cold-water corals (Spooner et al., 2016). They concluded that carbonate clumped isotopes can only be a useful proxy for paleotemperatures if species- or genus-specific calibrations are applied.
Marriott et al., 2004 first showed that Li/Ca ratios in *Porites* (warm-water coral of the order Sclearctinia) and seawater temperature correlated negatively $(4.9 \pm 1.8)\%$ per °C. This correlation is large compared to e.g. Sr/Ca dependencies (0.7%/1°C), making it a promising temperature proxy. Although Li/Ca in foraminifera shells does not show a clear temperature dependency (Delaney et al., 1985), the well-established deep-sea temperature proxy Mg/Ca in benthic foraminifera could be refined by analysing both Mg/Ca and Li/Ca (Bryan and Marchitto, 2008). The Li/Ca compensates carbonate ion and salinity influences on Mg/Ca, leading to an improved positive linear correlation of Mg/Li with seawater temperature, in particular for aragonitic foraminifera species. Investigating Li/Mg in the skeleton of several living cold-water coral species (Case et al., 2010) also asserted linear dependencies of the coralline Li/Mg ratios on temperature. Additionally, influences of seawater carbonate ions or salinity were ruled out. The achieved precision was ± 1.6 °C, calling for further calibrations. Raddatz et al., 2013 showed that in addition to seawater temperature, Li/Ca and Mg/Ca in *L. pertusa* are affected by seawater pH as well as coralline growth- and calcification rates. Mg/Li ratios, however did not exhibit these secondary effects. Possible correlations of Li/Mg in tropical corals (*Porites*) with seawater temperatures were tested by Hathorne et al., 2013a. Combining their data with the other three studies and hence benthic foraminifera, cold-water with tropical corals Hathorne et al., 2013a first suggested an inter-archive negative exponential correlation between Li/Mg and seawater temperature (Li/Mg = 5.16 exp(-0.0492 × T); Li/Mg in mmol/mol, T in °C). Analysing six different coral species, Montagna et al., 2014 determined a robust calibration curve to reconstruct seawater temperatures from Li/Mg ratios in aragonitic corals (Fig. 2.8). Both living or young (<100 a) zooxanthellate and azooxanthellate species from shallow and deep waters, as well as naturally grown corals and corals cultured in tanks were analysed. Hence, a wide range of environmental conditions in which corals grow was covered (e.g. temperature range: 0 – 28 °C). Similar to Hathorne et al., 2013a, they found that relative to Mg with increasing temperature less Li is incorporated roughly following a 5% decrease in Li/Mg per °C (Montagna et al., 2014). A strong negative exponential correlation ($r^2 = 0.975$, n = 49) between Li/Mg in the skeletons of corals and seawater temperature was derived:

$$\mathrm{Li/Mg}\left(\frac{\mathrm{mmol}}{\mathrm{mol}}\right) = 5.41\left(\frac{\mathrm{mmol}}{\mathrm{mol}}\right)\exp(-0.049\,(\pm 0.002)\,(1/^{\circ}C) \times \mathrm{T}), \qquad (2.7)$$

with a typical precision of ± 0.9 °C, based on measurement reproducibilities and the standard error of the calibration.
Montagna et al., 2014 discussed that Li/Ca and Mg/Ca exhibit the inner-skeleton mircoscale variations mentioned above (Chap. 2.2.4). In the fast growing COCs, laid down in the beginning of the calcification process, Li and Mg are enriched compared to in fibrous aragonitic parts subsequently overgrowing the COCs (Fig. 2.7). They conclude, that the areas exhibiting low Li/Ca and Mg/Ca probably grew slowly and close to thermodynamic equilibrium. Therefore,

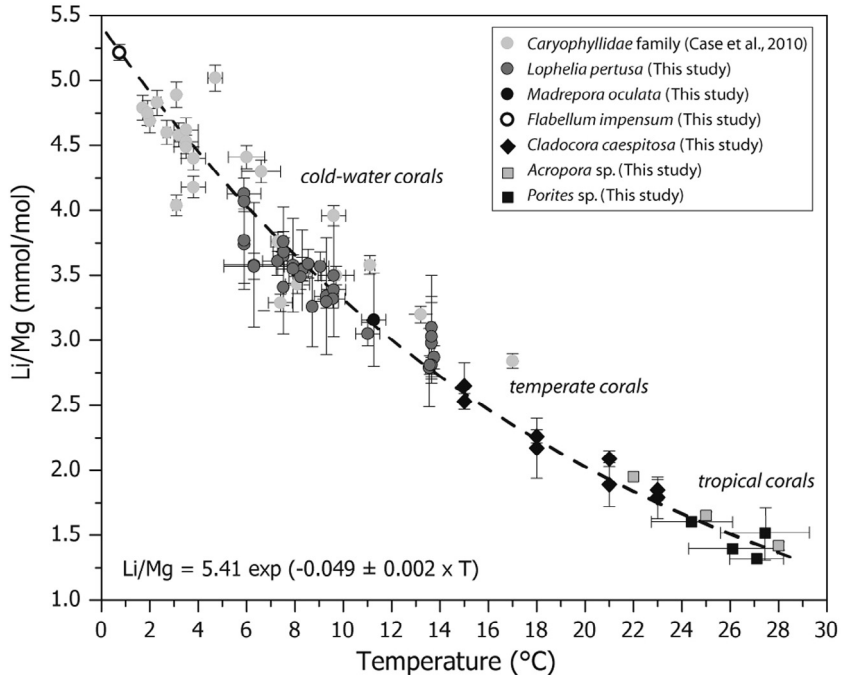

Figure 2.8: Li/Mg temperature calibration for CWCs
Figure taken from Montagna et al., 2014

unbiased environmental signals can potentially be found in the fibrous aragonitic part, making them the best areas for micro-scale geochemical analyses (Montagna et al., 2014). The effects of calcification rates or biological processes inside the skeleton are therefore similar for both elements. Microscale analyses rendered a Rayleigh-type incorporation of Li and Mg correlating positively with temperature (EQ. 2.8). Thus aragonitic coralline Li/Mg ratios are a robust proxy for paleotemperatures.

$$(\mathrm{X/Ca})_{\mathrm{Ar}} = (\mathrm{X/Ca})_{\mathrm{SW}}\, \mathrm{K_d^X F_{Ca}^{(K_d^X - 1)}} \tag{2.8}$$

$(\mathrm{X/Ca})_{\mathrm{Ar}}$ and $(\mathrm{X/Ca})_{\mathrm{Ar}}$ are the Element/Ca ratio in seawater or aragonite, $\mathrm{K_d^X}$ is the partition coefficient between seawater and aragonite ($\mathrm{K_d^X} = (\mathrm{X/Ca})_{\mathrm{Ar}}/(\mathrm{X/Ca})_{\mathrm{SW}}$) and $\mathrm{F_{Ca}}$ is the fraction of initial Ca in the fluid that has been precipitated (Montagna et al., 2014).
Recently, *L. pertusa* from the Norwegian margin (0.02 – 10.30 ka) were dated by U-series dating and analysed in a multi-proxy approach (δ^{11}B, U/Ca, Ba/Ca (see Chap. 2.6, 8 and Li/Mg ratios) to reconstruct the environmental boundary conditions of Norwegian CWC reef growth (Raddatz et al., 2016). Their Li/Mg-derived bottom water temperature reconstructions closely follow sea surface temperature (SST) patterns based on faunal assemblage (Sarnthein et al., 2003) and sub-SST (100 m water depth) determined from Mg/Ca ratios of the cold-water planktonic foraminifera (Aagaard-Sørensen et al., 2014), supporting the reliability of Li/Mg based temperature reconstruction in CWCs.

2.5 Water mass tracers

2.5.1 Radiogenic neodymium isotopes

One of the most used water mass tracers is the radiogenic isotopic composition of Nd, commonly denoted as εNd (EQ. 2.9). The radiogenic Nd isotope signature exhibits a quasi-conservative behaviour in the open oceans and the different oceanic water masses exhibit distinct Nd isotopic signatures. Thus, εNd can be used to identify and reconstruct the presence of different water masses. Acknowledging the huge potential of εNd and the need to understand all its underlying processes, GEOTRACES, currently the biggest global study investigating present day marine biogeochemical cycles of trace elements and their isotopes, appointed the characterisation of the marine distribution of radiogenic Nd and its radiogenic isotopes as one of the key parameters (www.geotraces.org, SCOR Working Group, 2007).
Parallel to this huge campaign effort to better constrain the distribution of radiogenic Nd in the ocean, Lacan et al., 2012 compiled a global data base of all seawater Nd concentration measurements combined with εNd analyses published until then. The data compilation contained 880 data points. Two recent publications (Flierdt et al., 2016 and Tachikawa et al., 2017 (NEOSYPA)) have updated this global data base. They expanded the data base from Lacan et al., 2012 by roughly 1000 seawater data points not collected in the scope of GEOTRACES, and 'historical Nd isotope and concentration data' (Flierdt et al., 2016). Additionally, hydrological parameters (Tachikawa et al., 2017; Flierdt et al., 2016), δ^{13}C and Δ^{14}C values of dissolved inorganic carbon and lateral distances from the data stations to the nearest continental margins at the ocean surface were compiled (Tachikawa et al., 2017). Furthermore, Tachikawa et al., 2017 included published archival εNd data (younger than 10 ka), including cold-water coral and leachates from Fe-Mn oxyhydroxides in bulk sediment; the archives used in this project.
But what causes the scientific interest in the present-day distribution of marine εNd?

The different oceanic water masses exhibit distinct Nd isotopic signatures that are derived from continental weathering, erosion and particle-seawater interaction (Lacan and Jeandel, 2005b; Goldstein and Hemming, 2003; Frank, 2002; Goldstein and O'nions, 1981; Piepgras et al., 1979). The residence time of εNd in the open ocean is approximately 360 – 700 a (Rempfer et al., 2011; Siddall et al., 2008; Tachikawa, 2003). Natural Nd isotopes are practically stable with regards to radioactive decay and nowadays only ^{143}Nd is radiogenically produced through the very slow alpha decay of ^{147}Sm. As the half life of ^{147}Sm is estimated to be 106 Ga (Stosch, 1999), isotopic differences in Nd are quite small. The Nd isotopic composition corresponds to ^{143}Nd/^{144}Nd and is expressed as

$$\varepsilon\mathrm{Nd}_{\mathrm{Sample}} = \left(\frac{\left(^{143}\mathrm{Nd}/^{144}\mathrm{Nd}\right)_{\mathrm{Sample}}}{\left(^{143}\mathrm{Nd}/^{144}\mathrm{Nd}\right)_{\mathrm{CHUR}}} - 1 \right) \times 1000\,, \tag{2.9}$$

which is the fractional deviation from the present-day 'bulk Earth' value $\left(^{143}\mathrm{Nd}/^{144}\mathrm{Nd}\right)_{\mathrm{CHUR}}$ = 0.512638 in parts per 10^4 (CHUR: Chrondric Uniform Reservoir; (Jacobsen and Wasserburg, 1980)). The two isotopic water mass end-members of the the major ocean water masses are the unradiogenic North Atlantic Deep Water, the most depleted in ^{143}Nd (εNd = -13.5 $\pm$ 0.5; (Piepgras and Wasserburg, 1987)), and the deep water of the North Pacific displaying the most radiogenic Nd signature (εNd = -2 to -3). In the modern ocean, the Nd isotopic composition has been shown to covary with salinity, silicate or PO_3 providing evidence for the validity as a water

mass tracer (Goldstein and Hemming, 2003; Blanckenburg, 1999). Radiogenic Nd isotopes are not known to be fractionated by biological activity or physical characteristics like temperature or salinity (Fig. 2.9) and have thus been treated as a quasi-conservative tracer for water mass sourcing and global ocean circulation for both present and past periods (Martin and Scher, 2004; Vance et al., 2004; Blanckenburg, 1999; for review: Goldstein and Hemming, 2003; Frank, 2002).

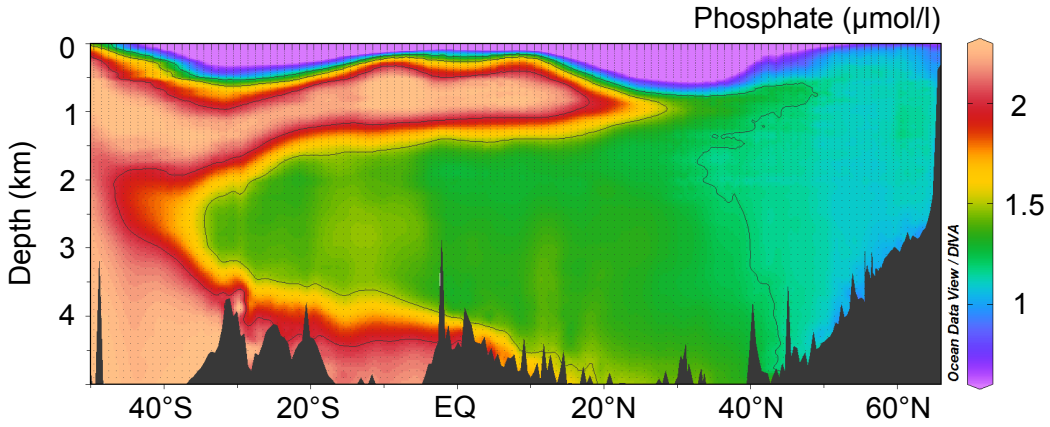

(a) PO_3 along a meridional west Atlantic section (Data from Garcia et al., 2013))

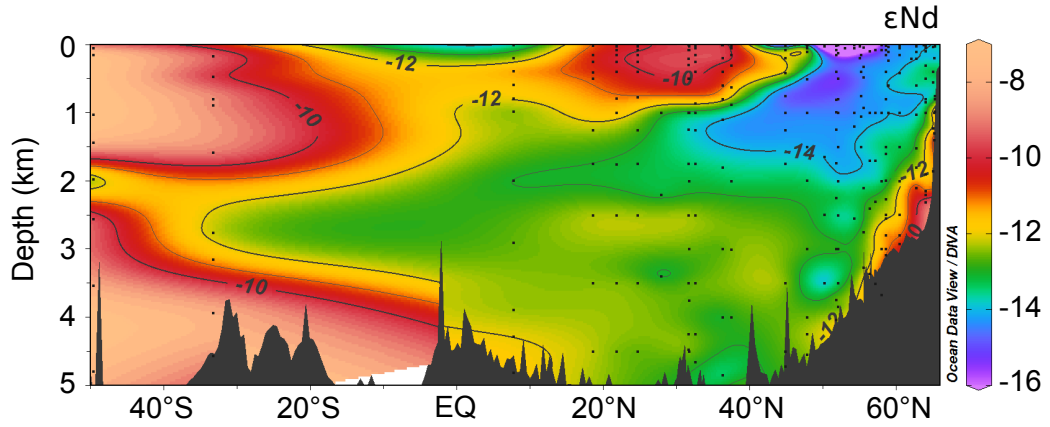

(b) εNd along a meridional West Atlantic section

Figure 2.9: Meridional west Atlantic transects of dissolved PO_3 and εNd
Both follow roughly the same pattern, in particular below 1000 m water depth, supporting the quasi-conservative behaviour of εNd in the ocean.
(a) The PO_3 concentration follows the advection of the main water masses: Antarctic Intermediate Water (upper red) and Antarctic Bottom Water (lower red) flow northward, while North Atlantic Deep Water (bluegreen) flows southward (data from Garcia et al., 2013).
(b) North Atlantic Deep Water is depleted in ^{143}Nd (lower εNd values) relative to most other water masses and can be distinguished from the upper Antarctic Intermediate Water and the dense Antarctic Bottom Water. (Black dots indicate positions of compiled measurements (Blaser, 2017; Flierdt et al., 2016)

However, there are still many open questions regarding radiogenic Nd concentrations and isotopes in the ocean. For example, it has been assumed that the Nd isotopic composition of NADW

has been uniform and constant through time. Recent studies give reason to doubt this simplification (Deaney et al., 2017; Roberts and Piotrowski, 2015; Wilson et al., 2014). The general processes producing the Nd isotopic compositions of water masses are known. However, some are not yet completely understood. For example, 'boundary exchange', which describes the interaction between sediments and seawater along continental margins (Wilson et al., 2012; Rempfer et al., 2011; Jeandel et al., 2007; Lacan and Jeandel, 2005b), is thought to play a major role in certain regions, but is not understood in detail (Jeandel, 2016). Another effect that has been found to be important in some regions (Northeast Pacific) is upward benthic fluxes of radiogenic Nd from sediment pore waters (Abbott et al., 2016; Du et al., 2016; Abbott et al., 2015a; Abbott et al., 2015b). Howe et al., 2016 suggested an influence of poorly chemically weathered detrital material on bottom water εNd signatures in the Labrador Sea.

In spite of these processes altering its quasi-conservative characteristic, εNd has evidently already served as a particularly useful paleoceanographic tracer for water masses. Several archives have been found suitable for εNd. For example, fish teeth and reductively cleaned or uncleaned foraminifera picked from marine sediments are considered to be two of the most reliable recorders (e.g. Horikawa et al., 2011; Martin and Scher, 2004; Vance and Burton, 1999), but are not found everywhere.

εNd in U/Th-dated cold-water corals was first introduced to reconstruct intermediate Northwest Atlantic signatures during the last glacial cycle (van de Flierdt et al., 2006). Robinson and Flierdt, 2009 combined ^{14}C-reservoir age determinations (Chap. 2.5.2) from CWCs with εNd analyses that suggested a reduced influence of NADW in the Southern Ocean during Heinrich stadial 1, a cold period 17,000 years ago, marked by partial collapse of the glacial Northern Hemisphere ice sheets (Heinrich, 1988).

In 2010 two studies systematically calibrated εNd in globally distributed aragonitic CWC skeletons (Copard et al., 2010; van de Flierdt et al., 2010). Both solitary and reef-forming species were investigated and compared to seawater signatures. However, only five of the coral-seawater comparisons could be done with nearby seawater sites. Recently, Struve et al., 2017 updated these two calibrations (Fig. 2.10). They analysed four species *D. dianthus, B. malouinensis, and F. curvatum* from the Drake Passage, and *M. oculata* from the North Atlantic (living or $\leqslant$ 467 a). Struve et al., 2017 were able to compare coral εNd to closely located seawater signatures that agreed well with already published seawater data from the respective region. The three species *D. dianthus, F. curvatum* and *M. oculata* could be confirmed as a suitable archive for seawater εNd signatures. However, the species *B. malouinensis* was found to exhibit deviations of up to 0.6 epsilon units, suggesting the need for further studies on this species. Nevertheless, up to this point six aragonitic cold-water coral species are reported to reliably trace seawater radiogenic Nd isotopes and can thus be used for paleoceanographic reconstructions.

In the last 10 years, εNd recorded in CWCs has been used successfully to gain new insight in paleoceanographic circulation patterns (Dubois-Dauphin et al., 2016; Wilson et al., 2014; Montero-Serrano et al., 2013; Copard et al., 2012; Copard et al., 2011; Montero-Serrano et al., 2011; Colin et al., 2010; Copard et al., 2010). Unfortunately, as discussed in chapter 2.2, CWCs do not grow in all parts of the global ocean. Additionally, they are sensitive to changes of the environmental conditions in the regions they grow. This has the advantage of possibly recording these changes, but also the disadvantage of reduced growth or even growth stops if the conditions become too hostile (e.g. Thiagarajan et al., 2013; Frank et al., 2011; Wienberg et al., 2010; Frank et al., 2009).

In addition to fish teeth, foraminifera and cold-water corals, acid-reductive extraction of trace

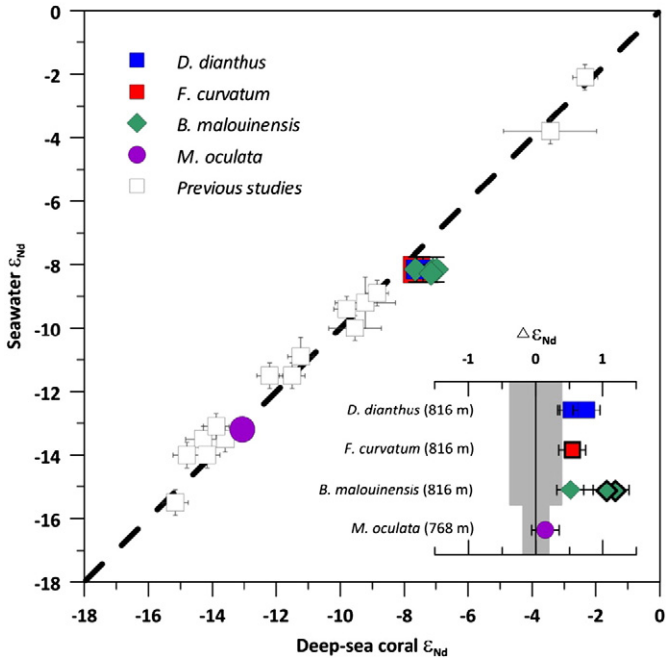

Figure 2.10: Modern calibration for εNd in aragonitic CWC (here 'deep-sea coral') skeletons White squares indicate modern calibration data from Copard et al., 2010; van de Flierdt et al., 2010. Coloured symbols are modern corals analysed in Struve et al., 2017 (Drake Passage: *D. dianthus, B. malouinensis, and F. curvatum*; North Atlantic *M. oculata*)
Inset: deviation of modern CWC εNd from ambient SW, expressed as $\Delta\varepsilon$Nd (only Struve et al., 2017). The grey bar represents the analytical uncertainty of the respective ambient SW measurement. Living corals are framed with a thick black line others are dated $\leqslant 467$ a.
Figure taken from Struve et al., 2017

metal enriched hydrogenetic Fe-Mn oxyhydroxides of the bulk sediment can be used (e.g. Gutjahr et al., 2007; Bayon et al., 2004; Piotrowski et al., 2004; Rutberg et al., 2000). However, potential contaminations due to labile terrigenous fractions like preformed continental Fe-Mn oxyhydroxides and radiogenic volcanic particles have been recognised to possibly alter the εNd signature extracted with these methods (Abbott et al., 2016; Blaser et al., 2016; Wilson et al., 2013; Elmore et al., 2011; Roberts et al., 2010; Bayon et al., 2004). To prevent such contaminations, Blaser et al., 2016 developed a leaching protocol for which the results agreed with data obtained from uncleaned foraminifera. Furthermore, it can easily be screened for contaminations (Blaser et al., 2016). This method was developed in the laboratories of the Institute of Environmental Physics (IUP, Heidelberg University), making it possible to apply his method on the two sediment cores analysed in this project.

2.5.2 ^{14}C-dating – reservoir ages

The most widely known method for dating fossil materials is radiocarbon or ^{14}C-dating. It was developed and first used in studies by W. F. Libby (e.g. Libby, 1952; Anderson and Libby, 1951). It is based on the radioactive carbon isotope ^{14}C, which is produced through the interaction of cosmic radiation and atmospheric nitrogen. In the atmosphere it mainly occurs as $^{14}CO_2$ with

$^{14}C/^{12}C \approx 10^{-12}$ (Currie, 2004). While still alive, any organic material takes up the atmospheric $^{14}C/^{12}C$ signature. After their death however, the ^{14}C uptake is terminated and the only process is ^{14}C decay with a half life of $t_{1/2} = 5730$ a ($\lambda = 1/8267$ a; (Godwin, 1962)). Knowing the initial $^{14}C/^{12}C$ ratio enables us to reconstruct the year of 'death'. Early publications used the 'Libby half life' of $t_{1/2_{Libby}} = 5568$ a ($\lambda = 1/8033$ a). This was found to be inaccurate as Libby assumed a constant atmospheric ^{14}C concentration through time. For reasons of comparisons the Libby age is still used for ^{14}C age determinations and reporting. Therefore, so-called 'conventional ^{14}C ages' have to be calibrated to obtain calender ages. The ^{14}C half-life limits the ages datable to periods between 200 and 40,000 to 50,000 a, depending on the condition/closed system behaviour of the archive.

When applying ^{14}C dating on CWCs, several additional factors have to be considered. The first correction is due to isotope fractionation, occurring both during the carbonate formation (here coralline skeleton) and during the measurement. To account for the fractionation the deviation of the $^{13}C/^{12}C$ ratio in the sample from $^{13}C/^{12}C$ in the so-called PDP-standard is used

$$\delta^{13C}C = \left(\frac{\left(^{13}C/^{12}C\right)_{\text{Sample}}}{\left(^{13}C/^{12}C\right)_{\text{PDP}}} - 1 \right) \times 1000\,. \tag{2.10}$$

The PDP-standard was a fossil from the Peedee formation in South Carolina, which had to be substituted by an artificial material VPDB due to consumption (Friedman et al., 1982). The measured $^{14}C/^{12}C$ ratio is normalised to an arbitrary set value of $\delta^{13C}C = -25‰$, the mean value of wood.

Second, changes in both the magnitude of the Earth's magnetic field and the distribution of ^{14}C throughout the atmosphere, ocean and land biomass alter the atmospheric ^{14}C content through time. Therefore, to correctly date archives a calibration for the initial atmospheric ^{14}C concentration ($^{14}C/^{12}C$ signature) is needed. This calibration curve is reconstructed from tree rings and other archives and is constantly discussed and further improved (IntCal13: Fig. 2.11; (Reimer et al., 2013)). Past atmospheric $^{14}C/^{12}C$ signatures are commonly reported as $\Delta^{14}C$ in reference to $^{14}C/^{12}C$ in year 1950.

$$\Delta^{14}C_{\text{Sample}} = \left(\frac{e^{^{14}\text{C Age}/8033}}{e^{\text{Cal Age}/8266}} \right) \times 1000\,. \tag{2.11}$$

Adkins et al., 2002 calibrated modern scleractinian corals with ambient seawater (Fig. 2.12). However, for marine archives and deep-sea ones in particular, a third effect has to be considered. The surface ocean is not in equilibrium with the atmosphere, but exhibits a lower $^{14}C/^{12}C$ signature accounting for roughly 350 – 400 a (Reimer et al., 2013). This 'reservoir effect' (r) is not constant over time (e.g. Waelbroeck et al., 2001). In addition, the benthic archive 'sees' a water mass that has not been in contact with the atmosphere for up to 1200 a. Therefore, the ^{14}C-age determined from dating a CWC is a combination of the coral age and the age of the ambient water mass.

There are two ways to describe the offset between coralline and atmospheric $\Delta^{14}C$. The first is $\Delta\Delta^{14}C = \Delta^{14C}C_{CWC} - \Delta^{14}C_{Atm}$, which is always negative (Fig. 2.11). The second way of accounting for the offset between atmosphere and deep ocean is the reservoir age R (Fig. 2.11). Assuming a closed system ^{14}C decay starting at the $\Delta^{14}C$ signature of the coral, the intersect

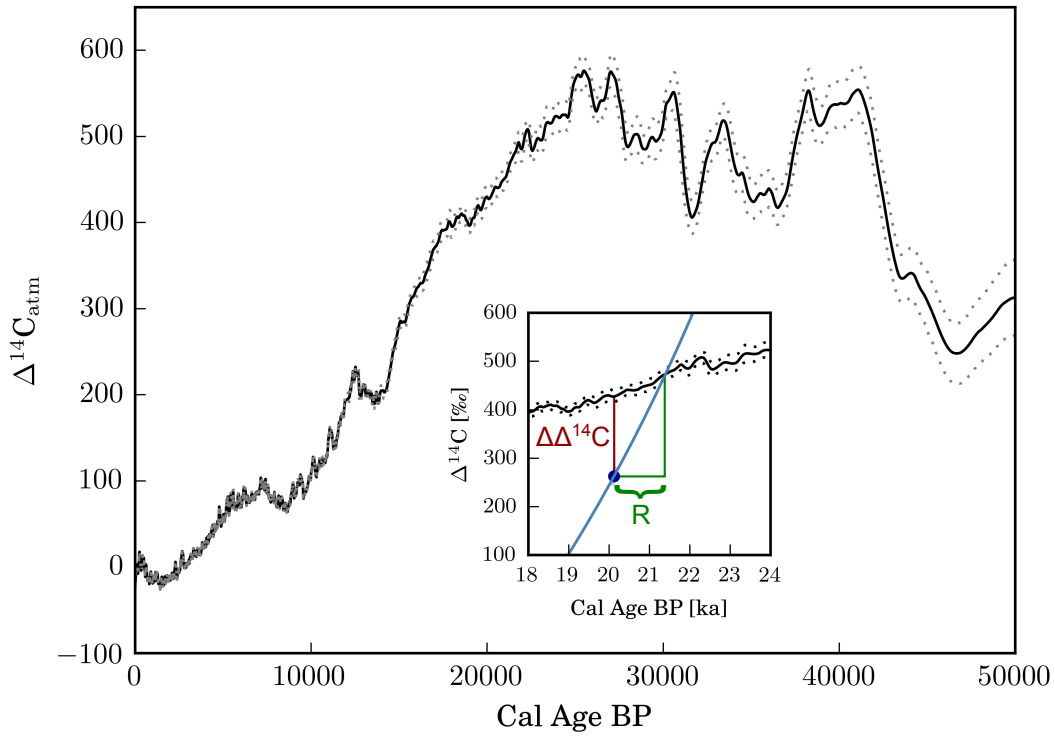

Figure 2.11: Atmospheric radiocarbon calibration IntCal13 and explanation for R and $\Delta\Delta^{14}C$
Calibration curve to account for atmospheric $^{14}C/^{12}C$ changes, given in age-corrected $\Delta^{14}C$ (Reimer et al., 2013). Changes are given relative to $^{14}C/^{12}C$ in year 1950, also referred to as Cal Age BP ('before present').
Inset: schematic explanation of the two terms $\Delta\Delta^{14}C$ (difference between atmospheric and coralline $\Delta^{14}C$; dark red) and ΔR (ventilation age; green) on an exemplary CWC data point. ΔR is determined through the intersect of the ^{14}C decay curve through the CWC data point and the IntCal13 (light blue line).

with the IntCal13 is determined. The difference between this extrapolated age (age BP) and the determined age BP (U-series dating) of the coral is the reservoir age (R; Fig. 2.11) of the water mass the coral grew in. If both reservoir age and reservoir effect are known, the time since the last contact with the atmosphere of the water mass, the ventilation age, can be derived by $\Delta R = R - r$ (Skinner et al., 2017; Adkins et al., 1998; Mangini et al., 1998).
Different water masses display different reservoir ages, with 'youngest' ages present in the surface mid-latitudes and the North Atlantic and the 'oldest' ages in the North Pacific. Therefore, like εNd, the reservoir age reconstructed from CWCs is a useful water mass tracer for oceanic circulation reconstructions both in the present (Sherwood et al., 2008) and in the past (Hines et al., 2015; Burke and Robinson, 2012; Mangini et al., 2010; Robinson and Flierdt, 2009; Eltgroth et al., 2006; Robinson et al., 2005; Frank et al., 2004; Schröder-Ritzrau et al., 2003; Goldstein et al., 2001; Adkins et al., 1998; Mangini et al., 1998). For example, Frank et al., 2004 reported mid-depth Northeast Atlantic radiocarbon variations during the Holocene both on millennial and centennial time scale, which they attributed to changes in Labrador deep convection. Considerably larger radiocarbon deviations could be observed by e.g. Mangini et al., 2010; Robinson et al., 2005; Adkins et al., 1998 reflecting major reorganisation of ocean interior circulation

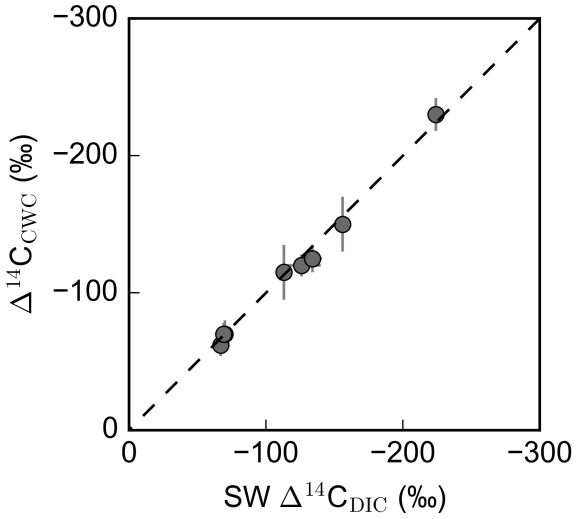

Figure 2.12: $\Delta^{14}C$ calibration on modern CWCs and dissolved inorganic carbon (DIC) in ambient seawater
Figure adapted from Adkins et al., 2002

coinciding with climate changes during the last glacial, the deglaciation and early Holocene.

2.6 Proxies for nutrient supply and utilization

As mentioned previously, the growth of CWCs is restricted by temperature, O_2 concentration, salinity, pH etc. (Chap. 2.2.1). However, the most important factor is the supply of sufficient food. Therefore, the search for a nutrient (phosphate, nitrate or silicic acid) proxy in CWCs has been a key concern.
Examples of established proxies in foraminifera for nutrient supply or utilization are for example δ^{13}C, Cd/Ca (Keigwin and Boyle, 1989), Ba/Ca (Lea and Boyle, 1990) and δ^{15}N (Altabet and Curry, 1989). In tropical corals Ba/Ca was successfully applied (Lea et al., 1989) in upwelling investigations.
The search for a nutrient supply or utilization proxy, closely linked to surface biological productivity (Chap. 2.2.1) in CWCs has turned out to be quite difficult. Early excitement caused by Montagna et al., 2006 who linked coralline P/Ca to deep-sea nutrients was dampened by Anagnostou et al., 2011. The linear correlation between seawater dissolved inorganic phosphorus (DIP) and P/Ca in aragonitic skeletons found by Anagnostou et al., 2011 was about a factor of 10 smaller than the one previously established by Montagna et al., 2006. This offset, probably caused by vital effects, has not yet been explained and further applications of P/Ca in CWC to gain insight into ambient nutrient conditions have not been published. Furthermore, Mason et al., 2011 reported that phosphorus in CWC skeletons is found in different chemical forms. Several studies on proteinaceous corals (*Porites*) also revealed a correlation between coralline P/Ca and seawater phosphorus (Chen and Yu, 2011; LaVigne et al., 2011; LaVigne et al., 2008), unfortunately also influenced by species effects which must be considered.
In proteinaceous corals, δ^{15}N has been used to reconstruct nutrient sources and cycling (e.g. Sherwood et al., 2011), but has not successfully been employed in CWCs. LaVigne et al., 2016;

LaVigne et al., 2011 calibrated Ba/Ca in tropical surface corals supporting its application to reconstruct surface ocean biogeochemical processes. In their study, Anagnostou et al., 2011 calibrated Ba/Ca of one CWC species to seawater signatures (*D.dianthus*). Further multi-species analyses by Spooner et al., submitted; Spooner, 2016 found a different seawater-coral correlation highlighting the need for additional evaluations.
Evidently, a reliable nutrient supply or utilization proxy in CWCs has not yet been found. In the last part of my thesis I will introduce the novel proxy Ba isotopes in CWCs, possibly a new tool for nutrient reconstructions?

Part I

Paleoceanographic Reconstructions over the Last 65 ka on Cold-Water Corals from the Gulf of Cádiz

3 Introduction

Paleoceanographic reconstructions were performed on two cold-water coral-bearing sediment cores and two hemipelagic sediment cores from the southern Gulf of Cádiz (sGoC). This region is of particular interest with respect to past climate and ocean dynamics as studies from this region could help identify the manner of the link between the Mediterranean Sea and the Atlantic. Water masses from three regions, the North Atlantic, the Mediterranean Sea and the Southern Ocean, compete at depths of 300 – 1500 m (Fig. 3.1 and 3.2; (Louarn and Morin, 2011)). Here, I will describe the present-day geological and oceanographic setting of that region.

The GoC is located between the southern Spanish and the northern Moroccan margin and

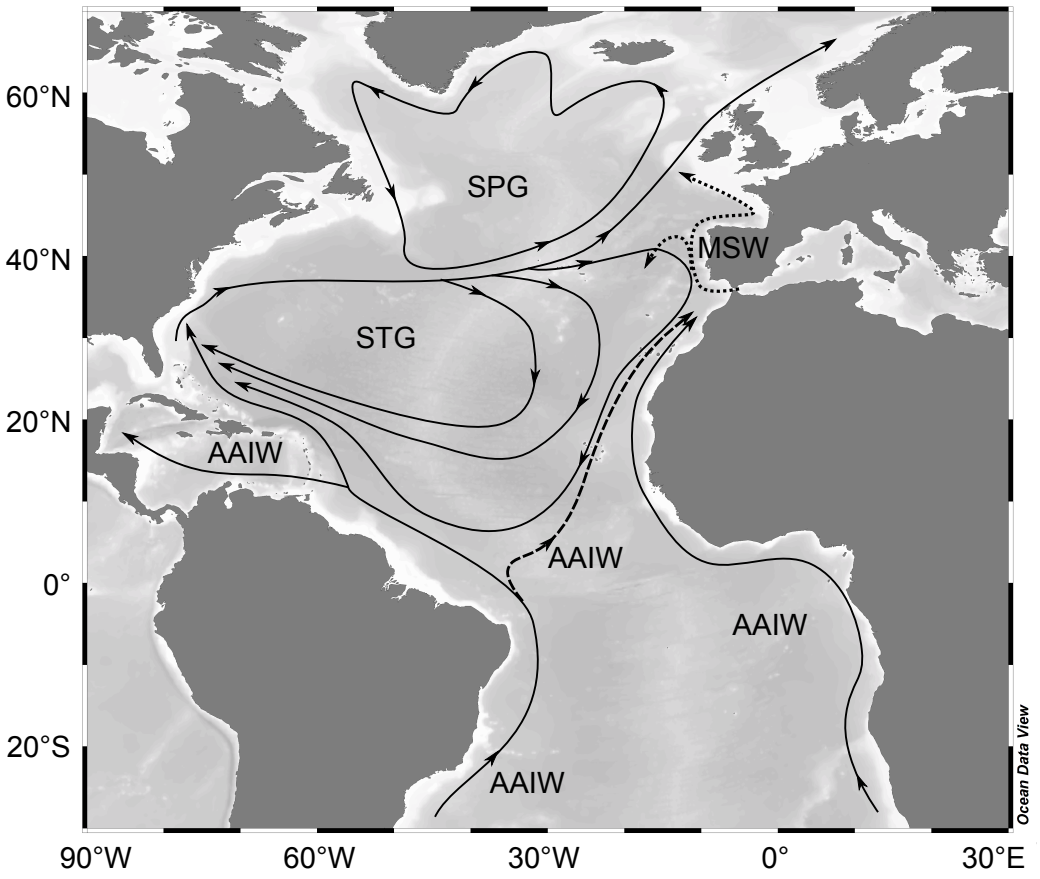

Figure 3.1: Simplified map of the intermediate circulation in the Atlantic ocean

connects the Atlantic with the Mediterranean Sea. Its complex topography results from the convergence of the African and Eurasian plates (2 – 4 mm/a). Tectonic activity leads to a complex system of channels and ridges (García et al., 2009).

The continental margins of the Iberian Peninsula (northern GoC) are lacking a marked continental rise (Hernández-Molina et al., 2006). The continental shelf subsides down to about 130 m,

where the continental slope starts. At 4000 m water depth the abyssal plain is reached. The slope is strewn with marginal valleys and furrows. Additionally, due to strong local bottom currents, large sediment depositions form contorite channels (Hernández-Molina et al., 2006). In contrast, the sGoC at the Moroccan margin is characterised by mud volcanoes and curved extensional faults (Foubert et al., 2008).

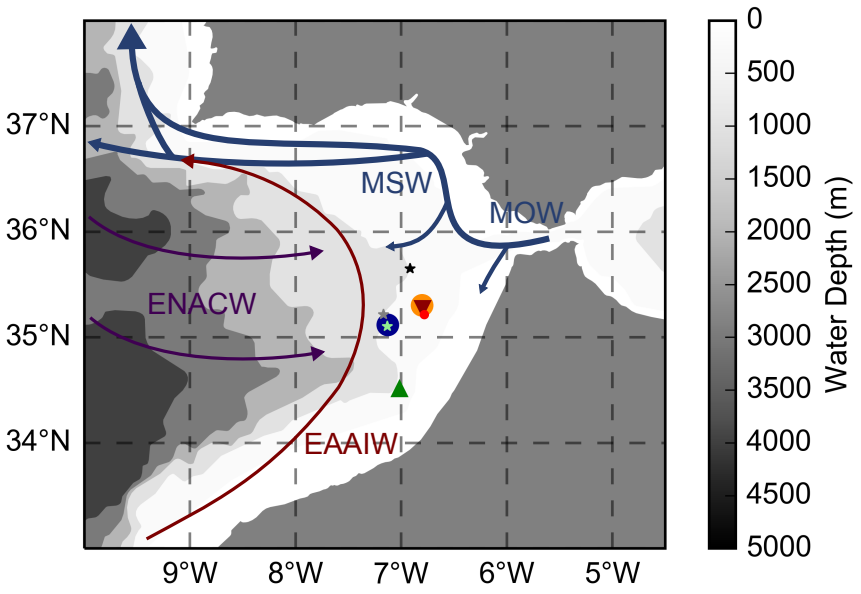

Figure 3.2: Simplified map of intermediate circulation in the GoC
CWC sample sites are shown as circles. Coral-bearing cores are MD08-3231 (orange) and GeoB-18141-01 (dark blue). Sediment cores are triangles, with MD08-3227 in dark red and MD04-2805-CQ in green. Small stars are seawater stations with GeoB-18136-01-10 (light green, Hebbeln et al., 2015) used for temperature, salinity and dissolved oxygen analyses and stations MOW1 (black), MOW2 (grey) and Beta1 (red) used for εNd analyses in chapter 6 (Dubois-Dauphin et al., 2016). The modern circulation of the three main water masses (MSW, ENACW, EAAIW) present in the depths of the sample locations are also shown.

The modern circulation in the GoC is dominated by the interaction between the Mediterranean Sea and the open Atlantic Ocean (Fig 3.2). Three main intermediate water masses are identified: the *Eastern North Atlantic Central Water* (ENACW), the *Mediterranean Outflow Water* (MOW), and the *Eastern Antarctic Intermediate Water* (EAAIW).
In the upper 100 m, the surface mixed layer above the thermocline, *Surface Atlantic Water* (SAW) characterised by temperatures above 16°C and a salinity around 36.4 psu is present (Criado-Aldeanueva et al., 2006, also see CTD profiles in Fig. 3.3, Tab. A.6). Below the SAW, in 100 – 600 m, *Eastern North Atlantic Central Water* (ENACW) flows from west to east. From top to bottom, ENACW exhibits salinities between 36.6 and 35.5 psu and temperatures of 16 to 11°C (Fig. 3.3 (a); (Louarn and Morin, 2011; Criado-Aldeanueva et al., 2006)). The ENACW consists of warm surface water from the North (*North Atlantic Central Water*, NACW; (Iselin, 1936)) that is modified by the basin gyre systems (*Subtropical Gyre* (STG) and *Subpolar Gyre* (SPG)) (Fig. 3.1). The two known ENACW sources originate from Celtic Sea and close to the Azores. They converge north-west of the Iberian Peninsula (Pollard et al., 1996; Fiúza, 1984; McCartney

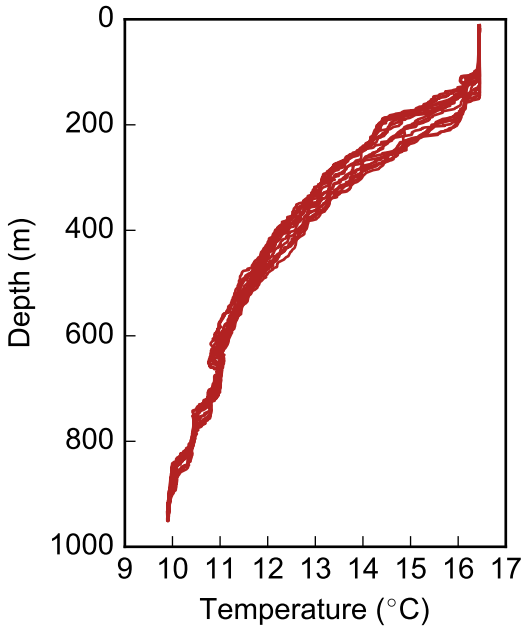

(a) CTD station GeoB-18136-01-10 temperature

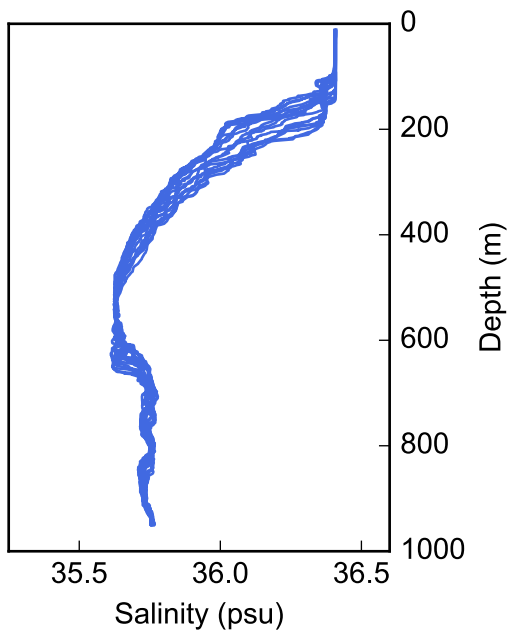

(b) CTD station GeoB-18136-01-10 salinity

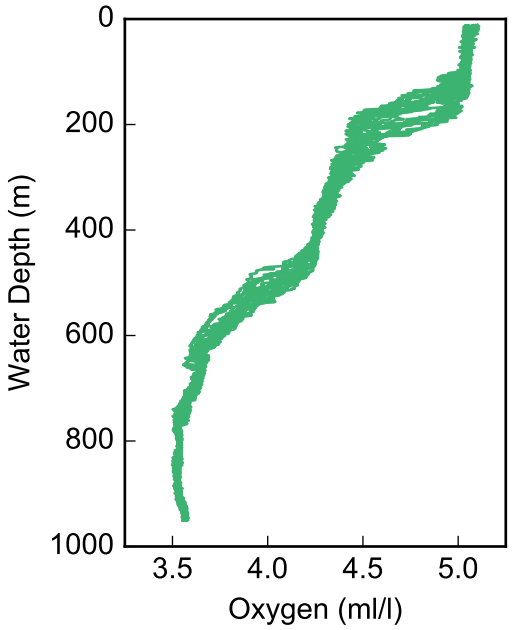

(c) CTD station GeoB-18136-01-10 oxygen

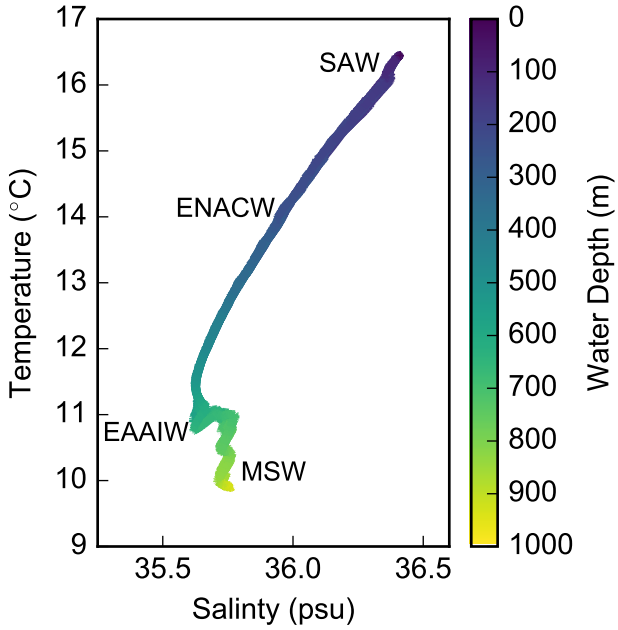

(d) CTD station GeoB-18136-01-10 salinity vs. temperature. The depth is shown as changing colour.

Figure 3.3: CTD station GeoB-18136-01-10 (7° 07.92'N, 35° 06.21'W, 990 m water depth)
(a-c) Temperature, salinity and dissolved oxygen profile
(d) Temperature vs. salinity with depth shown in the colour scheme (surface in purple and 990 m in yellow). The water masses present are indicated in their respective depths.
Figure adapted from Hebbeln et al., 2015

and Talley, 1982). ENACW can be distinguished from *Western North Atlantic Central Water* (WNACW) by higher salinities at a constant temperatures (Emery and Meincke, 1986).
At the Strait of Gibraltar, the cool and less saline *Atlantic Inflow Water* at the surface flows eastwards into the Mediterranean Sea, while the warm and highly saline (13.22 – 13.76°C, S > 36.2 psu; , Fig. 3.3 (a); (Dubois-Dauphin et al., 2016)) MOW enters the GoC westwards near the bottom of the rise ((Hernández-Molina et al., 2006); Fig 3.2). Compared to ENACW, MOW has lower nutrient and dissolved oxygen concentrations ((Rhein and Hinrichsen, 1993); Fig. 3.3 (b)). Due to the Coriolis force, the MOW is diverted north-westwards along the Spanish and Portuguese coast, flowing into the North Atlantic and mixing with mid-depth STG waters (Fig. 3.1). On its path, MOW is modified through mixing with the overlying ENACW. This modified MOW in the GoC is called *Mediterranean Sea Water* (MSW), characterised by similar salinities but colder temperatures than 'pure' MOW. The MSW is separated into two branches, the *Mediterranean Upper Water* (MSU, 500 – 800 m water depth) and the more saline *Mediterranean Lower Water* (MSL, 800 – 1200 m water depth) (Hernandez-Molina et al., 2014; Louarn and Morin, 2011; Hernández-Molina et al., 2006; Ambar and Howe, 1979).
From the south, EAAIW penetrates the present GoC at depths between 600 and 1000 m (proportion roughly 75%; (Mienis et al., 2012; Louarn and Morin, 2011; Cabeçadas et al., 2002)). Formed at the polar front in the Southeast Pacific, EAAIW is characterised by low salinities (< 35 psu; (Tsuchiya, 1989)). The EAAIW flows cyclonically through the GoC not reaching the Iberian margin (Louarn and Morin, 2011). At depths greater than 1.5 km, *Labrador Sea Water* (LSW) flows into the GoC following a similar path. However, sites analysed here lie between 500 and 1000 m water depth and are therefore not influenced by LSW.

4 Cold-water coral mound aggregation during the last 65 ka

4.1 Introduction

Throughout the Atlantic a vast diversity of reef morphologies is known today, from isolated colonies or small to large reefs or even gigantic carbonate mounds (Roberts et al., 2009). Reef and mounds can grow over periods of thousands to millions of years (Kano et al., 2007; Roberts, 2006; Freiwald et al., 2004). High resolution bathymetry allows careful mapping of mound structures. Seismic lines provided evidence of sediment covered reefs where cold-water coral (CWC) mounds were inactive. Additionally, ROV (remotely operating vehicle) videos from the sea floor documented the state (active/inactive) across numerous mounds in the Atlantic (e.g. Hebbeln et al., 2016a). However, given the thousands of known but unstudied coral reef structures in the Atlantic, solely few records exist. Several studies have revealed that CWC mounds do not aggregate continuously but exhibit periods over thousands of years with no CWC growth but possible erosion and even collapses (e.g. Stalder et al., 2015; López Correa et al., 2012; Raddatz et al., 2011; Frank et al., 2009; Eisele et al., 2008; Kano et al., 2007; Rüggeberg et al., 2007; Dorschel et al., 2005). Currently, one record of a drilled core penetrating a CWC mound is published (Kano et al., 2007). Ages of corals at the base of Challenger Mound are estimated to 2.7 Ma. Recently, during the 'MoccoMeBo' cruise in 2014 (Hebbeln et al., 2015) three additional CWC mounds could be fully penetrated using the *Bremen Sea Floor Drill Rig MeBo*.
CWC coral growth rates, in particular of the two frame-work forming species *L.pertusa* and *M. oculata*, are between 3 and 26 mm/a (e.g. Sabatier et al., 2012; Orejas et al., 2008; Gass and Roberts, 2006). However, little is known about possible common mound aggregation rates (MAR) and therefore mutual time scales that might underlie the different morphologies, shapes and histories of CWC mounds between the various regions of the Atlantic. A first compilation by Wienberg and Titschack, in press named extreme modern NE Atlantic MARs up to 1050 cm/ka (Norwegian shelf; (Titschack et al., 2015)) and slower glacial aggregation in more southern regions such as the GoC (Wienberg et al., 2010).
Here, two mound aggregation chronologies from the southern Gulf of Cádiz (sGoC) are explored. This region is of particular interest as it seemingly exhibits solely glacial CWC growth (Wienberg et al., 2010). Different glacial oceanic conditions, including the intensification of regional upwelling as well as colder (or denser) environments is suspected to have enhanced coral populations (Wienberg et al., 2010). Both cores provide evidence for extremely enhanced CWC growth and therefore higher mound aggregation rates in the temperate east Atlantic, which nowadays are observed in the NE Atlantic ($\sim$55°N; (Frank et al., 2009)). Updating the compilation of published data by Wienberg and Titschack, in press, now allows for first estimates of common time scales underlying CWC mound aggregation. The interpretations are based predominantly on U-series ages, which allows to consider time scales of several climate cycles (roughly 800 ka).

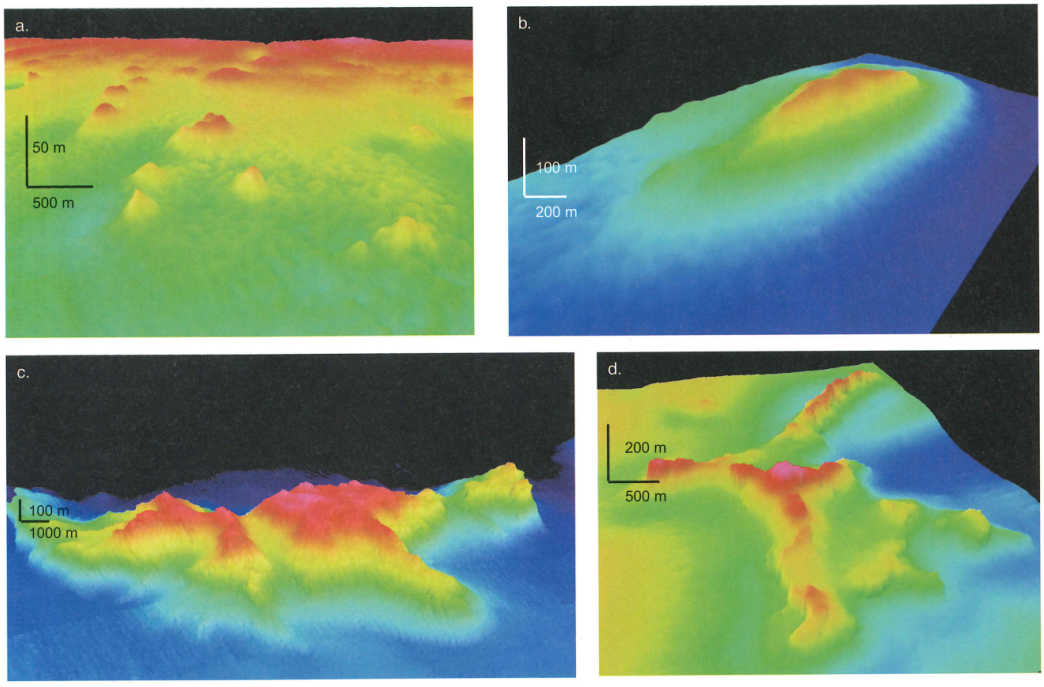

Figure 4.1: Different CWC mound morphologies seen in Multibeam data
Conical and near-conical mounds (a), a ridge-shaped mound in (b) and a 'giant' coral carbonate mound (c) from Rockall Bank are shown. Picture (d) displays the more complex morphology of Propeller Mound (Porcupine Seabight) where different mounds have merged together.
Figure taken from Roberts et al., 2009

4.2 Materials and analytical methods

4.2.1 Samples

Fossil CWCs (1 – 10 cm long) analysed for paleoceanographic reconstructions in the sGoC are from the two coral-bearing sediment cores MD08-3231 and GeoB-18141-01 (Fig. 3.2). The gravity core MD08-3231 (35°18.87'N, 06°48.05'W; 550 m water depth) was recovered during the *R/V Marion Dufresne* cruise 'MD169 MiCROSYSTEMS' in 2008 (Fig. 4.2, Tab. A.6; (Rooij et al., 2008)). 378 cm were retrieved on Gamma Mound from the Pen Duick Escarpment (PDE) using a core barrel of 575 cm. Already on board ship the core was divided into small sections of 5 cm in the upper 60 cm and 10 cm between 60 and 345 cm. The CWCs were roughly cleaned and placed into small plastic boxes for storage. From each section at least one CWC was chosen for analysis. Three sections (200 – 210 cm, 280 – 285 cm, 320 – 330 cm) only exhibited corals that showed strong biological diagenesis as well as physical and chemical weathering, and hence were not sampled. In total forty-eight CWCs of the three species *L. pertusa*, *M. oculata* and *D. dianthus* from core MD08-3231 were U-series dated.
The coral-bearing sediment core GeoB-18141-01 was recovered during the *Maria S. Merian* cruise 'MoccoMeBo' in 2014 (Hebbeln et al., 2015). It was retrieved on Wulle Mound in the southern deep belt of the Moroccan Atlantic CWC Province (MACP; 35°7.15'N, 07°7.74'W; 944 m; Fig. 4.4 , Tab. A.6; (Hebbeln et al., 2015)). GeoB-18141-01 is a MeBo drilling core, which means that the core is gradually drilled (drill bit diameter 55 mm) into the coral mound

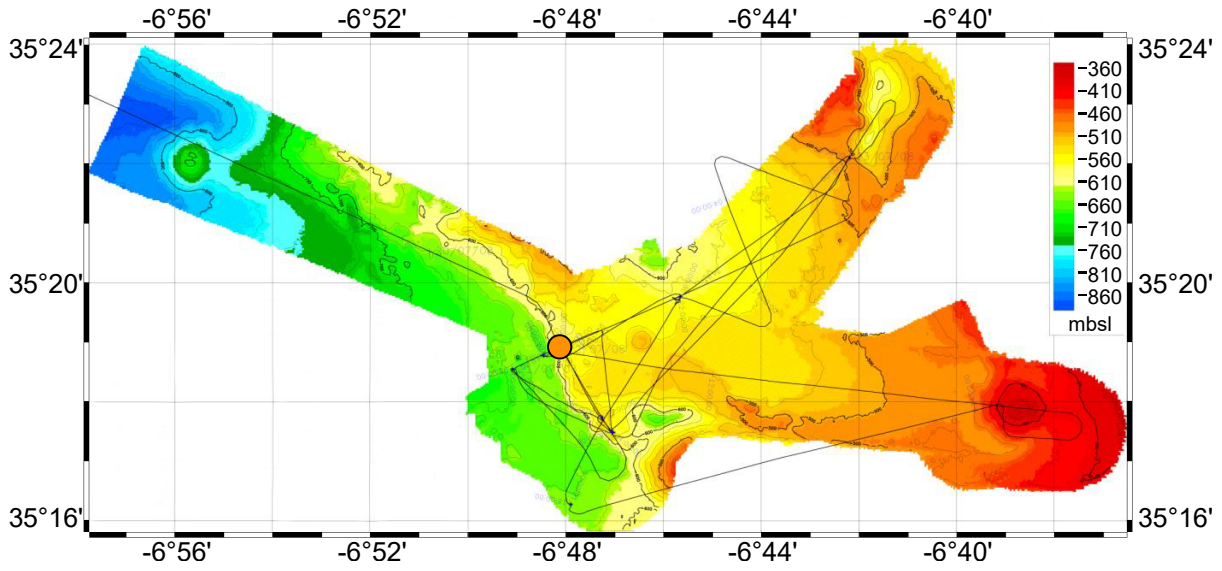

Figure 4.2: Bathymetry of Pen Duick Escarpment (PDE)
The location of the coral-bearing sediment core MD08-3231 is indicated by the orange circle. Figure adapted from Rooij et al., 2008

and not just dropped in one go like a gravity core (Hebbeln et al., 2015). Bremen Sea Floor Drill Rig MeBo (Fig.4.3(a)) allowed drilling to mound depths of more than 70 m taking roughly 30 h. The length of one core barrel and hence one stroke was 2.35 m plus core catcher (CC) (Fig. 4.3(b)). On board ship, the pilot sleeve and CC where first removed from the core barrel. The CC was transferred into a small tube and stored. Afterwards the liner was taken from the barrel. Due to an average recovery of 75% most liners were not filled completely (Tab. A.7). To prevent displacement of sediment inside the liners, they were cut to the length that was filled with sediment and CWCs. If sufficient material was abundant, the liner was divided into two sections with the length of section 1 at 1.2 m. Each liner was capped and frozen for 18 h after which they were cut in half and briefly described for coral abundances and preservation. The two halfs were carefully packed and stored at the MARUM core repository at the University of Bremen.
After roughly 33.5 m the sediment in of GeoB-18141-01 does not exhibit CWCs anymore, indicating the base of Wulle Mound. It should be noted that after Challenger Mound in the Porcupine Seabight (Kano et al., 2007) this is the second CWC mound fully penetrated. The drilling method of the MeBo drill can lead to a substantial material loss especially in the upper barrels, leading to recoveries down to 25.96% (Tab. A.7). Often gaps reflect a change in the structure of the material towards finer grained sediment or smaller sized coral fragments (rubble). However, changing the water pressure used to cool the drill might increase the loss of material. Many more effects can lead to arising gaps in the record seen in the age-depth profile (shaded blue boxes in Fig. 4.8).
In May 2015 GeoB-18141-01 was sampled in its upper 13 m, (barrels P1 – P6), which was the estimated range to cover the last 60 ka. Older CWCs from barrels P7 to P15 were analysed in Thomas Krengels' Master's project (Krengel, 2016) and his current PhD project at Heidelberg University (Germany). Roughly seventy CWCs were carefully retrieved from the sediment, of which the sixty best preserved were selected for analysis in this study. CWCs of the three species *L. pertusa*, *M. oculata* and *D. dianthus* were analysed by U-series dating.

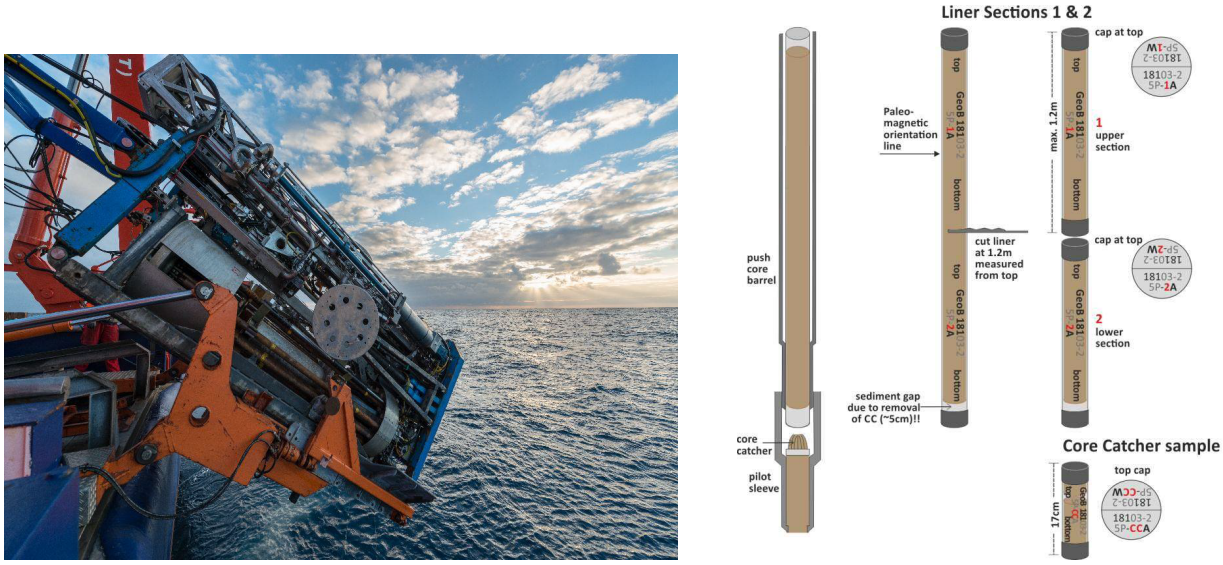

(a) (b)

Figure 4.3: Bremen Sea Floor Drill Rig MeBo (a) and explanation of core sections (b)
Figure taken from Hebbeln et al., 2015

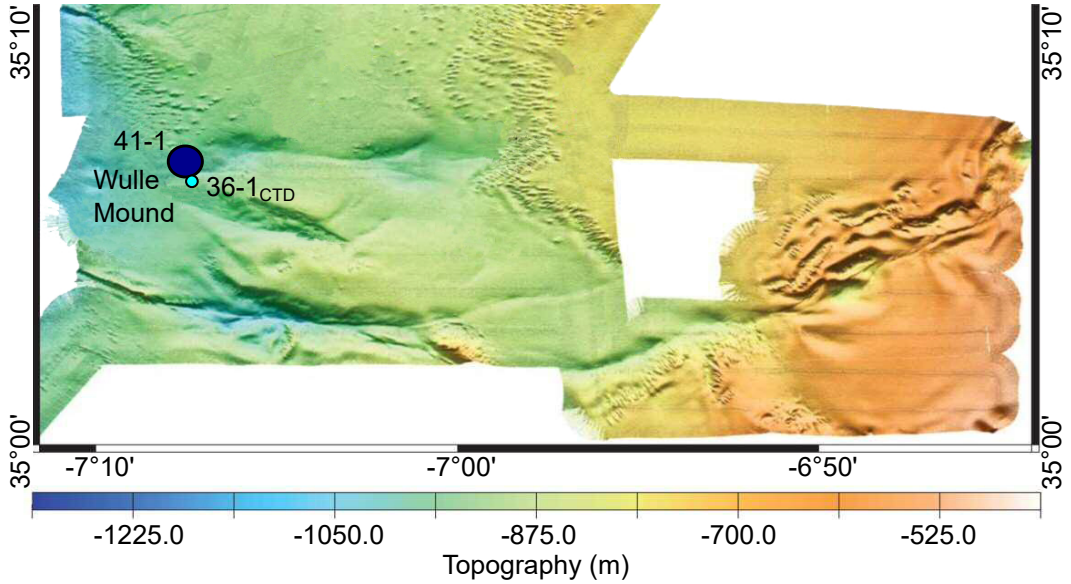

Figure 4.4: Bathymetry of the Moroccan Atlantic CWC Province (MACP)
The location of the coral-bearing sediment core GeoB-18141-01 is indicated by the blue circle.
Figure adapted from Hebbeln et al., 2015

4.2.2 U and Th extraction and analysis

U and Th extraction

The method to extract and purify U and Th from the fossil CWCs was modified after (Douville et al., 2010; Frank et al., 2004). Between 40 – 60 mg mechanically cleaned and carefully leached corals were dissolved in 7M HNO_3 and spiked with a TriSpike containing the three artificial isotopes ^{229}Th, ^{233}U and ^{236}U and passed through a column filled with UTEVA cation exchange resin. The columns were first cleaned with MilliQ, packed with 250 µl of the UTEVA resin and again cleaned with one column volume (1CV = 250µl) of MilliQ. After loading the column with 1CV 7M HNO_3 the sample was slowly given onto the column. The column was washed in three steps of 0.5 ml 7M HNO_3, after which the sample was collected. The elution process consisted of 1CV MilliQ, three steps of 0.5 ml 1M HCl, followed by three steps of 0.5 ml 3M HCl. The column was then stored in MilliQ, the samples evaporated overnight and redissolved in 300 µl 7M HNO_3. After loading the column with 7M HNO_3, the sample was again added onto the column. For the second column, the washing process of the first column was modified by adding 0.25 ml plus 0.5 ml 7M HNO_3. The elution process for the second column followed the first column, adding a last HF elution step with 3 x 0.5 ml 1M HF. After evaporating the samples they were prepared for the analysis on a Neptune Plus MC-ICP-MS (Multi Collector Inductively Coupled Plasma Mass Spectrometer) by dissolving in 2 ml of a 1% HNO_3 and 0.05% HF mixture. Blanks were treated similar to the samples with only two changes. The washing procedure was not applied and for the analysis the sample was dissolved in 0.3 ml 1% HNO_3 and 0.05% HF. The mean chemical yield achieved for the U and Th separation are 80% for Th and 98% for U. Chemical blanks are 0.1 fg for ^{230}Th, 1.2 fg for ^{234}U and 0.02 ng for ^{238}U (Wefing, 2016; Wefing, 2014).
The Neptune Plus MC-ICP-MS of the Institute of Environmental Physics (IUP) at Heidelberg University was installed in summer 2015. Early measurements of MD08-3231 CWCs during the Bachelor's project of Anne-Marie Wefing (Wefing, 2014) were therefore measured on an iCap Q ICP-MS (iCap Quadrupole Inductively Coupled Plasma Mass Spectrometer) already installed in the laboratory of IUP. These samples went through the same column chemistry but were dissolved in 0.5M HNO_3. Blanks were treated the same way as samples.

U and Th isotope analysis

The isotopes ^{229}Th, ^{230}Th, ^{232}Th, ^{233}U, ^{234}U, ^{235}U and ^{236}U were measured on a Thermo Fisher Neptune Plus MC-ICP-MS at the Institute for Environmental Physics (Heidelberg, Germany). The applied method was adopted from Arps, 2017; Wefing, 2016; Matos et al., 2015 and Douville et al., 2010 using a bracketing technique with the HU-1 standard (Cheng et al., 2000). The achieved reproducibility of the HU-1 standard is $^{234}U/^{238}U = 0.9997 \pm 0.0003$ and $^{230}Th/^{238}U = 1.0002 \pm 0.0005$ (Arps, 2017). Precisions with an average of 2.6 ‰ (range: 1.3 – 7.8 ‰) for thorium ratios and 1.0 ‰ (range: 0.2 – 4.1 ‰) for uranium ratios were achieved (2SD uncertainty; 113 measurements in 13 months). To calculate coral ages from measured ratios the half-life of ^{238}U after Cheng et al., 2000 was used. Improved values for half-lifes of ^{230}Th and ^{234}U were published in 2013 (Cheng et al., 2013). However, there is no consensus in the community on which half-life values will be used permanently, as the new values need to be confirmed independently. Therefore, in this project and for U-series age calculations cited in this project the older values were used.

Quality control of U-series ages

In a closed system, analysed CWCs should follow the seawater evolution curve of δ^{234}U and the activity ratio ^{230}Th/^{238}U (Chap. 2.3 EQ. 2.5), and exhibit only very little ^{230}Th derived by measuring ^{232}Th (Chap. 2.3). Frank et al., 2009 chose the upper limit for ^{232}Th at 10 ng/g. Their criteria was that the age correction due to ^{232}Th should not exceed the uncertainty of the measurement (personal discussion with the authors). However, the ε-precision (10^{-4}) achieved in most analysis here is considerably higher (Chap. 4.2.2; (Arps, 2017)), making the uncertainty more sensitive to age corrections due to ^{232}Th. The best case scenario for the reproducibility achieved here would be to set an upper ^{232}Th limit of 1 ng/g. This way even very young samples would not be affected by the ^{232}Th correction. However, for this study a ^{232}Th limit of 1 ng/g would lead to a loss of roughly 50% of the age data, which other than that do not show U-series open system behaviour. Therefore, I chose the artificial upper limit at 5 ng/g. Applying this limit 90% of the U-series data are preserved. Additionally, with a few exceptions, the correction due to ^{232}Th is still within the measurement uncertainty. Ages that shifted by more than their measurement uncertainty did not change by more than 250 a. As corals analysed are between 20 and 60 ka old, this correction is still within a reasonable range for the discussion of this work. For future studies though, I suggest to aim for ^{232}Th concentration below 1 ng/g because this limit implies, that the ε-dating precision achieved in our laboratory stays unaffected by initial Th corrections.
The last criterion used in this project to check the reliability of the U-series ages, are ^{14}C ages, presented and discussed in chapter 7.3. As will be shown, some CWC samples exhibit U/Th and ^{14}C ages that lead to Δ^{14}C signatures (EQ. 2.11, Chap. 2.5.2) lying above the atmospheric $\Delta^{14}C_{atm}$ of the respective time during which the corals grew (Fig. 7.2(a); or $\Delta\Delta^{14}C > 0$). As seawater is always lighter in ^{14}C than the atmosphere, signals like these cannot be accepted as reliable. Coral samples with this characteristic are considered to show U-series or ^{14}C open system behaviour and discarded from further discussions.

4.3 Results

For reasons of comparison with other studies, all U-series ages will be given as U/Th ages BP ('before present' defined as 1950). The Figure legends will be named 'U/Th Age BP', while in the text ages BP will be shortened to x ka.

4.3.1 Mound aggregation seen in MD08-3231

Forty-eight CWCs from core MD08-3231 were U-series dated in the course of this PhD project and one Bachelor's project, four of which twice (Tab. A.3; (Wefing, 2014)). Following the quality control described in chapter 4.2.2, twelve samples had to be discarded. Three corals (one measured twice) were rejected due to high ^{232}Th concentrations, one CWC did not follow the seawater evolution curve (Fig. 4.5) and eight (one measured twice) had to be discarded due to Δ14C > atmospheric Δ14C (Fig. 7.2(a), Chap. 7.3). Corals rejected due to their $\Delta\Delta^{14}$C are shown as open symbols in the age models.
U-series ages obtained cover 17 – 100 ka (Fig. 4.6, Tab. A.3). Several age-depth inversions can be seen in the uppermost 30 cm spanning ages between 17 ka and 22 ka. The most pronounced inversion is observed in section 15 – 20 cm. While the coral from the section above (10 – 15 cm) is

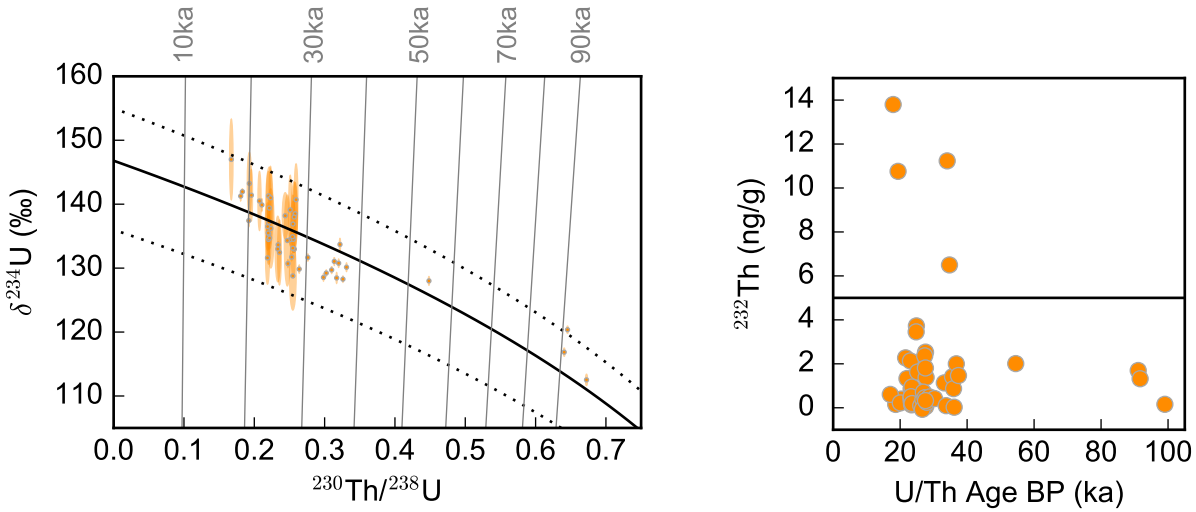

(a) (b)

Figure 4.5: MD08-3231: quality control of CWC U-series dating
(a) δ^{234}U and the activity ratio ^{230}Th/^{238}U of each dated CWC. The 2σ is displayed as shaded ellipsis. The seawater evolution curve (SEC) of δ^{234}U and ^{230}Th/^{238}U (EQ. 2.5) is shown in black with its empirical uncertainty as dashed grey line. The grey vertical lines indicate the time evolution in 10 ka steps.
(b) ^{232}Th (ng/g) in each CWC against their U-series age.
Data points outside the uncertainty of the SEC (one CWC) and/or with higher ^{232}Th concentrations than 5 ng/g (three CWCs of which one was measured twice) suggest an U-series open-system behaviour and are discarded in further discussions.

aged 20.38 ± 0.19 ka, the CWC in 17.5 cm is dated at 17.01 ± 0.30 ka. The respective ^{14}C age of the seemingly younger coral is 17.53 ± 0.05 ka and hence older than the U-series age. However, a second CWC from the same depth with a U-series age of 22.40 ± 0.09 ka exhibits a positive $\Delta\Delta^{14}$C (Fig. 2.11). Therefore, both corals from that depth section show signs for diagenesis and are rejected from further discussions. The other small scale inversions in the upper 30 cm of the core can possibly be explained by the exposure of the coral mound to ocean circulation during the last 30 ka moving lose material to slightly lower depths or erosion during the CWC reef growth. Moreover, the gravity core recovery technique might course these inversions. During the fall and burying of the gravity core, the uppermost layers are most vulnerable to possible movement as less boundaries are present at the surface than in the deeper core. A few smaller age-depth inversion between 90 and 190 cm (around 27 ka) are explained by positive $\Delta\Delta^{14}$C signatures of a few older CWCs (open symbols in Fig. 4.6 zoom). A second significant age-depth inversion can be observed in section 210 – 220 cm. The particular CWC grew at 27.57 ± 0.09 ka, while corals below and above date back to 33.19 ka and 30.27 ka respectively. However, in core depths above 180 – 190 cm CWCs are around 26.5 – 28.8 ka old, suggesting that this coral may have eroded from those mound depths. The deepest age-depth inversion can be observed between 250 – 260 cm and 260 - 270 cm. This is likely to be a results of mound erosion, because after the growth of these corals a 3 ka pause of CWC growth can be observed. Therefore, they were

possibly exposed to the ocean circulation for a longer time. The lack of well-preserved CWCs in depth section 240 – 250 reinforces this assumption.

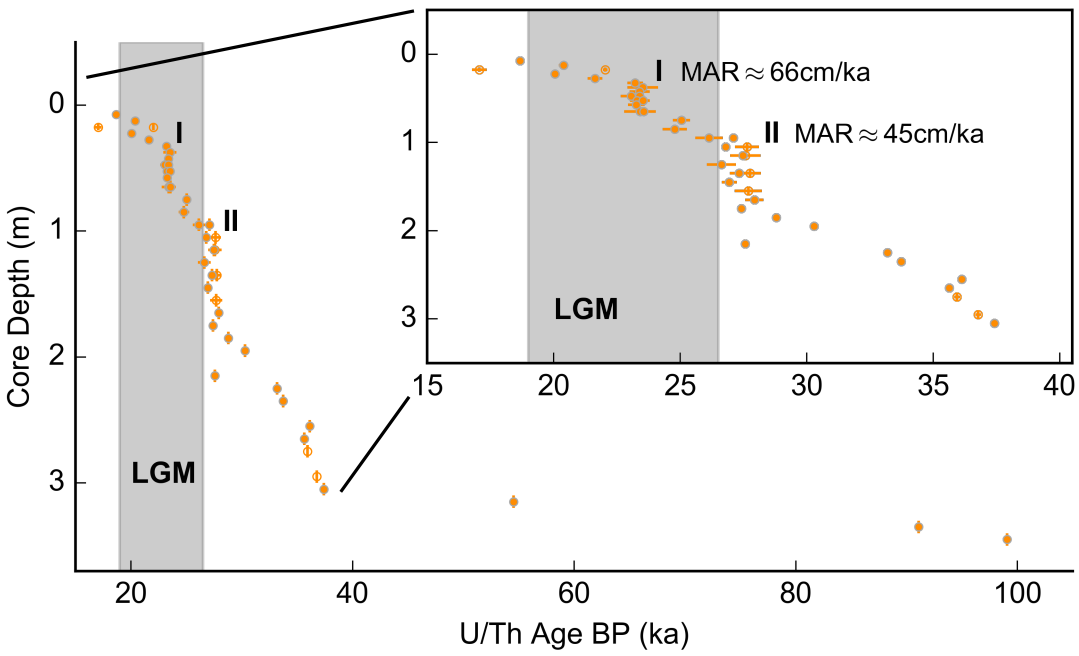

Figure 4.6: CWC mound aggregation seen in coral-bearing core MD08-3231 (Gamma Mound at PDE)
All corals grew during the last glacial. Only three CWC have ages above 40 ka. A few age-depth inversions can be seen. Some of these exhibit positive $\Delta\Delta^{14}C$ signatures (open symbols) and are discarded ffrom further discussions.
Two periods of increased mound aggregation can be observed (I and II). The timing of the LGM is shaded in grey.

Two increased CWC mound aggregation phases (I and II) can be observed (Fig. 4.6 zoom). The most pronounced mound aggregation phase (I) with a mound aggregation rate (MAR) of 66 cm/ka occurred 23.07 to 23.56 ka ago increasing the mound by 32.5 cm (n = 10). The second phase of increased mound aggregation (II) was 26.14 to 27.93 ka (n = 13). During that time the mound aggregated by 80 cm implying a MAR of 45 cm/ka. For the calculations of MARs I chose the youngest and oldest date of each period, which did not necessarily coincide with the uppermost and lowest located CWC. However, due to internal small scale erosions described in chapter 2.2.1 this is a reasonable approach. MARs obtained when using the uppermost and lowest CWC of each increased aggregation phase are 94 cm/ka (I) and 63 cm/ka (II). Between 185 and 305 cm core depth (28.80 – 37.42 ka, n = 10) a general trend of mound aggregation can be observed with an average MAR of 19 cm/ka. The overall MAR from present day to the oldest CWCs analysed from core MD08-3231 is 3 cm/ka, hence one order of magnitude lower than during enhanced aggregation. Considering only the ages seen in the core, the MAR is 4 cm/ka. Excluding the three single oldest CWCs (50 – 100 ka) a MAR of 16 cm/ka is obtained.

4.3.2 Mound aggregation seen in GeoB-18141-01

Sixty-four fossil CWCs from core GeoB18141-01 were U-series dated, with four coral samples dated twice (Tab. A.3). Due to quality control nine samples had to be discarded. Ten samples exhibited ^{232}Th concentrations above the limit of 5 ng/g, of which three CWCs were analysed twice and two were improved to fall below the ^{232}Th limit. Exhibiting a δ^{234}U of 169.4 ‰ at ^{230}Th/^{238}U = 0.21 sample 7511 fell off the seawater evolution curve (outside of range shown in Fig. 4.7).

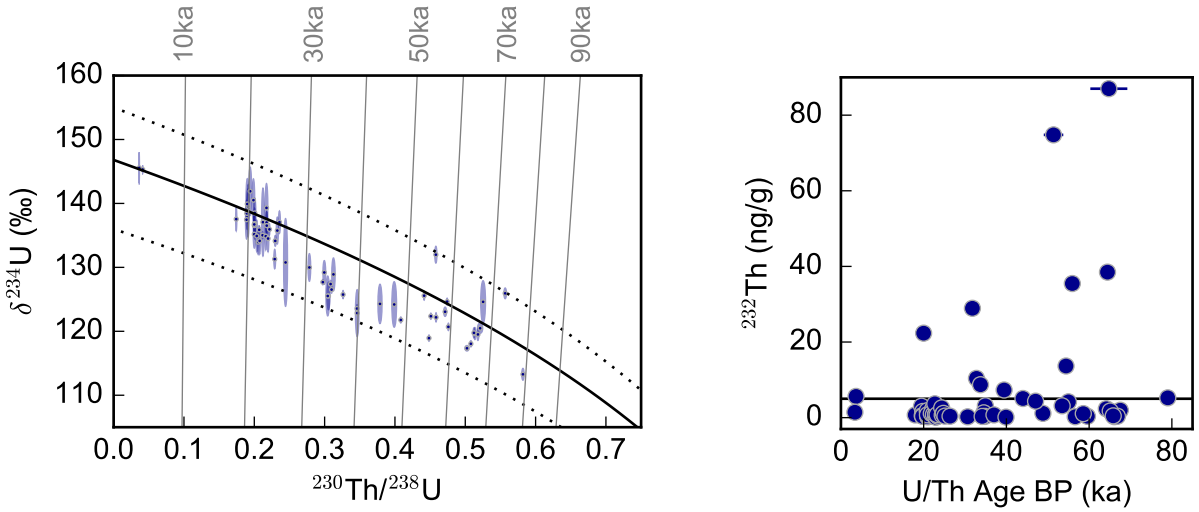

(a) (b)

Figure 4.7: GeoB-18141-01: quality control of CWC U-series dating
For a detailed description refer to Fig 4.5.

The upper 13 m of core GeoB-18141-01 contained CWCs between 3 and 70 ka (Fig. 4.8). It is important to note that the gaps in depth do not necessarily result from a lack of CWCs in the sediment of the core, but can originate from the sampling technique. Depths in which the liners were empty, hence material was lost, are indicted by the shaded blue boxes in Fig. 4.8 (for explanation see Chap. 4.2.1, Tab. A.7). For these sections we cannot assume periods without mound aggregation. In fact, if ages from CWCs in one barrel continue at the same ages like the CWCs sampled from the barrel below it can be assumed that the lost material exhibited similar ages (shaded blue boxes (a) and (b) in Fig. 4.8).
As for core MD08-3231 only few significant age-depth inversions can be observed. Small scale age-depth inversions seen in core depths from 5.61 to 0.7 m are possibly due to both the drilling technique and internal small scale CWC erosions during the mound aggregation (inner circle of Fig. 2.6). The most pronounced age-depth inversion is seen in the first section of barrel 5 at an age of 67.54 ± 0.68 ka and 10.82 m core depth (Fig. 4.8). The two CWCs below sampled from the core catcher (CC) of barrel 5, are both significantly younger (59.58 ± 0.19 and 58.59 ± 0.35 ka) agreeing better with mound growth pattern from CWCs above the inversion (53.47 ka in 10.55 m core depth). No conclusive reason for this age-depth inversion could be found. Therefore, a resampling of barrel 5 is advisable. The small inversion of the two CC corals of barrel P4 can easily be a result of the material ‘falling’ into the CC or small scale internal reef erosions. In

general, age-depth inversions seen in core depths 10 – 12.6 m can both be a result of the drilling technique or small reef erosions during times the mound aggregated more slowly.

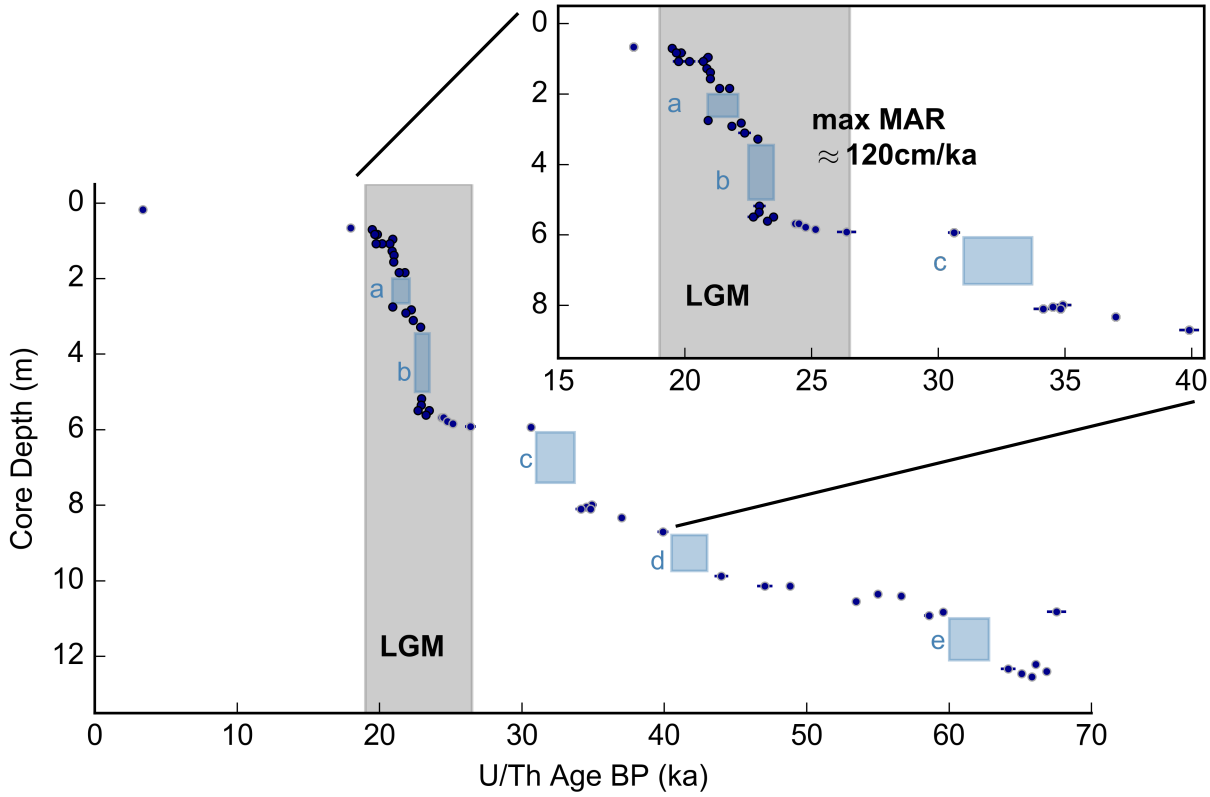

Figure 4.8: CWC mound aggregation seen in coral-bearing core GeoB-18141-01 (Wulle Mound at MACP)
Blue shaded boxes correspond to depths for which there was no recovery in the barrel. The timing of the LGM is shown by the shaded grey area. One period of extremely enhanced mound aggregation (MAR ≈ 120 cm/ka) is observed around 23 ka (data points with black edges).

Here, the lack of corals in blue shaded depths is interpreted solely due to the lost material and not as periods without mound aggregation. Apart from one CWC at 3.38 ka found in upper 20 cm, all corals dated fell into glacial periods (Fig. 4.8). The most striking feature seen in core GeoB-18141-01 from Wulle Mound is the extremely enhanced mound aggregation during the Last Glacial Maximum (LGM, grey shaded area in Fig. 4.8 zoom), in particular between 19.48 ± 0.15 ka and 23.49± 0.08 ka (n = 22, data points with black edges in Fig. 4.8). The mound aggregation rate for the entire LGM is 76 cm/ka (n = 27). The maximal MAR observed, however, lies between 0.7 and 5.61 m depth and is 122 cm/ka (19.48 ± 0.15 ka to 23.49± 0.08 ka; n = 22). This number is obtained by accounting for the small age-depth inversions, hence using the oldest and youngest ages found in this part. The ages of the starting and ending depths result in a MAR of 130 cm/ka. Additionally, the age model suggests a nearly continuous growth from 34 to 67 ka ago with an overall MAR of roughly 14 cm/ka. The mean MAR seen in the top 12.6 m GeoB-18141-01 analysed here is 6.6 cm/ka.

4.4 Discussion

4.4.1 Cold-water coral occurrence in the southern Gulf of Cádiz

First U/Th ages for coral bearing core MD08-3231 were already provided by Frank et al., 2011 and Dubois-Dauphin et al., 2016 (red stars in Fig. 4.9). Four of the thirteen samples, including

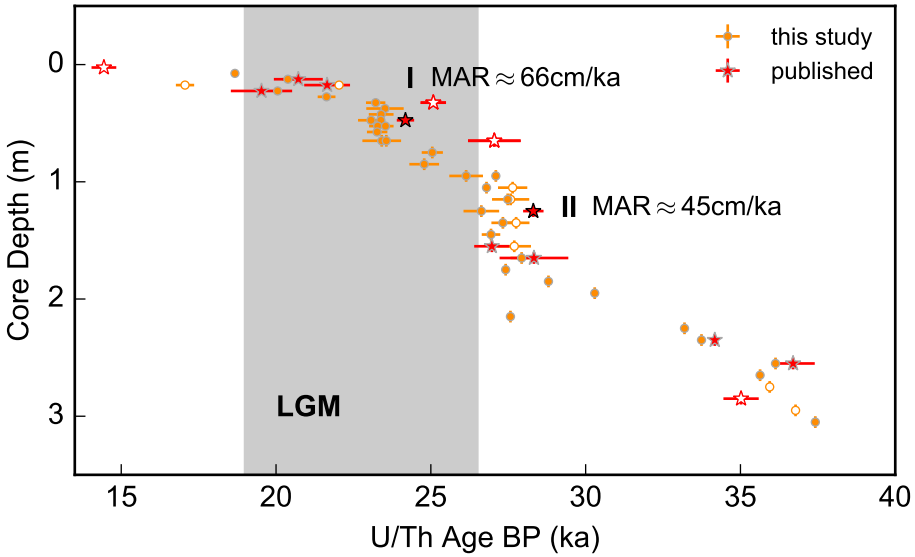

Figure 4.9: MD08-3231 U-series ages including samples U/Th dated by Frank et al., 2011 and Dubois-Dauphin et al., 2016
Samples measured in this work are shown as orange circles (open symbols represent CWCs with $\Delta\Delta^{14}C > 0$), while published analyses are indicated by red stars. Stars with grey edges are standard, open stars are data points that did not pass the ^{232}Th quality control applied here and black edges hint towards a positive $\Delta\Delta^{14}C$. The grey shaded area represents the LGM.

the CWC dated at ~14.5 ka, do not pass the ^{232}Th quality control applied in this study (open stars). CWCs from the upper 30 cm and in depths of about 255 cm follow the same pattern of age-depth inversions observed from the U-series dating in this project. The coral from mound aggregation phase I is slightly older than all the other corals analysed here. The same can be observed for the CWC from depth 125 cm (stars with black edge). Samples from the data set of this project exhibiting similar shifts to older ages during mound aggregation phase II, are all rejected due to positive $\Delta\Delta^{14}C$ (Fig. 4.6). This suggests that these two samples, U-series dated by Dubois-Dauphin et al., 2016; Frank et al., 2011, might also follow this pattern. Therefore, these samples should be treated with care. Within uncertainties, the other seven U-series ages agree with the CWCs dated here. However, no extra information is gained from the formerly analysed CWCs and most uncertainties are significantly larger than here. Hence, in the discussions hereafter, the age model of MD08-3231 will solely be based on the dating analysis of this study. The samples analysed by Dubois-Dauphin et al., 2016; Frank et al., 2011 will be discussed again in the context of εNd analysis in chapter 6.

The general restriction of active mound aggregation to the last glacial seen in both coral bearing cores MD08-3231 and GeoB-18141-01 confirms previous studies (Fig. 4.10; (Frank et al., 2011;

Wienberg et al., 2010; Wienberg et al., 2009)). By analysing surface collected CWCs and various corals retrieved from box or gravity cores the predominant occurrence of CWCs during glacial stages could be established (Wienberg et al., 2010). A few video observations showed scarce live CWC patches with diameters of 10 to 20 cm in the sGoC (Wienberg et al., 2009 and references therein). Furthermore, some fossil Holocene corals (0.65 – 2 ka) were found in the northern GoC (nGoC) at the Iberian margin (Wienberg et al., 2010), however, only of the solitary species *Dendrophyllia alternata*. The youngest dated framework-forming CWCs in the sGoC grew during the Younger Dryas (YD, 12.5 – 11.4 ka; Dansgaard et al., 1989), the last reversion to near glacial conditions during deglaciation (Fig. 4.10). Additionally, the majority of formerly dated CWCs grown during the last glacial did not exceed ages of 45 ka. Several CWCs were dated to the glacial periods of Marine Isotope Stages MIS 6, 8 and 10 (Krengel, 2016; Frank et al., 2011; Wienberg et al., 2010).

Combining the data sets by Wienberg et al., 2010 and Frank et al., 2011 with the CWC dates measured in this project, a nearly continuous growth during MIS 2 to 4 (11.4 – 71 ka) can bee seen (middle panel of Fig. 4.10). The time periods during MIS 2 – 4 lacking dated corals are possibly just due to the fact that the corals which grew during those times simply have not been found and analysed yet. In fact, the missing recovery of the coral bearing core GeoB-18141-01 could possibly have filled some of the gaps observed.

Wienberg et al., 2010 proposed relatively cold surface conditions and a significantly increased biological productivity during the last glacial suggested by high abundances of the planctonic foraminifera species *G. glutinata*. This was attributed to an enhanced upwelling. Prior 16 ka, the Azores Front was shifted northward, compared to today at 30°N, and penetrated the GoC (33 – 37°N) (Rogerson et al., 2004). This shift was indicated by an increased abundance of the deep-dwelling foraminifera *G. scitula*, that grow in water depths from 100 to 700 m and are characteristic for cool surface waters and enhanced vertical mixing (Pérez-Folgado et al., 2003; Schiebel et al., 2002). Additional to a stronger upwelling, grain size analysis of sediment cores in the sGoC hint towards an increased input of aeolian dust from the Sahara (Wienberg et al., 2010). By providing more iron and manganese, this would favour the primary production in the surface waters and consequently possibly the food supply for the CWC mounds below.

The deep MACP on which GeoB-18141-01 was recovered, is located in water depths of about 880 – 970 m. Merely, five corals of the published data originate from the shallow MACP between water depths of 720 – 820 m. All other published CWCs were retrieved from similar water depths as core MD08-3231 in about 550 m, most also from PDE. Between 12 and 40 ka ago conditions favouring CWC growth seem to have reached both depths in which the CWC mounds aggregated. However, corals older than 40 ka are mainly from the deeper coral bearing core GeoB-18141-01. This strongly suggests different conditions for the two depth regimes studied during this time.

The southern deep belt of the MACP (GeoB-18141-01) follows the seaward edge towards the Atlantic of large sedimentary lobes (Hebbeln et al., 2015). The only other known setting of extensive CWC mounds in similarly large water depths are found at the Irish margin (Hebbeln et al., 2015). In these areas strong bottom currents providing the flourishing CWC reefs with food were identified (Dorschel et al., 2005). Possibly, a similar bottom current delivered food to the deeper MACP mounds, but did not pass the CWC mounds of the PDE prior to about 40 ka. As described in chapter 2.2.1, various additional complex circulation patterns often provide flourishing CWC mounds with the needed food (Mienis et al., 2007; White et al., 2005). Without the analysis of further proxies resolving the two depth regimes, that can identify different water masses present during that time or give hints for the food supply, it is difficult to assess this

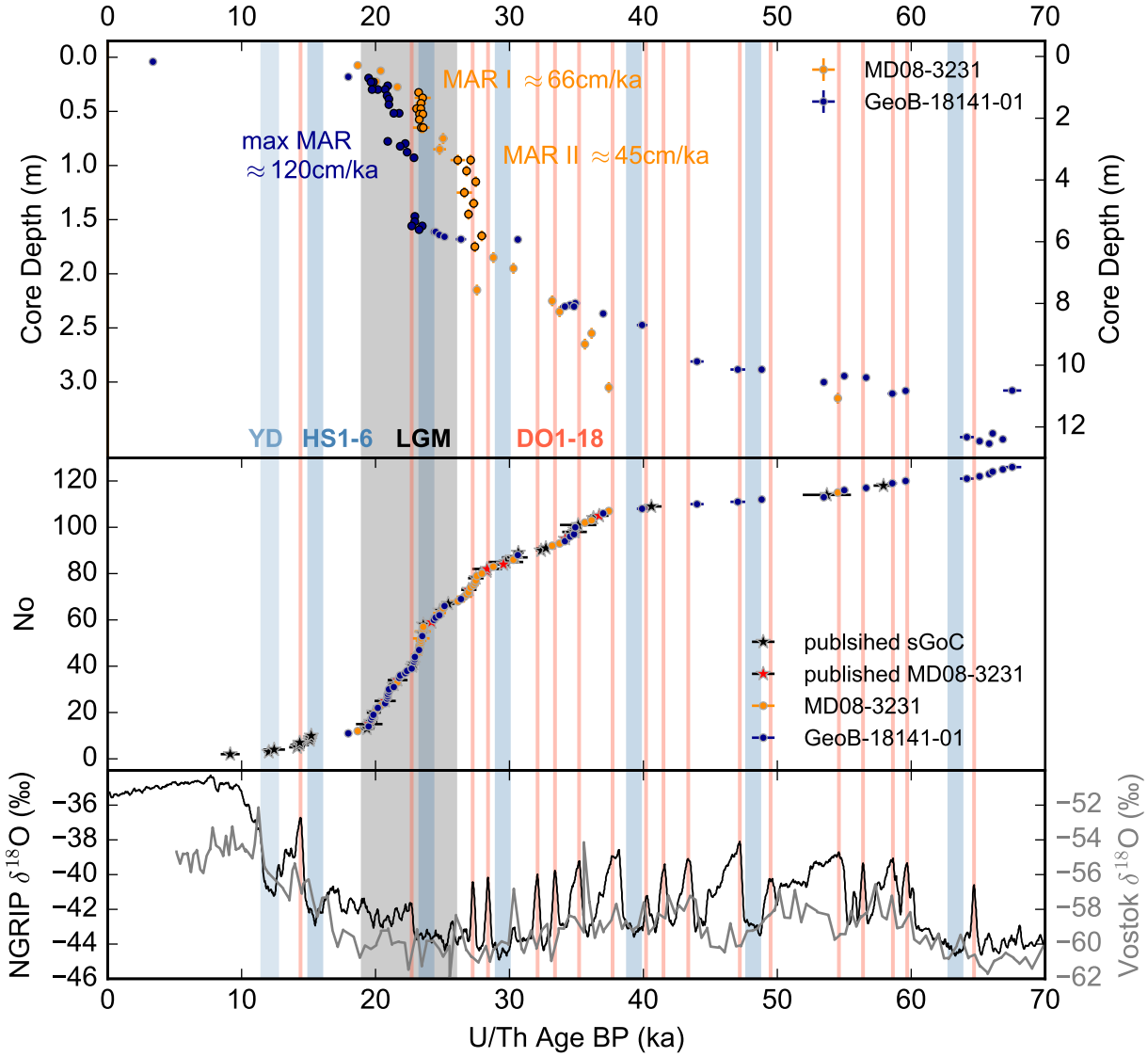

Figure 4.10: CWC appearance and mound aggregation vs. atmospheric climate records
upper panel: age-depth models for both coral-bearing cores (MD08-3231 in orange, GeoB-18141-01 in blue) with enhanced mound aggregation phases represented by symbols with black edges.
mid panel: Compilation of published reef-forming CWCs ages from the sGoC (stars) and data of this study. Red stars are published MD08-3131 data, black stars are CWC from the sGoC (Frank et al., 2011; Wienberg et al., 2010).
lower panel: atmospheric climate development over the last 70 ka from the Arctic (NGRIP) and Antarctic (Vostok) ice core (Landais et al., 2008; Andersen et al., 2004). The Last Glacial Maximum is shown as the grey shaded area. Red lines represent Dansgaard-Oeschger cycles 1 – 18 and light blue bars Heinrich stadials 1 – 6 and Younger Dryas.

question further. A first step towards the analysis of these environmental conditions was part of this PhD project and will be presented in chapters 5 to 7. However, it should already be noted here, that the published paleoceanographic record provided by CWCs from the sGoC could be

extended in this study from about 40 to 70 ka by analysing CWCs from the deeper located MACP.

4.4.2 Peak mound aggregation in the southern Gulf of Cádiz

For the following discussion, it is important to note that a lack of corals in the two coral bearing cores does not represent the whole CWC mound or even the complete region in which they were sampled. Possibly, additional sampling of cores just a few metres away from each core site or on a different mound in the same CWC province would close a few of the smaller time gaps in the records. This does not apply for long-term gaps like the lack of substantial CWC occurrence during the Holocene and the CWC decline 40 ka at the shallower site (MD08-3231) or 70 ka at Wulle Mound (GeoB-18141-01) ago.
As described in chapter 4.3 both coral-bearing cores MD08-3231 and GeoB-18141-01 suggest enhanced mound aggregation phases between 19 and 30 ka (upper panel in Fig. 4.10). The increased mound aggregation at around 27 ka of Gamma Mound at PDE (MAR II $\approx$ 45 cm/ka) cannot be observed in the deeper located core sampled on Wulle Mound in MACP. The single dated CWC of core GeoB-18141-01 at around 30 ka was found in the core catcher. Therefore, it is hard to say, if the lack of corals between 6 and 7.5 m is a result of no corals present at MACP, or lost material during the drilling procedure. However, in water depths around 550 m, favourable conditions for CWC mound aggregation must have prevailed.
The equality of ages above and below the two LGM depth ranges lacking corals (Chap. 4.3.2, Fig. 4.8, 4.10) indicates that both gaps have featured corals that grew during the same time period. Following this assumption, increased MAR I $\approx$ 66 cm/ka in MD08-3231 at 23 ka is simultaneous with the start of the extremely fast mound aggregation recorded in the deeper core GeoB-18141-01 (122 cm/ka; Fig. 4.10). This strongly suggests similar oceanic and environmental conditions for both coral mound sites during this short-term period of roughly 500 – 1000 years. While the CWC mound aggregation slows down severely afterwards at Gamma Mound, Wulle Mound continues to aggregate rapidly until the end of the LGM at 19 ka. Therefore, oceanic and environmental conditions probably shifted slightly with less favourable but tolerable conditions at Gamma Mound.
In core GeoB-18141-01, possibly all corals missing due to recovery between 3.45 and 5 m also grew around 23 ka ago, indicated by the framing coral ages. This would imply an even higher MAR for that time on the order of 1000 cm/ka, which is similar to the growth rates of a single *L. pertusa* coral (Chap. 2.2.3). However, this number is highly speculative and should be treated with care. Therefore, in the further discussions the period for enhanced mound aggregation seen in GeoB-18141-01 will be set as the whole core depth range between 0.7 and 5.61 m (23.5 – 19.5 ka).
Period II of increased aggregation in MD08-3231 coincides with the Dansgaard-Oeschger cycle DO 3 (lower panel and coloured bars of Fig. 4.10). The other phase of enhanced growth (I), concurrent with the start of high MAR in GeoB-18141-01, lies at the transition of the subsequent HS 2 (Heinrich stadial) and DO 2. These, are linked to extremely fast and severe changes in Atlantic circulation and intensity of *Mediterranean Outflow Water* (Bahr et al., 2015; Voelker et al., 2006). Evidently, involved oceanic changes greatly improved the living conditions for the CWCs. However, the two records here do not show a reoccurring correlation between DOs or HS and increased CWC mound aggregation between 30 and 70 ka.
To this day, similarly high MARs above 50 cm/ka have mainly been recorded for the Holocene

(e.g. Matos et al., 2015; Stalder et al., 2015; López Correa et al., 2012; Frank et al., 2009). The only other sites with significant glacial mound aggregation were found more south at the Brazilian margin (Ruckelshausen, 2013), off Mauritania (Eisele et al., 2011) and recently at the Angolan margin (Beisel, 2017; Roesch, 2017; Wefing, 2016).
The underlying oceanic and environmental conditions in the sGoC possibly explaining the different aggregation characteristics observed in the two coral-bearing cores, in particular the extremely fast MARs, will be investigated in chapters 5 to 7.

4.4.3 A general view on aggregation rates of cold-water coral mounds

To investigate common CWC mound aggregation characteristics, all published data of coral bearing cores from CWC mounds with at least two CWC ages were compiled (Tab. 4.1). Including this study, the compilation consists of 28 studies about 16 different CWC mound provinces investigated in 61 coral-bearing sediment cores (Beisel, 2017; Matos et al., 2017; Roesch, 2017; Douarin et al., 2016; Krengel, 2016; Wefing, 2016; Fink et al., 2015; Matos et al., 2015; Stalder et al., 2015; Raddatz et al., 2014; Douarin et al., 2013; Fink et al., 2013; Ruckelshausen, 2013; Fink et al., 2012; López Correa et al., 2012; Eisele et al., 2011; Frank et al., 2011; Mangini et al., 2010; Van der Land et al., 2010; Wienberg et al., 2010; Frank et al., 2009; Mienis et al., 2009; Wienberg et al., 2009; Eisele et al., 2008; Dorschel et al., 2007; Kano et al., 2007; Frank et al., 2004; this study).
Using the recovery and the oldest age of each core the average MAR (MAR_{av}) was calculated. Additionally, the MAR_{ana} for the analysed depth (depth in core of deepest and most shallow CWC) and ages covered (maximal to minimal age) was determined. Furthermore, the age-depth models of cores with more than two dated CWCs were analysed in more detail for possible maximal and minimal MARs (MAR_{max}, MAR_{min}). The criterion for maximal MAR was a clear occurrence of an increased aggregation phase, compared to the general aggregation pattern seen in the respective core. The MAR for this phase was calculated using the same strategy for the starting and ending age of such a period as for the two coral-bearing cores analysed in this study (Chap. 4.3.1). Hence, the MAR was obtained using the youngest and oldest age, not necessarily coinciding with the age of the shallowest and deepest coral of the respective period. Minimal MARs were calculated for phases in which a general continuous mound aggregation could be observed, however, relatively slow with respect to the general age-depth model. Here, periods clearly lacking an overall coral growth, like the Holocene in the two cores investigated here, were not taken into account. For example, in core GeoB-18141-01 a minimal MAR would not be calculated between the shallowest CWC in 0.17 m and the next coral in 0.66 m, as compared to the general aggregation in the core this single coral does not represent an active CWC mound aggregation phase (Fig. 4.8, 4.10). In contrast, the slower aggregation seen in the deeper part of the core (e.g. between 50 and 60 ka; Fig. 4.8, 4.10) would be analysed for minimal MAR considerations as a general aggregation, seen from more than one CWC age, can be observed. Coral-bearing cores for which maximal and minimal MAR evaluation could not be done, MAR_{av} and if available MAR_{ana} were used as MAR_{mim} and/or MAR_{max}.
The values of MARs were rounded to the third decimal place, chosen as the highest decimal place for which each core had a $MAR_{min} > 0$. A statistical assessment shows that the mean value for the different MAR categories (MAR_i, i= av, ana, min, max) is always considerably larger

than the median (Tab. 4.1). Due to the unsymmetric distribution of the MAR values, this is not surprising. Therefore, for further considerations the median of each MAR category will be used. The median of MAR_{av} is 85 cm/ka, with a minimal MAR_{av} of 0.1 cm/ka and a maximum of 127.4 cm/ka. While the median of MAR_{min} is comparable to the one of MAR_{av} (med: 6.9 cm/ka, max and min as MAR_{av}), the median of MAR_{max} is considerably larger (med: 6.9 cm/ka, max: 1486.5 cm/ka & min: 0.1 cm/ka). This is mainly due to the fact that about 3/4 of MAR_{min} were filled by MAR_{av}.

Typical heights of larger mounds vary between 40 m in shelfs or regions like the GoC (Hebbeln et al., 2015; Foss et al., 2005) and 150 m in regions like the Northwest European margin or the Alboran Sea (Hebbeln et al., 2015; Wheeler et al., 2007). Therefore, for smaller mound heights, this would lead to base ages between roughly 135 ka and 580 ka and the base age of about 470 ka for MAR_{av} considerations. For higher mounds base ages would be about 510 ka (MAR_{max}), 1.8 Ma (MAR_{av}) and 2.2 Ma (MAR_{min}) respectively.

A closer analysis of the table reveals a bias towards faster MARs for sites located in the Mediterranean Sea. The Atlantic medians are 19.5 cm/ka (MAR_{max}), 4.4 cm/ka (MAR_{av}) and 3.9 cm/ka (MAR_{min}), leading to base ages for small mounds of 205 ka, 907 ka and 1.03 Ma respectively. Higher mounds potentially reach base ages between 770 ka and 3.88 Ma and MAR_{av} implies 3.40 Ma. In contrast, studies on CWC mounds in the Mediterranean Sea reveal median MAR_i of 127.5 cm/ka, 27.2 cm/ka and 18 cm/ka suggesting base ages of 31 – 147 ka for shallow and 118 – 831 ka for higher mounds. A difference in the observations between Atlantic and Mediterranean CWC mounds can have two reasons. First, this observation is merely an artefact due to the regional distribution of the published data. The amount of different regions and hence coral-bearing cores analysed is significantly smaller for the Mediterranean Sea than for the Atlantic. It is possibly that by chance Mediterranean mounds exhibiting relatively high MARs were sampled. Second, there is a difference between CWC mounds in the Atlantic and in the Mediterranean Sea. Possible reasons could be linked to the near closed basin characteristic of the Mediterranean Sea and linked ocean dynamics and environmental conditions. However, this is highly speculative and needs to be investigated with further drillings on Mediterranean CWC mounds.

It is important to note, that MAR_{max} and therefore minimal base ages are unrealistic scenarios. No core analysed by the 28 studies with numerous dated CWCs exhibited an age-depth model with MAR_{max} prevailing throughout the whole core. Further high resolution core dating needs to resolve, if a similar discrepancy can be observed for MAR_{min} compared to MAR_{av}, or if those two numbers generally lie closer together. This data compilation does not allow to draw a clear line between minimal and average MARs.

Including the investigated core GeoB-18141-01 from Wulle Mound, presently only one other mound was penetrated fully. Challenger Mound in the Porcupine Seabight Province (150 m high) was dated to a base age of 2.7 Ma, which is in a similar range as the base limit found here (Raddatz et al., 2014; Kano et al., 2007). Wulle Mound (30 m high) has a base age of about about 500 ka (Krengel, 2016, unpublished data by T. Krengel) lying in the range for smaller mounds. An additional MeBo drilling coral-bearing core from Brittlestar Ridge down to 70 m into the CWC mound roughly covering half of the total mound height. Lowest ages about $\sim$ 500 ka (Krengel, 2016). Extrapolating similar cycles of active CWC mound aggregation and inactive phases, a base age of about 1 Ma was estimated, which is on the same order as maximal base ages of Mediterranean mounds obtained from the compilation.

The compilation suggests that CWC mounds found in the ocean do not exceed ages above roughly 3.4 Ma. This coincides with the mid-Pliocene warm period and the gradual onset grad-

ual onset and further amplification of Northern Hemisphere glaciation (Fedorov et al., 2013; Shackleton et al., 1984). While it is clear that CWC mound are unlikely to be older than about 3.4 Ma, it remains open if base ages on this order can be observed for the majority of CWC provinces, or if the CWC growth spread from a certain region. To improve our understanding of the timing for mound initiation and their aggregation rates, considerably more drillings of long coral-bearing cores, ideally penetrating whole CWC mounds are of great importance. Additionally, high resolution age determination are substantial to obtain reliable age-depth models. For ages until 800 ka U-series dating can be used. However, samples older than 500 ka often exhibit large uncertainties due to possible U-series open-system behaviour. Sr-isotopes can be used for dating samples older than 500 ka, however this dating technique is also related to large uncertainties (0.1- 1 Ma, (Raddatz et al., 2014; Kano et al., 2007). Therefore, in addition to more and well selected sample material, a dating method reaching back to several million years with smaller uncertainties should be developed. A possible dating tool could be U/Pb dating covering 1 – 4.5 Ma.

4.5 Conclusions

In this study, the reconstruction of cold-water coral growth in the southern Gulf of Cádiz during the last glacial was extended by 30 ka, from 14 – 40 ka in previous studies to 18 – 70 ka here. U-series dating of two coral-bearing cores from to different water depths (550 m and 950 m) revealed that between 18 and 40 ka CWCs were able to flourish at both the Pen Duick Escarpment (PDE) and in the Moroccan Atlantic CWC Province (MACP). However, prior to 40 ka, CWC mound aggregation seems to have been reduced to the deeper of the two provinces (MACP).
Additionally, for the first time glacial mound aggregation rates (MAR) above 50 cm/ka, and $>$ 100 cm/ka during the LGM in particular, were recorded for the temperate East Atlantic. In the modern ocean, similarly high MARs were previously mainly reported in the North Atlantic or the Mediterranean Sea, with records of significant glacial mound aggregation limited to southern sites.
The observed high MARs call for a better understanding of past environmental conditions favouring the flourishing CWC mound, particularly during the LGM. This question will be addressed in the course of this thesis by investigating seawater temperatures from coralline Li/Mg ratios, εNd signatures and water mass reservoir ages recorded in the individual corals.

The compilation of all published data on MAR allowed for an extrapolation of maxima CWC mound ages in the ocean. Potentially, first CWC larvae settled around 3.4 Ma, which coincides with the mid-Pliocene warm period and the gradual onset and further amplification of Northern Hemisphere glaciation.
Wulle Mound clearly showed how strongly MARs can vary even at one site, not only between states of inactive and active CWC growth, but also between different periods of active CWC occurrence. A gravity core might have retrieved the upper 4 m, covering part of the extremely high MAR during the LGM. Extrapolating this aggregation rate for the whole height of this mound would lead to an extreme underestimation of the base age. This clearly highlights the need to precisely date CWCs at the base of CWC mounds rather than extrapolating MARs observed in the upper few metres. This can only be achieved by the recovery of further long coral-bearing cores extending over several tens or even a few hundred meters, that penetrate numerous coral mounds. A more extensive spatial coverage of such cores throughout known CWC provinces

in the Atlantic and the Mediterranean Sea will enable us to further improve the estimation of potential common time scales or distinguish differences in the evolution of CWCs in the various regions.

Table 4.1: Compilation of published coral-bearing cores and their mound aggregation rates (MAR)
MAR_{ana} is MAR for the analysed depth in cores, Average MAR is MAR with repsect to the recovery, Max and Min MARs are the maximal and minimal MARs found in each core. For site abbreviations please refer to list of abbreviations (Chap. D)

Reference	Core	Location	Water Depth (m)	Analysed Depth (m)	Recovery (m)	# U/Th & ^{14}C Ages	Min Age (ka)	Max Age (ka)	MAR_{ana} (cm/ka)	Max MAR (cm/ka)	Min MAR (cm/ka)	Average MAR (cm/ka)
Dorschel et al., 2007	GeoB6728-1	PS	749	3.68	3.68	4	143	261	3.1	3.1	1.4	1.4
Dorschel et al., 2007	GeoB6729-1	PS	711	2.68	2.68	3	53	300	1.1	1.1	0.9	0.9
Dorschel et al., 2007	GeoB6730-1	PS	704	3.58	3.58	4	93	207	3.1	3.1	1.7	1.7
Raddatz et al., 2014; Kano et al., 2007	U1317E	PS	800	154	154	28	600	2700	7.3	68.9	1.0	5.7
Eisele et al., 2008	GEOB9214-1	PS	793	1.98	3.78	2	9.17	299	0.7	1.3	0.7	1.3
Eisele et al., 2008	GEOB9213-1	PS	852	3.12	4.62	2	8.68	269	1.2	1.7	1.2	1.7
Frank et al., 2009	MD012459G	PS	610	4.5	4.5	10	4.3	9.7	83.3	291.7	15.8	46.4
Frank et al., 2011; Frank et al., 2009	MD012463G	PS	888	9	9	16	0.26	324	2.8	19.0	2.8	2.8
Frank et al., 2011; Frank et al., 2009	MD012451G	PS	762	4.07	4.07	9	0.3	230.4	1.8	7.6	0.8	1.8
Frank et al., 2004	ENAM 9915BX	RB	725	0.5	0.5	3	-0.045	696	0.1	0.1	0.1	0.1
Frank et al., 2009	MD01-2454G	RB	747	2.73	2.73	36	0.015	10.88	25.1	103.0	9.7	25.1
Frank et al., 2009	MD012455G	RB	637	1.93	1.93	13	0.1	11	17.7	66.2	16.0	17.5
Mienis et al., 2009	M2003-23	RB	673	3.18	3.18	6	0.051	363	0.9	9.3	0.8	0.9
Van der Land et al., 2010	M2001-28	RB	671	1.6	1.6	2	0.83	11	15.7	15.7	14.5	14.5
Van der Land et al., 2010	M2001-43	RB	634	1.54	1.54	3	0.11	10.9	14.3	14.3	14.1	14.1
López Correa et al., 2012	STJ-325-430	STJ	407	2.62	3.23	2+2	10.822	10.896	24.0	29.6	24.0	29.6
López Correa et al., 2012	STJ-325-472	STJ	262	5.65	5.65	12+12	1.615	9.851	68.6	1486.5	57.4	57.4
López Correa et al., 2012	STJ-325-470	STJ	386	2.68	2.68	1+3	10.4335	11.5675	236.3	236.3	23.2	23.2
López Correa et al., 2012	STJ-325-482	STJ	479	4.2	4.2	0+2	0.478	7.165	62.8	62.8	58.6	58.6
López Correa et al., 2012	TRD-325-359	TRD	315	4.08	4.98	5+6	2.427	3.91	275.1	275.1	127.4	127.4
Douarin et al., 2016; Douarin et al., 2013	+56-08/929VE'	MR	127	3.51	3.51	8	3.367	4.256	394.8	438.9	82.5	82.5
Douarin et al., 2016; Douarin et al., 2013	+56-08/930VE	MR	134	4.39	4.39	21	1.702	3.537	239.2	376.3	124.1	124.1
Wienberg et al., 2010	GeoB9031	nGoC	897	1.5	1.5	3	20.92	45.94	6.0	6.0	3.3	3.3
Wienberg et al., 2010	GeoB9018	nGoC	702	2.72	2.72	3+1	14.65	283.8	1.0	1.0	1.0	1.0
Wienberg et al., 2010; Wienberg et al., 2009	GeoB9032	nGoC	843	0.47	0.47	2	17.15	41.17	2.0	2.0	1.1	1.1
Wienberg et al., 2010; Wienberg et al., 2009	GeoB9070	PDE	594	5.2	5.2	3+2	23.5	166	3.6	12.4	3.1	3.1
Frank et al., 2011; Wienberg et al., 2010	GeoB12103	PDE	591	4.44	4.44	6	22.83	49.63	16.6	38.8	8.9	8.9
Wienberg et al., 2010	GeoB12104	PDE	590	4.91	4.91	3	23.57	342.29	1.5	3.8	1.4	1.4
Wienberg et al., 2010	GeoB12102	PDE	585	4.93	4.93	5	57.93	164.02	4.6	20.2	3.0	3.0
Frank et al., 2009	M2004-05	PDE	543	1.25	2.34	3	113	129.8	7.4	7.4	1.0	1.8
Frank et al., 2011; Wienberg et al., 2010	M2004-02	PDE	523	4.03	4.03	13	9.15	262.8	1.6	19.5	1.5	1.5
Frank et al., 2009	GeoB12712	PDE	716	4.88	4.88	5+1	345.5	500	3.2	3.2	1.0	1.0
Frank et al., 2009	GeoB12722	PDE	882	4.26	4.26	3	32.37	194.3	2.6	2.6	2.2	2.2
Frank et al., 2009	MD08-3212	PDE	525	0.58	0.58	5	11.08	311.2	0.2	1.5	0.2	0.2
Frank et al., 2009	MD04-2804G	PDE	530	0.4	0.4	2	287	318	1.3	1.3	0.1	0.1
Frank et al., 2009; **this study**	MD08-3231	PDE	550	3.45	3.45	11+1 / **36+23**	14.78	99.05	4.1	66.0	3.5	3.5
Frank et al., 2009	GeoB12740	shal. MACP	739	3.5	3.5	4+3	14.34	41.26	13.0	13.0	8.5	8.5
Frank et al., 2009	GeoB12743	shal. MACP	827	1.43	1.43	3+2	27.49	53.7	5.5	5.5	2.7	2.7

Reference	Core	Location	Water Depth (m)	Analysed Depth (m)	Recovery (m)	# U/Th & ^{14}C Ages	Min Age (ka)	Max Age (ka)	MAR$_{ana}$ (cm/ka)	Max MAR (cm/ka)	Min MAR (cm/ka)	Average MAR (cm/ka)
Krengel, 2016; **this study**	GeoB18141-1 P1-13	deep MACP	944	14.92	30	19 / **50+13**	3.88	347.88	4.3	122.0	8.6	8.6
Eisele et al., 2011	GEOB11569-2	MA	444	4.875	4.875	20	14.24	61.34	10.4	70.8	7.9	7.9
Roesch, 2017; Wefing, 2016, Beisel, 2017	GeoB20933-1	AM	338	9.6	9.6	54+22	0.465	33.58	29.0	225.0	24.7	28.6
Matos et al., 2015	TRACOS2010-76	NCM	443	2.21	2.4	4	5.6	6.84	178.2	178.2	35.1	35.1
Matos et al., 2015	TRACOS2010-69	NCM	335	0.18	0.18	2	0.244	0.712	38.5	38.5	25.3	25.3
Matos et al., 2015	TRACOS2010-10	NCM	393	0.275	0.275	2	0.198	0.698	55.0	55.0	39.4	39.4
Matos et al., 2015	TRACOS2010-10	NCM	337	0.2	0.2	2	0.212	0.942	27.4	27.4	21.2	21.2
Matos et al., 2015	TRACOS2010-55	NCM	436	0.14	0.14	2	0.153	0.873	19.4	19.4	16.0	16.0
Matos et al., 2015	GeoB-16310-3	GoM	573	1.56	1.56	15	1.56	224.28	0.7	32.1	3.9	0.7
Matos et al., 2015	GeoB-16313-2	GoM	553	2.08	2.08	4	3.98	7.75	55.2	55.2	26.8	26.8
Matos et al., 2015	GeoB-16318-1	GoM	556	4.37	4.37	7	4.49	99.14	4.6	10.0	4.4	4.4
Mangini et al., 2010	ENG-111 (C1)	BM	621	2.97	2.97	17+10	8.202	19.502	26.3	44.2	5.7	15.2
Mangini et al., 2010	PC21210009 (C2)	BM	781	0.68	0.68	13+10	12.612	29.272	4.1	7.2	2.3	2.3
Ruckelshausen, 2013	MXL-030	BM	626	3.85	3.85	29+18	11.761	89.928	4.9	27.1	3.2	4.3
Ruckelshausen, 2013	K-GLC-PPT-06	BM	808	9.94	9.94	16+7	4.728	27.017	44.6	384.2	36.8	36.8
Fink et al., 2015	GeoB11135-2	SoS	634	2.83	4.7	0+2	3.756	5.783	139.6	139.6	48.9	81.3
Fink et al., 2012	GeoB11185-1	SMLCP	612	0.92	0.92	7	1.786	13.348	8.0	110.0	6.9	6.9
Fink et al., 2012	GeoB11186-1	SMLCP	628	1.35	1.35	7	2.725	11.956	14.6	89.9	11.3	11.3
Fink et al., 2013	GeoB13728-2	MCP	343	2.95	2.95	6	2.913	13.194	28.7	133.1	22.4	22.4
Fink et al., 2013	GeoB13729-1	MCP	442	3.75	3.75	5	9.81	11.206	268.6	268.6	33.5	33.5
Fink et al., 2013	GeoB13730-1	MCP	338	4.27	4.27	7	2.563	13.291	39.8	122.0	32.1	32.1
Stalder et al., 2015	TTR17-401G	MCP	251	5.6	5.6	0+7	5.426	13.023	73.7	212.1	13.7	43.0
Krengel, 2016	GeoB18118-2	MCP	329	65.35	68.55	51	10.26	521.84	12.8	74.4	3.9	13.1
Mean							35	169	44.5	101.1	16.8	19.9
SE									10.3	26.6	3.3	3.5
Median							6	41	10.4	29.8	6.9	8.5
Deviation from Median									40.1	95.8	15.2	17.2
Age with mound hight of 40 m									386	135	580	472
Age with mound hight of 150 m									1449	506	2176	1768
Atlantic Median									6.0	19.5	3.9	4.4
Atlantic Deviation									36.2	91.0	15.0	16.1
Base Age with mound hight of 40 m									667	205	1034	907
Base Age with mound hight of 150 m									2502	770	3878	3403
Mediterranean Median									34.2	127.5	18.0	27.2
Mediterranean Deviation									57.2	44.7	12.6	13.0
Base Age with mound hight of 40 m									117	31	222	147
Base Age with mound hight of 150 m									438	118	831	551

5 Li/Mg-temperatures seen in cold-water corals from the last 65 ka

5.1 Introduction

Here, I present the application of the thermometer Li/Mg in aragonitic corals on the coral-bearing sediment cores GeoB-18141-01 and MD08-3231 from the sGoC (4.2.1). Corals analysed grew from 3 ka (1 sample) to 65 ka ago, with an extremely enhanced LGM mound aggregation ($\sim$ 66 cm/ka in MD08-3231 to $\sim$ 122 cm/ka in GeoB18141-01) (Chap. 4.3). Therefore, the discussion on changes of intermediate water temperatures and thermocline characteristics will focus on this time period, investigating the environmental conditions favouring the flourishing coral reef.

5.2 Materials and methods

Each fossil CWC U-series dated for mound aggregation analysis (Chap. 4) was investigated for its Li/Mg ratio (Tab. A.4). Due to a lack of sample material, three CWCs were not analysed for Li/Mg ratios. For details concerning the coral-bearing sediment cores refer to chapter 4.2.1 and table A.3. Present temperatures in the respective water depths of the cores are 11.2 °C in 550 m (MD08-3231) and 9.9 °C in 944 m (GeoB-18141-01) with less than 2°C annual temperature variations (whole CTD-profile in Fig. 3.3 and 5.2).

From the mechanically cleaned sample for the U/Th analysis (Chap. 4.2.2) an extra 12.2 – 12.8 mg aliquot was taken for Li/Mg analysis following Montagna et al., 2014. The coral fragment was dissolved in 10 ml 0.5M HNO_3. To attain a maximum Ca concentration of 10 µg/ml a portion of the dissolved sample was diluted. Measurements were carried out on an iCap Q^{TM} ICP-MS at the Institute of Environmental Physics (IUP), Heidelberg, Germany. The analytical measurement methods were introduced in our laboratory by Förstel, 2014. In that study, the uncertainty of the temperature

$$\mathrm{T}\,(^{\circ}\mathrm{C}) = \frac{1}{0.049 \pm 0.002} \times \ln\left(\frac{\mathrm{Li/Mg}}{5.41\,\frac{mmol}{mol}}\right) \tag{5.1}$$

(after EQ. 2.7) was investigated. It evolves from the uncertainties of the empirically determined factor 0.049 ± 0.002 and analytical Li/Mg uncertainty. With increasing temperatures its uncertainty increases. Even if statistical reproducibilities of Li/Mg are ignored, a seawater temperature of 26°C already exhibits an uncertainty > 1°C, which is larger than the estimation by Montagna et al., 2014. Cold-water corals usually grow in water temperatures between 4 and 10°C. Assuming for example a temperature of 5°C, an analytical Li/Mg uncertainty of 5% is allowed to achieve a total temperature uncertainty of 1°C. With analytical uncertainties of Li/Mg ratio

measurements in this study between 1 and 2%, the largest contribution to the temperature reconstruction lies in the empirical calibration curve. A conservative estimation of the combined Li/Mg reproducibility and calibration curve uncertainty lead to an external reproducibility for temperature of 1°C (Lausecker, 2015).
Additionally, one has to keep in mind that for a temperature of 0°C only the Li/Mg reproducibility is considered because Montagna et al., 2014 used the °C-scale, keeping the y-intersect fixed. Using the total temperature scale in Kelvin instead, would lead to a more variable calibration curve in the lower temperature regime (Förstel, 2014).
Analysing several living or young CWCs (< 100 a) the calibration curve (Montagna et al., 2014) was reconstructed ascertaining the reliability of the in-house measurements (Fig. 5.1(a)) for reconstructions of temperatures from coralline Li/Mg measurements (Lausecker, 2015). Additionally, a number of samples was measured in both the laboratories of IUP and at LSCE (Laboratoire des Sciences du Climat et de l'Environnement, Gif-sur-Yvette, France) (Krengel, 2016). The Li/Mg ratios measured agreed well with each other, providing high confidence in the applied methods (Fig. 5.1(b)). The instrumental drift was monitored and corrected using the in-house standard ICE-CTD 20PL501-6-C4 (ICE20). Its Li/Mg ratio is 4.08 ± 0.08 mmol/mol (Lausecker, 2015).

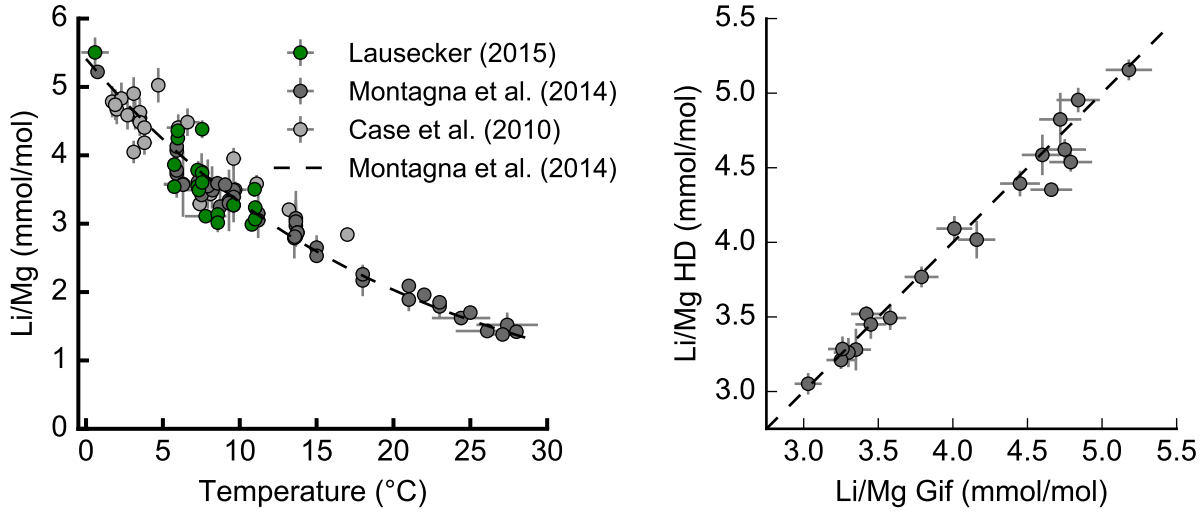

(a) In-house Li/Mg-temperature calibration

(b) Inter-laboratory comparison

Figure 5.1: Calibration of the Li/Mg thermometer in CWCs at the laboratory of IUP
(a) The calibration curve for Li/Mg temperatures (black dashed line) was reconstructed to ascertain the reliability of the in-house measurements (Lausecker, 2015). Green circles are measurements performed at IUP laboratory and grey and dark grey circles represent data used for the calibration (Montagna et al., 2014; Case et al., 2010).
(b) Twenty CWCs were measured at IUP and LSCE showing the same results (Krengel, 2016).

5.3 Results

Li/Mg ratio measurements of the CWCs from cores GeoB-18141-01 and MD08-3231 were carried out over a period of three years (Tab. A.4) as part of the Bachelor's project Rieger, 2015 and this PhD project.
Temperatures at CTD station GeoB-18136-01-10 (35 ° 06.21'N, 7 ° 07.92'W, 990 m) nowadays are 11.2 °C in 550 m and 9.9 °C in 944 m, implying a temperature gradient between these two depths (∂T/∂z) of about 0.33 °C/100 m. Taking past glacial-interglacial sea-level changes into account (LGM-today ≈ -130 m; (Lambeck et al., 2014; Waelbroeck et al., 2002)) during the LGM the mounds were located in about 420 m and 810 m water depth. In these depths the present day temperatures are 11.9 °C and 10.3 °C, hence ∂T/∂z = 0.4 °C/100 m.

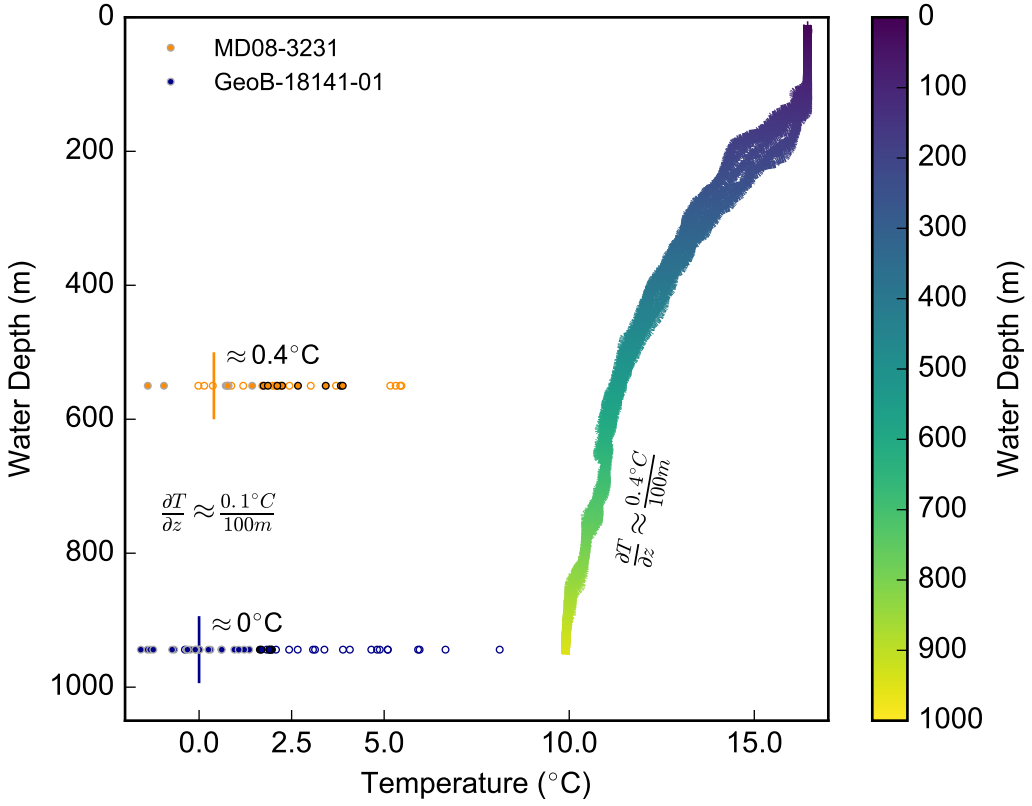

Figure 5.2: Coralline Li/Mg temperatures compared to the modern seawater temperature profile of CTD station GeoB-18136-01-10
Filled coloured symbols (MD08-3231: orange, GeoB-18141-01:blue) with grey and black edges depict LGM CWCs and CWCs grown during DO 2 respectively. Open symbols represent Li/Mg temperatures recorded in CWCs not grown during the LGM. The vertical coloured bars indicate the LGM mean temperature. On the left the temperature profile of station GeoB-18141-01-10 is shown with changing colour representing the water depth (Hebbeln et al., 2015).

The single coral from core GeoB-18141-01 that grew 3.88 ± 0.05 ka years ago suggests an ambient seawater temperature of 8.1 ± 1.4 °C agreeing with warm seawater temperatures during the Holocene (closest GeoB-18141-01 coral to modern T-profile in Fig. 5.2 and 5.3). The stop of flourishing reef growth coincides with the end of the LGM and the start of atmospheric warming

recorded in Arctic and Antarctic ice cores (Chap. 4.4; lowest panel in Fig. 4.10). Seawater temperatures during the LGM reconstructed from the fossil CWCs in which the coral reef flourished were 1.7 ± 0.8 °C (n = 14, 2σ of mean) (MD08-3231) and 0.3 ± 0.4 °C (n = 26, 2σ of mean) (GeoB-18141-01) (Fig. 5.3). This leads to a modern-LGM temperature anomaly of about -9.5 °C in both water depths. For sea-level change adjusted depths the temperature anomaly of -10.2 °C and -10 °C is even larger. The different temperatures in the water depths of the coral-bearing cores, imply an overall LGM temperature gradient between both sites of 0.35 °C/100 m, which is similar to the modern gradients both accounting for sea-level changes and for present depths of the cores.

However, the constantly cold climate signal during the LGM is overlain by the climate signal of the Dansgaard-Oeschger cycle DO 2 (22.7 ka), seen in Arctic ice cores like NGRIP (Fig. 5.3, Andersen et al., 2004; Dansgaard et al., 1993). DO cycles are characteristic for the Northern Hemisphere, describing a seesaw temperature pattern with a rapid warming over decades followed by a much slower cooling over centuries to millennia (Dansgaard et al., 1993). Coinciding with DO 2, corals from MD08-3231 show a punctuated increase of temperature to about 3.7 ± 0.2 °C (n = 3, 2σ of mean). Compared to the overall LGM temperature of MD08-3231, corals this implies an increase of about 2 °C. Corals that grew during the LGM but not during DO 2, exhibit a mean temperature of 0.4 ± 0.8 °C (n = 6, 2σ of mean). This leads to a DO 2 temperature increase of roughly 3.3 °C. Although less pronounced, in the deeper core GeoB-18141-01 a similar pattern can be observed. Temperatures during DO 2 increase to 1.8 ± 0.1 °C (n = 3, 2σ of mean), which is 1.5 °C warmer than the total LGM mean and 1.8 °C warmer than the mean over LGM corals not grown during DO 2 (0 ± 0.4 °C, n = 21, 2σ of mean). The temperature gradient between the two water depths of the cores obtained when considering the DO 2 is roughly 0.48 °C/100 m and therefore higher than modern conditions. $\partial T/\partial z$ calculated from the CWCs grown during LGM, but not coinciding with the DO 2 warming is about 0.1 °C/100 m which is significantly smaller than the temperature decrease observed today for both the modern depths of the cores and the sea level change adjusted depths.

Between 26 and 70 ka most seawater temperatures reconstructed from corals were significantly warmer (2.08 – 6.66 °C), following the Northern Hemisphere climate signal seen in the NGRIP ice core, in particular the occurrence of DOs. As the atmospheric climate, these warmer temperatures are still clearly lower than the present warmer temperature conditions in the GoC.

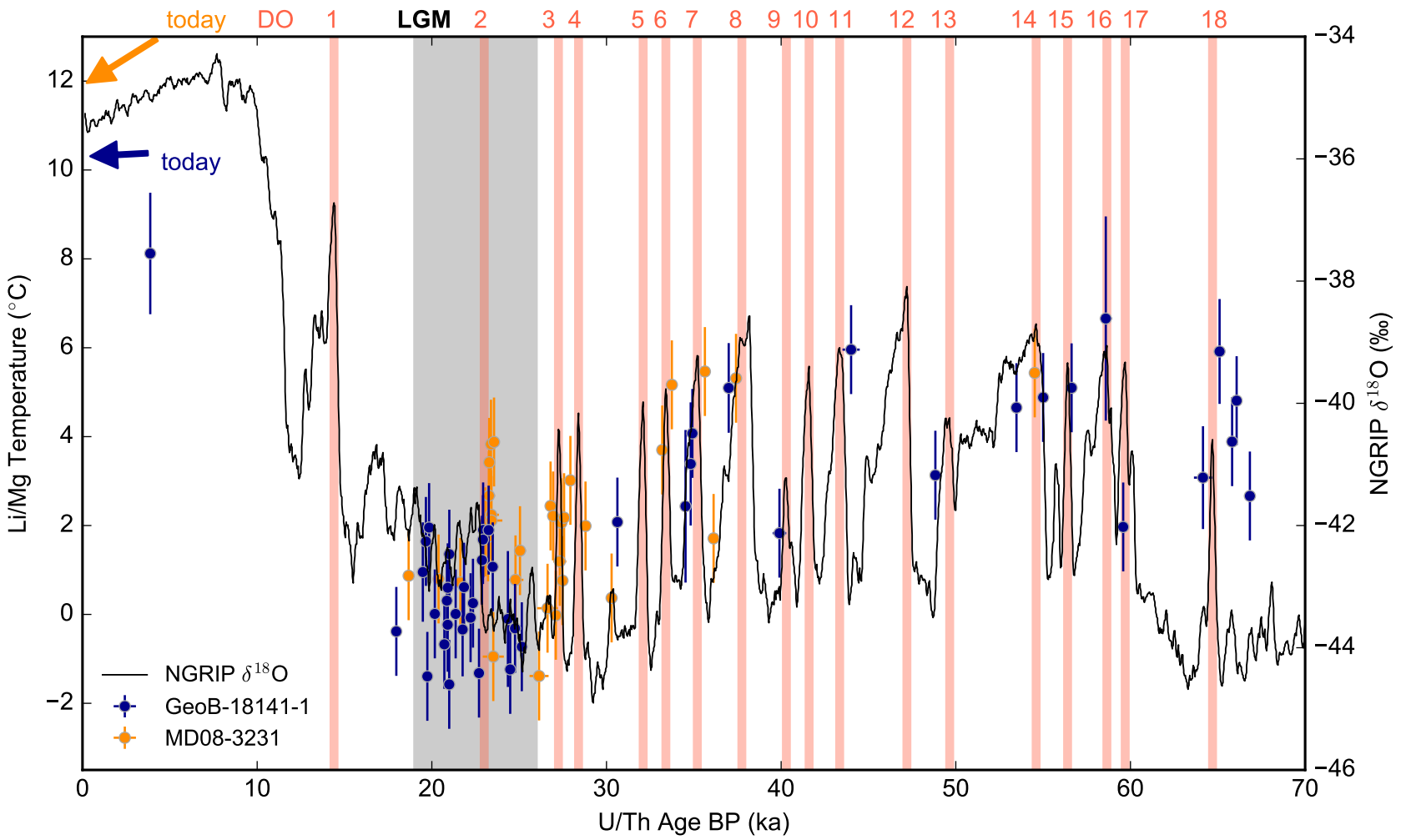

Figure 5.3: CWC Li/Mg temperatures from both cores compared to the NGRIP Arctic ice core climate signal (Andersen et al., 2004) MD08-3231 temperatures are shown in orange, GeoB-18141-01 as blue symbols and the ice bore δ^{18}O record as the black line. DO cycles 1 – 18 are represented by red and the LGM by grey shaded areas (Clark et al., 2009; Dansgaard et al., 1993).

5.4 Discussion

Two striking features are observed in the temperature reconstructions. First, the temperature development reconstructed from the CWCs is, on first order, synchronous with the atmospheric climate changes observed in Northern Hemisphere ice cores (Fig. 5.3). Both long-term trends and punctuated events are recorded in apparent coralline Li/Mg temperatures from the sGoC. Second, intermediate water temperatures during the LGM, excluding the observed DO 2 warming, seem to have been extremely cold reaching down to -1.57 $\pm$ 1°C (Fig. 5.3), and imply a temperature gradient between the two core sites a factor 4 smaller than present conditions (Fig. 5.2).
The absolute values of extremely cold temperatures reconstructed here from corals dated back to the LGM have to be considered in more detail. From a physico-chemical point of view, the minimum temperature obtained of -1.57 $\pm$ 1°C can be reached in seawater. However, seawater temperatures this cold, are presently only found in polar regions. Moreover, a study on planctonic foraminifera indicated that unlike for Heinrich stadials (HS 1 and 4) the northern polar front did not reach the Iberian margin during the late LGM (19 – 24 ka) (Fig. 5.4; (Eynaud et al., 2009)). In addition, a synthesis of studies on sea surface temperatures (SST) during the LGM, MARGO (Muiltiproxy Approach for Reconstruction of the Glacial Ocean Surface; (Waelbroeck et al., 2009)), reconstructed a modern-LGM SST anomaly for the Gulf of Cádiz by only about -1 to -2 °C (Fig. 5.5). This leads to the question how intermediate waters in the sGoC can exhibit such extreme cooling, not seen by planctonic foraminifera living in the surface waters just above.

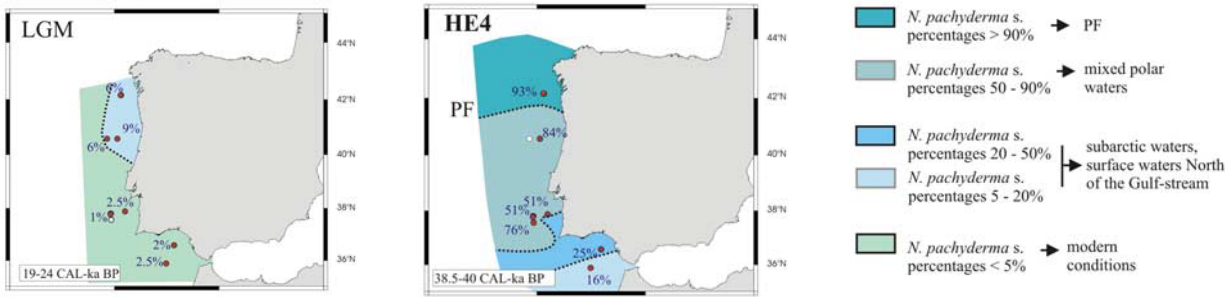

(a) (b)

Figure 5.4: The southward penetration of the polar front along the Iberian margin during the late LGM and HS 4 reconstructed from foraminifera assemblages
(a) During the late LGM (19 – 24 ka) the polar front did not reach the Iberian margin.
(b) stadials like HS 4 (here HE 4) exhibit a southward shift of the polar front to around 40 – 42°N.
The figure was adjusted from Eynaud et al., 2009

Two directions of arguments can be taken to explain the extremely high modern-LGM anomalies about -10 ° observed for both sites: first, The empirically determined Li/Mg-temperature calibration curve needs revision. Second, The reconstructed temperatures describe conditions of the thermocline and intermediate waters in the sGoC caused by upwelling of polar masses and/or advection of an intermediate water mass that was formed in polar regions.
Here, I will focus first on a possible deviation from the calibration curve. Afterwards, potential oceanic implications that could explain the extreme temperatures during the LGM will be described.

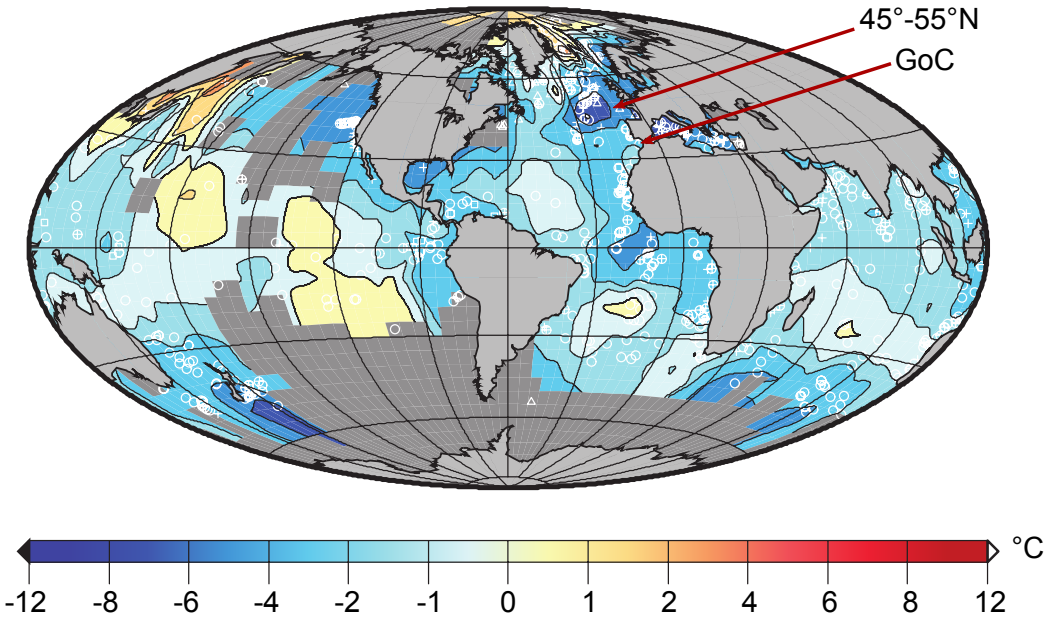

Figure 5.5: Annual SST anomaly reconstructions for the LGM from MARGO project
Note the anomalies for the sGoC around 2°C and the particularly negative anomaly in the Northeast Atlantic between ∼45°N and ∼55°N.
Figure taken from Waelbroeck et al., 2009

5.4.1 Critical examination of the Li/Mg-temperature proxy

The first assumption made, when the coralline Li/Mg temperature proxy was introduced, was a constant seawater [Li] and [Mg] concentration through time, both on global and regional scales. Therefore, Li/Mg changes observed in aragonite corals could be linked to purely seawater temperature changes. This assumption is reasonable, as yet, no oceanic [Li]/[Mg] change has been reported.
The calibration curve used to derive the temperature from the Li/Mg ratio in the aragonite skeleton of the CWCs was obtained from an empirical study by Montagna et al., 2014. This study was based on a data set containing different species of corals with aragonite skeletons which grew in water temperature between 0.75 and 28 °C. In the low temperature regime (below 5.9 °C), Montagna et al., 2014 only had one data point at 0.75 °C. A comparison between the obtained calibration and further Li/Mg-temperature analysis by Case et al., 2010 showed a good agreement for temperatures between 1.7 and 3.8 °C. However, a closer inspection of investigated CWC from Case et al., 2010, reveals that CWCs grown in warmer sea temperatures (4.7 – 13.2 °C) exhibits mostly Li/Mg values above the calibration. Furthermore, no inter-laboratory calibration was done between those two studies. Additionally, the calibration curve is calculated using the °C scale rather than the total temperature Kelvin scale (Chap. 5.2) and the y-intersect at 0°C is kept fixed. Therefore, strictly speaking the calibration curve by Montagna et al., 2014 is not calibrated for temperatures below 0°C. Hence, additional analyses of modern CWCs grown in temperatures below 6°C is advisable, to re-evaluate the calibration curve by Montagna et al., 2014 in the cold temperature regime.
Another important aspect are vital effects induced by the corals (Chap. 2.2.4). The species found in the coral bearing cores GeoB-18141-01 and MD08-3231 were mainly *L. pertusa* and *M. oc-*

ulata. While modern *L. pertusa* are known to tolerate temperatures between -1.8 and 14.9°C, most presently active mounds are found in water temperatures between 6.5 and 8 °C (Wienberg and Titschack, in press; Davies and Guinotte, 2011; Davies et al., 2009). *M. oculata* preferentially grow in slightly warmer conditions 8.5 – 10 °C (Wienberg and Titschack, in press). Corals analysed during the LGM were mostly *L. pertusa*. This suggests that LGM temperatures were at least tolerable for *L. pertusa* growth and too cold for the species *M. oculata*. Species investigated for the calibration were found in regions that are known to exhibit comfortable seawater temperatures or cultivated in aquariums under species preferred conditions (Montagna et al., 2014). Although within the tolerable range, reconstructed temperatures for the LGM are clearly below the preferred temperatures of *L. pertusa*. Up to this point, we do not know if CWCs and *L. pertusa* in particular, that grow in water temperatures just durable, alter their aragonite skeleton and hence possibly the Li/Mg ratio. It is not unlikely that under stress, the inner-skeleton microscale variations of element/Ca ratios and therefore the vital effects change (Chap. 2.2.4 and 2.4). To rule out vital effects as a cause of Li/Mg ratio changes, either microscale analysis of cultured aragonitic corals under comparably cold conditions or naturally grown corals known to have grown under stress, is needed.
The last effect, possibly altering coralline Li/Mg ratios is diagenesis. However, samples for which diagenesis was suspected were identified by the quality control of U-series and ^{14}C dating. Typically U/Ca ratios (µmol/mol) in CWC skeletons are one and three orders of magnitude smaller than Li/Ca (10 µmol/mol) and Mg/Ca (mmol/mol), respectively (Montagna et al., 2014; Anagnostou et al., 2011). Therefore U-series dating is likely more sensible to processes altering the skeleton. To this point, we have not found indications for diagenesis affecting Li/Mg ratios, but not U-series dating.

In spite of these open questions concerning the calibration curve, their is an extremely good correlation between reconstructed intermediate seawater temperature variations and atmospheric climate changes both for long-term patterns and punctuated events recorded in ice cores (Fig. 5.3). This fact provides high confidence in coralline Li/Mg ratios as a qualitative temperature proxy. The considerations above suggest that quantitative considerations, in particular in the cold regime, might not be as precise as believed. This suspension has not been confirmed but urges the need for a re-evaluation.

5.4.2 The thermocline and intermediate waters during the LGM

Setting aside the particular oceanic setting in the GoC with its different water masses a key change can be observed for the thermocline. The modern temperature gradient with depth (∂T/∂z) lies between 0.33 and 0.4 °C/100 m, depending if modern-LGM sea level changes are considered. In contrast, the LGM ∂T/∂z for CWCs, not following the temperature increase attributed to DO 2, is 0.1 °C/100 m (Fig. 5.2). As LGM surface temperatures are only about 2°C colder than today (Eynaud et al., 2009; Waelbroeck et al., 2009), an extreme rise towards shallower depths and a flattened vertical structure of the thermocline is suggested (Fig. 5.6). This would lead to a stronger density gradient between surface and intermediate waters, resulting in a further inhibited diffusional exchange between the two water bodies. In the following considerations, discussing possible oceanic scenarios for the LGM, this change in the vertical thermocline will be termed 'flattened' thermocline.
A model for the Atlantic, forced by a freshening of surface waters in high latitudes predicted a

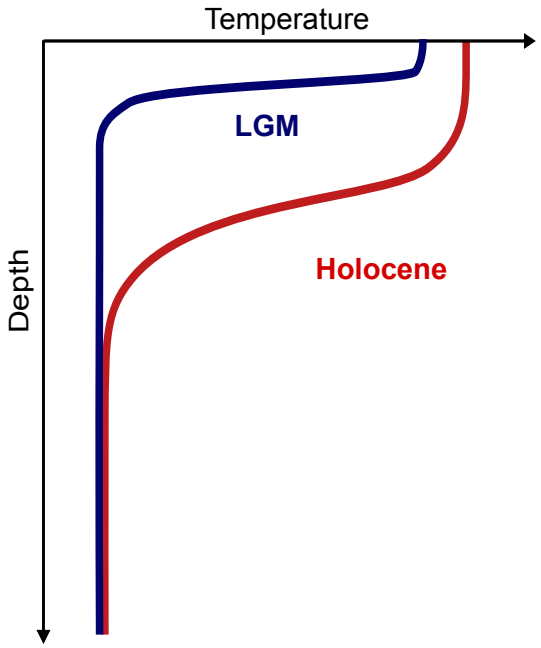

Figure 5.6: Proposed schematic view on thermocline change between the Holocene and the LGM
A deep thermocline during the Holocene (red line) is replaced by an extremely flattened thermocline during the LGM (blue line).

deepening of the thermocline in tropical regions (Fedorov et al., 2007). The LGM is defined as the period of the last glacial with the maximal volume of ice sheets and lowest sea level conditions, leaving the ocean relatively saline (Clark et al., 2009). In combination with the overall colder temperatures during the last glacial this could explain the more flattened thermocline. Such a scenario would imply a general flattening of the Atlantic thermocline and should be observable in other regions. A study on CWCs from the Angolan margin reported intermediate water temperatures around 2° for the LGM (Roesch, 2017). Further temperature reconstructions on thermocline CWCs from other regions in the Atlantic, grown during the LGM, are needed to confirm this scenario.
Another possibility to explain a more homogeneous temperature distribution in intermediate depths is upwelling. The increased growth of CWCs was explained by an enhanced biological productivity, suggested by foraminifera assemblage analysis (Wienberg et al., 2010). The increase in biological surface productivity was attributed to frontal upwelling of intermediate waters caused by a northward shift of the Azores current from around 30°N today, reaching into the GoC prior to 16 ka (Rogerson et al., 2004). However, if upwelling was the cause of the flattened thermocline, colder temperatures would also have reached the surface waters. One could argue that upwelling strongly varies throughout the year and foraminifera only record SSTs during the time they grow. However, in this case we would expect that during the times of high foraminifera abundances the temperature would be at its lowest, compared to the rest of year. Additionally, unlike foraminifera, CWCs most likely calcify their skeleton during the entire year, therefore showing a temperature signal averaged over short-termed fluctuations like seasonal upwelling. Hence, temperature signals recorded in foraminifera from the GoC should exhibit a stronger cooling, if upwelling was the main cause for the flattened thermocline. Although it is unlikely

that upwelling was the main reason for the flattened thermocline, it cannot completely be rule out.

Both scenarios presented, imply a penetration of an extremely cold intermediate water mass into the GoC. The only water masses exhibiting temperatures around 0°C today are polar water masses formed in the Arctic or Antarctic region. In the GoC water masses of both northern (*Eastern North Atlantic Central Water*; ENACW) and southern origin (*Eastern Intermediate Antarctic Water*; EAAIW) are present. While MSW also plays an important role in the GoC, it is very unlikely that water formed in the Mediterranean Sea reached polar temperatures. Reported glacial temperatures for the deeper Alboran Sea range between 8 and 10°C (Cacho et al., 2006).
A wind-induced southward shift of the Arctic polar front during HS 1 and 4 to about 41°N was evident in foraminifera assemblages, however, this shift was less pronounced for the late LGM after HS 2 (19 – 24 ka) (Fig. 5.4,5.5; (Eynaud et al., 2009; Waelbroeck et al., 2009)). Modern ENACW is *North Atlantic Central Water* (NACW) modified by the basin gyre systems *Subtropical Gyre* (STG) and *Subpolar Gyre* (SPG) (Iselin, 1936). It consists of two branches, formed in the Celtic Sea (∼46°N) and close to the Azores (∼35°N), merging north-west of the Iberian Peninsular (Fiúza, 1984; McCartney and Talley, 1982). Following the MARGO project (Fig. 5.5; Waelbroeck et al., 2009), the region in which the Azores branch of ENACW is formed shows a modern-LGM temperature anomaly of about -5°C. Present potential temperatures of this warmer ENACW source are $\theta = 13 - 18.5$°C (Fiúza, 1984), suggesting another source for the temperature anomaly reconstructed from the CWCs. The region from which the second branch originates, the Celtic Sea, exhibits modern-LGM temperature anomalies of up to -10°C (Fig. 5.5, Waelbroeck et al., 2009). Present potential temperatures of this ENACW source are $\theta = 10.0 - 12.2$°C (McCartney and Talley, 1982). Therefore, if the composition of the ENACW shifted towards a near pure Celtic sourced ENACW, intermediate water temperatures in the GoC could have dropped to the here reconstructed LGM temperatures around 0°C.
The second source of polar waters is the Antarctic polar region. Based on first analyses of εNd in CWCs from MD08-3231 (Fig. 4.9, Fig.6.8), a stronger northward penetration of more pure EAAIW was proposed during DOs (Dubois-Dauphin et al., 2016). However, EAAIW would have to maintain the cold temperature it exhibits at its polar origin over a significantly longer path crossing the warmer tropical region. Recently, Roesch, 2017 showed that although LGM Li/Mg temperatures also dropped significantly (∼ -6°C) in intermediate waters at the Angolan margin, minimal EAAIW temperatures reached were around 2°C. These reconstructions were performed in the same laboratory as this study using identical methods. This suggests, that while EAAIW could have caused a large temperature drop down to 2°C, observed intermediate temperatures around 0°C could not have been reached by EAAIW alone.
Here, it should be noted, that both scenarios could explain the presence of a cold intermediate water mass in the GoC, although first hints towards the ENACW scenario were given. Hence, it is possible that extreme temperatures obtained during the LGM are not, as first suspected, an artefact of the calibration, but mirror polar waters advancing south or northwards along the eastern Atlantic basin boundary at thermocline depths.

5.4.3 Stadial / interstadial temperature changes recorded in cold-water corals

The intermediate water temperatures reconstructed from CWCs in the sGoC coincide with Northern Hemisphere climate signals, in particular stadial and interstadials (HS, DO in Fig. 5.3). Tem-

perature oscillations span 0 – 6°C, which is about half the offset between present and LGM conditions. This difference in magnitude of fast short-termed changes in relation to the maximal offset between the Holocene and the LGM, reflects the same differences in magnitude seen in the climate signals from the Arctic ice core NGRIP.
Additionally, although colder intermediate water temperatures, typically down to ∼1°C, were reconstructed between 27 and 70 ka, the extremely cold temperatures during the LGM were not reached. Therefore, intermediate water temperature are not coldest during the southern-most position of the polar front (during HS), but during the period with lowest sea-levels and a general southward shift of the polar front which was less pronounced. In contrast SSTs, show coldest conditions in the GoC and a southern-most position of the Arctic polar front during stadials HS 1 (15.9 – 18.3 ka) and HS 4 (38.5 – 40 ka), but not during the late LGM (19 – 24 ka) (Fig. 5.4; (Eynaud et al., 2009)). This suggests a decoupling of surface and intermediate temperatures evolution, which could be explained by different contributions of source regions of mid-depth water masses penetrating the GoC (Chap. 5.4.2).
The strong correlation between stadials/interstadials oceanic changes in the sGoC and climate variations observed in NGRIP, confirms previous evidence from sediment cores in the nGoC (Bahr et al., 2015; Voelker et al., 2006). They also found a close correlation between rapid climate events observed in δ^{18}O of ice cores and changes in prevailing water masses in the nGoC. Both studies suggested a strengthening of MOW during stadials/interstadials. Additionally, a strengthening of MOW was proposed for glacial times like the LGM (Rogerson et al., 2005), with a deepening of the MSW in the nGoC. It remains open how these observations influenced the oceanic conditions in the sGoC.
Although this data set already shows a clear correlation between intermediate temperatures and short-termed climate changes, several gaps are left open in the record. Further analysis of CWC cores from the PDE and the MACP could fill these gaps and possibly resolve the periods of rapid change themselves. A first hint that this approach is realistic, can for example be seen during the climate cooling period around 35 ka, during which temperatures from four corals of both cores show a similar rapid decline. With growth rates of *L. pertusa* between 5 and 26 mm/a (Orejas et al., 2008; Gass and Roberts, 2006; Mortensen, 2001; Mortensen et al., 1998), high resolution multi-sampling analyses on well-preserved larger CWC fragments even have the potential to resolve the decadal warming periods of DOs.

5.5 Conclusions

A close correlation between thermocline temperatures, reconstructed from coralline Li/Mg ratios, and long-term atmospheric climate signals recorded in ice cores was established. Additionally, punctuated cooling or warming events seem to have influenced the intermediate temperature significantly. This clearly highlights the unique potential of the Li/Mg temperatures from CWCs as a proxy for the mid-depth thermal structure of the ocean.
A particularly high temporal resolution was achieved for the main growth period between 19 and 28 ka for which mean temperatures around 0°C were reconstructed. This observed glacial cooling of intermediate waters exceeds expectations from simple ocean models. Therefore, although physically possible, these polar temperatures strongly suggest the need to re-evaluate the empirical calibration curve relating coralline Li/Mg to absolute seawater temperatures. In addition to identifying possible systematic bias, further calibration efforts could reduce the uncertainty of the calibration itself to even below 1°C. This is currently the main contribution to the external

reproducibility of this temperature proxy, because analytical uncertainties of Li/Mg ratios are only around 1 – 2%.
Nevertheless, two possible scenarios that could explain the observed Li/Mg temperatures were proposed. The cooling of thermocline waters in the sGOC to 0°C can only be explained by the penetration of a mid-depth polar water mass (EAAIW or ENACW) into the temperate east Atlantic. This would lead to a strong rise of the thermocline towards shallow depths and to an increased density gradient between surface waters and the intermediate ocean. Due to the highly stratified water column downward diffusion of heat from the relatively warm mixed surface layer would be further inhibited.

Currently, ocean models for past, present and future ocean dynamics consider reconstructions from deep and surface water archives. Therefore, the highly dynamical thermocline, which represents the link between these two regimes, is often not well represented and unconstrained by observations. While the observations presented in this study are based on only two records from one region, it is clear that analyses on CWCs from different locations throughout the Atlantic have the potential to provide further evidence of the importance of thermocline dynamics when considering future and past oceanic dynamics. Furthermore, multi-sampling analyses on large CWC fragments can provide records of decadal temperature variabilities, for example tracing the movement of cold fronts. Therefore, conceptual and computational models simulating rapid oceanic changes, in particular during Heinrich stadials or Dansgaard-Oeschger cycles, could possibly be improved greatly by implementing observations of past temperature dynamics in typical thermocline depths (70 – 1000 m) retrieved from CWCs.

In the following two chapters 6 and 7, radiogenic Nd isotopes (εNd) and ^{14}C-reservoir ages will be analysed. Both proxies have the potential to trace water mass changes to indicate the presence of polar water masses in sGoC and can therefore help to further assess the proposed scenarios.

6 Changes in water mass provenance recorded by εNd in CWCs and sediment

6.1 Introduction

In this study, I combine εNd of two independent paleoceanographic archives to gain insight into water mass provenance changes to further verify or confute the proposed penetration of polar waters into the southern Gulf of Cádiz. The εNd analysis on the CWCs, already U-series dated and analysed for Li/Mg temperatures, will be combined with εNd records of Fe-Mn oxyhydroxides in bulk sediment of two hemipelagic sediment cores exhibiting high accumulation rates. This will enable me to fill time gaps left by the CWC analyses, including the period of deglaciation. Additionally, during periods of overlapping records both differences and similarities of CWCs to sediment will be highlighted, providing supplementary information and confirming observed patterns.

6.2 Materials and methods

6.2.1 Seawater profiles of modern εNd in the sGoC

Present εNd signatures of the three main water masses before entering the GoC are -9.4 for pure *Mediterranean Outflow Water* (MOW) at the Strait of Gibraltar (Tachikawa et al., 2004), around -11.2 for *Eastern Antarctic Intermediate Water* (EAAIW) south of the GoC (Stichel et al., 2015; Rickli et al., 2009) and -11 to -12 for *Eastern North Atlantic Central Water* (ENACW; Stichel et al., 2015). Nd concentrations and salinities are $\sim$ 25 pmol/kg and $>$ 38.4 psu (MOW), $\sim$ 22 pmol/kg and 35 psu (EAAIW), and $\sim$ 15 – 18 pmol/kg and 35.5 psu (ENACW). Therefore, EAAIW and ENACW do not differ strongly in εNd and are mainly distinguishable by salinity analyses.
Seawater Nd analysis in the sGoC were recently carried out on three stations (Fig. 6.1; (Dubois-Dauphin et al., 2017a; Dubois-Dauphin et al., 2016)). Compared to the Northeast Atlantic, where εNd varies between -16.5 and -9.5 (Lacan and Jeandel, 2005a), signatures in the GoC cover a small range of -11.7 to -9.4. Water masses present in the sGoC were allocated to their respective depths by εNd, salinity and temperature analyses: *Subarctic Water* (SAW), ENACW, EAAIW and *Mediterranean Sea Water* (MSW: upper (MSU) and lower (MSL)) (Fig. 6.1(b); (Dubois-Dauphin et al., 2017a)).
Present isotopic compositions of radiogenic Nd at the depth of MD08-3231 (Gamma Mound) are estimated by the deepest seawater analysis from station Beta-1 (35°17.46'N, 06°47.16'W;

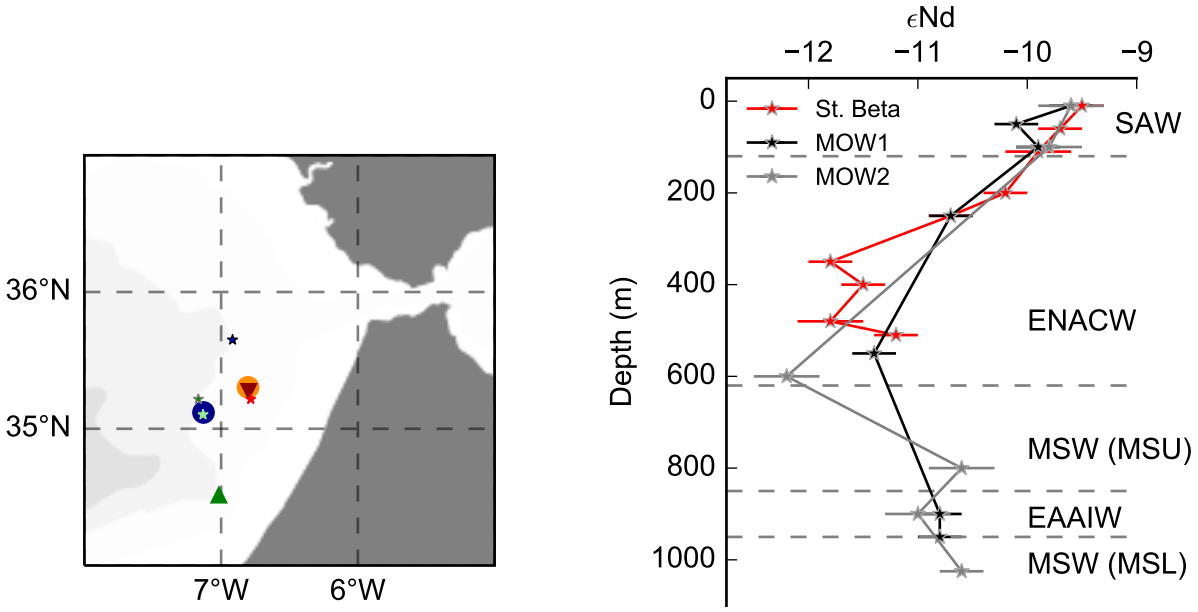

(a) Site locations for εNd analysis

(b) εNd profiles for seawater stations

Figure 6.1: (a) Map of site locations for the εNd analysis
Coral sites are shown as circles with MD08-3231 (orange) and GeoB-18141-01 (blue). Sediment cores are depicted as triangles with MD08-3227 (dark red) and MD04-2805-CQ (green). Small stars are seawater stations with GeoB-18136-01 (lightgreen; (Hebbeln et al., 2015)) used for temperature, salinity and dissolved oxygen analysis and stations MOW1 (black), MOW2 (grey) and Beta-1 (red) used for εNd analysis in this chapter.
(b) εNd profiles of the three seawater stations MOW1, MOW2 and Beta-1. The colours are the same as in (a) (data from Dubois-Dauphin et al., 2017a; Dubois-Dauphin et al., 2016).

510 m water depth; Fig. 6.1(a)), exhibiting -11.2 ± 0.2 ε units (Fig. 6.1(b); (Dubois-Dauphin et al., 2017a; Van Rooij et al., 2013)). An εNd of about -10.9 ± 0.4 in 994 m water depth for GeoB-18141-01 (Wulle Mound) was extrapolated from station MOW2 located close to this core (35°13.11'N, 07°10.56'W, 1025 m water depth; Fig: 6.1(a)). As for the temperature reconstructions, past sea-level changes have to be taken into account. For the LGM this implies ≈ -130 m (Lambeck et al., 2014) while for the Marine Isotope Stage 3 (MIS 3) the global sea-level was 60 - 80 m lower than during the Holocene (Spratt and Lisiecki, 2016). Hence, during the LGM the reefs grew in roughly 420 m and 810 m water depth corresponding to present day εNd values of -11.5 ± 0.4 and -10.7 ± 0.4, respectively. Assuming that circulation patterns remained unchanged during the LGM and only sea-level varied, according to Fig: 6.1(a) Gamma Mound would have bathed in ENACW and Wulle Mound would have been washed in a larger fraction of MSW. Therefore, a change in water mass observed by the CWCs of the deeper core is expected (GeoB18141-01). During MIS 3, water depths were 470 – 490 m for MD08-3231 and 860 – 880 m for GeoB-18141-01. Hence, taking only MIS 3 sea-level changes into account, both coral reefs would still bath in the same water masses as in modern times.
In addition to the two coral-bearing cores MD08-3231 and GeoB-18141-01, two hemipelagic sediment cores with high accumulation rates (14 – 100 cm/ka) from the sGoC were analysed

for radiogenic εNd (Fig. 6.1(a), Chap. 6.2.3). Estimated modern εNd signatures in the depth of sediment core MD08-3227 (642 m) are between -11.2 and -11.9. As εNd signatures in depths between 400 and 700 m vary, this range was chosen between the lowest data point of profile station Beta-1 and the extrapolation of profile MOW 2 to the water depth of MD08-3227. Considering sea-level changes, MD08-3227 was located in ∼ 510 m during the LGM and in 560 – 580 m paleo water depth during MIS 3. This leads to a corresponding εNd range of -11.2 to -12.7 (LGM) and -11.2 to -12.6, where -11.2 is the signature of station Beta-1 (above MD08-3227). For the southern located core MD04-2805-CQ (859 m water depth), the seawater profile MOW2 is used. Estimated εNd signatures are -10.8 ± 0.4 in modern conditions and -11.2 ± 0.4 (∼ 730 m) when LGM sea level changes are applied.
It should be noted that the estimation of εNd signatures at the core sites relies on very few measurements that are unlikely to capture the range of hydrodynamic variability at each site.

6.2.2 Cold-water coral bearing cores

Due to low Nd concentrations in CWCs on the order of ng/g (Nd/Ca), sample sizes required for radiogenic Nd isotope analysis are roughly 500 mg aragonite. As coral fragments retrieved from the sediment cores MD08-3231 and GeoB-18141-01 were sometimes small or porous, not every coral dated could be analysed for its Nd isotopes. In total fifty-eight well-preserved fossil CWCs were analysed for their radiogenic Nd isotopes, twenty-eight from MD08-3231 and thirty from GeoB-18141-01. For details concerning the coral-bearing sediment cores please refer to chapter 4.2.1 and table A.3.

6.2.3 Hemipelagic sediment cores

Piston core MD08-3227 (35°16.28'N, 06°47.89'W; 642 m water depth) was recovered on the same cruise as the coral-bearing core MD08-3231 (Tab. A.6; (Rooij et al., 2008)). The working half was stored in Ostend, Belgium, and analysed in detail by Delivet, 2017, who also determined the age model for the upper 17 m used here (Fig. 6.2(b), Tab. A.8). Sediment accumulation in core MD08-3227 was high during the last glacial (33 - 46 ka: 86 cm/ka). After a major hiatus between 33 and 19 ka the accumulation rate during deglaciation and Holocene was about a third of glacial accumulation (28 cm/ka).
Radiogenic Nd isotope analyses were performed on the archive half stored in the core repository of LSCE (Gif-sur-Yvette, France). Sampled U-channels (small rectangular plastic liners) were cut into 2 cm pieces at IUP and freeze-dried. For the Nd analysis the core was sampled every 10 cm in the top metre and every 20 cm down to 11 m core depth, which corresponds to a time resolution of 230 to 715 a per sample.
Sediment core MD04-2805-CQ (34°30.99'N, 07°00.99'W; 859 m water depth) was retrieved in 2004 during the *R/V Marion Dufresne* cruise 'MD 140 / Priviledge' (Tab. A.6; (Turon et al., 2004)). The age model of MD04-2805-CQ covers ages from 5 to 28 ka (Fig. 6.2(a) and Tab. A.8; ()Penaud et al., 2010)). The glacial accumulation rate between 28 and 21 ka was about 59 cm/ka, decreasing to 16 cm/ka from 21 to 16 ka. This is followed by a significant increased accumulation of 100 cm/ka until 14.51 ka after which sediment accumulation slows to 14 cm/ka stopping 5.8 ka ago.
Radiogenic Nd analyses were done on part (f) stored at EPOC (Environnements et Paléoenvironnements Océaniques et Continentaux, University of Bordeaux, France). Samples from U-channels

were cut into 1 cm pieces at IUP and freeze-dried. For the Nd analysis sediment core MD08-2805 CQ was sampled every 5 cm in the top metre and every 10 cm for core depths below, corresponding to a time resolution between 50 and 360 a.

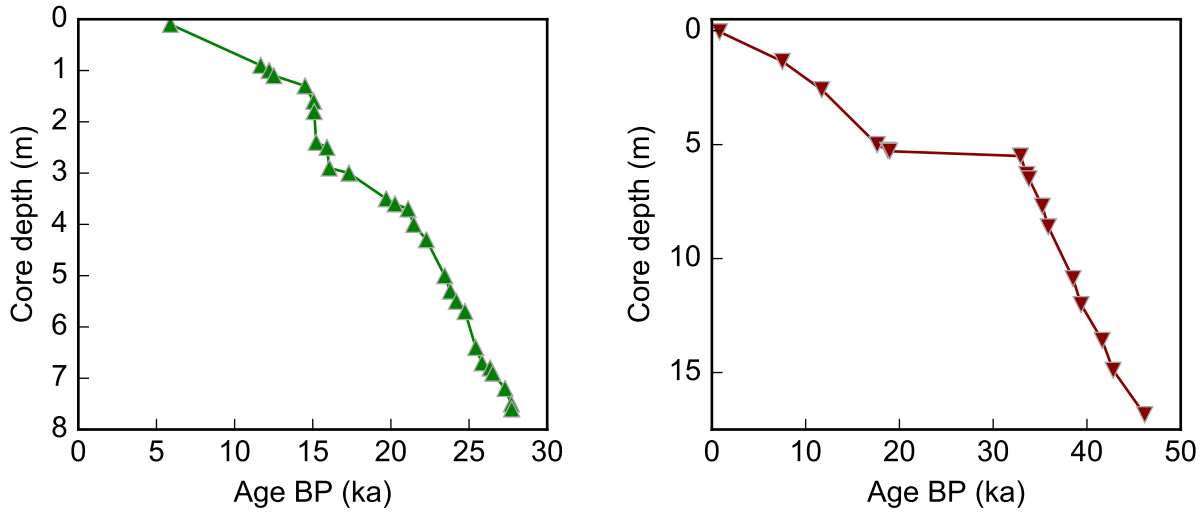

(a) Depth-age model of MD04-2805-CQ

(b) Depth-age model of MD08-3227

Figure 6.2: Depth-age models of hemipelagic sediment cores based on foraminifera ^{14}C dates and $\delta^{18}O$ stratigraphy
(a) The sediment core MD04-2805-CQ covers a period of 5 – 27 ka (Penaud et al., 2010).
(b) The top 17 m of sediment core MD08-3227 cover the time period 0 – 48 ka with a hiatus between 19 and 33 ka (Delivet, 2017).

6.2.4 Methods

Cold-water Corals

From the mechanically cleaned coral samples for U/Th analysis (Chap. 4.2.2) an extra ∼ 500 mg aliquot was taken for Nd-analysis. Mechanical cleaning and chemical Nd extraction procedures were adapted after Copard et al., 2010 and extracted Nd fractions were analysed on a Thermo-Scientific Neptune Plus Multi-Collector Inductively Coupled Plasma Mass Spectrometer (MC-ICP-MS) (Dubois-Dauphin et al., 2017a; Pöppelmeier, 2016). Corals from MD08-3231 were analysed in two batches. The first batch was prepared and analysed during Niclas Rieger's Bachelor's project in 2015 (Rieger, 2015). These corals were prepared and analysed at LSCE. The second batch of CWCs from MD08-3231 and CWCs from core GeoB-18141-01 was analysed at IUP in 2017. The mechanical and chemical cleaning protocol and Nd extraction procedures were identical in both laboratories. MC-ICPMS measurement procedures of $^{143}Nd/^{144}Nd$ ratios at LSCE are described by Dubois-Dauphin et al., 2017a and $^{143}Nd/^{144}Nd$ analysis at IUP in Pöppelmeier, 2016. The external reproducibility (2σ) for measurements at LSCE of 0.24 ε units were obtained from repeated measurements of the La Jolla standard (Tab. 6.1; (Lugmair et al., 1983)). Analysis at IUP yielded an external reproducibility of 0.17 ε units deduced from repeated JNdi-1 (Tanaka et al., 2000) and in-house target analysis called VWR (Tab. 6.1). The analytical

uncertainty for each CWC was taken as the larger of its internal and external reproducibility. Due to the quality control for U-series dating, two data points from core MD08-3231 and four data points from GeoB-18141-01 were discarded (Chap. 4.3.2). Additionally, four CWCs from core GeoB-18141-01 exhibiting extremely low Nd intensities during measurements on the mass spectrometer (< 1 V in ^{144}Nd) leading to relatively high uncertainties (typically > 0.4 ε units) were also considered unreliable.

Sediment

After freeze-drying the sediment, samples were milled to a homogeneous powder of which 250 to 300 mg were taken for Nd-analysis. The extraction of the authigenic Nd from Fe-Mn oxy-hydroxides in bulk sediment was performed after Blaser et al., 2016. The instrumental analysis of sediment core MD04-2805-CQ was carried out in January and April 2016 (Helmholtz Centre for Ocean Research, Kiel, Germany). External reproducibilities, determined by repeated measurements of standard JNdi-1 and the secondary in-house target 50SPEX, were between 0.12, 0.17 and 0.21 ε units varying between sessions (Tab. 6.1: MD04-2805-CQ). The analytical uncertainty for each sample was taken as the larger of its internal and the external reproducibility.
Sediment core MD08-3227 was chemically prepared at IUP in June 2017. Instrumental analysis on MC-ICP-MS was performed in September 2017. Repeated analyses of JNdi-1 and the in-house target VWR lead to an external reproducibility of 0.23 ε units (Tab. 6.1).
No inter-calibration between the three laboratories has been performed. Therefore, additional uncertainties might be introduced by the fact that measurements were carried out at three institutes. However, the analysis of the same standards with similar results gives confidence in the different results.

Table 6.1: Summary of standards and in-house targets for radiogenic Nd isotope analysis. Grey cells symbolise 2σ used for the respective session.

Measurement	Standard	$^{143}Nd/^{144}Nd$	$2\sigma(^{143}Nd/^{144}Nd)$	n	$2\,\sigma$ (ε unit)
Lugmair et al., 1983	La Jolla	0.511858	0.000007		
Tanaka et al., 2000	JNdi-1	0.512115	0.000006		
MD08-3231 Gif	La Jolla	0.511856	0.000012	(n = 19)	0.24
MD08-3231 IUP	JNdi-1	0.512098	0.000008	(n = 73)	0.16
MD08-3231 IUP	VWR	0.512210	0.000008	(n = 10)	0.17
GeoB-18141-01 IUP	JNdi-1	0.512098	0.000008	(n = 73)	0.16
GeoB18141-01 IUP	VWR	0.512210	0.000008	(n = 10)	0.17
MD04-2805-CQ GEOMAR 1a	JNdi-1	0.512132	0.000006	(n = 18)	0.11
MD04-2805-CQ GEOMAR 1a	50SPEX	0.511087	0.000009	(n = 17)	0.17
MD04-2805-CQ GEOMAR 1b	JNdi-1	0.512068	0.000018	(n = 25)	0.35
MD04-2805-CQ GEOMAR 1b	50SPEX	0.511084	0.000011	(n = 12)	0.21
MD04-2805-CQ GEOMAR 1c	JNdi-1	0.512112	0.000006	(n = 20)	0.12
MD04-2805-CQ GEOMAR 1c	50SPEX	0.511086	0.000007	(n = 10)	0.13
MD04-2805-CQ GEOMAR 2a	JNdi-1	0.512020	0.000008	(n = 15)	0.15
MD04-2805-CQ GEOMAR 2a	50SPEX	0.511088	0.000005	(n = 7)	0.12
MD04-2805-CQ GEOMAR 2b	JNdi-1	0.512013	0.000014	(n = 14)	0.27
MD04-2805-CQ GEOMAR 2b	50SPEX	0.511091	0.000007	(n = 11)	0.14
MD08-3227 IUP	JNdi-1	0.512115	0.000012	(n = 84)	0.37
MD08-3227 IUP	VWR	0.512206	0.000012	(n = 12)	0.23

6.3 Results

6.3.1 Radiogenic Nd isotopes recorded in cold-water corals

For both sites of coral-bearing cores, glacial isotopic compositions of radiogenic Nd reconstructed from aragonitic cold-water corals are shifted towards more radiogenic signatures (1.5 – 3 ε units) compared to present seawater (Fig. 6.3, Tab. A.1 and A.6).
CWCs from core MD08-3231 exhibit LGM εNd signatures of -9.13 $\pm$ 0.19 (n = 10, 2σ of mean) (Fig. 6.3(a)). Within uncertainties no variations can be observed within the period of the LGM. Variations in εNd occurred from 26.6 $\pm$ 0.59 ka to 27.6 $\pm$ 0.9 ka and 33.74 $\pm$ 0.8 ka to 33.19 $\pm$ 0.09 ka, suggesting rapid water mass changes that coincided with DO cycles 3 and 6 (Fig. 6.3(a) & 6.4). Around DO 3, four CWCs show slightly less radiogenic Nd than the LGM signal with an average of -9.53 $\pm$ 0.22 (n = 4, 2σ of mean) and a maximum decrease to -9.71 $\pm$ 0.25. At the same time five CWCs recorded signatures similar to the LGM (-9.10 $\pm$ 0.11; n = 5, 2σ of mean). A jump occurred from -9.94 $\pm$ 0.24 to -9.09 $\pm$ 0.24 which coincides with the rapid warming during DO 6. All other CWCs in MD08-3231 grown during MIS 3 recorded moderately less radiogenic signatures of -9.40 $\pm$ 0.13 (n = 5, 2σ of mean), which is similar to the less radiogenic signal around DOs.
In GeoB-18141-01, CWCs that grew during the LGM recorded a higher variation of εNd signatures than MD08-3231 (-9.29 $\pm$ 0.44; n = 12, 2σ of mean). This is mainly due to an excursion towards less radiogenic Nd signatures around 22 ka with an average of -9.60 $\pm$ 0.05 (n = 3, 2σ of mean) and the lowest signature at -9.66 $\pm$ 0.22 (Fig. 6.3(b)). At the start of this period which coincides with DO 2, an εNd signature of -9.03 $\pm$ 0.17 was recorded in one coral (Fig. 6.4), suggesting a similarly rapid water mass change as recorded in MD08-3231 around DO 3. Excluding this excursion, GeoB-18141-01 and MD08-3231 εNd signals during LGM are equal within their uncertainties (-9.19 $\pm$ 0.31; n = 9, 2σ of mean). A second fast variation occurred between 34.53 $\pm$ 0.11 ka and 34.82 $\pm$ 0.10 ka, although no direct correlation to a DO cycle or other rapid climate changes as Heinrich stadials can be observed. Other CWCs in MIS 3 recorded εNd signatures around -9.37 $\pm$ 0.13 (n=5, 2σ of mean), equal within uncertainties to MD08-3231.

6.3.2 Radiogenic Nd isotopes recorded in hemipelagic sediment

Sediment core MD04-2805-CQ covers the complete period between 27.8 and 5.2 ka exhibiting a variable time resolution. The material in the analysed depth of core MD08-3227 accumulated between 38.6 and 0.6 ka with a major hiatus (covering the LGM) between 33 and 18.6 ka. A hiatus is often caused by strong currents hindering the accumulation of sediment or reflects winnowing of deposited sediment. The resumption of sediment accumulation at core site MD08-3227 coincides with the end of increased CWC growth observed in both coral-bearing cores. MD08-3227 is located close to MD08-3231 and stronger currents are known to favour high CWC activity by delivering food (e.g. Mienis et al., 2007; Dorschel et al., 2005; White et al., 2005). Thus, possibly, the strong currents delivering food to the CWCs are the cause for the hiatus observed in sediment core MD08-3227.
Similar to εNd signatures of the CWCs, glacial Fe-Mn oxyhydroxides in bulk sediment from both hemipelagic sediment cores show more radiogenic glacial Nd isotope signatures than present-day conditions with an offset of about 1.4 – 3.1 ε units (Fig. 6.4, Tab. A.2).
The MIS 3 signature recorded in MD08-3227 (37.7 – 33 ka) is -9.32 $\pm$ 0.23 (n=21, 2σ of mean). This signal is equal to εNd recorded in CWCs from both coral-bearing cores. The constant

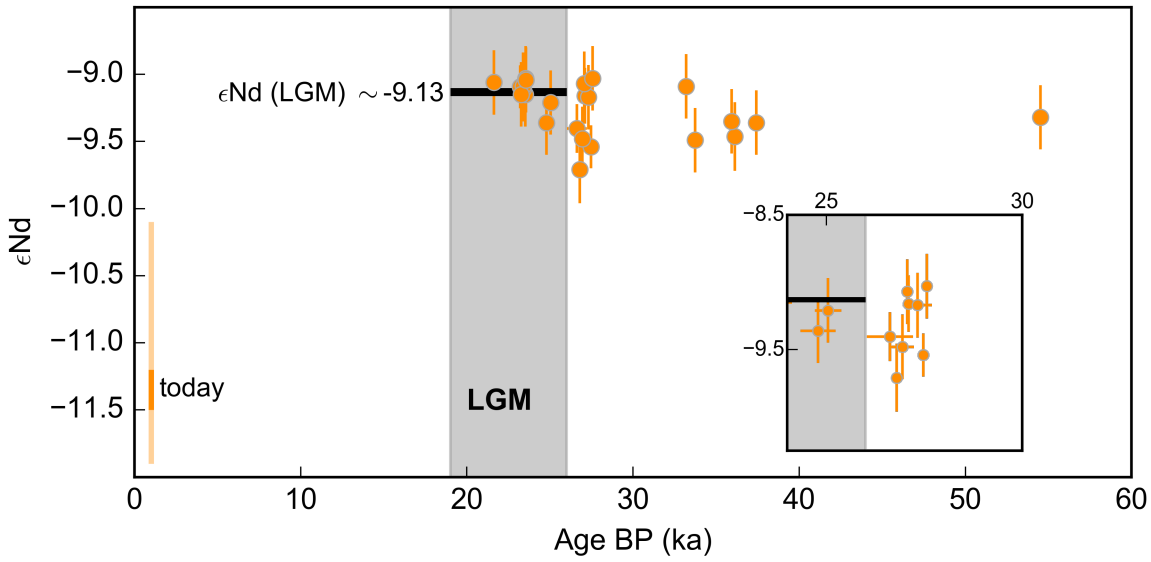

(a) ε Nd signatures recorded in CWCs from MD08-3231

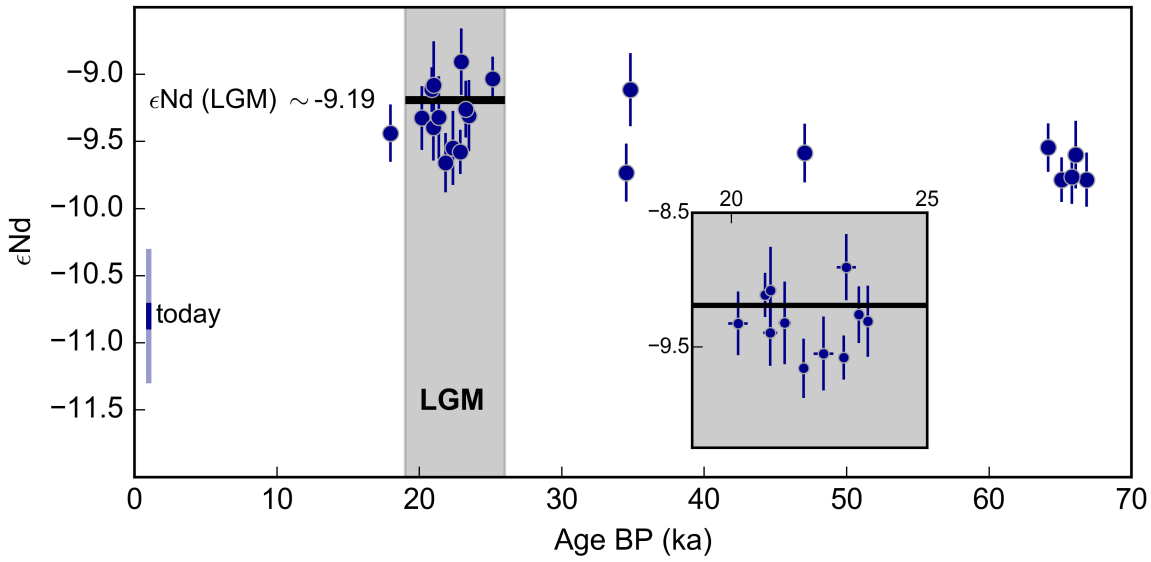

(b) ε Nd signatures recorded in CWCs from GeoB-18141-01

Figure 6.3: εNd signatures in CWCs
Black bars depict the mean over the LGM (grey shaded area). Estimated modern seawater signatures at the core sites are given as the orange/blue bar on the left with shaded bars representing the uncertainty. The zooms highlight the variation around 27 ka (MD08-3231, (a)) and 23 ka (GeoB-18141-01, (b)).

conditions were interrupted by two fast variations between 38.6 and 37 ka and around 33.5 ka coinciding with DO 8 and 6. The variation around DO 8 spans -9.15 ± 0.23 to -9.73 ± 0.23. The εNd range during DO 6 is slightly larger spanning signatures from -9.94 ± 0.23 to -9.08 ± 0.23. Additionally, the rapid change in εNd around DO 6 was also observed in MD08-3231 CWCs. The fast changes in water mass provenance around 27 ka with signatures between -9.26 ± 0.21

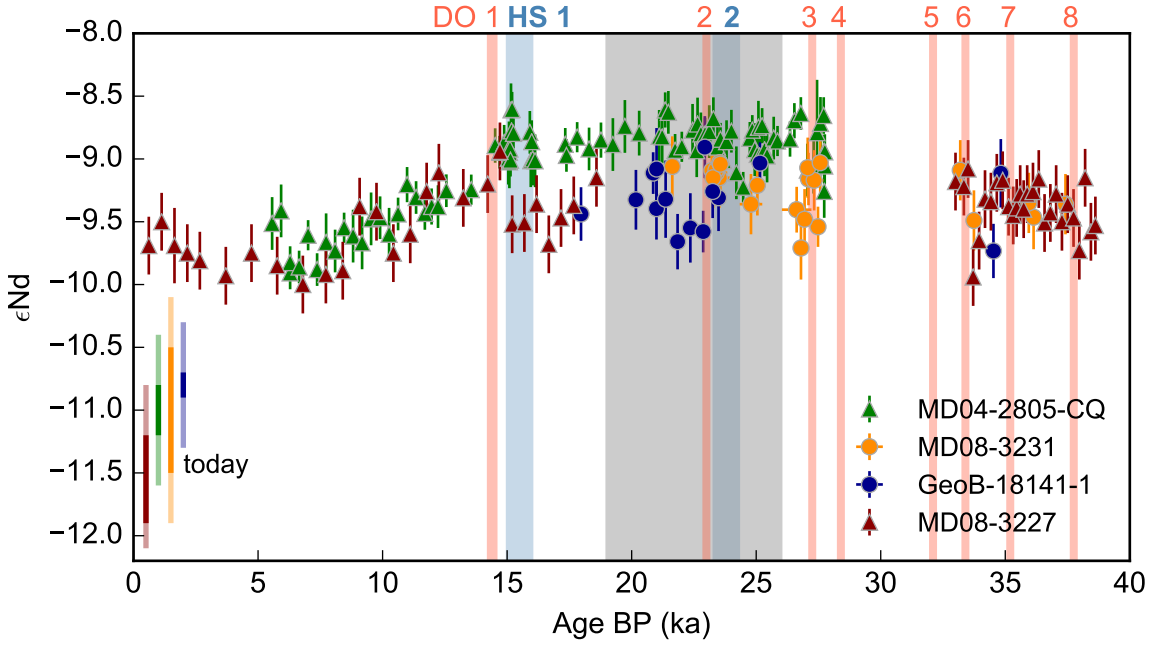

Figure 6.4: Radiogenic Nd isotopes in hemipleagic sediment and coral-bearing cores
Sediment cores are shown as triangles with green for MD04-2805-CQ and red for MD08-3227. Coral bearing cores have circular symbols in blue (GeoB-18141-01) and orange (MD08-3231). Ranges for seawater εNd signatures extrapolated from measurements by Dubois-Dauphin et al., 2017a; Dubois-Dauphin et al., 2016 are shown on the left as bars with shaded bars for uncertainties (same colours as cores).
Red lines show DOs 1 – 8, blue shaded areas HS 1 and 2 , and the LGM is represented by the grey shaded area.

and -8.64 ± 0.13 recorded in the lowest depths of MD04-2805-CQ coincide with DO 3 and were also observed in MD08-3231 CWCs (Fig. 6.4). The overall constant εNd signature during the LGM (-8.84 ± 0.26; n = 35, 2σ of mean) is interrupted by a further rapid excursion towards less radiogenic signals at around 24.5 ka to -9.22 ± 0.12 (n = 2). This excursion, coinciding with the start of HS 2 known for extreme oceanic changes on very short time scales, is possibly seen in MD08-3231 CWCs. However, the slight trend towards less radiogenic Nd isotopic composition recorded in the corals is within uncertainties. Comparing LGM signatures between the CWCs and hemipelagic sediment signals, CWCs recorded slightly less radiogenic εNd than seen in MD04-2805-CQ. GeoB-18141-01 LGM signatures are offset to the sediment of MD04-2805-CQ by -0.34 ε units and MD08-3231 CWCS are -0.29 less radiogenic, which is equal within uncertainties (Fig. 6.4).
18.6 ka ago, sediment started accumulating again at site MD08-3227. This coincides with the end of CWC occurrence in both coral-bearing cores (Fig. 4.6 and 4.8), suggesting a weakened current not providing the CWCs with sufficient food. εNd signals from 18.6 – 15.2 ka are -9.44 ± 0.3 (n = 7, 2σ of mean) and equal within uncertainties to signatures in LGM CWCs, in particular from core GeoB-18141-01. This implies an offset of 0.6 ε units towards less radiogenic signals to the more southern located sediment core MD04-2805-CQ. At around 15 ka the εNd signatures (∼ -8.9, n = 18 for MD04-2805-CQ and n = 1 for MD08-3227) of both sediment cores converge,

coinciding with the periods of HS 1 and DO 1. During deglaciation, both follow the same trend towards less radiogenic isotopic compositions of Nd to -9.87 ± 0.13 (n = 2) in MD08-2805-CQ and -10 ± 0.23 in MD08-3227 at 6.9 ka. This implies an εNd change of about -1.1 ε units. At this time, least radiogenic signals are reached, although still exhibiting an offset to modern seawater signatures between 0.5 and 2 ε units. In the uppermost layers MD04-2805-CQ exhibits a small excursion towards more radiogenic isotopic compositions before accumulation stopped. Signatures between 6 and 0.6 ka reconstructed from MD08-3227 did not change within uncertainties (-9.7 ± 0.12; n = 8, 2σ of mean). The uppermost layer dated to 0.6 ka (-9.69 ± 0.23) implies an offset to the measured modern seawater εNd value close to the sample site of around 1.3 – 2.4 ε units.

6.4 Discussion

This is the first study that directly combines records of the exact same tracer in two independent archives. Both archives, cold-water corals and Fe-Mn oxyhydroxides in bulk sediment, provided complementary information on εNd signatures resolving different time scales, periods and locations in the sGoC.
As expected, CWCs precisely dated by U-series dating, overall exhibit more frequent εNd fluctuations than the εNd evolution recorded in sediment affected by bioturbation. However, most of the fluctuations that are not observed in the sediment records are within uncertainties of εNd analyses in corals. Therefore, improvement of the external reproducibility for εNd analyses is needed to discern if the variations observed in the coral record are an artefact of our analyses or if they capture short-termed fluctuations not resolved in the archive sediment. While the gap of coral growth during deglaciation and Holocene could be filled by adding the sediment based records, a gap between 28 and 33 ka remains open.

Despite these limitations, the isotopic composition of radiogenic Nd recorded in CWCs and Fe-Mn oxyhydroxides in bulk sediment revealed several important patterns. First, where present, glacial CWCs and MD08-3227 sediment signatures are equal, while MD04-2805-CQ is slightly more radiogenic in εNd (0.29 – 0.6 ε units). Second, the largest change in εNd (-1.1 ε units) can be observed in both hemipelagic sediment cores and occurs during deglaciation (15 – 6.9 ka). Third, εNd signals retrieved from modern sediment leachates (MD08-3227) exhibit more radiogenic isotopic compositions than modern seawater signatures at the core sites (∼ 1 – 2 ε units).
In the following, the apparent modern offset between εNd in core top Fe-Mn oxyhydroxides in bulk sediment and seawater will be examined. Afterwards, the εNd evolution will be considered in combination with Li/Mg temperatures (Chap. 5) to discuss possible oceanic scenarios, that could have prevailed in the past and lead to the observed radiogenic Nd isotope evolution along the Moroccan shelf.

6.4.1 The modern sediment to seawater offset in εNd

The three intermediate water masses entering the GoC are MOW, ENACW and EAAIW (Chap. 3). As mentioned in chapter 6.2, the present εNd signature and Nd concentration [Nd] of the MOW end-member is -9.4 and ∼ 25 pmol/kg respectively (Tachikawa et al., 2004), while EAAIW (-11.2 and [Nd] ∼ 22 pmol/kg) (Stichel et al., 2015; Rickli et al., 2009) and ENACW (-11 to -12 and [Nd] ∼ 15 – 18 pmol/kg) (Stichel et al., 2015) have similar εNd values, prior to entering the

GoC.
The modern εNd signature recorded in the core top of MD08-3227 is -9.7 $\pm$ 0.23, hence significantly higher than the from measurements extrapolated seawater value of (-11.2 to -11.9) $\pm$ 0.4. Assuming MOW as the main water mass and either ENACW or EAAIW as the water mass mixing into MOW, the mixing can be described as

$$f_{MOW} \times [Nd]_{MOW} \times \varepsilon Nd_{MOW} + f_i \times [Nd]_i \times \varepsilon Nd_i = [Nd]_m \times \varepsilon Nd_m \quad (6.1)$$

with i = ENACW or EAAIW, and εNd_m representing the measured signature. $f_{i,MOW}$ is the fraction in % of MOW or i in the present water mass 'mixture'. $[Nd]_m$ can be calculated by

$$[Nd]_{MOW} \times \varepsilon Nd_{MOW} + [Nd]_i \times \varepsilon Nd_i = [Nd]_m \quad (6.2)$$

and

$$f_{MOW} + f_i = 1 \quad (6.3)$$

The proportion of entrained EAAIW or ENACW needed to obtain the observed MSW signature of -9.7 ranges from around 15% to 30%. The required dominant water mass suggested by core top analyses of MD08-3227 is MOW (70 – 85%). However, seawater salinities observed from any seawater profile suggest salinities between 35.6 and 36 maximum at the core site MD08-3227. Therefore, maximum MOW proportions expected from salinity mixing models lie between 4 and 30% (e.g. Louarn and Morin, 2011). Applying these proportions of MOW, εNd signatures observed in modern seawater are reached.
There are two directions of argumentation that can be taken to explain this clear discrepancy between modern core top εNd and seawater signatures, extrapolated from nearby seawater profiles. Either the isotopic composition of radiogenic Nd isotopes reconstructed from sediment leachates does not mirror seawater conditions above the sediment, or the seawater values extrapolated from the measured profiles are not representative for the water mass seen by the archive sediment.
Using leachates of Fe-Mn oxyhydroxides in bulk sediment to extract the εNd signatures of the authigenic fraction, always leaves the possibility that part of the detrital fraction is also leached into solution during the leaching procedure with acid. However, Blaser et al., 2016 established the here used method including numerous tests to avoid leaching of the detritus. The only tests in which signatures were shifted towards more radiogenic signatures were performed on sediment sections containing large amounts of volcanic ash particles (Blaser et al., 2016), but in the sGoC no source for significant amounts of ash particles is known. Additionally, elemental ratios like Al/Nd used to identify detrital leaching (Gutjahr et al., 2007) did not show any salience. Furthermore, it was shown that the detrital fraction of sediment in the sGoC obtains εNd signatures around -11.8, which was attributed to Saharan dust (Grousset et al., 1988). Therefore, if part of the detrital fraction was leached into solution, the signals measured should exhibit less radiogenic signals than seawater.
Other possible process that can alter the radiogenic isotopic composition of Nd of the sediment are pore water processes carrying Nd through the sediment. A study from the North Pacific showed that core top signatures resembled pore water εNd signatures rather than seawater signatures just above (Du et al., 2016). But, the North Pacific is characterised by low oxygen bottom waters not found in the modern Atlantic and similar studies have not made these observations for any Atlantic sediments. However, for the Moroccan margin it should be noted that sediment fluid venting was recorded, indicated by the presence of mud-volcanoes and punctuated gas hydrate

leakage from the sediment (e.g. Foubert et al., 2008). CH_4 reduction can lead to an acidification of pore waters, which could result in the remobilisation of Nd, subsequently imprinting the local bottom waters. Nevertheless, this process is unlikely to have caused the seawater to core top offset, as such a presence of gas leakages should have been visible in the bottom water samples studied in Dubois-Dauphin et al., 2017a; Dubois-Dauphin et al., 2016.

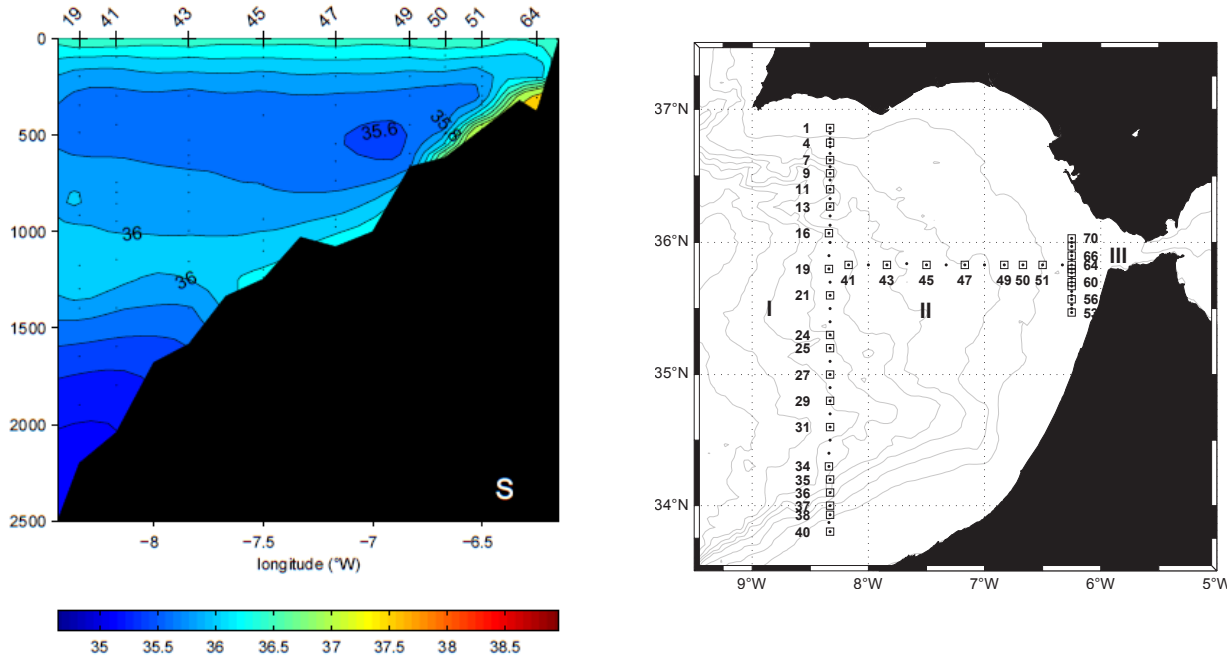

(a) Salinity section along the shelf

(b) Sites of salinity analysis used for section in (a)

Figure 6.5: An extremely narrow MSW layer is observed by a salinity maximum in depths between roughly 200 and 700 m cascading down the shelf in front of the Strait of Gibraltar. Figure adjusted from Louarn and Morin, 2011

An east-west section starting just outside the Strait of Gibraltar down the shelf shows how close to the sea floor MSW creeps down the slope (Fig. 6.5; (Louarn and Morin, 2011)). If seawater samples were not taken right above the sea floor, it is possible that the bulk of MSW was not sampled. In the case of station Beta-1 and MOW2, however, this is unlikely as the deepest seawater εNd analyses were performed on samples taken 10 and 25 m above sea floor in an area of rough topography.

Another process that could change the radiogenic Nd isotopic composition is based on the complex bathymetry of the shelf. Internal diurnal waves change water masses present in certain depths on hourly time scales. This can be observed at CTD station GeoB-18141-01-10, which was sampled several times as a 'yoyo' station over a time period of 10 hours (Fig. 6.6(a) – 6.6(d)) (MoccoMeBo cruise 2014; (Hebbeln et al., 2015)). Temperature and salinity anomalies can be observed throughout all depths, in particular between roughly 150 m and 400 – 500 m water depth. The time scale on which anomalies occur seems to coincide with tidal cycles, suggesting a periodic pattern. No measurements of currents were carried out, which leaves the question whether flow directions change accordingly open. This observation implies that, while oceanic archives at one location record the mean over the observed variation, the punctuated timing of

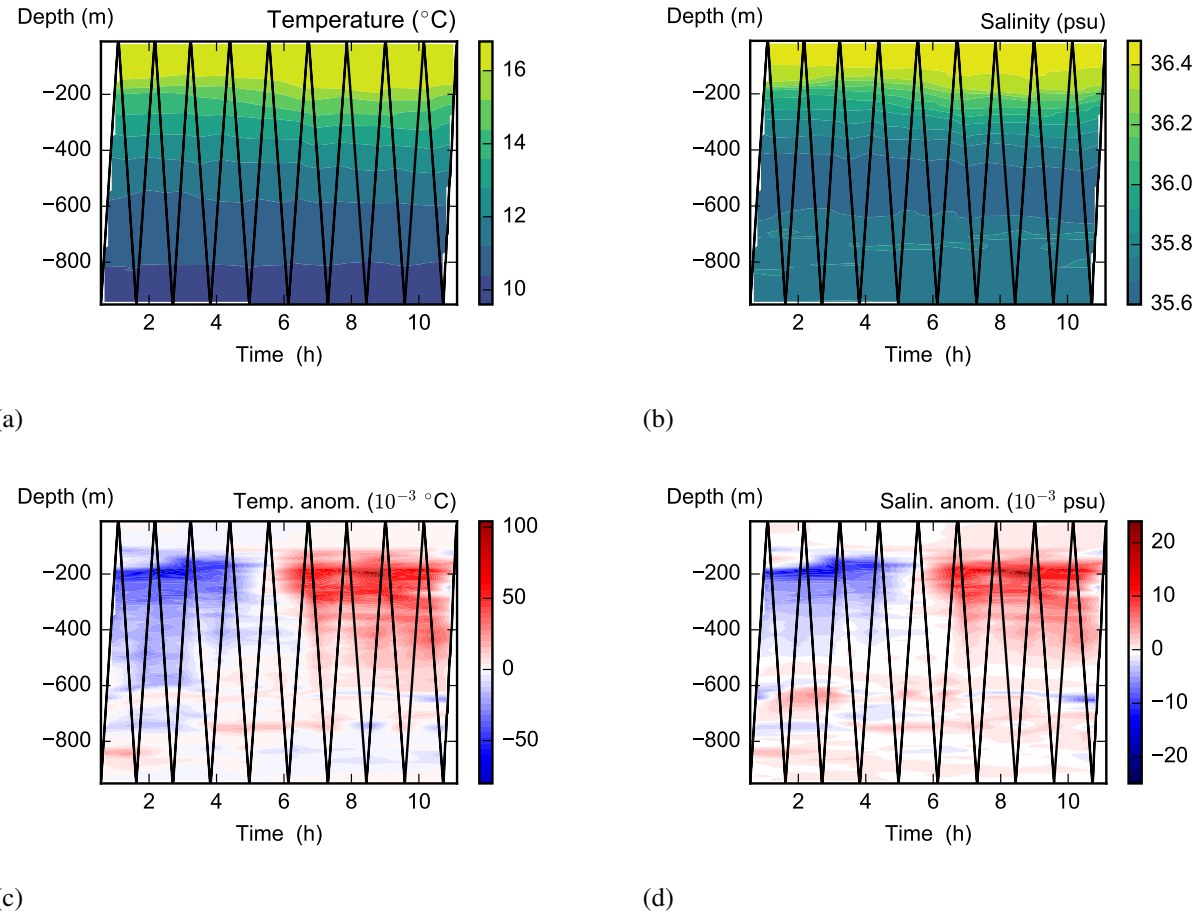

Figure 6.6: Yoyo CTD station GeoB-1841-36-(01-10)
Over 10 h, several CTD profiles were taken at station GeoB-18136 recording internal waves roughly coinciding with tidal time scales.
Figure adjusted from Hebbeln et al., 2015

seawater sampling does not capture the regional dynamics of conditions in a given depth, but only a snapshot. Furthermore, it is not unlikely that seasonal, annual and decadal changes of prevailing wind and flow regimes additionally influence the highly variable water mass exchange across the thermocline in the sGoC.
Moreover, the complex bathymetry can lead to differing conditions at closely located sample sites. During the MoccoMeBo cruise (Hebbeln et al., 2015), a triangular course was sampled taking nine CTD profiles along the way (Fig. 6.7). Covering merely 20' latitude (∼ 37 km) and 10' longitude (∼ 15 km), significant differences between 600 and 1000 m depths, in particular in salinity and hence water mass provenance, could be observed. While some profiles showed an increase in salinity below 600 m, others exhibited near constant salinities. Although station Beta-1 (510 m, Fig. 6.1) is located only 8 km south and 2 km west from sediment core MD08-3227 (644 m), it does not reach the depth from which MD08-3227 was recovered. Particularly between 500 and 650 m, seawater εNd profiles suggest significant changes and even a water mass change from ENACW to MSW (Fig. 6.1(b)). Therefore, station MOW2 was included in the estimate εNd at site MD08-3227. While it covers the water depth of MD08-3227, it is located 6 km

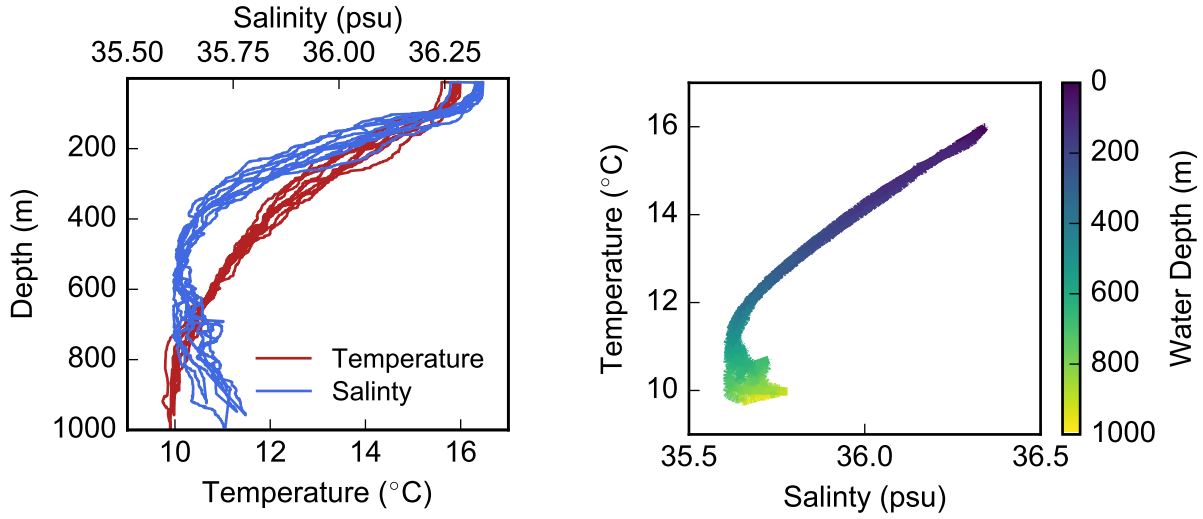

(a) (b)

Figure 6.7: CTD triangle GeoB-18152-60
Nine CTD profiles were taken in a triangular course covering 20' latitude and 10' longitude. Some profiles exhibit an increase in salinity between 600 and 1000 m depth, while others do not change significantly, suggesting the presence of a different water mass on very small regional scales.
Figure adjusted from Hebbeln et al., 2015

south and 34' west, hence involving an uncertain regional bias.
It should be noted that such an offset between modern sediment core top and ambient seawater εNd analyses was observed at other sites, especially in regions known to exhibit spatial and temporal variation of present ocean conditions (Blaser et al., 2016; Elmore et al., 2011; Roberts et al., 2010). In addition to leachates of Fe-Mn oxyhydroxides in bulk sediment, these studies analysed εNd recorded in foraminifera and fish teeth. To better understand the difference between analyses of sediment core tops (bulk leachates, foraminifera, or fish teeth) and seawater, repeated seawater sampling directly above the sediment over hours, days, seasons and years would be required.
Though the significant difference between modern seawater and sediment core top analyses remains partly unexplained, in the following I will discuss the implications of radiogenic Nd isotope changes in the past. The discussions are based on the assumption that the observed offset between modern seawater and core top sediment is a results of the 'snapshot' seawater sampling taken not directly at the depth or site of core MD08-3227. Therefore, εNd signatures of both archives will be discussed as past seawater characteristics. It is important to note, that the addition of CWC analyses to the sediment further provides confidence in the recorded signals. Thorough cleaning of CWCs removes FeMn-coatings, which should eliminate the signal of Nd-precipitation in sediment pore water.

6.4.2 εNd in cold-water corals from the GoC

Previous studies on glacial εNd signatures recorded in CWCs from the GoC showed considerably larger variations than observed in this study (Fig. 6.8; (Dubois-Dauphin et al., 2016; Montero-Serrano et al., 2011)). Previous analyses also included samples from coral-bearing core MD08-3231 (Fig. 6.8: small orange circles with grey errorbars). However, measurements of Dubois-Dauphin et al., 2016 were performed on a Thermal Ionisation Mass Spectrometer (TIMS) detecting Nd-oxide isotopes, leading to partly higher uncertainties than in analyses conducted here using MC-ICP-MS and measuring radiogenic Nd isotopes directly. Therefore, higher variations observed by Dubois-Dauphin et al., 2016 are probably due to these uncertainties. Within uncertainties, CWC εNd data from southern (Fig. 6.8: stars and triangles) and three glacial CWCs from the nGoC agree with CWCs εNd signatures from MD08-3231 and GeoB-18141-01 (Dubois-Dauphin et al., 2016; Montero-Serrano et al., 2011).

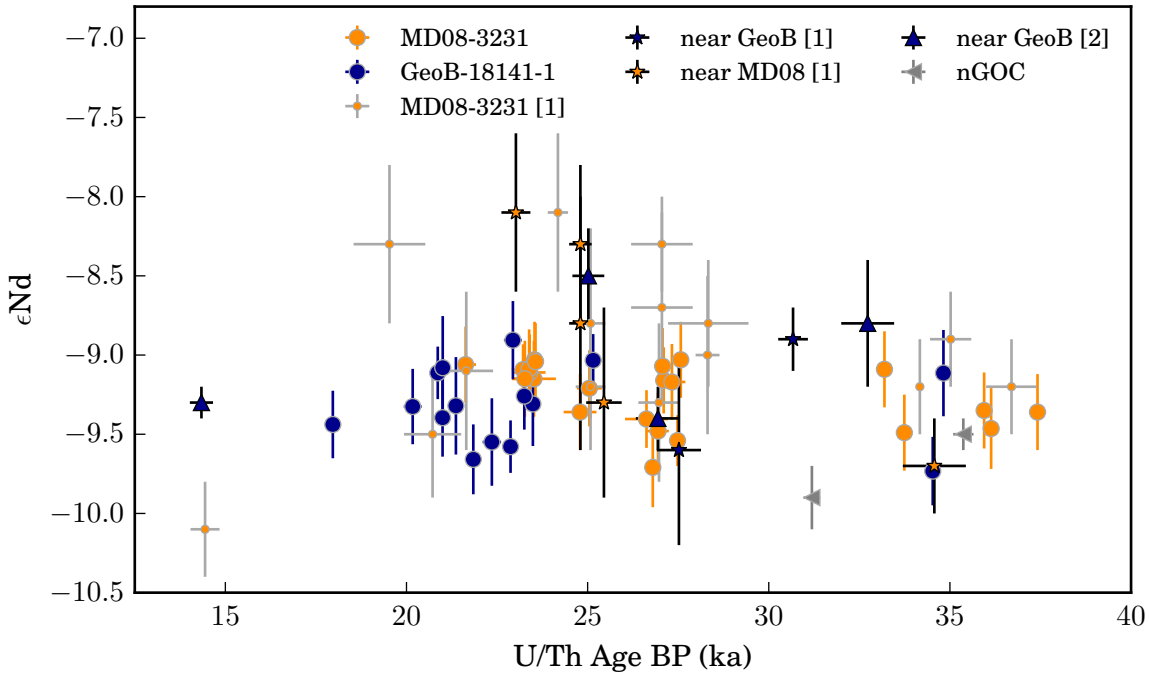

Figure 6.8: Published data of CWC εNd in the GoC
CWCs from cores analysed here are orange (MD08-3231) and blue (GeoB18141-01) circles. MD08-3231 [1] CWCs analysed by Dubois-Dauphin et al., 2016 are depicted as small orange circles with grey errorbars. Stars with black errorbars are sGoC CWCs analysed by Dubois-Dauphin et al., 2016 ([1]) and triangles by Montero-Serrano et al., 2011 ([2]) with filling colour indicating if the coral site was close to MD08-3231 or GeoB-18141-01. Two nGoC CWCs are shown as grey sideways triangles.

6.4.3 Glacial water masses in the sGoC

All four εNd records from the sGoC exhibit overall constant glacial signatures with mean values around -9.32 ± 0.23 (MD08-3227), -9.19 ± 0.31 (MD08-3231), -9.13 ± 0.19 (GeoB-18141-01)

and -8.84 ± 0.26 (MD04-2805-CQ) interrupted by short-termed excursions, mostly towards less radiogenic signals. Mean signatures are more radiogenic than any modern signature of end-members MOW, ENACW or EAAIW prior to entering the GoC. Therefore, radiogenic Nd isotopic compositions between -9.32 and -8.84, and a maximum signature of -8.59 in particular, cannot be reached with present εNd signatures of the end-members, suggesting a change of at least one end-member. As MOW was shown to have exhibited a constant signature throughout the last glacial, deglaciation and the Holocene (e.g. Dubois-Dauphin et al., 2017b), either ENACW or EAAIW must have had a different radiogenic Nd isotopic composition than today.
The signature of EAAIW in the region it is formed nowadays is between -7 and -9 (Stichel et al., 2012; Jeandel, 1993). Dubois-Dauphin et al., 2016 proposed a stronger contribution of EAAIW Nd reaching the GoC which could explain the observed shift towards more radiogenic signals. This scenario could also explain the 80% of the modern-LGM temperature anomaly recorded in glacial CWCs based on Li/Mg analyses (Chap. 5.3, 5.4). However, lets assume an initial glacial EAAIW εNd signature of -7 at its region of formation in the Southern Ocean: in this scenario, the εNd records from CWCs and sediment in the sGoC imply that EAAIW would not reach the sGoC in its pure condition but would have already mixed with a less radiogenic water mass. This mixing could also involve a concurring warming of EAAIW which would possibly prevent the presence of polar seawater temperatures reconstructed from CWCs grown during the LGM (Chap. 5.3, 5.4). In contrast, an εNd of -9 for the glacial EAAIW in its formation region, would imply that possibly unmodified EAAIW reached the sGoC and could therefore also explain the polar temperatures.
The second potential glacial source for radiogenic εNd signatures is ENACW. In the Northeast Atlantic, εNd signatures were shifted from -14 to -12 today towards more radiogenic signals between -4.9 and -8.2 during the LGM (4000 – 1150 m) (Blaser, 2017; Roberts and Piotrowski, 2015). As discussed in chapter 5.4.2, the modern ENACW has two sources of which the one in the Celtic Sea is most likely the source that could have caused polar temperatures in intermediate waters of the sGoC. This region is located relatively close to the sites recording radiogenic Nd isotope signals for the LGM (Blaser, 2017; Roberts and Piotrowski, 2015). Thus, for both water masses EAAIW and ENACW, possible scenarios exist that could lead to more radiogenic signatures in the sGoC.

Between 28 and 15 ka, the most southerly hemipelagic sediment core (MD04-2805-CQ) recorded εNd values more radiogenic than at sites of coral-bearing cores and MD08-3227 further north. The offset is between 0.29 and 0.6 ε units, implying a significant gradient of the εNd on a relatively small distance of ∼ 86 km. The more radiogenic signature at the site of MD04-2805-CQ, hints towards a more dominant influence of the end-member exhibiting the glacial increase in radiogenic Nd.
With the start of the warming period at around 15 ka (DO 1, also called Bølling-Allerød, (Dansgaard et al., 1993) sediment records converge and follow the same decline in signatures to -10 ± 0.23 at 6.9 ka. The difference in εNd of -1.1 ε units implies a significant change in either water mass provenance or the conversion of the proposed glacial εNd signatures of EAAIW and/or ENACW into modern conditions. Afterwards, a slight trend back to more radiogenic Nd can be observed in both sediment cores. Similar characteristics during deglaciation were also observed in the deep North Atlantic, but not yet in intermediate depths between 70 and 1000 m (Blaser, 2017; Lippold et al., 2016).
Rapid εNd changes recorded at all four studied sites occur around short-termed climate cycles

DO 1 (see above), DO 2, 3, 6 and 8. Typically, in the presented data εNd signals during the rapid warming of DOs are more radiogenic, while shortly prior and subsequent to the warmer phase less radiogenic signatures down to -9.94 ± 0.23 prevailed. This characteristic hints towards extremely fast water mass changes in the temperate Northeast Atlantic thermocline. The less radiogenic water mass could possibly have been be MOW. The shifts towards more radiogenic signals just before and after DOs could be caused by the predominant present of EAAIW and/or ENACW in the sGoC, which were proposed to exhibit more radiogenic εNd signatures during the last glacial than today.
Additionally, an excursion towards more negative εNd values at the start of HS 2 is seen in MD04-2805-CQ. The decrease in εNd suggests a punctuated reduction of the modified glacial end-member at the southern site in about 200 a, coinciding with the typical time scale of Heinrich Events (iceberg discharge at the start of HS; (Hemming, 2004)). This excursion is not clearly seen in the CWC records. However, this might be caused by the lack of εNd analyses on CWCs coinciding directly with this time period.
Dubois-Dauphin et al., 2016 also proposed a scenario in which they attributed more radiogenic signatures around DO cycles to an enhanced influence of EAAIW. However, several studies observed a strengthening of MOW in the nGoC during stadials and interstadials (Bahr et al., 2015; Voelker et al., 2006). With the data of this study it is difficult to resolve this contradiction. High resolution analyses on CWCs and sediment from nGoC could provide insight into changes of the east Atlantic boundary currents.

The εNd variations occurring synchronous to fast oceanic changes suggest a correlation in intermediate waters between εNd and Li/Mg temperatures recorded in the CWCs, which also follow the Northern Hemisphere climate observed in ice cores (Chap. 5). However, no such correlation between εNd signatures and Li/Mg temperatures can be observed in the coralline record (Fig. 6.9). While reconstructed temperatures span about a third of the whole temperature range covered by the modern end-members, only a small fraction of εNd signals is observed for the glacial record in the sGoC. These considerations are based on the characteristics of the modern end-members in their region of formation. Instead of ENACW, *Labrador Sea Water* (LSW) is used as the northern end-member. LSW is the densest variety of *Subpolar Mode Water* (SPMW) which is a main fraction of northern intermediate waters and therefore also ENACW (Lacan and Jeandel, 2005a). In its region of formation it exhibits εNd signatures between -13 and -14.2 and temperatures around 5.5 – 8.5°C. LSW is also present in the GoC in depths below 1.5 km, therefore not flooding the depths of the sample sites (Louarn and Morin, 2011). It should be noted, that the end-members depicted represent modern conditions while coralline data describe the last glacial. These considerations again emphasise that, as discussed above and in chapter 5.4.2, end-member characteristics today cannot explain the observed values, in particular during the LGM. The close correlation of the observed variability in temperature and εNd to DOs and HS, highlights the potential influence of the highly dynamic thermocline on the reorganisation of the Atlantic. Until now, this aspect was mostly overlooked as most studies focused solely on deep and surface ocean reconstructions.

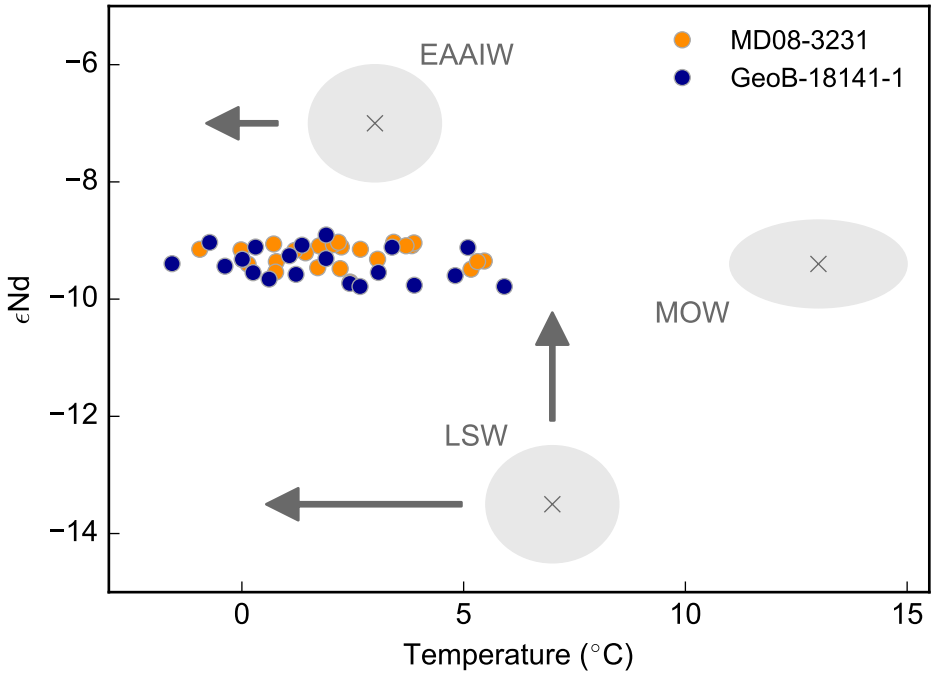

Figure 6.9: εNd vs. Li/Mg temperatures recorded in CWCs in relation to end-member water masses
Coral data points of GeoB-18141-01 (blue) and MD08-3231 (orange) are compared to the end-members (grey circles) of the water masses in the sGoC. Here, EAAIW is considered for its region of formation. LSW is used as the northern end-member as ENACW can be described as greatly modified LSW (see text for explanation). The arrows indicate the directions in which the end-member characteristics of EAAIW and LSW would have to shift to explain the recorded temperature and εNd signals.

6.5 Conclusions

The data set presented in this study is unique in its combination of two different and independent archives from one region both recording seawater εNd signatures. εNd analysis in CWCs provided a glacial record of intermediate waters in the temperate Northeast Atlantic from an archive that was precisely dated and recorded signatures during the individual growth period of each coral. εNd signatures recorded in CWC represent averages over merely a decade or a few years, therefore CWC records exhibited more frequent fluctuations than sediment based records. However, the discontinuous character of the obtained εNd evolution left gaps that were bypassed by analyses of two high accumulation rate sediment cores. As expected, both archives traced similar oceanic patterns on centennial and longer time scales. Furthermore, a general agreement in recorded εNd signals and differences in fast changes and amplitudes can be observed in the data set here. However, the difference in time resolution leads to slightly different timings and/or amplitudes of changes.
Compared to present εNd signatures, a systematic shift towards more radiogenic Nd isotopes was recorded for the last glacial (1.5 to 3 ε units). However, the extent of this shift cannot be explained by modern εNd signatures of the three end-members EAAIW, ENACW and MOW. As

for temperature, changes in the radiogenic Nd isotopic composition of the MOW end-member could be ruled out. Therefore, this shift supports the hypothesis that at least one of the two end-members EAAIW and ENACW must have undergone severe changes between today and the last glacial (Chap. 5). However, as for temperature considerations, no scenario could be ruled out completely. To discern whether EAAIW or ENACW underwent severe changes between the last glacial and the Holocene, further studies on archives located north and south of the GoC are substantial. Such a glacial change in the end-member εNd could also help to explain the gradual trend recorded in the two hemipelagic sediment cores towards less radiogenic signals (-1.1) during deglaciation.
Additionally, rapid changes coinciding with fast climate events (DO and HS) could be observed in CWC and sediment records. But, implied changes are difficult to explain without further knowledge on the glacial end-member that changed. Furthermore, punctuated changes observed are relatively small which demonstrates the need to further improve the precision of the Nd isotope measurements.

The observed offset between seawater εNd and core top analysis of sediment could not be explained with the data presented in this study. It can either be a result of a Nd remobilisation in pore waters or stem from the 'snapshot' characteristic of seawater samples. Punctuated seawater measurements used to establish the modern εNd signatures at the sites of the archives represent signals on an even shorter time scale of a certain time on a particular day. Due to its long residence time (360 – 700 a) variations of εNd signatures on time scales of days, years or decades can only be caused by existing gradients within the investigated region, which is the case in the sGoC. In archives, these gradients in seawater εNd signals would be averaged over decades, centuries or even millennia, which possibly induces a bias when comparing seawater to archive analysis. To further assess this problem, repeated seawater sampling directly above the archive site over hours, days, seasons and years would be required.

7 Reservoir ages recorded in cold-water corals

7.1 Introduction

The use of εNd as a water mass tracer in the southern Gulf of Cádiz was somewhat hampered by the fact that modern EAAIW and EAAIW exhibit similar signatures before entering the GoC. Additionally, it was shown that one of these two end-members entering the GoC must have undergone severe changes in εNd between the last glacial and the Holocene. Reservoir age reconstructions from coupled U-series and ^{14}C dating represent a second proxy to trace water masses. Recently, it was shown that reservoir ages of EAAIW off Angola increased during the LGM (Beisel, 2017; Roesch, 2017), suggesting that in the case of a stronger influence of EAAIW a similar increase in reservoir ages should be observed in the GoC. Therefore, in this study, CWCs from the two coral-bearing cores will be radiocarbon dated to gain insight into prevailing reservoir ages during the last glacial. Sampled CWCs were already analysed for their U-series age, Li/Mg temperature reconstructions and εNd signatures of the surrounding water mass, which will allow to interpret the ^{14}C results in light of the findings in previous chapters 4 – 6.

7.2 Materials and methods

Thirty-three CWCs of core MD08-3231 were analysed for their radiocarbon age, two of which were dated twice. Twenty-eight analyses were done in the course of three Bachelor's projects with sixteen corals by Wefing, 2014 and six by each Rieger, 2015 and Beisel, 2017. Of core GeoB-18141-01 only thirteen CWCs were analysed, six of which were radiocarbon dated by Elvira Beisel (Beisel, 2017). The sample sizes needed were between 15 – 20 mg, taken as an aliquot from the CWC piece cleaned for U-series and Li/Mg analysis.
Instrumental analyses were carried out on an AMS (Accelerator Mass Spectrometer) at the radiocarbon laboratory Klaus-Tschira-Labor (KTL) at the Curt-Engelhorn-Centre Archaeometry gGmbH in Mannheim, Germany. The AMS used was adapted from the MICADAS-System ('MIni CArbon DAting SYstem') developed at ETH Zurich (Wacker et al., 2010; Synal et al., 2007). Details concerning the MICADAS set-up in Mannheim are described in Kromer et al., 2013. For the AMS ^{14}C analysis graphite samples are needed in the ion source of the accelerator. Therefore, the preparation of the CWCs consisted of two parts. In the first step the CWCs were hydrolysed with carbon dioxide extraction. Afterwards, the extracted carbon dioxide was graphitised (Beisel, 2017; Therre, 2016).
The long-term average blank activity on the AMS in KTL, Mannheim is between 0.2 and 0.4 pmc. pmc is 'percent modern carbon', which is an equivalent unit for the activity ratio of a

sample.

$$\mathrm{pmc_{meas}} \equiv \frac{\mathrm{A_{SN}}}{\mathrm{A_{ON}}} \times 100\% = e^{-\lambda_{\mathrm{Libby}} \times \mathrm{t_{14C}}} \tag{7.1}$$

with $\mathrm{A_{SN}}$ the activity ratio of the examined sample normalised to the activity of the oxalic acid standard in relation to the year of reference 1950, λ_{Libby} is the decay constant after Libby, 1952, and $\mathrm{t_{14C}}$ the radiocarbon age of the sample.
To assess the long-term reproducibility, the International Atomic Energy Agency (IAEA) standard IAEA-C2 was used. It is a travertine standard obtained from a fresh-water deposition near Munich, Germany with a reference value of 41.14 ± 0.03 pmc. The long-term value of IAEA-C2 samples prepared in the IUP laboratory and measured at KTL in Mannheim between February 2015 and July 2017 is 40.74 ± 0.39 pmc (SE, relative SE is 0.95%), which is roughly 1 SE lower than the reference value. Three additional in-house standards made of three different stalagmites were also monitored (HD-Larga, HD-CG and HD-Bu-1 (Therre, 2016)). Their long-term analyses started in March 2016 and show similar reproducibilities. Due to the more extensive statistical assessment of IAEA-C2, the international standard is used as the external reproducibility.

7.3 Results

Due to the reservoir age (R) of the water mass the coral grew in (Fig. 2.11 in Chap. 2.5.2), the single Holocene coral has an older ^{14}C than U-series age (Fig. 7.1, Tab. A.5). In contrast, glacial ^{14}C ages are younger than the U-series ages, which at first sight seems contradictory. However, the initial atmospheric radiocarbon concentration used to calculate the radiocarbon age was set to 1950 which underestimated glacial conditions. The glacial atmospheric radiocarbon concentrations were significantly higher than today (Fig. 2.11), hence, ^{14}C ages seem younger than U-series ages. The convergence of ages from both dating tools towards the end of the LGM around 19 ka, suggests that the higher atmospheric ^{14}C concentration roughly accounts for the reservoir age of the water mass the corals grew in.
In general, both age-depth models of cores MD08-3231 and GeoB-18141-01 show less age-depth inversions in their radiocarbon ages than in the U-series dates. The multiple inversions observed for the U/Th ages in the upper 30 cm of core MD08-3231 are not seen in the ^{14}C ages (Fig. 7.1(a)). In fact, the sample showing the most extreme U-series inversion compared to neighbouring corals has the same radiocarbon ages as other corals in those depths. This suggests U-series open system behaviour, i.e. exchange of uranium and its decay products with the environment embedding the corals. Therefore, this coral was discarded in prior and following discussions. The other U-series inversions between core depths 70 – 160 cm are also smaller in ^{14}C ages and most are equal within uncertainties. The last two corals from that growth phase (160 – 180 cm) exhibit slightly older ^{14}C-ages (1 ka) while U-series ages fall into the same range as corals above. Additionally, the age inversion apparent for the U/Th dates in these depths cannot be observed in the ^{14}C-ages.
CWCs analysed from GeoB-18141-01 show only one ^{14}C-age inversion from core depth 5.68 to 5.86 m (Fig. 7.1(b)). However, this inversion cannot be seen in the U/Th age model. The youngest coral that grew around 3.7 ka BP exhibits radiocarbon and U/Th ages lying extremely close to another.

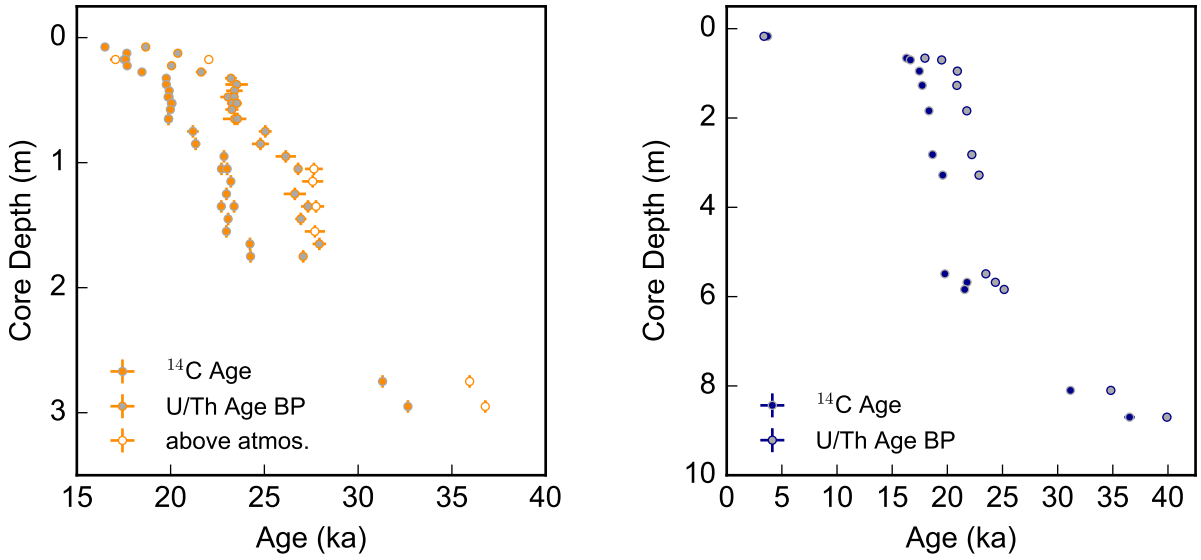

(a) ^{14}C vs. U-series age models of MD08-3231

(b) ^{14}C vs. U-series age models of GeoB-18141-01

Figure 7.1: ^{14}C vs. U-series age models of both coral-bearing cores
(a) MD08-3231 ^{14}C ages (orange symbols with grey edges) are shown versus U-series ages (grey symbols with orange edges). White symbols with orange edges are samples with Δ^{14}C above the atmosphere.
(b) GeoB-18141-01 ^{14}C ages (blue symbols with grey edges) are shown versus U-series ages (grey symbols with blue edges)
As is convention, uncertainties for ^{14}C ages are given as 1σ.

7.3.1 Δ^{14}C in relation to atmospheric Δ^{14}C changes

Combining the U-series age with the ^{14}C age, Δ^{14}C of the water mass in which the CWC grew can be calculated based on Equation 2.11 (Chap. 2.5.2). This is compared to the calibration curve IntCal13, describing atmospheric changes of $\Delta^{14}C_{atm}$ (Reimer et al., 2013) (Fig. 7.2(a) and 7.2(b)). The uncertainties of coralline Δ^{14}C versus U/Th age are shown as ellipses. As Δ^{14}C depends on the U/Th age (BP), ellipses are tilted by angle θ. Ellipses contain the uncertainties of the U-series (2σ), ^{14}C dating (2σ) and the IntCal13 (σ). The python script used to calculate the ellipses is based on a Monte Carlo method (Chap. A.1.2).
Seven CWCs of core MD08-3231 show Δ^{14}C values that lie above the atmospheric signature of the respective U/Th age (Fig. 7.2(a)). However, positive offsets ($\Delta\Delta^{14}$C, Fig. 2.11) for seawater in relation to the atmosphere express an unphysical behaviour. As mentioned in chapter 4.3, this behaviour is therefore interpreted as U-series open system behaviour and corals showing this characteristic were discarded in the discussions.
The data set of MD08-3231 exhibits a few data points with considerably larger uncertainties than other data points. This results from the fact that CWCs from MD08-3231 were dated over a period of several years. During this time, the U-series dating could be improved significantly by installing the Thermo Fisher Neptune Plus MC-ICP-MS at IUP. Ages with larger uncertainties are due to U-series dating on the ICP-QMS (Chap. 4.2.2).
During the LGM, a trend starting with a smaller offset $\Delta\Delta^{14}$C to the atmosphere (-62 $\pm$ 30 ‰,

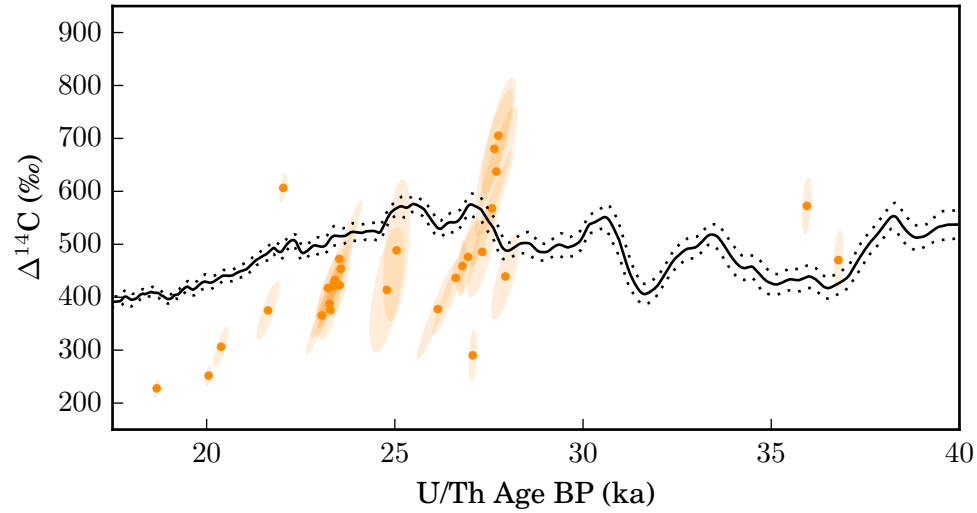

(a) Δ^{14}C of MD08-3231

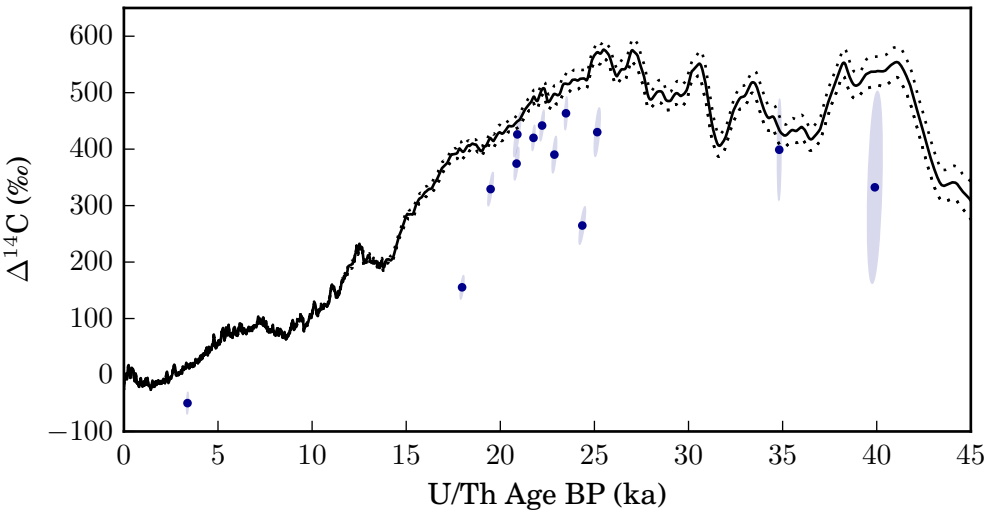

(b) Δ^{14}C of GeoB-18141-01

Figure 7.2: Δ^{14}C of MD08-3231 and GeoB-18141-01 CWCs
(a) Seven CWCs have larger Δ^{14}C signatures than the atmosphere during the time the CWCs grew. This suggests U-series open system behaviour and therefore these corals were discarded in prior and further discussions.
(b) All Δ^{14}C signatures of GeoB-18141-01 are below the calibration curve IntCal13.
IntCal13 and its uncertainty 1σ is shown as black line and scored line respectively (Reimer et al., 2013).

R: 0.38 ± 0.16 ka) and larger values at the end of the LGM can be observed (-180 ± 20 ‰, R: 1.23 ± 0.14 ka) (Fig 7.3). Around 23 ka, this trend is interrupted by a large variation ranging from a $\Delta\Delta^{14}$C of -40 ± 98 to -136 ± 66 ‰ (R: $0.29 \pm 0.62 - 0.91 \pm 0.44$ ka). This period coincides with DO 2 and HS 2. Prior the LGM ($\sim$ 27 ka three CWCs), a larger variation is observed spanning offsets of -$62 \pm 105 - 282 \pm 51$ ‰ (R: $0.26 \pm 0.42 - 1.23 \pm 0.30$ ka), which coincides

roughly with DO 3. Directly after DO 3, $\Delta\Delta^{14}C$ generally increases again. It should be noted that due to the higher uncertainties of early U-series dating most of these variations are within error.

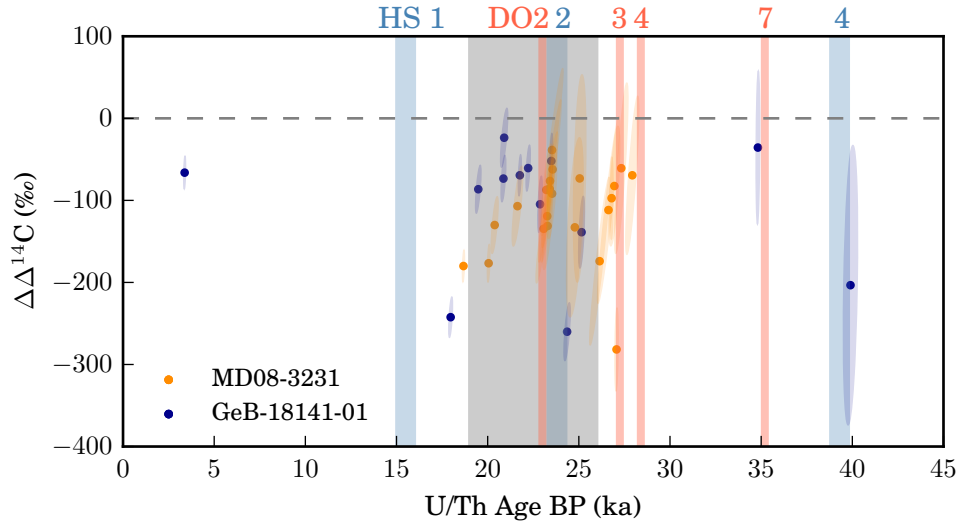

(a) $\Delta\Delta^{14}C$ of both cores

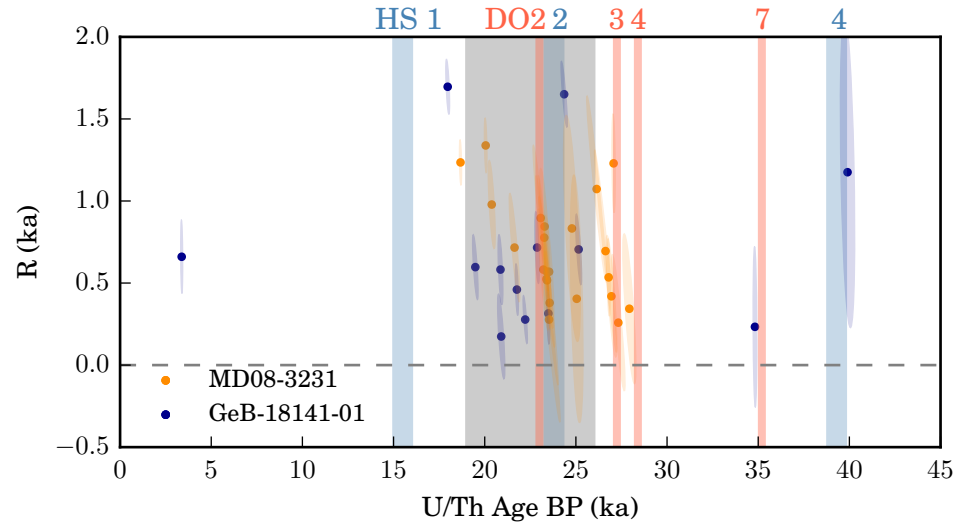

(b) R of both cores

Figure 7.3: $\Delta\Delta^{14}C$ and R of both coral bearing cores
CWCs from MD08-3231 are shown as orange and from GeoB-18141-01 as blue symbols. Ellipses show the uncertainty of $\Delta\Delta^{14}C$ (a) and R (b).
LGM is shown as grey shaded area, HS 1,2 & 4 as blue bars and DO cycles are depicted as red bars. Only HS or DOs occurring around analysed CWC are shown.

Unlike MD08-3231, GeoB-18141-01 does not exhibit any CWCs with $\Delta^{14}C$ values above the atmospheric value of that time (Fig. 7.2(b)). In general, CWCs follow the atmospheric $\Delta^{14}C$ changes with an offset of around -64 $\pm$ 47‰ (n = 8, 2σ of mean), during the MIS 3, the LGM and the Holocene. Three CWCs exhibit significantly lower $\Delta\Delta^{14}C$ at 17.97 $\pm$ 0.05 ka, 24.36 $\pm$ 0.06 ka

and 39.90 ± 0.47 ka between -204 ± 170 and -260 ± 36 ‰ (R: 1.18 ± 0.95 – 1.65 ± 0.20 ka). While two of these coincide with HS 2 and 4, the third CWC does not coincide with a known climate or atmospheric radiocarbon perturbation. The trend of larger $\Delta\Delta^{14}C$ towards the end of LGM observed in MD08-3231 cannot be observed clearly. A slight possible shift towards larger $\Delta\Delta^{14}C$ within uncertainties (Fig 7.3). During this period, GeoB-18141-01 $\Delta\Delta^{14}C$ values are generally smaller than in CWCs from MD08-3231, suggesting a slightly 'younger'/better ventilated water mass at the deeper site.

7.4 Discussion

Unlike εNd, which is treated as a quasi-conservative tracer for water masses that is transported and changed only through horizontal advection and mixing, radiocarbon ages have to be treated with more care. Intermediate waters are in contact with the overlying well ventilated surface waters, hence eddy diffusion can take place between these two water bodies. Surface Nd concentrations are significantly lower than in the rest of the water column, whereas dissolved inorganic carbon (DIC) concentrations do not differ severely, but have the highest radiocarbon fraction in the surface layer. Hence, the downward diffusion of radiocarbon 'young' surface water can lead to a better ventilated water mass (smaller R) than expected from the advection of the intermediate water mass (Broecker et al., 1990b). Additionally, ^{14}C is part of the global carbon cycle and therefore affected by variations in the carbon cycle as seen for example in the calibration curve IntCal13 (Reimer et al., 2013). Part of this carbon cycle is the carbon uptake by organic matter in the surface ocean that sinks through the water column and remineralises. The remineralisation mainly occurs in the intermediate ocean reducing the apparent reservoir age of the intermediate water mass. However, due to the phosphate limitation in biological productivity, this process can only alter the ^{14}C concentration by up to 4 – 10% and is thus a minor source of ^{14}C variability in mid-depth waters (Broecker and Peng, 1982).
In this study, I assume that the intermediate water masses investigated here are only minimally affected by eddy diffusional exchange with the surface ocean. This assumption is based on the observed upward shift of the glacial thermocline (Chap. 5) that lead to an increase in the density gradient between the two water bodies, hence reducing eddy diffusivity in the glacial ocean (Chap. 7.5). To confirm this assumption, a model forced by a similar thermocline temperature scenario assumed here investigating the diffusional transport would be needed.

After a critical examination of the data, oceanic implications that can be drawn from radiocarbon analyses will be discussed and put into the context of the two scenarios proposed to have prevailed in the last glacial.

7.4.1 Critical examination of the $\Delta^{14}C$ record from cold-water corals

The two oldest coral samples of GeoB-18141-01 both exhibit high $\Delta^{14}C$ uncertainties when compared to the other eleven analyses. This is mainly due to the radiocarbon dating method itself as these two ages are relatively close to the ^{14}C-dating limit of 40 ka resulting from the ^{14}C half-life of 5730 a. To interpret these two data points more reliably a larger amount of samples of this time period would be necessary. Therefore, these two data points will be excluded from further discussions.
In a previous study, fast $\Delta^{14}C$ changes with increasing $\Delta\Delta^{14}C$ following the decay of ^{14}C, similar

to MD08-3231 signals around 23 and 28 ka (DO 3 and 2, HS 2) were observed off Brazil around HS 1, HS 2 and YD (Mangini et al., 2010). The observed ageing of the water mass was attributed to a reduction of North Atlantic deep water formation and an increase of the influence of southern intermediate waters at the Brazilian margin. However, changes observed were significantly larger than in this study. Furthermore, the rapid variability recorded by MD08-3231 corals is mainly within analytical uncertainties. The large $\Delta^{14}C$ uncertainties of most MD08-3231 CWCs is mainly due to U-series dating. Early analyses on ICP-QMS lead to considerably higher reproducibilities than on MC-ICP-MS (Arps, 2017), resulting in the higher $\Delta^{14}C$ uncertainties (Chap. 4.2.2). Moreover, ^{14}C analysis could also be improved between the first measurements in 2014 and analyses of GeoB-18141-01 and six of the samples from MD08-3231 (Beisel, 2017; Therre, 2016). Hence, older measurements, including these fast changes, cannot be interpreted reliably without additional U-series and ^{14}C dating and will therefore be neglected in the further discussion.

Excluding the GeoB-18141-01 coral around 40 ka, three other corals from both coral-bearing cores (27.07 ± 0.09 ka, 24.36 ± 0.18 ka & 17.97 ± 0.10 ka) recorded a significantly increased offset to the atmosphere $\Delta\Delta^{14}C$ and water mass reservoir age R. However, the coral exhibiting the excursion towards larger reservoir ages coinciding with DO 3 ($\sim$ 27 ka) has to be treated with special care. A clear age-depth inversion with samples above is apparent in U-series dating but is not observed in the ^{14}C chronology. This strongly suggests that the U-series age possibly underestimates the real age which would lead to an overestimation of the reservoir age. Thus, a second U-series analysis of this sample is needed to reliably interpret this data point. A similar behaviour cannot be observed for the two corals from GeoB-18141-01. Several studies have shown that during periods of rapid climate and oceanic changes (HS 1 and 2, YD) reservoir ages of northern and southern sourced waters have increased significantly (Thornalley et al., 2015; Burke and Robinson, 2012; Mangini et al., 2010; Robinson et al., 2005; Schröder-Ritzrau et al., 2003; Adkins et al., 1998). However, only one coral of the two GeoB-18141-01 samples coincides with such a rapid change ($\sim$24 ka at the start of HS2) while the other sample ($\sim$18 ka) does not fall into a period known during which a HS, DO occurred. Furthermore, these two signals of extremely 'old' water masses are only seen by one coral each. Further radiocarbon analysis on CWCs that grew during the same time could confirm the observed amplitude of the water mass ageing. To prevent an overinterpretation of these two corals, these two corals will not be discussed further.

7.4.2 Oceanic implications of reservoir ages in the Gulf of Cádiz

A recent study on coupled U-series and radiocarbon ages from CWCs off the Angolan margin showed that $\Delta^{14}C$ followed the atmosphere with an offset of about -70 ‰ during the Holocene and MIS 3, while LGM corals recorded a water mass with $\Delta\Delta^{14}C \sim$ -170 ‰ and R $\sim$ 1.2 ka (Fig. 7.4; (Roesch, 2017)). In contrast, $\Delta^{14}C$ reconstructions in this study (excluding CWCs discussed above, Chap. 7.4.1) do not follow this clear pattern. Within uncertainties, most GeoB-18141-01 corals exhibit the same $\Delta\Delta^{14}C$ both during the Holocene and the LGM. Merely two CWCs recorded slightly larger $\Delta\Delta^{14}C$, one during early LGM ($\sim$ 25 ka) and one coinciding with DO 2 (Fig. 7.4). During the late LGM, two corals of MD08-3231 recorded larger $\Delta\Delta^{14}C$ (or reservoir ages R). It should be noted that the following interpretation relies on these four single corals. Unlike the large variations in $\Delta\Delta^{14}C$ of two GeoB-18141-01 CWCs discussed in the section above, these are discussed in more detail as the changes observed are similar to the am-

plitude of changes reported in the record of Angola in both timing and amplitude (Beisel, 2017; Roesch, 2017).

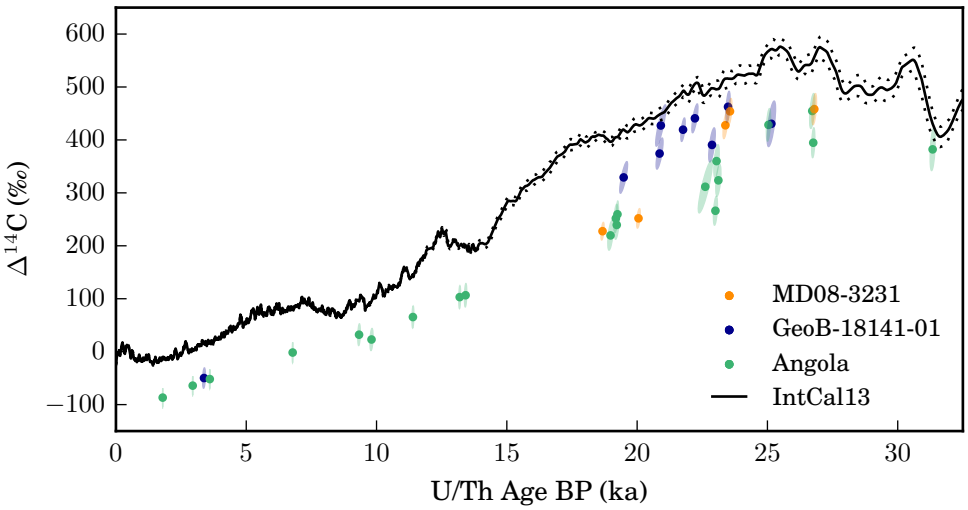

(a) Δ^{14}C sGoC vs. Angolan margin

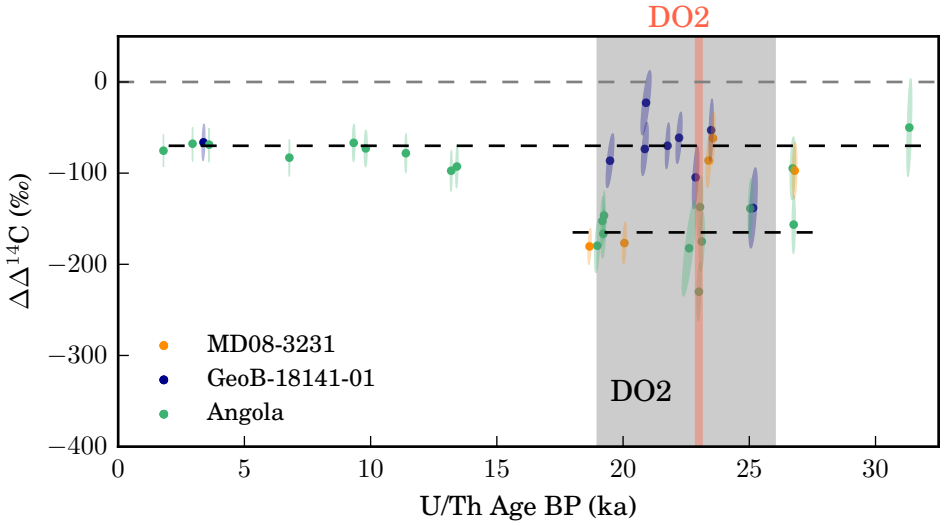

(b) $\Delta\Delta^{14}$C sGoC vs. Angolan margin

Figure 7.4: Δ^{14}C and $\Delta\Delta^{14}$C in the sGoC and off Angola
MD08-3231 CWCs (orange), GeoB-18141-01 (blue) are compared to CWCs from Scary Mound on the Angolan margin (light green, Beisel, 2017; Roesch, 2017). sGoC signatures vary between Holocene and LGM $\Delta\Delta^{14}$C values recorded in Angolan CWCs (black dashed lines). DO 2 is shown as the red line, and the LGM as grey shaded area. Atmospheric $\Delta^{14}C$ is shown in (a) as black line (IntCal13; (Reimer et al., 2013)).

Older water mass reservoir ages (higher $\Delta\Delta^{14}$C) at the early and late LGM are similar to water mass characteristics at the Angolan site (Beisel, 2017; Roesch, 2017). This strongly suggests an increased influence of EAAIW in the sGoC during those times. Here, 'increased influence' of

EAAIW should be interpreted as a less modified EAAIW on its path from its formation region in the Southern Ocean to the sGoC via the Angolan margin. However, another coral (GeoB-18141) grown during the late LGM follows the smaller offset to the atmosphere of around -70 ‰. Hence, either the seawater masses prevailing at the different depths of the CWC provinces in the sGoC were different, or periods with increased EAAIW influences were really short and therefore not recorded by corals with slightly different ages. It should be noted that no clear differences could be observed in Li/Mg temperature and εNd reconstructions for the late Holocene. Another less pronounced shift towards larger reservoir ages (GeoB-18141-01) coincides with a variation in $\Delta\Delta^{14}$C recorded in Angolan corals and the DO 2. The ageing of the sGoC water mass is less pronounced, hinting towards merely a slight increase in EAAIW provenance.
The two corals of GeoB-18141-01 that recorded a higher offset of Δ^{14}C to the atmosphere, exhibited εNd signatures -9.58 $\pm$ 0.17 (23 ka) -9.03 $\pm$ 0.17 (25 ka). One of the late LGM MD08-3231 corals was analysed for εNd recording -9.06. Therefore, oldest reservoir age signals suggesting predominantly less modified EAAIW in the sGoC coincide with least radiogenic signatures. Additionally, Li/Mg temperatures reconstructed on the same Angolan corals were around 2°C (Roesch, 2017). While in the sGoC recorded temperatures cooled down to around 0°C, 8 of the 10°C difference between Holocene and LGM could be explained by the dominant EAAIW. Therefore, this observation strongly suggests that at least during short intervals of the LGM EAAIW was the dominant water mass in the sGoC. Previous studies linked stronger EAAIW influences to rapid climate events like DO cycles or HS (Dubois-Dauphin et al., 2016; Pahnke et al., 2008). A close correlation to these, could not be resolved in this study which might be due to lack of data capturing these short termed events.
However, it is important to note that while punctuated periods of increased EAAIW provenance could possibly be reconstructed at both CWC provinces in the sGoC, no long-term dominance for the entire LGM can be drawn from this data set. Most Δ^{14}C recorded for the water mass the corals bathed in (mainly GeoB-18141-01), followed the atmosphere with a constant offset similar to the one during the Holocene. Both the other two end-members ENACW or MOW are expected to be well-ventilated during the LGM. Considering the results and implications of chapters 5 and 6, MOW can be ruled out as the main water mass present in the depths of the coral sites.
Hence, the ensemble of the reservoir age reconstructions, Li/Mg temperatures and εNd signatures suggests that both scenarios proposed in chapters 5.4.2 and 6.4.3 of changed EAAIW and ENACW end-members (just before entering the GoC) prevailed during the LGM and that sGoC CWCs were alternately bathed in waters of dominant EAAIW and ENACW. This would imply a modified glacial EAAIW exhibiting polar temperatures, more radiogenic εNd signatures and older reservoir ages and a glacial ENACW also characterised by even colder temperatures and more radiogenic εNd signatures (Fig. 6.9) but low reservoir ages and therefore well ventilated.

7.5 Conclusions

Δ^{14}C reconstructions were performed on the same cold-water corals of cores GeoB-18141-01 and MD08-3231 for which Li/Mg temperatures and εNd signatures were analysed. Overall, Δ^{14}C followed the atmospheric Δ^{14}C evolution with an offset of $\Delta\Delta^{14}\text{C} \sim$ -(60 – 70) ‰. A few short-term excursions with larger $\Delta\Delta^{14}$C implying a less ventilated water mass were recorded in CWCs from both cores. The amplitude of the water mass ageing was the same as a recently reported LGM increase in reservoir ages recorded in CWCs from the Angolan margin. In contrast,

Holocene CWCs grown there recorded young reservoir ages similar to the Holocene sample of GeoB-18141-01 and LGM corals that bathed in the well ventilated water mass. Therefore, short time periods with an increase in reservoir ages are interpreted as times during which EAAIW was the dominant water mass in the intermediate depths of the southern Gulf of Cádiz (sGoC). However, while punctuated periods of suggested EAAIW dominance were recorded in sGoC corals from intermediate waters, the majority of LGM CWCs bathed in a well ventilated water mass. This strongly hints towards a subsequent alternation between periods of dominant EAAIW and periods during which well ventilated ENACW or MOW were predominantly present in the intermediate sGoC. Combining this observation with the records gained from Li/Mg temperatures and εNd signatures, MOW can be ruled out as the possible main contribution. Therefore, the ensemble of proxies and archives investigated suggests a seesaw pattern of intermediate waters changing between predominant ENACW and ENACW. In this scenario glacial ENACW and EAAIW both exhibit polar temperatures and more radiogenic εNd signatures than in the modern ocean and were distinguishable by their reservoir ages, with glacial ENACW better ventilated than glacial EAAIW.
This proposed scenario is mainly based on observation from one region and needs to be validated in future studies. As proposed for temperature and εNd, these studies should be performed on archives north and south of the GoC. The first results of Angolan corals already showed the great potential benefit from such studies. However, the coralline record from the Angolan margin did not cover the times during which younger reservoir ages were observed in the sGoC. Therefore, analysis filling these gaps are needed. Additionally CWCs of coral-bearing core MD08-3231 U-series dated on an ICP-QMS should be remeasured to improve the uncertainty of the Δ^{14}C reconstruction. This would allow to discern if variations observed for those CWCs were an artefact of the higher uncertainty, or reflected thermocline ventilation changes. Furthermore, additional CWCs of core GeoB-18141-01 could be ^{14}C-dated to support the findings.

Considering the information gained by the ensemble of CWC growth analysis, Li/Mg temperature, εNd and reservoir age reconstructions, a main factor influencing the coral growth and therefore mound aggregation was neglected: the availability of sufficient food. Currently, no reliable proxy in the archive CWC has been introduced that records past nutrients or the closely linked surface biological productivity. In the next part of this thesis, I will investigate the potential of nutrient reconstructions from Ba isotopes in CWCs. In contrast to the paleoceanographic reconstructions performed for the Gulf of Cádiz, this calibration study will be based on 'living' or very young corals (< 1000 a) from three sites throughout the entire Atlantic.

Part II

Establishing a New Proxy:

Ba Isotopes in Cold-Water Corals

8 Barium isotope fractionation in cold-water corals

This project was carried out at the Department of Earth Sciences at the University of Oxford where I spent 11 months (Feb. – Dez. 2016) of my PhD working as part of Prof. Gideon Henderson's research group.
This chapter will be submitted to the journal Earth and Planetary Science Letters. Figures and Tables are equal to the ones in the script of the paper.

8.1 Introduction

Cold-water corals (CWC) are distributed throughout the global oceans in waters ranging from just a few meters to abyssal depths of several thousand meters (Roberts, 2006). In contrast to traditional paleoceanographic archives such as sediment cores, CWCs can be dated precisely beyond the ^{14}C age range by U-series (Spooner et al., 2016; Margolin et al., 2014; Burke et al., 2010; Douville et al., 2010; Potter et al., 2005; Cheng et al., 2000; Mangini et al., 1998). Hence, oceanic changes on centennial, decadal, yearly or even seasonal time scales can be elucidated from geochemical and isotope tracers in CWCs. Despite this advantage, only a small number of paleoceanographic tracers have been established and applied in CWCs (Robinson et al., 2014). Biological factors, so-called 'vital' effects, alter some elemental and isotopic systems, e.g. $\delta^{13}C$, $\delta^{18}O$ or Li/Ca, limiting their use as oceanic tracers (Raddatz et al., 2013; Case et al., 2010; Rollion-Bard et al., 2009; Adkins et al., 2003). However, temperature and water mass provenance have been successfully retrieved from other elemental and isotope tracers (Robinson et al., 2014).
Barium has an enigmatic oceanic chemistry that has been studied for many years. The nutrient-like distribution of dissolved Ba in seawater $[Ba]_{SW}$ is closely correlated with silicate ($Si(OH)_4$) (Wolgemuth and Broecker, 1970; Chow and Goldberg, 1960). But numerous studies suggest that the oceanic Ba cycle is not directly linked to the silicate or carbonate cycle (Monnin et al., 1999; Bishop, 1988). While regenerative dissolved Ba enriches deep ocean concentrations, its removal in the upper ocean is attributed to the precipitation of barite ($BaSO_4$), even though seawater is mostly under-saturated in $BaSO_4$. This behaviour can possibly be explained by the decay of organic matter in settling particles releasing Ba into a microenvironment until a $BaSO_4$-saturation is reached (Paytan and Griffith, 2007; Bishop, 1988; Dehairs et al., 1980).
A new-found ability to precisely measure naturally occurring fractionation between Ba isotopes may provide a tool with which more insight into the processes controlling the Ba cycle in the ocean can be gained. Recent Ba-isotope studies have focussed on fractionation processes during experimental precipitation of $BaCO_3$ or $BaSO_4$ (van Zuilen et al., 2016; Böttcher et al., 2012; von Allmen et al., 2010), in igneous rocks (Nan et al., 2015; Miyazaki et al., 2014), in soils and sediments (Bridgestock et al., in review; Bullen and Chadwick, 2016), and in seawater (Bridgestock et al., in review; Bates et al., 2017; Hsieh and Henderson, 2017; Cao et al., 2016; Horner

et al., 2015). During barite, $BaCO_3$ and $BaMn[CO_3]_2$ precipitation experiments, the solid phase preferentially incorporates the lighter isotopes, leaving the solution relatively heavy in Ba isotopes (van Zuilen et al., 2016; Böttcher et al., 2012; von Allmen et al., 2010). Surface barite formation and its dissolution in the deep ocean lead to an inverse profile for Ba isotopes compared to dissolved Ba concentration, with light Ba isotopic compositions in the deep ocean and heavy isotopic compositions of Ba in surface waters (e.g. Horner et al., 2015). Further studies on Ba isotopes have the potential to provide insight about the oceanic Ba cycle, the ocean's biological pump, deep water mass provenance (Bates et al., 2017; Horner et al., 2015), riverine inputs (Cao et al., 2016) and changes in hydrothermal inputs (Hsieh and Henderson, 2017). To investigate past changes in these processes, CWCs could be a promising archive.

Over the years, several studies have shown that, as for inorganic aragonite, the Ba/Ca ratio in foraminifera, calcitic corals and aragonitic CWCs reflects Ba concentrations in ambient seawater $[Ba]_{SW}$ (LaVigne et al., 2011; Lea and Boyle, 1993). Recently, calibrating the Ba/Ca in CWCs to reconstruct past $[Ba]_{SW}$ has been a focus of research (Spooner et al., submitted; LaVigne et al., 2016; Anagnostou et al., 2011).

Only one published study has presented Ba isotope analysis of coralline carbonate (Pretet et al., 2016). That study measured Ba isotopes in cultured tropical scleractinian corals grown in Mediterranean seawater. A variable fractionation between seawater and cultured coral aragonite ranging from -0.02 ‰ (*Acropora sp.* and *Porite sp.*) and -0.35 ‰ (*Stylophora sp.* and *Montipora sp.*) was found. The Ba isotopic composition of natural CWCs was also reported; two *Lophelia pertusa* (*L. pertusa*) samples from the Norwegian shelf were analysed and found to have $\delta^{138/134}$Ba values of 0.25 ± 0.11 ‰ and 0.3 ± 0.11 ‰. The isotopic composition of Ba is defined in reference to the SRM NIST 3104a standard

$$\begin{aligned} \delta^{138/134}\mathrm{Ba}_{\mathrm{NIST}_{3104a}} &= \left(\frac{\left(^{138}\mathrm{Ba}/^{134}\mathrm{Ba}_{\mathrm{sample}}\right)}{\left(^{138}\mathrm{Ba}/^{134}\mathrm{Ba}_{\mathrm{NIST}_{3104a}}\right)} - 1 \right) \times 1000 \\ &= \left(\frac{\mathrm{R}_{\mathrm{sample}}}{\mathrm{R}_{\mathrm{NIST}_{3104a}}} - 1) \right) \times 1000 \end{aligned} \tag{8.1}$$

which we abbreviate to $\delta^{138/134}$Ba.

In this study, the first detailed study of the $\delta^{138/134}$Ba in natural CWCs in comparison to that of the seawater in which they grew is presented. This data set includes thirty-six well-characterised specimens from eight different genera from the North Atlantic, the Equatorial Atlantic, and the Drake Passage (Southern Ocean). The samples cover a wide range of environmental conditions, Ba concentrations, and seawater Ba isotopic compositions. This allows for a systematic assessment of the Ba isotope fractionation during coral growth and the use of CWCs as an archive for past seawater $\delta^{138/134}$Ba.

8.2 Materials and analytical methods

8.2.1 Samples

Thirty-six CWCs and ambient seawater samples from three ocean regions were selected for Ba isotope analysis. The locations were south of Iceland in the North Atlantic (Reykjanes Ridge and Hafadjup), in the Equatorial Atlantic (Carter Seamount), and in the Drake Passage (Burd-

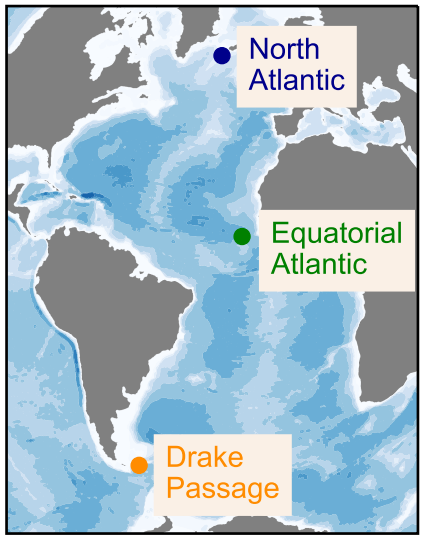

Figure 8.1: Locations of CWC and ambient seawater sample sites
For exact coordinates please refer to Tab. 8.1 and Tab. A.11.

Table 8.1: Locations of CWC and ambient seawater sample sites for Ba analysis
For exact coordinates of each coral please refer to Tab. A.11.

Station	Latitude	Longitude	Covered depths (m)	Analysed depths (m)
Hafadjup CWC	63° 16.82' – 63° 20.52'N	19° 34.11' – 19° 35.75'W	363 – 680	363 – 680
Hafadjup SW	63° 19.02 'N	19° 36.72'W	360 – 680	360 – 680
Reykjanes Ridge CWC	62° 36.45' – 63° 5.13'N	24° 59.27' – 24° 32.53'W	209 – 698	209 – 698
Reykjanes Ridge SW	62° 53.34'N	24° 50.88'W	238 – 338	238 – 338
Carter Seamount CWC	5° 36.66' – 9° 13.37'N	21°16.49' – 26° 57.46' W	265 – 2318	265 – 2318
JC094 CTD 2 SW	9° 17.1'N	21° 38.0' W	0 – 4524	0 – 4524
Burdwood Bank	54° 50.26' – 54° 50.33'S	62° 7.11' – 62°14.99'W	334 – 1879	334 – 1879
NBP1103 CTD 21	55° 3.25' S	62° 81' W	0 – 4110	0 – 2250
NBP1103 CTD 100	60° 33.85' S	65° 29.57' W	0 – 3100	0 – 1500

wood Bank) (Fig. 8.1, Tab. 8.1). They were chosen to cover a wide range of temperature and salinity (e.g. T: 2 – 11.5°C; S = 34.29 – 35.32 psu), Ba concentrations and Ba isotopic compositions (Fig. 8.2, Tab. A.11 and A.9). Eight different coral taxa (identified to either genus or species level) of living or young (less than 1000 a) CWCs were sampled: *Lophelia pertusa* (*L. pertusa*), *Madrepora oculata* (*M. oculata*), *Desmophyllum dianthus* (*D. dianthus*), *Balanophyllia sp.*, *Caryophyllia sp.*, *Dasmosmillia sp.*, *Flabellum sp.* and *Javania sp.* (Tab. A.10, A.11). Icelandic corals were collected during the ICECTD cruise (2012) using theVictor 6000 ROV (remotely operating vehicle). Simultaneously, seawater samples (125 ml) were directly filled into acid cleaned PEP bottles by the ROV (Frank et al., 2012). They were stored at room temperature. Three months prior to Ba-isotope analysis seawater samples were acidified to a pH of 1.5 by adding purified, concentrated HCl. Equatorial Atlantic samples from Carter Seamount were recovered during the JC094 cruise in 2013 (Spooner et al., 2016; Robinson, 2014). The corals were collected by an ISIS ROV. Ambient seawater samples are from CTD station 2 and were

already analysed by Bates et al., 2017. CWCs from Burdwood Bank in the Drake Passage were collected in 2011 during cruise NBP1103 using a small basket dredge and trawls (Chen et al., 2015; Margolin et al., 2014; Robinson and Waller, 2011). Depths and coordinates given here are the average for each retrieval event. Seawater samples are from CTD station 21 and were taken by a Sea-Bird 991plus CTD in PVC Niskin bottles, immediately filtered with 0.4 µm Acropak cartridge filters, acidified with 4 ml concentrated HCl and stored at room temperature. As Burdwood Bank is positioned north of the polar front, an additional seawater profile close to Sars Seamount (cruise NBP1103, station 100) south of the polar front was analysed.
Temperature and salinity were determined according to Spooner et al., 2016. Details regarding the complete coral collection are summarised in Tab. A.10, A.11 and A.9.

8.2.2 Ba extraction and analysis

All samples (corals and seawater), except for the seawater samples analysed by Bates et al., 2017 (CTD 2 cruise JC094), were prepared and analysed at the Earth Sciences Department of the University of Oxford. Ba isotopes of both seawater and CWC samples were measured on a thermal ionisation mass spectrometer (TIMS; Thermo Scientific Triton), using a ^{137}Ba-^{135}Ba double spike to correct for mass fractionation during the chemical procedure and instrument analysis (Hsieh and Henderson, 2017). For seawater analyses, $\sim$ 50 ml of seawater was precisely weighed and spiked with a known quantity of the double spike. After an equilibrating period of 24 h, 3 ml of 0.9 M Na_2CO_3 solution were added to co-precipitate Ba with $CaCO_3$. The precipitate was centrifuged and cleaned with 18 MΩ cm^3 water (MilliQ). After dissolving the precipitate in HCl, column separation was applied twice using the cation exchange resin AG50-X8 (200 – 400 mesh) to purify Ba from the matrix elements (Horner et al., 2015; Nan et al., 2015; Foster et al., 2004, here used method in Bridgestock et al., in review). To remove organics leached from the resin, 7.5 M HNO_3 and 9.8 M H_2O_2 were alternatingly added to the samples and evaporated. This procedure was repeated three times.
Cold-water coral samples were rinsed with fresh water on board ship. Living corals were bleached to remove external organic tissue and washed again in fresh water. All corals were dried and stored at room temperature until analysis. The cleaning procedure was adapted from Copard et al., 2010 and Pretet et al., 2016. CWCs were thoroughly mechanically cleaned using a dremel tool, removing FeMn-coatings and organic residues. To remove any further contamination CWCs were then washed three times in MilliQ in acid cleaned Teflon vials and leached in very weak HCl. Leaching was performed by covering the sample with MilliQ and adding drops of 2 M HCl until small bubbles could be seen around the aragonite. Leaching lasted for five minutes before rinsing three times with MilliQ again. Afterwards, samples were dried and weighed (45 – 70 mg). The sample size was chosen to have more than 300 ng of Ba for isotope measurements. This sample size also reduced the influence of intra-skeletal variability in e.g. centres of calcification (COC), thickening deposits (TO), or small contaminant inclusions (Spooner et al., submitted; Adkins et al., 2003). Samples were dissolved in 5 ml 7.5 M HNO_3 and spiked with a known quantity of ^{137}Ba-^{135}Ba double spike (Hsieh and Henderson, 2017). To ensure spike equilibration, samples were heated to 90 – 100 °C for at least 12 h following spike addition. CWC samples were subsequently dried down, dissolved in 3 M HCl, dried again and redissolved in 1 ml 3 M HCl. Ba purification by cation exchange chromatography follows the procedure for seawater samples (Bridgestock et al., in review).
For seawater samples the total procedural Ba blank was between 0.19 and 1.6 ng (n = 4) repre-

senting maximal 0.16% of Ba processed in samples. Most of the Ba blank is added with the Na_2CO_3 used for co-precipitation, so blanks for coral samples processed without this step were far lower: 0.02 – 0.24 ng (n = 5) accounting for maximal 0.02% of the total Ba processed in samples. No blank correction for either seawater or coral samples was applied.
Purified samples were dissolved in 1 – 2 µl 2 M HCl and loaded on a previously outgassed single Re filament adding 1 – 2 µl Ta_2O_5-H_3PO_4 activator (Hsieh and Henderson, 2017). To stabilise the ion beams during the analysis the activator was loaded on the filament prior to the samples. Ba isotopes were analysed on a Thermo Scientific Triton TIMS. Within 30 – 45 min the filaments were heated to roughly 1450 – 1550 °C. By further increasing the temperature to 1600 to 1650 °C for a few minutes before decreasing the temperature back to approximately 1500 °C, a stable signal was achieved.
For corals samples typical ion beams during the analysis were 8 – 10 V for ^{138}Ba. Seawater samples yielded slightly smaller $^{138}Ba^+$ beams of 3 – 7 V and frequently showed a less stable beam signal. Seven Faraday cups simultaneously detected the masses 138^+, 137^+, 136^+, 135^+, 134^+, 140^+ and 139^+, with the latter reflecting $^{140}Ce^+$ and $^{139}La^+$ monitored to account for possible isobaric interferences on ^{136}Ba and ^{138}Ba. No 140^+ and 139^+ above background signals were detected during any analysis. One analysis consisted of 54 blocks each containing 10 ratio measurements, with a measurement integration time of 8.4 s. To monitor the electronic baseline the X-Symmetry of the instrument was adjusted to divert the ion beams before each block. Blank analyses were only measured for 20 – 30 blocks. To correct for instrumental mass bias using the double-spike compositions, all raw data was processed offline according to Hsieh and Henderson, 2017. The isotopic analysis and the known spike mass added to each sample also provided precise Ba concentration.
The standard JCp-1 consisting of powdered coral (Hathorne et al., 2013b) was also analysed three times. It was prepared in the same way as CWCs samples but without the mechanical and chemical cleaning steps.

8.3 Results

8.3.1 Reproducibility

Repeated analyses of the SRM NIST 3104a standard using similar beam sizes for seawater samples lead to a long-term external reproducibility of ± 0.03 ‰ (2σ; Bridgestock et al., in review; Hsieh and Henderson, 2017). Repeated analyses of the coral standard JCp-1 yielded a Ba isotopic composition of $\delta^{138/134}$Ba = 0.25 ± 0.03 ‰ (2σ, n = 3), which is slightly lower than two other analysis that measured 0.29 ± 0.03 ‰ (Horner et al., 2015) and 0.26 ± 0.1 ‰ (Pretet et al., 2016). This might be explained by a slight $\delta^{138/134}$Ba inhomogeneity of JCp-1 batches between the different laboratories. Hence, a laboratory inter-calibration on the same JCp-1 batch is needed. Several duplicates of seawater and coral samples confirm the external reproducibility achieved (Tab. A.10, Bridgestock et al., in review). Two studies (Bridgestock et al., in review; Hsieh and Henderson, 2017), also measured at University of Oxford, further verify these results for seawater and sediment samples. The reproducibility for the Ba concentration of the repeated coral standard and these sample measurements was ± 2 – 3% (1σ) and is taken as the 1σ of Ba concentration measurements in this study. With an average of 7.94 µmol/mol ± 2%; n = 3 our Ba/Ca of the JCp-1 standard is higher than the mean value by Hathorne et al., 2013b of 7.465 ± 0.655, but lies within uncertainties. Any analyses yielding a larger internal Standard

Error for $\delta^{138/134}$Ba than the standard reproducibility were considered unreliable, discarded for this study and remeasured.

8.3.2 $\delta^{138/134}$Ba in seawater profiles

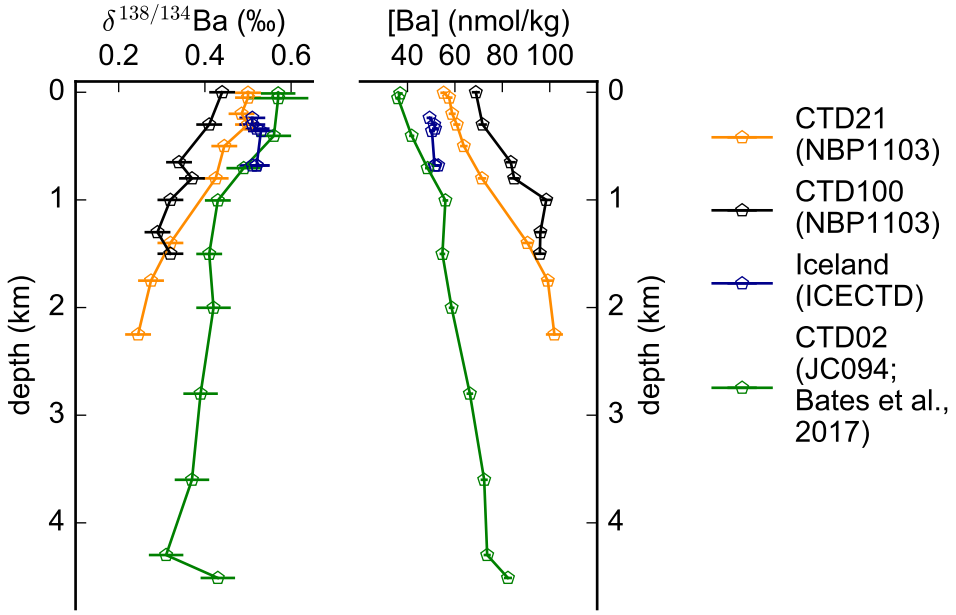

Figure 8.2: Seawater profiles for dissolved Ba concentrations $[Ba]_{SW}$ and Ba isotopic compositions $\delta^{138/134}$Ba
At all locations, station CTD 21 (Burdwood Bank, orange), CTD 100 (Sars Seamount, black), Iceland (Reyjanes Ridge and Hafadjup, blue), and CTD 02 (Carter Seamount) (Bates et al., 2017), the well-established anti-correlation between $[Ba]_{SW}$ and $\delta^{138/134}$Ba can be observed. Both profiles from cruise NBP1103 potentially reach deeper, but were not analysed in abyssal depths as only depths with coral growth were considered for this study. Station CDT 100 will not be discussed further as corals from Sars seamount were not analysed here.

The seawater profile from Burdwood Bank (CTD 21) in the Drake Passage shows the established anti-correlation between $[Ba]_{SW}$ and $\delta^{138/134}$Ba (Fig. 8.2, Tab. A.9). $[Ba]_{SW}$ is 55.2 nmol/kg in surface waters and increases to 102 nmol/kg in 2250 m water depth[1]. The isotopic composition of Ba decreases from 0.5 ‰ to 0.25 ‰ with depth.
Tropical Atlantic water samples, measured and described in detail by Bates et al., 2017 (CTD 2, cruise JC094), show a similar behaviour with Ba concentrations increasing from 37.9 in the surface to 84.6 nmol/kg at 4512 m and $\delta^{138/134}$Ba decreasing from 0.57 ‰ to 0.31 ‰. Note, that Ba concentrations from Bates et al., 2017 were initially given in nM and have been recalculated here to nmol/kg by assuming a seawater density of 1.027 kg/l.
Seawater samples from Reykjanes Ridge and Hafadjup, south of Iceland, only cover the depths 238 to 680 m from which corals were analysed (Fig. 8.2). Both $[Ba]_{SW}$ and $\delta^{138/134}$Ba are nearly constant within uncertainties: 49.3 – 52.9 nmol/kg and 0.51 – 0.53 ‰ respectively.

[1]Deeper samples were available, but were not measured because no corals were analysed below 2250m depth.

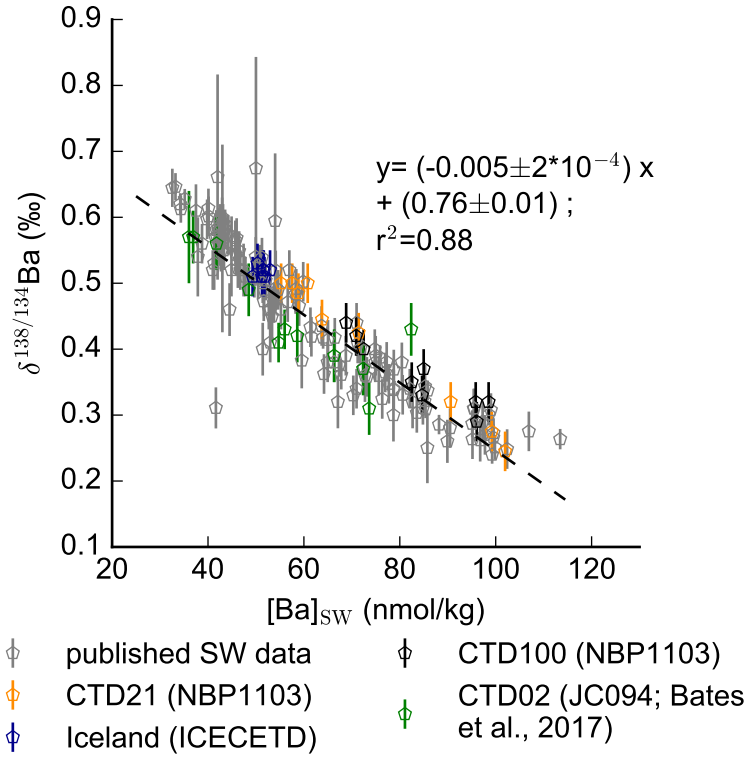

Figure 8.3: $\delta^{138/134}Ba_{SW}$ against $[Ba]_{SW}$ for samples from this study and published data (Bridgestock et al., in review; Bates et al., 2017; Hsieh and Henderson, 2017; Pretet et al., 2016; Horner et al., 2015). Data from Cao et al., 2016 was not included in this summary as their seawater samples had uncharacteristically high Ba isotopic compositions. Our data agree well with the other studies. Note that seawater Ba isotopic composition at the coral sites cover nearly the total observed range of oceanic $\delta^{138/134}$Ba recorded in the other studies.

The seawater samples analysed in this study cover nearly the total observed range of $\delta^{138/134}$Ba in seawater and confirm published data (Fig.8.3; (Bridgestock et al., in review; Bates et al., 2017; Hsieh and Henderson, 2017; Cao et al., 2016; Pretet et al., 2016; Horner et al., 2015)). Isotopic compositions of Ba from publications originally reporting in $\delta^{137/134}$Ba were converted into $\delta^{138/134}$Ba by multiplying by a factor of 1.3 (after Horner et al., 2015). The closest seawater profiles were used to compare seawater $\delta^{138/134}$Ba with the coral analyses. To obtain $\delta^{138/134}Ba_{SW}$ in the water depths in which the corals grew, the values of the next highest and lowest water signature were linearly extrapolated (Fig. 8.2, 8.5 and Tab. A.10, A.9).

8.3.3 Ba/Ca in cold-water corals

To calculate Ba/Ca_{CWC} we assumed a coralline Ca concentration of 40% (Roberts et al., 2009). For seawater samples a Ca concentration of 1.03×10^{-7} nmol/kg (Henderson and Henderson, Gideon M., 2009) was taken to determine Ba/Ca_{SW} values. Ba/Ca for corals varied between 7.5 and 16.3 µmol/mol, while seawater samples spanned 3.9 to 9.7 µmol/mol (Fig. 8.4a, Tab. A.10). A linear least squares regression renders $Ba/Ca_{CWC} = 1.8\ (\pm\ 0.4, 2\sigma)\ Ba/Ca_{SW} + 0.7\ (\pm\ 2.6)$ with a correlation factor of $r^2 = 0.67$. Therefore, the overall partition coefficient $D_{CWC/SW}$(Ba) (i.e.

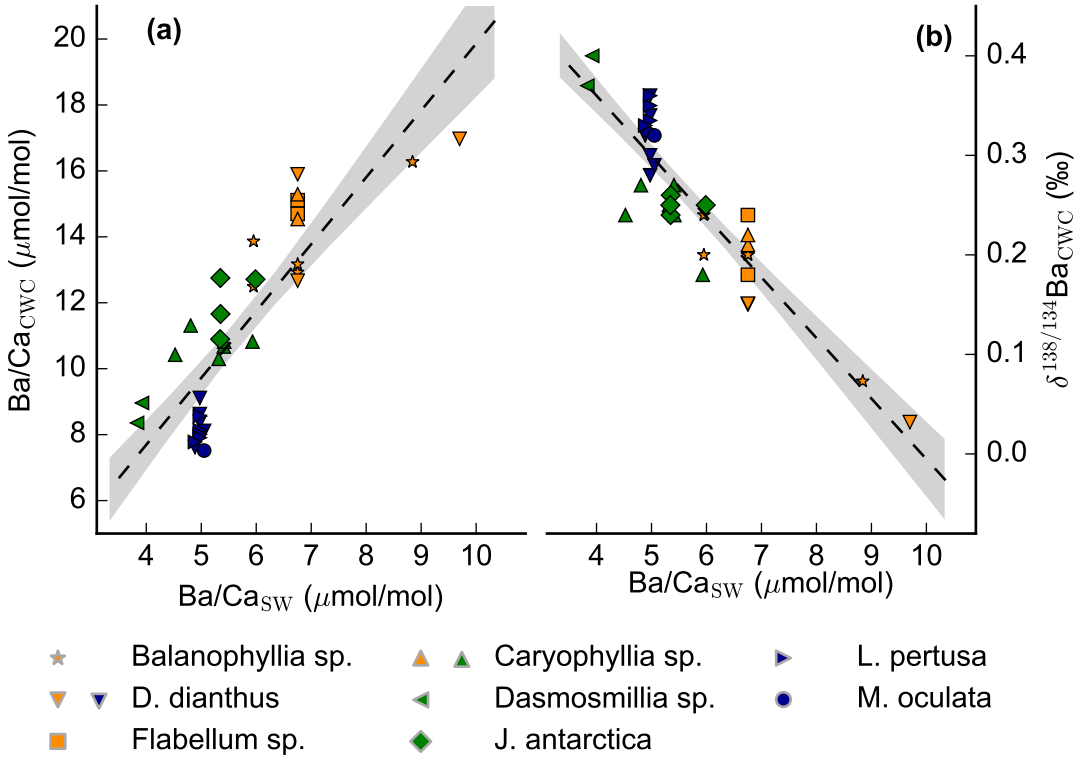

Figure 8.4: Ba/Ca in CWCs and ambient seawater (a) and seawater Ba/Ca$_{SW}$ influence on coralline $\delta^{138/134}$Ba (b)
(a) A linear fit (black dashed line) through our data (coloured symbols, colour scheme: see Fig. 8.2 or 8.5) renders: Ba/Ca$_{CWC}$ = 1.8 ($\pm$ 0.4) Ba/Ca$_{SW}$ + 0.7 ($\pm$ 2.6) with a correlation factor of r^2 = 0.67 (0.95 confidence interval as shaded grey area)
(b) Similar to seawater $\delta^{138/134}$Ba a close anti-correlation to Ba concentration (here as Ba/Ca$_{SW}$) can be observed for coralline $\delta^{138/134}$Ba. The correlation factor r^2 is 0.82.

(Ba/Ca)$_{CWC}$/(Ba/C)$_{SW}$) observed is 1.8 ± 0.4 (2σ). The partition coefficient calculated separately for each CWC in this study covers a range from 1.5 to 2.4.

8.3.4 $\delta^{138/134}$Ba in cold-water corals

CWCs of eight different taxa were analysed from Burdwood Bank (Fig. 8.4b – 8.6, Tab. A.10, A.11). Taxa from Burdwood Bank included five *Balanophyllia sp.*, two *Flabellum sp.*, two *Caryophyllum sp.* and three *D. dianthus*, with samples taken from depths ranging from 334 to 1829 m. Isotopic compositions are $\delta^{138/134}$Ba = 0.24 ‰ in shallow corals and 0.03 ‰ in the deeper corals (Fig. 8.5), reflecting the decrease in seawater $\delta^{138/134}$Ba with depth. At each depth, CWC $\delta^{138/134}$Ba values agree with each other within external reproducibility, regardless of species. The fractionation of Ba between corals and seawater can be expressed by the isotope fractionation factor

$$\alpha = \frac{R_{CWC}}{R_{SW}} \tag{8.2}$$

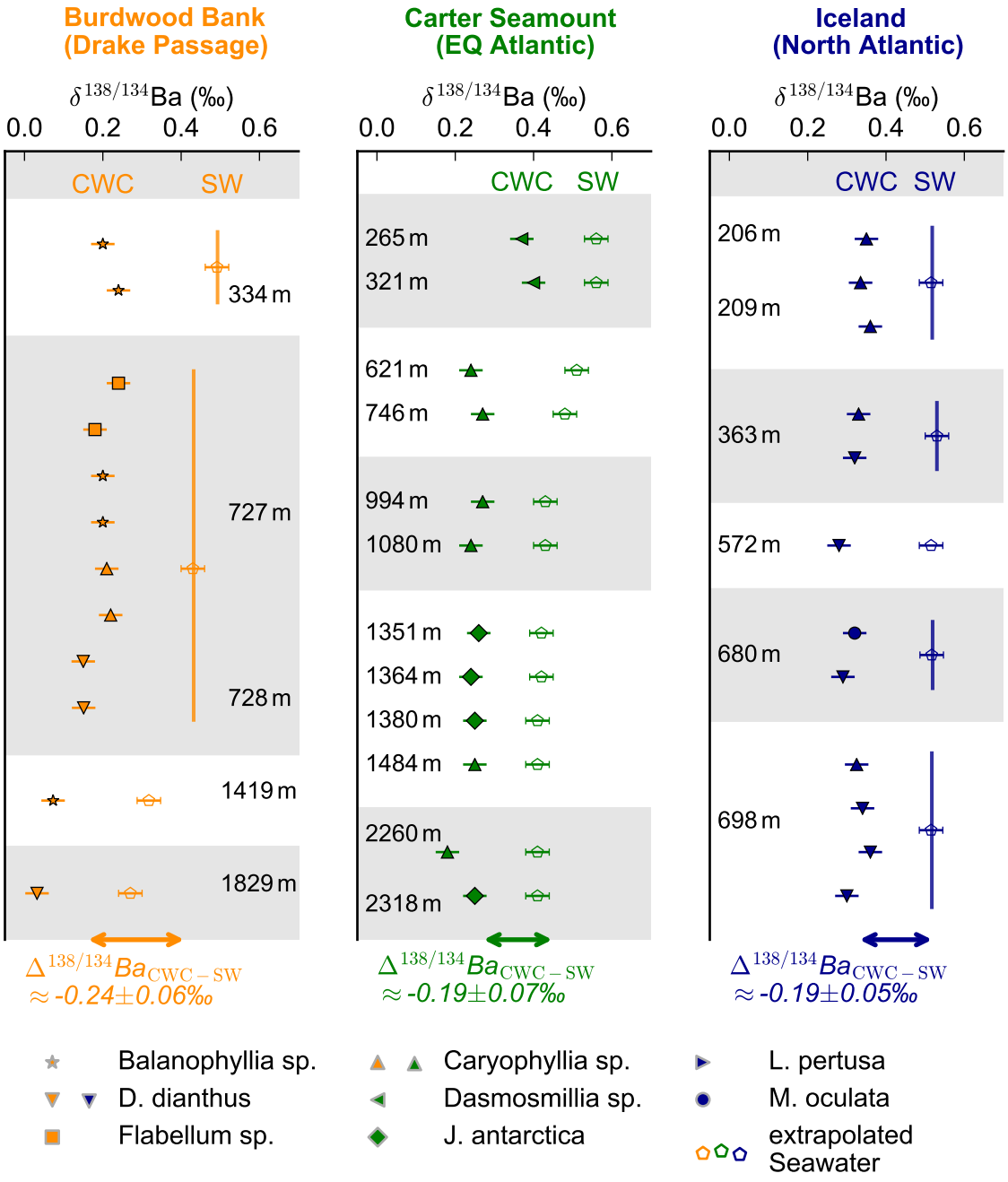

Figure 8.5: $\delta^{138/134}$Ba in CWCs at all three sites compared to ambient seawater
CWCs are shown as filled symbols and seawater signatures as open symbols. Seawater values are linearly extrapolated to the depth each coral grew in. All CWCs are isotopically lighter than ambient seawater, with higher Ba isotopic compositions in shallower depths than in deeper waters. Within uncertainties all sites show a similar overall fractionation. The mean fractionation of Burdwood Bank corals is $\Delta^{138/134}Ba_{CWC\text{-}SW} = -0.24 \pm 0.06$ ‰ while Carter Seamount and Iceland corals both fractionate by -0.19 ± 0.07‰, ± 0.05‰, respectively.

or the enrichment factor

$$\begin{aligned} \varepsilon &= (\alpha - 1) \times 1000 \\ &\approx \Delta^{138/134}Ba_{CWC\text{-}SW} \\ &= \delta^{138/134}Ba_{CWC} - \delta^{138/134}Ba_{SW} \end{aligned} \tag{8.3}$$

with an external analytical 2σ of ± 0.04 ‰ propagated from the analytical 2σ of $\delta^{138/134}$Ba (± 0.03 ‰). Individual enrichment factors range from -0.19 ‰ to -0.29 ‰ with an average of -0.24 ± 0.06 ‰. The uncertainty of the average is assumed to be the larger of either the propagated external reproducibility or the 2σ obtained when averaging over a number of corals.
Taxa analysed from Carter Seamount include two *Dasmosillia sp.*, six *Caryphyllia sp.*, and four *Javania sp.* covering water depths from 265 to 2318 m. $\delta^{138/134}$Ba varies from 0.18 – 0.40 ‰ associated with enrichment factors of -0.16 to -0.27 ‰, with a mean of -0.19 ± 0.07 ‰.
CWC analysed from Iceland only cover shallow water depths between 206 and 698 m. Three species, six *D. dianthus*, five *L. pertusa*, and one *M. oculata*, show an isotopic composition of 0.28 – 0.36 ‰. The enrichment $\Delta^{138/134}Ba_{CWC\text{-}SW}$ between seawater $\delta^{138/134}$Ba and coral $\delta^{138/134}$Ba is -0.16 to -0.24 ‰ also averaging to -0.19 ± 0.05 ‰.
The fractionation $\Delta^{138/134}Ba_{CWC\text{-}SW}$ between cold-water corals and seawater averaged over all locations and species is -0.21 ± 0.08 ‰ (2σ; 2SE = ± 0.01 ‰) (α(Ba) = 0.99979 ± 0.00008) (Fig. 8.6). Averaging separately for each species leads to a Ba fractionation between -0.17 and -0.25 ‰ (Fig. 8.6 and Tab. A.12). The genus *Balanophyllia sp.* (n = 5) shows the largest Ba fractionation of -0.25 ± 0.01 ‰ (2SE) while *Javania sp.* (n = 4) fractionate Ba by only -0.17 ± 0.01 ‰. The two genus with the highest variability in $\Delta^{138/134}$Ba were *D. dianthus* and *Caryophyllia sp.* with values ranging from -0.16 ‰ to -0.28 ‰ averaging to -0.22 ± 0.02 ‰ (2SE), and -0.16 ‰ to -0.27 ‰ averaging to -0.21 ± 0.03 ‰ (2SE), respectively.

8.4 Discussion

8.4.1 Constancy of $D_{CWC/SW}$(Ba)

The mean partition coefficient derived by a linear fit to all data is $D_{CWC/SW}$ (Ba) = 1.8 ± 0.4 (2SE, see Fig. 8.4a), and for separate samples covers a range from 1.5 to 2.4. These values are similar to those in previous studies (Spooner et al., submitted; Anagnostou et al., 2011). Anagnostou et al., 2011's results ($Ba/Ca_{CWC} = 1.4\,(\pm 0.3)\,Ba/Ca_{SW} + 0\,(\pm 2)$) did not reveal a significant correlation between the partition coefficient and seawater temperature, salinity or pH. Spooner et al., submitted analysed possible environmental impacts on D in more detail confirming the Anagnostou et al., 2011 finding, and indicating that D is independent of seawater nutrient content and oxygen concentrations. Data in this study supports the previous finding that incorporation of Ba into CWCs does not depend on seawater temperature (Fig. 8.8a), salinity, pH or nutrient content significantly, but happens at constant D values. This supports the use of CWCs to reconstruct past oceanic Ba concentrations, with potential application to assess past biogeochemical cycling of Ba, and/or ocean circulation.

8.4.2 Constancy of $\Delta^{138/134}Ba_{CWC\text{-}SW}$

With a mean enrichment factor of -0.21 ± 0.08 ‰ (Fig. 8.6) all thirty-six coral samples analysed in this study are isotopically lighter in ^{138}Ba than ambient seawater. The incorporation of lighter isotopes during carbonate fractionation agrees with other isotope systems such as Ca (e.g. Fantle and DePaolo, 2007; Böhm et al., 2006), Sr (e.g. Raddatz et al., 2013; Fietzke and Eisenhauer, 2006), Mg (e.g. Yoshimura et al., 2011) and Li (e.g. Rollion-Bard et al., 2009; Marriott et al., 2004). The most likely explanation for the fractionation is a kinetic effect combined with biological impacts (e.g. Böhm et al., 2006; DePaolo, 2004). A first study analysed two *L. pertusa* from

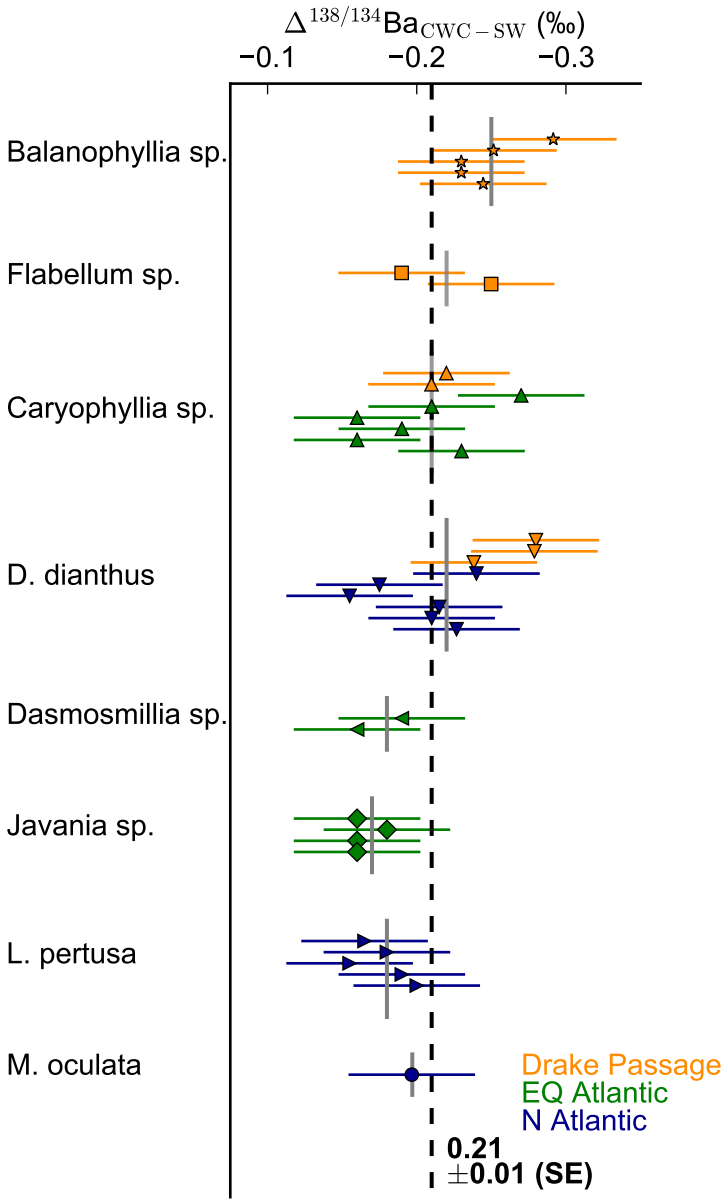

Figure 8.6: $\Delta^{138/134}Ba_{CWC}$ for each species / genus separately
The overall fractionation between CWCs and seawater is $\Delta^{138/134}Ba_{CWC}$ = -0.21 ± 0.08 ‰ (2σ and 0.01 ‰ 2SE). Maximal species specific fractionation is $\Delta^{138/134}Ba_{CWC}$ = -0.25 ± 0.02 ‰ for *Balanophyllia sp.* and minimal $\Delta^{138/134}Ba_{CWC}$ = -0.17 ± 0.01 ‰ for *Javania sp.* (uncertainties are the larger of external reproducibility and 2σ from averaging). The species *D. dianthus* shows the largest variability in $\Delta^{138/134}Ba_{CWC}$ with a range of -0.16 to -0.28 averaging to -0.22 ± 0.03 ‰.

the Norwegian margin exhibiting $\delta^{138/134}$Ba of 0.25 ± 0.11 and 0.3 ± 0.11 (Pretet et al., 2016), which is equal within uncertainties to the corals from the North Atlantic (Hafadjup and Reykjanes Ridge) analysed here. Further analyses on cultured aragonitic scleractinian corals showed a more variable fractionation than observed here (Pretet et al., 2016). Tropical corals were cultured

in an aquarium filled with Mediterranean surface water off Monaco. The fractionation varied between -0.02 ‰ (*Acropora sp.* and *Porite sp.*) and -0.35 ‰ (*Stylophora sp.* and *Montipora sp.*), implying a significantly higher variance (Fig. 8.7).

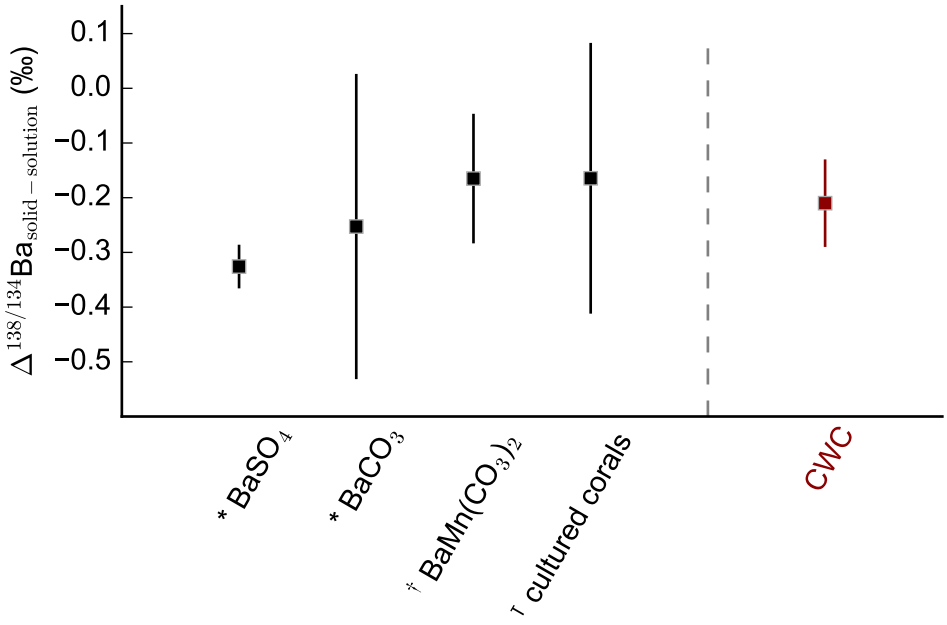

Figure 8.7: Comparison of $\Delta^{138/134}$Ba to published precipitation experiments
* $BaCO_3$ and * $BaSO_4$ precipitates were analysed by von Allmen et al., 2010, † $BaMn(CO_3)_2$ by Böttcher et al., 2012 and ᵀ cultured tropical corals by Pretet et al., 2016. Uncertainties are 2σ over published samples.
The variation seen in precipitates is larger than for all thirty-six natural CWCs analysed in this study (red).

Inorganic precipitation experiments of $BaCO_3$, $BaSO_4$ and $BaMn(CO_3)_2$ showed a similar preference for incorporation of lighter isotopes, with a maximal fractionation of -0.4 ‰ observed between solution and precipitate (Böttcher et al., 2012; von Allmen et al., 2010) (Fig.8.7). Compared to these studies and Pretet et al., 2016, the analytical reproducibility for $\Delta^{138/134}$Ba could be improved by a factor of about 4. The theory of an equilibrium fractionation leads to an expected fractionation for the $BaSO_4$ precipitation in the water column of $\Delta BaSO_4$-SW = -0.28 ± 0.10 ‰ (Horner et al., 2015) matching our results.
There is no correlation between water temperature (between 2 and 12 °C) and Ba isotope fractionation ($\Delta^{138/134}$Ba) observed in this study (Fig. 8.8(b) and Tab. A.11). No previous study has assessed the temperature dependency of $\Delta^{138/134}$Ba on $CaCO_3$ formation, although no temperature dependence of fractionation in laboratory grown $BaCO_3$ precipitates was found (von Allmen et al., 2010). A possible effect of precipitation rates was observed for the Ba fractionation into $BaCO_3$ precipitates with a larger fractionation for slower precipitation rates. Transferring this observation to the higher variance seen in the cultured corals compared to the natural coral analysed in this study cannot explain the observed discrepancy. Growth rates of cultured corals were considerably higher (20 – 45 mm/a; (Pretet et al., 2016)) than for natural corals (*D. dianthus*: 0.5 – 3.1 mm/a and *L. pertusa*: 5 – 26 mm/a (Orejas et al., 2008; Gass and Roberts, 2006;

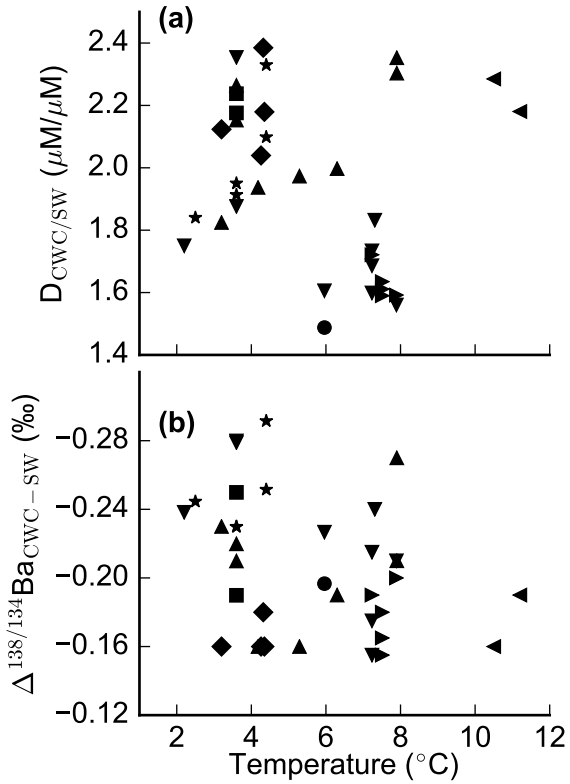

Figure 8.8: Temperature dependency of $D_{CWC/SW}$ (a) and $\Delta^{138/134}Ba_{CWC}$ (b)
In both cases, no correlation to temperature can be observed. Correlation factors are: r^2 ($D_{CWC/SW}$) = 0.02 and r^2 ($\Delta^{138/134}Ba_{CWC}$) = 0.12.
Symbols denote different species. Please refer to Fig. 8.5.

Mortensen, 2001; Mortensen et al., 1998). Therefore, if CWCs followed the behaviour of $BaCO_3$ precipitates, all faster grown cultured corals should exhibit a lower fractionation of Ba isotopes than natural corals. This cannot be observed. In fact, the fractionation observed in this study lies in the middle of the fractionation range reported by Pretet et al., 2016 and not at the upper end. Additionally, growth rates of the species analysed in this study differ noticeably, but did not have a significant effect on the fractionation of Ba.
No substantial correlation between the fractionation and nutrient availability could be observed (see PO_4 in Tab. A.11). Analyses of other environmental factors like pH, salinity etc. provided no clear evidence for significant impacts on Ba fractionation (Tab. A.11). Furthermore, there was no substantial influence of dissolved Ba concentration in seawater on the Ba fractionation (r^2 = 0.16; Fig. 8.9).
Different species span a range of the enrichment factors from -0.17 ± 0.01 ‰ (2SE) (*Javania sp.*) to -0.25 ± 0.02 ‰ (*Balanophyllia sp.*) (Fig. 8.6). However, this possible species or vital effect lies within 2σ of the overall fractionation between seawater and CWCs $\Delta^{138/134}Ba_{CWC\text{-}SW}$ (± 0.08 ‰). The tendency of CWCs from the Drake Passage compared to the Equatorial and North Atlantic of -0.05 ‰ (Fig. 8.5) also lies within the uncertainty of the enrichment factor and may hence be insignificant. Furthermore, these two effects could potentially be influenced or even induced by the other. Species that indicate an overall higher fractionation than the average

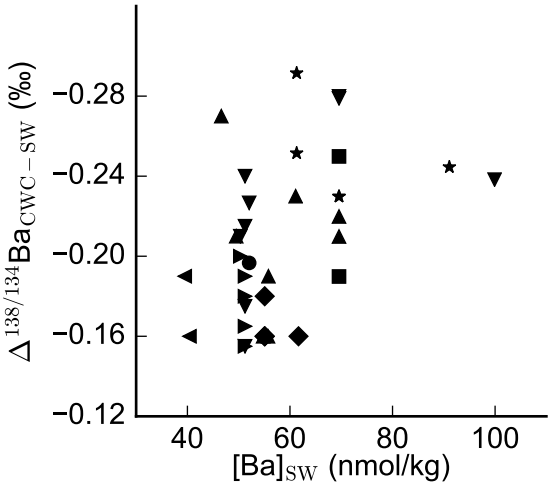

Figure 8.9: Influence of dissolved Ba concentration in seawater on $\Delta^{138/134}Ba_{CWC}$
No correlation between $[Ba]_{SW}$ and Ba fractionation can be observed ($r^2 = 0.16$). Symbols denote different species. Please refer to Fig. 8.5.

over all CWCs $\Delta^{138/134}Ba_{CWC\text{-}SW}$ seem to have mainly grown in the Drake Passage. Hence, a more detailed study is needed to make a conclusive argument about possible vital effects of species from or the conditions in the Drake Passage (Southern Ocean) on $\Delta^{138/134}Ba_{CWC\text{-}SW}$.

8.4.3 $\delta^{138/134}$Ba: a new proxy for paleoceanography

Recent studies have demonstrated a strong linear relationship between $\delta^{138/134}$Ba and [Ba] in seawater across the full range of modern open-ocean [Ba] values (Bates et al., 2017; Hsieh and Henderson, 2017; Horner et al., 2015). Local deviations from this relationship could provide evidence for local inputs of Ba with distinct isotope compositions. Variation in the nature of the global relationship may also have occurred in the past indicating changes in the global biogeochemical cycling of Ba through time. The fact that both $D_{CWC/SW}$ (Ba) and $\Delta^{138/134}Ba_{CWC\text{-}SW}$ are found to be constant for CWCs regardless of growth environment in this study, suggests that measurements on fossil corals would allow reconstruction of the past ocean relationship between [Ba] and $\delta^{138/134}$Ba. Analysis of coralline Ba/Ca by itself can provide information about the [Ba] of the water the coral grew in, with possible implications for changing productivity or water circulation at the location of growth. However, measurements of this parameter alone cannot provide information about local inputs of Ba, nor possible changes in the whole oceanic We can demonstrate the potential accuracy of seawater reconstruction from cold water corals based on the data of this study. A constant $D_{CWC/SW}$ (Ba) (Chap. 8.3.3) and $\Delta^{138/134}Ba_{CWC\text{-}SW}$ (Chap. 8.3.4) are assumed to 'reconstruct' the modern seawater relationship between dissolved [Ba] and $\delta^{138/134}$Ba (Fig. 8.10). As before we assumed a fixed seawater Ca content to convert Ba/Ca_{SW} into $[Ba]_{SW}$ (nmol/kg). The reconstructed seawater relationship has slope and intersect values that are equal, within uncertainty, to the relationship observed in seawaters in this and previous studies (Fig. 8.10). The average $\delta^{138/134}$Ba deviation of each reconstructed seawater value from the best-fit line through all seawater observations is 0.03‰ indicating the likely level to which reconstruction of past seawater composition is possible. This level of uncertainty is sim-

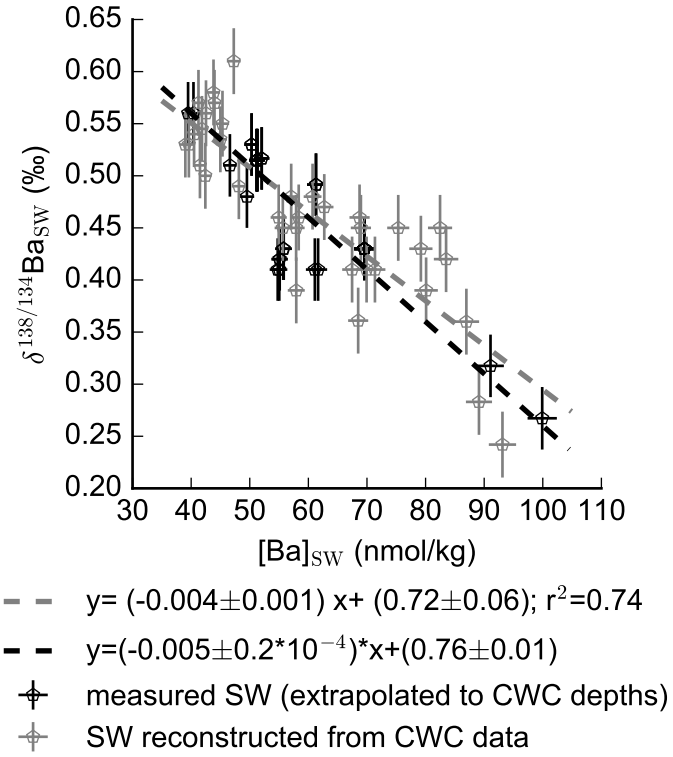

Figure 8.10: Comparison between measured seawater $[Ba]_{SW}$ and $\delta^{138/134}$Ba extrapolated to the depths the CWCs grew in (black) and 'reconstructed' seawater data (grey)
The reconstruction was achieved by applying the constant partition coefficient and isotopic fractionation of Ba on the measured CWC data. Uncertainties shown are the external reproducibilities from our measurements. The reconstructed data agree very well with the originally measured data. Additionally, the well-established relationship between $[Ba]_{SW}$ and $\delta^{138/134}$Ba is reconstructed by a linear fit (reconstructed: grey dashed line; published seawater data: black dashed line and see Fig. 8.3).

ilar to the uncertainty of an individual Ba isotope analysis, suggesting that the range of values observed for $\Delta^{138/134}Ba_{CWC\text{-}SW}$ and $D_{CWC/SW}$ (Ba) in this study are largely due to uncertainty in measurement, rather than due to systematic differences within the dataset. Furthermore, the level of uncertainty is small relative to the observed geographical variation in the modern ocean (Fig. 8.3), suggesting the ability to provide useful reconstructions of the Ba cycle in the past.
Therefore, the capabilities of the tracer $\delta^{138/134}$Ba to provide new insight into nutrient cycling and continental upwelling (Bates et al., 2017; Horner et al., 2015), riverine inputs (Cao et al., 2016) or changes in hydrothermal inputs (Hsieh and Henderson, 2017) in the modern ocean, could be extended to records of changes in the past.

8.5 Conclusions

The first detailed study of the isotopic composition of Ba ($\delta^{138/134}$Ba) in cold-water corals (CWC) was presented using eight different coral taxa. Corals from the North Atlantic, the

Equatorial Atlantic, and the Drake Passage were analysed, covering a wide range of environmental conditions, Ba concentrations, and Ba isotopic compositions. An average enrichment factor of $\varepsilon_{Ba} \approx \Delta^{138/134}Ba_{CWC\text{-}SW}$ = -0.21 $\pm$ 0.08 ‰ was observed that did not depend on seawater dissolved Ba concentration, temperature, salinity, pH or nutrients. Constancy of the partition coefficient for Ba, found in previous studies, was also confirmed ($D_{CWC/SW}$ (Ba) = 1.8 $\pm$ 0.4), regardless of the growth environment. The constancy of elemental partitioning and isotope fractionation indicate that coupled [Ba] and $\delta^{138/134}$Ba analysis in CWCs can be used to reconstruct the local and global relationship between seawater [Ba] and $\delta^{138/134}$Ba. New information about inputs of Ba and past global oceanic cycling of Ba will be gained. This offers the possibility to trace, changes in riverine and hydrothermal inputs,the biological pump and nutrient cycling in the past ocean.

9 Conclusions and outlook

In this thesis, a multi-proxy and multi-archive approach was used to investigate intermediate ocean dynamics in the southern Gulf of Cádiz (sGoC) over the last 65 ka. This region is of particular oceanographic interest as it links the Atlantic Ocean to the Mediterranean Sea. Southern and northern sourced Atlantic water masses interact with Mediterranean water, leading to a highly dynamic oceanic system, in particular in the thermocline between 300 and 1000 m water depth. Periods such as the Last Glacial Maximum (LGM) and rapid cooling and warming events Heinrich stadials (HS) or Dansgaard Oeschger cycles (DO) are connected to a reorganisation of the Atlantic overturning circulation (Adkins, 2013). However, understanding the exact processes involved in the ocean's reorganisation remain a major frontier of paleoceanography. Studies have focussed on the warm well-mixed surface ocean and the slowly moving deep ocean waters storing carbon and heat. The thermocline studied here, which represents the link and a buffer between these two water bodies, has been widely overlooked.
Here, cold-water corals (CWCs) from two closely located coral-bearing cores retrieved in different water depths were analysed. On the basis of U-series dating of the CWCs, the evolution of mound aggregation was investigated. Additionally, Li/Mg temperature analyses were carried out and water mass reservoir ages were obtained from coupling ^{14}C to U-series dating. Furthermore, the εNd evolution tracing water mass changes was recorded in the CWCs and fort the first time extended by the independent archive of two neighbouring hemipelagic sediment cores.

These paleoceanographic proxies cannot deliver information on another important aspect for the understanding of thriving CWC colonies: the food supply. When this PhD project began, no reliable proxy for nutrients or surface biological productivity recorded in CWCs was available. For example, the element ratios P/Ca or Cd/Ca had to be discarded as both are influenced greatly by biological processes in the coral, so-called vital effects (e.g. Anagnostou et al., 2011; Montagna et al., 2006; Keigwin and Boyle, 1989). Therefore, I investigated the potential of Ba isotopes to reconstruct changes in nutrients or surface biological productivity in the last part of my thesis.

Paleoceanographic reconstructions in the southern Gulf of Cádiz

The basis of paleoceanographic reconstructions on CWCs is our ability to precisely date them by U-series dating. The evolution of coral growth obtained from the two coral-bearing cores from the Pen Duick Escarpement (PDE, 550 m) and the Moroccan Atlantic CWC Province (MACP, 950 m) revealed that, unlike previously reported for the last glacial, CWCs in the sGoC did not only occur between 40 – 14 ka, but active mound aggregation already started around 65 ka (Chap. 4). However, prior to 40 ka, CWC mound aggregation seems to have been reduced to the deeper of the two provinces (MACP). For the first time, glacial mound aggregation rates (MAR) above 50 cm/ka, and in particular higher than 100 cm/ka during the LGM, were recorded for the temperate East Atlantic. Similarly high MARs are presently mainly reported for the North

Atlantic or the Mediterranean Sea, while glacial records placed thriving coral mounds to more southern sites.

To investigate the environmental conditions that lead to this thriving CWC mounds, Li/Mg temperatures were analysed on the same corals, with a particular focus on the main growth period during the LGM (Chap. 5). Intermediate water temperatures obtained for the LGM were around 0°C, implying a modern-LGM anomaly of roughly -10°C. However, sea surface temperature records (SST) merely suggested a modern-LGM anomaly of about -2°C (Eynaud et al., 2009; Waelbroeck et al., 2009). This implies a strong rise of the thermocline towards shallow depths and an increased density gradient between surface and intermediate waters. This temperature profile could only be caused by the penetration of a polar mid-depth water mass into the GoC. Three water masses dominate the intermediate water in the GoC: *Mediterranean Sea Water* (MSW), which is *Mediterranean Outflow Water* (MOW) modified by Atlantic water, *Eastern North Atlantic Central Water* (ENACW) and *Eastern Antarctic Intermediate Water* (EAAIW). As MOW was reported to exhibit glacial temperatures between 8 and 10°C, an increased influence of this water mass cannot explain the polar temperatures at the CWC sites (Cacho et al., 2006). Both other water masses could have possibly cooled down to polar temperatures. However, a study from the Angolan margin recently reported Li/Mg temperatures of 2°C during the LGM, which can only explain -8°C of the modern-LGM anomaly observed for the sGoC.

To further gain insight into the water mass provenance in the sGoC radiogenic Nd isotopes (εNd) were analysed. For this part of my PhD project, I extended the coralline record of the two coral-bearing cores by additionally analysing Fe-Mn oxyhydroxides in bulk sediment of two independent hemipelagic sediment cores retrieved near the coral sites. One of sediment cores was recovered from PDE, while the other site is situated $\sim$ 85 km south of the coral sites. All four εNd records from the sGoC exhibit overall constant glacial signatures with mean values ranging from -9.32 $\pm$ 0.23 to -9.13 $\pm$ 0.19 for the three northern sites and -8.84 $\pm$ 0.26 for the slightly southerly located sediment core. Compared to present εNd signatures, a systematic shift towards more radiogenic Nd isotopes was recorded in the last glacial (1.5 – 3 ε units). The extent of this shift cannot be explained by modern εNd signatures of the three water masses entering the GoC, as present εNd of MOW, EAAIW and ENACW are all less radiogenic prior to entering the GoC. Again, MOW could be ruled out as the water mass undergoing glacial-Holocene changes (Dubois-Dauphin et al., 2017b). Therefore, at least one of the two end-members ENACW and EAAIW entering the GoC, both exhibiting modern εNd signatures around -11.2, must have changed severely, supporting the hypothesis of dominant glacial polar ENACW or EAAIW provenance in the sGoC.

The slightly more radiogenic signature in the southerly sediment core compared to the three northern sites (85 km distance) suggests that the changed glacial end-member was even more dominant in the south. At the start of the deglaciation warming period around Bølling-Allerød (15 ka), the two sediment records converged and followed the same trend towards less radiogenic signatures which stopped around 6 – 7 ka. This change in εNd (1.1 ε units) could possibly represent the shift of one or both of the end-members ENACW and EAAIW from glacial to modern conditions.

An additional water mass provenance proxy used is the reservoir age of water masses (R) obtained from coupled ^{14}C and U-series dating of CWCs. During the LGM a well ventilated water mass was reported, similar to Holocene conditions. This constant signal was interrupted by four punctuated increases in R. The amplitude of the water mass ageing during these events was the same as a recently reported LGM increase in reservoir ages recorded in CWCs from the Angolan

margin. This suggested EAAIW dominance recorded in sGoC corals from intermediate waters during these punctuated periods, however, the majority of CWCs bathed in a well ventilated water mass during most of the LGM.
Considering the ensemble of proxies and archives analysed in the sGoC, a seesaw pattern of intermediate waters changing between predominant ENACW and EAAIW is proposed. In this scenario glacial ENACW and EAAIW both exhibit polar temperatures and more radiogenic εNd signatures than in the modern ocean and were distinguishable by their reservoir ages, with glacial ENACW better ventilated than glacial EAAIW.

In addition to these regional implications, the paleoceanographic records revealed several further reaching aspects relevant for global paleoceanographic reconstructions.
A compilation of published records on mound aggregation allowed for an extrapolation of maximal CWC mound base ages in the ocean. Based on this summary the timing of initial CWC larvae settlement was determined to roughly 3.4 Ma. This coincides with the mid-Pliocene warm period and the gradual onset and further amplification of Northern Hemisphere glaciation. To further improve this first estimate of the start of coralline mound aggregation, it is essential to get better constraints on base ages of CWC mounds throughout the entire ocean. The result of this compilation, and the low number of long drilling cores in particular, have clearly highlighted the risk of over- or underestimating the mound aggregation rate if only the top few meters of a mound are analysed. Only fully penetrating CWC mounds and dating bottom CWCs can yield reliable time scales for the evolution of CWC mounds. This also implies the introduction of new precise dating tools on CWCs resolving the required time scale, which could possibly be achieved by U/Pb dating that covers ages of $1-4.5$ Ma.
A close correlation between the intermediate water Li/Mg temperature record and long-term atmospheric climate signals recorded in ice cores was found. Moreover, the significant impact of rapid warming and cooling events, DO cycles, on the intermediate temperatures could be resolved for the first time. This clearly highlights the huge potential of Li/Mg temperatures from CWCs as a proxy for changes in the mid-depth thermal structure of the ocean. A similar correlation was observed in the εNd record. While general long-term glacial signals were constant, this was overlain by a few punctuated variations that coincided with DO cycles. Models for oceanic dynamics in the past, present and future currently consider only reconstructions from deep or surface waters. The highly dynamical thermocline linking and buffering these two water bodies, however, is usually not well represented and unconstrained by observations. The observations in Li/Mg and εNd are only based on up to four records from one oceanic region. Still, they clearly highlight the potential benefit that can arise from implementing records of past mid-depth temperature and water mass provenance dynamics. A wider record of regions throughout the Atlantic ocean could further provide evidence of the importance of the mid-depth ocean and the thermocline in particular. Multi-sampling on large coral fragments could provide records of yearly or decadal variability that could for example trace cold or warm fronts.
However, it should be noted that, while physically possible, the particularly cold temperatures recorded during the LGM reaching down to -1.57 $\pm$ 1°C strongly suggest the need to re-evaluate the calibration curve that links coralline Li/Mg to seawater temperatures. In the present calibration curve (Montagna et al., 2014) the low temperature regime below $\sim$6°C is not well represented, which was the main temperature range investigated in this study. In addition to Li/Mg measurements of modern CWCs collected from seawaters below 6°C, analysis of CWCs grown under stress, possibly causing vital effects, is highly recommended. Such a re-evaluation could

resolve possible systematic biases and potentially reduce the uncertainty of the calibration curve below 1°C, which is currently the main source of external uncertainty. While such a re-evaluation could possibly reduce the anomaly observed in this project by a few degrees, it is unlikely to yield temperatures warmer than e.g. 4°C, which would still imply a modern-LGM offset of at least -6°C.

The combination of the same tracer in two co-located but independent marine archives, εNd in CWCs and from Fe-MN oxohydrates in bulk hemipelagic sediments, is unique. While CWCs provided an εNd record of the temperate Northeast Atlantic in a precisely datable archive, hemipelagic sediment cores are relatively dated using stable isotope stratigraphy and radiocarbon dating, which implies partially unknown reservoir effects. εNd signatures in CWCs are averaged over a few years to a decade while bioturbation and other mixing processes lead to time resolutions in the sediment between 50 and 715 a per sample. This was observable in more frequent variations in the CWC record. Though providing a higher time resolution, the CWC record left several gaps that could mostly be bypassed by the sediment analysis that showed a continuous accumulation. As expected, both archives traced similar centennial or longer oceanic patterns but differed slightly in timing and/or amplitude of observed changes in εNd.

An offset of 1.3 – 2.4 ε units between seawater εNd signatures and modern core top analysis was reported in this thesis. This offset could not be explained with the data set of this study. One possible cause is the remobilisation of Nd in pore waters. It could also result from the 'snapshot' characteristic of the modern seawater samples, representing the water mass provenance at a point in time, i.e. a specific time of day. It has been shown that internal waves coinciding with the time scale of tide cycles can be observed in the complex bathymetry of the GoC. Due to the long residence time of εNd (360 – 700 a), variations of εNd signatures on time scales of days, years or decades can only be caused by existing gradients within the investigated region, which is clearly the case for the sGoC. In archives like hemipelagic sediment cores these variations would be averaged over centuries or even millennia, possibly introducing a bias. It should be noted that similar offsets have been observed in other archives and locations showing fast spatial and temporal variations in present oceanic conditions. To better understand the difference between the εNd signature in seawater and modern sediment core tops, extensive seawater analysis directly above the archive would have to be carried out over hourly, daily, seasonal, inter-annual and decadal time scales.

To better constrain the oceanic dynamics of the three water masses present in the sGoC and discern between a glacially modified EAAIW and/or ENACW, the record compiled in this study should be extended by additional multi-proxy analyses on archives both slightly north and south of the GoC. This would provide the urgently needed information about the two glacial end-members prior to entering the GoC. Such archives could be CWCs from coral-bearing cores off Mauritania (south, current Master's project of Hannah Schneider) and from the Galicia Bank (north, current Bachelor's project of Hanna Rosenthal). When including the Angolan margin, this could possibly even resolve the spatial evolution of EAAIW on its long path from its region of formation in the Southern Ocean to the GoC. Additionally, the ^{14}C record of both coral-bearing cores from the sGoC will be completed which will provide a more continuous record of reservoir age reconstructions.

Ba isotope fractionation into cold-water corals

The ensemble of proxies analysed for the paleoceanographic reconstructions cannot provide information about the most important factor favouring or limiting active CWC growth: the supply of sufficient food. Prior to this project, no reliable proxy in CWCs tracing the availability of nutrients or the closely linked surface biological productivity was available. The nutrient-like distribution of Ba in the ocean gave rise to the idea that Ba could trace nutrients and/or changes in the biological pump. However, the processes involved in the Ba cycle are not well understood. Recently, studies on coupled Ba isotopes ($\delta^{138/134}$Ba) and concentration [Ba] in seawater highlighted the great potential of this new proxy to better understand the Ba cycle (e.g. Horner et al., 2015).
Here, a first systematic study of δ^{138}Ba in CWCs was conducted to investigate if CWCs are a suitable archive for seawater Ba isotopes. Modern corals of eight different taxa, from the North Atlantic, the Equatorial Atlantic and the Drake Passage were analysed, covering a wide range of environmental conditions, Ba concentrations and δ^{138}Ba. The average enrichment factor between CWCs and seawater $\varepsilon_{Ba} \approx \Delta^{138/134}Ba_{CWC\text{-}SW} = -0.21 \pm 0.08$ ‰ did not depend on dissolved Ba concentrations in seawater, temperature, salinity pH or nutrients. Therefore, applying this constant fractionation, δ^{138}Ba from CWCs can be used to reconstruct seawater δ^{138}Ba signatures. Furthermore, as proposed by previous studies (Spooner et al., submitted; Anagnostou et al., 2011), constancy of the partition coefficient of Ba could be confirmed ($D_{CWC/SW}$ (Ba) = 1.8 ± 0.4). This strongly indicates that coupled [Ba] and $\delta^{138/134}$Ba analysis in CWCs can be used to reconstruct the past relationship between seawater [Ba] and $\delta^{138/134}$Ba on both regional and global scales from which new knowledge about the past global oceanic Ba cycle can be gained. With this knowledge, the potential of $\delta^{138/134}$Ba to trace changes in the biological pump and nutrient supply, riverine or hydrothermal inputs will greatly be improved.

Future studies on $\delta^{138/134}$Ba recorded in fossil CWCs will be based on two approaches.
First, fossil corals of the same species analysed in this study that grew during a period of different climate and oceanic conditions from today, e.g. the LGM, should be investigated. Coupled [Ba] and $\delta^{138/134}$Ba analysis of a few sites covering a wide range of oceanic conditions and $\delta^{138/134}$Ba could provide insight about possible modern-LGM changes in the Ba cycle.
Second, a study over a longer time period on a coral-bearing core known to have recorded oceanic changes could offer proof that changes in surface biological productivity and/or nutrient supply are recorded in coralline $\delta^{138/134}$Ba. For this study, the two coral-bearing cores from the Gulf of Cádiz analysed in the first part of this PhD project provide a unique opportunity to test the potential of $\delta^{138/134}$Ba as a nutrient and /or surface productivity proxy on a cold-water coral record that is already well characterised with regard to other environmental conditions.

10 Published and submitted publications of the author

Dubois-Dauphin, Q. Bonneau, L., Colin, C., Montero-Serrano, J.-C., Montagna, P., Blamart, D., Hebbeln, D., Van Rooij, D., Pons-Branchu, E., Hemsing, F., Wefing, A.-M., and Frank, F. (2016). "South Atlantic Intermediate Water Advances into the North-East Atlantic with Reduced Atlantic Meridional Overturning Circulation during the Last Glacial Period: HYDROLOGY OF THE NORTH ATLANTIC". In: *Geochemistry, Geophysics, Geosystems* 17.6, pp. 2336–2353. DOI: 10.1002/2016GC006281.

Spooner, P. T., Robinson, L. F., and Hemsing, F. (submitted). "Ba/Ca Ratio in Cold-Water Coral Skeletons Records Seawater Dissolved Ba Concentration". In: *Chemical Geology.*

Science never solves a problem without creating ten more.

George Bernard Shaw

A Supplementary material

A.1 Southern Gulf of Cádiz

A.1.1 Data

Table A.1: εNd results from both coral-bearing cores MD08-3231 and GeoB-18141-01
Samples denoted with * did not pass the U-series quality control, †samples exhibited $\Delta\Delta^{14}C > 0$ suggesting U-series open system behaviour and $^{\bullet}$ denoted samples with ^{144}Nd intensities <1V during MC-ICPMS analyses.
CWCs from MD08-3231 were analysed in the course of this PhD one Bachelor's projects (Rieger, 2015) denoted by [2], which were measured at LSCE in Gif-sur-Yvette. All CWCs from GeoB-18141-01 were analysed during this project.

Lab No (HD)	Lab No (Gif)	^{143}Nd/^{144}Nd	2σ	εNd ‰	int. 2σ ‰	ext. 2σ ‰
MD08-3231						
6576 *[2]		0.512178	0.000012	-8.97	0.23	0.23
6447 [2]	764	0.512171	0.000011	-9.06	0.22	0.24
6533		0.512172	0.000007	-9.09	0.14	0.17
6577 [2]	765	0.512167	0.000011	-9.15	0.21	0.24
6578 [2]	766	0.512167	0.000011	-9.15	0.21	0.24
8402		0.512172	0.000013	-9.09	0.25	0.25
6449 [2]	767	0.512173	0.000009	-9.03	0.18	0.24
6579 [2]	768	0.512169	0.000005	-9.11	0.10	0.24
8403		0.512174	0.000012	-9.04	0.24	0.24
6580 [2]	769	0.512167	0.000012	-9.15	0.23	0.24
6581 [2]	770	0.512156	0.000011	-9.36	0.22	0.24
8404		0.512168	0.000011	-9.16	0.21	0.21
6450 †[2]	771	0.512145	0.000004	-9.58	0.09	0.24
8405		0.512140	0.000013	-9.71	0.25	0.25
8406		0.512149	0.000008	-9.54	0.15	0.17
6583		0.512156	0.000009	-9.40	0.18	0.18
6451 [2]	772	0.512166	0.000012	-9.17	0.23	0.24
6453 [2]	773	0.512150	0.000010	-9.48	0.19	0.24
7009 [2]	774	0.512171	0.000010	-9.07	0.19	0.24
7010 [2]	775	0.512162	0.000008	-9.25	0.15	0.24
7020 [2]	781	0.512173	0.000010	-9.03	0.19	0.24

Lab No (HD)	Lab No (Gif)	$^{143}Nd/^{144}Nd$	2σ	εNd ‰	int. 2σ ‰	ext. 2σ ‰
7019 [2]	780	0.512170	0.000012	-9.09	0.22	0.24
7018 [2]	779	0.512150	0.000012	-9.49	0.24	0.24
8408		0.512153	0.000013	-9.46	0.26	0.26
7015 [2]	777	0.512150	0.000006	-9.49	0.12	0.24
7014 [†2]	778	0.512157	0.000005	-9.35	0.10	0.24
7021 [2]	782	0.512156	0.000010	-9.36	0.19	0.24
7022 [2]	783	0.512158	0.000010	-9.32	0.19	0.24
GeoB-18141-01						
7545		0.512154	0.000011	-9.44	0.21	0.21
7508 •		0.512173	0.000023	-9.07	0.45	0.45
7547 •		0.512138	0.000017	-9.74	0.33	0.33
7549		0.512160	0.000012	-9.33	0.24	0.24
7510		0.512171	0.000008	-9.11	0.17	0.17
7551		0.512173	0.000017	-9.08	0.33	0.33
7511 *		0.512168	0.000010	-9.17	0.20	0.20
7552		0.512156	0.000013	-9.40	0.25	0.25
7553		0.512160	0.000016	-9.32	0.31	0.31
7555 *		0.512153	0.000013	-9.45	0.25	0.25
7556		0.512143	0.000011	-9.66	0.22	0.22
7515		0.512148	0.000014	-9.55	0.28	0.28
7513		0.512147	0.000008	-9.58	0.16	0.17
7516		0.512181	0.000013	-8.91	0.25	0.25
7559		0.512161	0.000014	-9.31	0.27	0.27
7517		0.512163	0.000011	-9.26	0.21	0.21
7518 •		0.512137	0.000021	-9.78	0.40	0.40
7519		0.512175	0.000008	-9.03	0.16	0.17
7563 •		0.512147	0.000025	-9.58	0.49	0.49
7522		0.512139	0.000011	-9.73	0.22	0.22
7523		0.512171	0.000014	-9.11	0.27	0.27
7524 *		0.512170	0.000017	-9.12	0.33	0.33
7520 *		0.512154	0.000012	-9.45	0.23	0.23
7569		0.512147	0.000011	-9.59	0.22	0.22
7575		0.512146	0.000013	-9.60	0.25	0.25
7105		0.512149	0.000009	-9.55	0.18	0.18
7576		0.512136	0.000010	-9.78	0.20	0.20
7111		0.512136	0.000007	-9.79	0.14	0.17
7577		0.512137	0.000010	-9.76	0.20	0.20

Table A.2: εNd data from hemipelagic sediment cores MD04-2805-CQ and MD08-3227
MD04-2805-CQ analyses were performed at MARUM (Kiel, Germany), MD08-3227 samples were measured at IUP (Heidelberg, Germany).
* denoted samples with ^{144}Nd intensities <1V during MC-ICPMS analyses were discarded.

Lab No (HD)	Depth (cm)	σ (cm)	Age (ka BP)	^{143}Nd/^{144}Nd	2σ	εNd (‰)	int. 2σ (‰)	ext. 2σ (‰)
MD08-3227								
1572 *	0.5	0.5	5.20	0.512190	0.000005	-8.69	0.09	0.12
1353	5.5	0.5	5.56	0.512148	0.000005	-9.51	0.09	0.21
1362	10.5	0.5	5.93	0.512153	0.000005	-9.41	0.11	0.21
1383	15.5	0.5	6.29	0.512128	0.000005	-9.91	0.10	0.13
1383	15.5	0.5	6.29	0.512132	0.000005	-9.83	0.10	0.13
1379	20.5	0.5	6.65	0.512131	0.000005	-9.86	0.10	0.13
1574	25.5	0.5	7.01	0.512143	0.000005	-9.61	0.09	0.12
1406	30.5	0.5	7.37	0.512129	0.000005	-9.88	0.10	0.13
1523	35.5	0.5	7.73	0.512141	0.000012	-9.67	0.23	0.23
1327	40.5	0.5	8.09	0.512137	0.000004	-9.73	0.08	0.17
1555	45.5	0.5	8.45	0.512147	0.000004	-9.55	0.08	0.12
1374	50.5	0.5	8.82	0.512143	0.000005	-9.61	0.11	0.21
1347	55.5	0.5	9.18	0.512140	0.000005	-9.67	0.10	0.21
1339	60.5	0.5	9.54	0.512150	0.000005	-9.48	0.10	0.21
1323	65.5	0.5	9.90	0.512151	0.000006	-9.47	0.11	0.17
1371	70.5	0.5	10.26	0.512144	0.000005	-9.60	0.10	0.21
1402	75.5	0.5	10.62	0.512152	0.000005	-9.44	0.09	0.13
1540	80.5	0.5	10.98	0.512164	0.000005	-9.20	0.10	0.14
1415	85.5	0.5	11.34	0.512159	0.000005	-9.31	0.10	0.13
1410	90.5	0.5	11.70	0.512152	0.000005	-9.43	0.09	0.13
1547	95.5	0.5	11.97	0.512155	0.000007	-9.38	0.14	0.14
1334	100.5	0.5	12.23	0.512155	0.000004	-9.38	0.08	0.17
1378	110.5	0.5	12.56	0.512162	0.000005	-9.25	0.10	0.13
1516	120.5	0.5	13.56	0.512162	0.000006	-9.24	0.11	0.12
1518	130.5	0.5	14.52	0.512180	0.000007	-8.89	0.14	0.14
1404	140.5	0.5	14.70	0.512177	0.000006	-8.95	0.11	0.13
1537	150.5	0.5	14.88	0.512181	0.000005	-8.87	0.10	0.14
1369	160.5	0.5	15.05	0.512175	0.000005	-8.99	0.10	0.21
1341	170.5	0.5	15.08	0.512179	0.000005	-8.91	0.09	0.21
1357	180.5	0.5	15.09	0.512173	0.000005	-9.02	0.09	0.21
1541	180.5	0.5	15.09	0.512177	0.000005	-8.95	0.09	0.14
1349	190.5	0.5	15.11	0.512179	0.000005	-8.92	0.09	0.21
1412	200.5	0.5	15.13	0.512174	0.000004	-9.01	0.08	0.13
1345	210.5	0.5	15.16	0.512195	0.000006	-8.61	0.12	0.21
1401	220.5	0.5	15.18	0.512186	0.000005	-8.78	0.10	0.13

Lab No (HD)	Depth (cm)	σ (cm)	Age (ka BP)	$^{143}Nd/^{144}Nd$	2σ	εNd (‰)	int. 2σ (‰)	ext. 2σ (‰)
1521	230.5	0.5	15.20	0.512195	0.000006	-8.61	0.11	0.14
1556	240.5	0.5	15.25	0.512185	0.000005	-8.80	0.09	0.12
1331	250.5	0.5	15.91	0.512185	0.000004	-8.79	0.08	0.17
1375	260.5	0.5	15.95	0.512174	0.000005	-9.01	0.10	0.21
1324	270.5	0.5	15.99	0.512182	0.000004	-8.86	0.08	0.17
1364	280.5	0.5	16.02	0.512175	0.000004	-9.00	0.09	0.21
1354	290.5	0.5	16.12	0.512174	0.000006	-9.01	0.12	0.21
1380	300.5	0.5	17.33	0.512181	0.000004	-8.88	0.08	0.13
1403	301.5	0.5	17.38	0.512176	0.000006	-8.97	0.11	0.13
1570	310.5	0.5	17.81	0.512184	0.000005	-8.83	0.09	0.12
1326	320.5	0.5	18.29	0.512179	0.000004	-8.92	0.08	0.17
1548	330.5	0.5	18.77	0.512182	0.000005	-8.85	0.10	0.14
1342	340.5	0.5	19.25	0.512181	0.000006	-8.89	0.12	0.21
1337	350.5	0.5	19.73	0.512188	0.000005	-8.74	0.10	0.21
1531	360.5	0.5	20.30	0.512185	0.000009	-8.79	0.18	0.18
1367	370.5	0.5	21.11	0.512184	0.000005	-8.82	0.09	0.21
1359	380.5	0.5	21.23	0.512184	0.000006	-8.82	0.11	0.21
1551	390.5	0.5	21.35	0.512195	0.000005	-8.61	0.09	0.14
1330	400.5	0.5	21.47	0.512194	0.000004	-8.63	0.08	0.17
1382	410.5	0.5	21.74	0.512178	0.000005	-8.93	0.09	0.13
1515	420.5	0.5	22.01	0.512180	0.000005	-8.90	0.11	0.12
1562 *	430.5	0.5	22.28	0.512196	0.000022	-8.59	0.43	0.43
1340	440.5	0.5	22.45	0.512186	0.000005	-8.77	0.10	0.21
1370	450.5	0.5	22.61	0.512178	0.000005	-8.93	0.09	0.21
1356	452.5	0.5	22.65	0.512189	0.000005	-8.72	0.10	0.21
1321	460.5	0.5	22.78	0.512185	0.000004	-8.80	0.09	0.17
1409	470.5	0.5	22.95	0.512185	0.000006	-8.80	0.11	0.13
1346	480.5	0.5	23.11	0.512186	0.000006	-8.78	0.12	0.21
1329	490.5	0.5	23.28	0.512191	0.000004	-8.68	0.08	0.17
1366	500.5	0.5	23.45	0.512179	0.000006	-8.91	0.12	0.21
1413	510.5	0.5	23.57	0.512183	0.000005	-8.84	0.10	0.13
1381	520.5	0.5	23.69	0.512174	0.000004	-9.01	0.08	0.13
1322	530.5	0.5	23.81	0.512182	0.000004	-8.86	0.07	0.17
1332	540.5	0.5	24.00	0.512186	0.000005	-8.78	0.10	0.17
1373	550.5	0.5	24.20	0.512169	0.000005	-9.11	0.11	0.21
1553	560.5	0.5	24.48	0.512163	0.000006	-9.22	0.12	0.12
1405	570.5	0.5	24.74	0.512183	0.000007	-8.84	0.13	0.13
1566	580.5	0.5	24.84	0.512186	0.000004	-8.77	0.08	0.12
1350	590.5	0.5	24.94	0.512178	0.000005	-8.93	0.09	0.21
1348	600.5	0.5	25.04	0.512176	0.000004	-8.96	0.08	0.21
1338	605.5	0.5	25.09	0.512188	0.000004	-8.75	0.08	0.21
1363	610.5	0.5	25.14	0.512176	0.000005	-8.97	0.10	0.21
1543	620.5	0.5	25.24	0.512188	0.000006	-8.74	0.12	0.14

Lab No (HD)	Depth (cm)	σ (cm)	Age (ka BP)	$^{143}Nd/^{144}Nd$	2σ	εNd (‰)	int. 2σ (‰)	ext. 2σ (‰)
1355	630.5	0.5	25.34	0.512178	0.000005	-8.93	0.10	0.21
1372	640.5	0.5	25.44	0.512176	0.000005	-8.98	0.09	0.21
1325	660.5	0.5	25.70	0.512183	0.000004	-8.83	0.08	0.17
1569	670.5	0.5	25.86	0.512182	0.000004	-8.86	0.08	0.12
1407	680.5	0.5	26.36	0.512183	0.000007	-8.84	0.14	0.14
1524	690.5	0.5	26.53	0.512190	0.000007	-8.70	0.13	0.14
1411	700.5	0.5	26.79	0.512193	0.000005	-8.64	0.09	0.13
1358	710.5	0.5	27.05	0.512170	0.000005	-9.09	0.10	0.21
1351	720.5	0.5	27.31	0.512171	0.000005	-9.07	0.10	0.21
1365	730.5	0.5	27.44	0.512185	0.000022	-8.79	0.42	0.42
1343	740.5	0.5	27.58	0.512189	0.000006	-8.72	0.11	0.21
1377	750.5	0.5	27.71	0.512192	0.000007	-8.65	0.15	0.15
1414	759.5	0.5	27.73	0.512178	0.000005	-8.94	0.10	0.13
1335	760.5	0.5	27.73	0.512161	0.000006	-9.26	0.11	0.21
1535	770.5	0.5	27.75	0.512172	0.000005	-9.06	0.09	0.14
1534	772.5	0.5	27.76	0.512178	0.000006	-8.94	0.12	0.14
MD08-3227								
3037	1	1	0.61	0.512145	0.000007	-9.69	0.13	0.23
3084	11	1	1.13	0.512157	0.000006	-9.5	0.11	0.23
3075	21	1	1.64	0.512151	0.000016	-9.69	0.3	0.23
3055	31	1	2.16	0.512143	0.000005	-9.75	0.11	0.23
3058	41	1	2.66	0.512140	0.000006	-9.81	0.13	0.23
3071	61	1	3.71	0.512135	0.000007	-9.93	0.14	0.23
3061	81	1	4.74	0.512142	0.000006	-9.75	0.11	0.23
3050	101	1	5.77	0.512136	0.000006	-9.85	0.12	0.23
3040	121	1	6.80	0.512133	0.000007	-10	0.13	0.23
3044	141	1	7.72	0.512135	0.000006	-9.92	0.11	0.23
3047	161	1	8.40	0.512141	0.000007	-9.89	0.14	0.23
3031	181	1	9.08	0.512162	0.000005	-9.38	0.1	0.23
3078	201	1	9.76	0.512160	0.000006	-9.42	0.12	0.23
3065	221	1	10.43	0.512145	0.000006	-9.75	0.12	0.23
3068	241	1	11.11	0.512154	0.000007	-9.6	0.14	0.23
3081	261	1	11.77	0.512169	0.000007	-9.26	0.13	0.23
3083	281	1	12.26	0.512176	0.000006	-9.11	0.12	0.23
3090 *	301	1	12.75	0.512208	0.000007	-8.6	0.13	0.23
3087	321	1	13.24	0.512170	0.000006	-9.31	0.12	0.23
3039	361	1	14.22	0.512171	0.000006	-9.2	0.11	0.23
3080	381	1	14.71	0.512184	0.000006	-8.94	0.13	0.23
3089	401	1	15.20	0.512156	0.000007	-9.52	0.14	0.23
3086	421	1	15.69	0.512156	0.000005	-9.51	0.1	0.23
3054	441	1	16.18	0.512162	0.000007	-9.36	0.14	0.23

Lab No (HD)	Depth (cm)	σ (cm)	Age (ka BP)	$^{143}Nd/^{144}Nd$	2σ	εNd (‰)	int. 2σ (‰)	ext. 2σ (‰)
3060	461	1	16.67	0.512147	0.000006	-9.68	0.12	0.23
3092	481	1	17.16	0.512157	0.000008	-9.47	0.16	0.23
3033	501	1	17.68	0.512163	0.000006	-9.37	0.11	0.3
3064	521	1	18.59	0.512177	0.000007	-9.15	0.13	0.23
3043 *	541	1	32.83	0.512171	0.000006	-9.19	0.12	0.23
3046	561	1	33.00	0.512175	0.000007	-9.18	0.13	0.23
3070 *	581	1	33.17	0.512171	0.000054	-9.21	1.05	1.05
3077	601	1	33.34	0.512172	0.000006	-9.22	0.12	0.23
3073	621	1	33.51	0.512180	0.000007	-9.08	0.14	0.23
3067	641	1	33.71	0.512133	0.000006	-9.94	0.11	0.23
3057	661	1	33.95	0.512149	0.000006	-9.65	0.12	0.23
3049	681	1	34.19	0.512165	0.000006	-9.32	0.12	0.23
3036	701	1	34.42	0.512169	0.000005	-9.34	0.1	0.23
3069	721	1	34.66	0.512174	0.000007	-9.19	0.14	0.23
3051	741	1	34.90	0.512173	0.000007	-9.17	0.14	0.23
3038	761	1	35.13	0.512165	0.000006	-9.38	0.12	0.23
3056	781	1	35.32	0.512162	0.000006	-9.45	0.12	0.23
3082	801	1	35.46	0.512163	0.000007	-9.39	0.14	0.23
3062	821	1	35.60	0.512166	0.000007	-9.28	0.13	0.23
3088	841	1	35.74	0.512162	0.000006	-9.4	0.13	0.23
3045	861	1	35.88	0.512172	0.000006	-9.28	0.12	0.23
3032	881	1	36.11	0.512170	0.000006	-9.26	0.11	0.23
3066	901	1	36.35	0.512176	0.000007	-9.16	0.14	0.23
3048	921	1	36.58	0.512155	0.000007	-9.51	0.13	0.23
3059	941	1	36.81	0.512160	0.000006	-9.43	0.12	0.23
3076	961	1	37.04	0.512168	0.000006	-9.28	0.13	0.23
3072	981	1	37.28	0.512157	0.000006	-9.5	0.12	0.23
3053	1001	1	37.51	0.512164	0.000008	-9.36	0.16	0.23
3035	1021	1	37.74	0.512159	0.000007	-9.47	0.13	0.23
3091	1041	1	37.97	0.512146	0.000007	-9.73	0.14	0.23
3079	1061	1	38.21	0.512173	0.000007	-9.15	0.14	0.23
3042	1081	1	38.44	0.512154	0.000008	-9.58	0.16	0.23
3093	1101	1	38.62	0.512155	0.000008	-9.53	0.16	0.23

Table A.3: U-series dating results from both coral-bearing cores MD08-3231 and GeoB-18141-01
Samples denoted with * did not pass the U-series quality control, †samples exhibited $\Delta\Delta^{14}C > 0$ suggesting U-series open system behaviour, 'depth' corresponds to depth in core, 'AR' = activity ratio
CWCs from MD08-3231 were U-series dated in the course of this PhD, and one Bachelor's projects (Wefing, 2014[1]), all CWCs from GeoB-18141-01 were dated during this this project.

Lab No (HD)	label	depth (cm)	σ (cm)	^{238}U (µg/g)	2σ (µg/g)	^{232}Th (ng/g)	2σ (ng/g)	$^{230}Th/^{238}U$ AR	2σ AR	$^{230}Th/^{232}Th$ AR	2σ AR	$\delta^{234}U$ (‰)	2σ (‰)	Age uncor. (ka)	2σ (ka)	U/Th Age (ka)	U/Th Age (ka BP)	2σ (ka)	$\delta^{234}U_i$ (‰)	2σ (‰)
8400	MD08-3231-7.5	7.5	2.5	4.4258	0.0002	0.1529	0.0006	0.1806	0.0005	15914	80	141.26	0.74	18.75	0.06	18.74	18.67	0.06	148.94	0.78
6446 [1]	MD08-3231-12.5	12.5	2.5	4.7910	0.0100	0.3959	0.0018	0.1958	0.0017	7243	70	141.40	4.00	20.47	0.21	20.45	20.38	0.19	149.80	4.20
6532 †[1]	MD08-3231-17.5	17.5	2.5	3.8580	0.0110	0.6087	0.0042	0.1673	0.0024	3256	51	147.00	6.30	17.16	0.28	17.12	17.06	0.30	154.20	6.60
8401 †	MD08-3231-17.5	17.5	2.5	2.5552	0.0001	1.3309	0.0032	0.2108	0.0006	1230	5	139.88	0.97	22.23	0.07	22.10	22.04	0.09	148.90	1.04
6576 *[1]	MDO8-3231-22.5	22.5	2.5	4.0281	0.0090	10.7575	0.0501	0.1930	0.0030	221	4	143.24	4.89	20.11	0.35	19.45	19.38	0.48	151.34	5.17
6576 *[1]	MDO8-3231-22.5	22.5	2.5	3.3503	0.0001	13.7983	0.0302	0.1831	0.0004	136	0	141.96	0.50	19.01	0.05	17.99	17.92	0.51	149.36	0.57
8411	MD08-3231-22.5	22.5	2.5	3.5655	0.0002	0.2215	0.0009	0.1922	0.0006	9452	48	137.43	0.95	20.14	0.07	20.12	20.05	0.07	145.50	1.00
6447 [1]	MD08-3231-27.5	27.5	2.5	4.5160	0.0160	2.2722	0.0152	0.2074	0.0022	1260	15	140.50	4.60	21.82	0.29	21.70	21.63	0.29	149.40	4.90
6533 [1]	MD08-3231-32.5	32.5	2.5	3.6940	0.0090	0.4376	0.0026	0.2203	0.0029	5707	81	141.30	3.80	23.31	0.33	23.28	23.22	0.31	150.90	4.00
6577 [1]	MDO8-3231-37.5	37.5	2.5	3.5251	0.0091	0.8661	0.0043	0.2235	0.0047	2781	60	136.21	6.18	23.82	0.58	23.76	23.69	0.57	145.67	6.61
6577 [1]	MDO8-3231-37.5	37.5	2.5	3.1533	0.0001	0.3057	0.0007	0.2205	0.0006	6937	24	137.17	0.46	23.44	0.07	23.41	23.35	0.07	146.55	0.49
6578 [1]	MD08-3231-42.5	42.5	2.5	4.2781	0.0084	0.3182	0.0019	0.2204	0.0033	9057	145	134.48	3.86	23.48	0.40	23.46	23.40	0.40	143.70	4.13
6534 [1]	MD08-3231-47.5	47.5	2.5	3.7900	0.0090	2.1317	0.0123	0.2190	0.0035	1191	20	136.50	3.70	23.27	0.42	23.13	23.07	0.42	145.70	4.00
8402	MD08-3231-47.5	47.5	2.5	3.7034	0.0002	0.2347	0.0008	0.2204	0.0008	10580	51	135.36	0.88	23.47	0.09	23.45	23.39	0.09	144.63	0.94
6448 [1]	MD08-3231-52.5I	52.5	2.5	4.1520	0.0110	0.8597	0.0055	0.2199	0.0020	3246	35	135.50	4.10	23.40	0.23	23.35	23.28	0.28	144.80	4.40
6449 [1]	MD08-3231-52.5II	52.5	2.5	4.0130	0.0120	0.9446	0.0047	0.2231	0.0020	2903	28	141.00	4.90	23.66	0.27	23.60	23.53	0.26	150.70	5.20
6579 [1]	MD08-3231-57.5	57.5	2.5	3.9019	0.0090	0.5048	0.0031	0.2188	0.0027	5152	70	131.60	4.10	23.36	0.33	23.33	23.27	0.33	140.57	4.38
6535 [1]	MD08-3231-65	65	5	3.0440	0.0080	0.1333	0.0013	0.2214	0.0051	15463	382	139.40	6.40	23.49	0.59	23.48	23.41	0.63	149.00	6.80
8403	MD08-3231-65	65	5	3.3706	0.0002	0.1916	0.0010	0.2218	0.0006	11876	68	134.70	0.86	23.64	0.08	23.63	23.56	0.08	144.00	0.92
6580 [1]	MDO8-3231-75	75	5	5.2948	0.0136	1.6271	0.0095	0.2358	0.0026	2338	28	132.45	5.07	25.38	0.33	25.30	25.24	0.34	142.27	5.44
6580 [1]	MDO8-3231-75	75	5	4.7224	0.0001	3.7263	0.0077	0.2339	0.0006	903	3	133.65	0.52	25.12	0.07	24.93	24.86	0.13	143.40	0.56
6581 [1]	MD08-3231-85	85	5	3.8745	0.0105	3.4542	0.0162	0.2334	0.0037	798	13	132.99	5.13	25.08	0.47	24.85	24.79	0.48	142.67	5.51
6536 [1]	MD08-3231-95	95	5	3.4900	0.0100	0.0944	0.0007	0.2440	0.0042	27579	509	138.20	3.60	26.21	0.52	26.20	26.14	0.54	148.80	3.90
8404	MD08-3231-95	95	5	3.3249	0.0011	0.4609	0.0015	0.2513	0.0008	5525	25	134.47	1.01	27.20	0.09	27.17	27.10	0.11	145.20	1.09
6450†[1]	MD08-3231-105	105	5	3.1690	0.0130	0.0540	0.0005	0.2554	0.0032	45894	660	134.50	6.00	27.71	0.44	27.71	27.64	0.47	145.50	6.50
8405	MD08-3231-105	105	5	4.5761	0.0005	0.3700	0.0010	0.2478	0.0007	9355	38	130.71	0.61	26.89	0.09	26.87	26.80	0.09	141.02	0.65
6582†[1]	MD08-3231-115	115	5	3.9690	0.0100	2.5314	0.0135	0.2548	0.0047	1216	23	128.78	5.34	27.80	0.60	27.64	27.58	0.60	139.25	5.78
8406	MD08-3231-115	115	5	2.9437	0.0002	0.1473	0.0005	0.2543	0.0008	15505	69	134.90	1.00	27.56	0.09	27.55	27.48	0.10	145.80	1.10
6583 [1]	MD08-3231-125	125	5	3.2162	0.0066	-0.0695	-0.0008	0.2470	0.0044	-34780	-734	134.32	7.11	26.70	0.60	26.69	26.63	0.58	144.84	7.68
6451 [1]	MD08-3231-135I	135	5	3.0430	0.0150	2.3620	0.0132	0.2550	0.0025	1006	10	136.90	4.50	27.59	0.28	27.39	27.33	0.37	147.90	4.90
6452†[1]	MD08-3231-135II	135	5	3.0790	0.0180	1.3820	0.0071	0.2581	0.0031	1771	20	138.50	4.90	27.93	0.36	27.82	27.75	0.43	149.80	5.30
6453 [1]	MD08-3231-145	145	5	4.1550	0.0200	0.7114	0.0032	0.2511	0.0022	4517	39	139.10	5.40	27.05	0.31	27.01	26.94	0.30	150.10	5.80
6584†[1]	MDO8-3231-155	155	5	2.9694	0.0089	1.8119	0.0095	0.2567	0.0042	1280	22	137.99	5.51	27.80	0.50	27.61	27.55	0.54	149.19	5.96
6584†[1]	MD08-3231-155	155	5	3.7067	0.0002	0.3723	0.0009	0.2569	0.0006	7802	27	132.97	0.52	27.94	0.08	27.91	27.84	0.08	143.89	0.56
6454 [1]	MD08-3231-165	165	5	3.9030	0.0180	0.2519	0.0013	0.2594	0.0026	12375	127	140.70	5.60	28.01	0.36	28.00	27.93	0.36	152.30	6.10
7009	MDO8-3231-175	175	5	3.5319	0.0001	0.4581	0.0008	0.2532	0.0005	5957	16	131.72	0.57	27.51	0.06	27.48	27.42	0.07	142.36	0.62
8407[1]	MD08-3231-185	185	5	4.5278	0.0002	0.4913	0.0014	0.2639	0.0007	7412	29	129.85	0.64	28.89	0.10	28.87	28.80	0.09	140.89	0.70
8306[1]	MD08-3231-195	195	5	4.8462	0.0014	0.4195	0.0015	0.2762	0.0009	9723	46	131.66	0.56	30.38	0.12	30.36	30.29	0.11	143.46	0.61
7020	MDO8-3231-285	215	5	3.4684	0.0001	0.3253	0.0006	0.2547	0.0007	8306	27	133.12	0.59	27.66	0.08	27.64	27.57	0.09	143.94	0.63
7019	MDO8-3231-275	225	5	4.1936	0.0001	1.1324	0.0018	0.2984	0.0006	3377	9	128.55	0.59	33.33	0.09	33.26	33.19	0.09	141.22	0.64
7018	MDO8-3231-265	235	5	3.6806	0.0002	0.0955	0.0002	0.3023	0.0006	35534	104	129.23	0.49	33.81	0.08	33.81	33.74	0.08	142.19	0.54
7017*	MDO8-3231-255	245	5	4.1349	0.0002	11.2337	0.0227	0.3100	0.0007	347	1	129.71	0.56	34.80	0.09	34.12	34.05	0.35	142.84	0.63
7016*	MDO8-3231-245	255	5	3.6926	0.0002	6.4986	0.0150	0.3138	0.0007	543	2	131.05	0.63	35.24	0.10	34.80	34.74	0.24	144.60	0.70
8408	MD08-3231-245	255	5	2.5498	0.0002	0.0261	0.0001	0.3218	0.0009	95958	601	133.70	0.94	36.21	0.13	36.20	36.13	0.13	148.10	1.00

Lab No (HD)	label	depth (cm)	σ (cm)	^{238}U (µg/g)	2σ (µg/g)	^{232}Th (ng/g)	2σ (ng/g)	^{230}Th/^{238}U AR	2σ AR	^{230}Th/^{232}Th AR	2σ AR	δ^{234}U (‰)	2σ (‰)	Age uncor. (ka)	2σ (ka)	U/Th Age (ka)	U/Th Age (ka BP)	2σ (ka)	$\delta^{234}U_i$ (‰)	2σ (‰)
7015	MDO8-3231-235	265	5	4.2549	0.0002	1.4135	0.0028	0.3171	0.0008	2913	9	128.46	0.85	35.78	0.11	35.70	35.63	0.12	142.10	0.94
7014†	MDO8-3231-225	275	5	3.4495	0.0001	0.8704	0.0018	0.3200	0.0008	3865	13	130.77	0.65	36.07	0.11	36.01	35.94	0.11	144.78	0.72
7012†	MDO8-3231-205	295	5	3.5365	0.0001	2.0006	0.0032	0.3261	0.0006	1757	4	128.27	0.50	36.99	0.09	36.85	36.78	0.11	142.35	0.55
7021	MDO8-3231-305	305	5	3.3525	0.0001	1.4668	0.0028	0.3311	0.0008	2315	7	130.14	0.67	37.59	0.11	37.48	37.42	0.12	144.69	0.75
7022	MDO8-3231-315	315	5	3.7544	0.0001	2.0102	0.0040	0.4483	0.0010	2563	8	128.00	0.68	54.72	0.15	54.59	54.52	0.17	149.36	0.80
7023	MDO8-3231-335	335	5	3.7658	0.0001	1.6953	0.0028	0.6407	0.0012	4353	11	116.86	0.64	91.27	0.27	91.16	91.10	0.27	151.20	0.84
7024*	MDO8-3231-345	345	5	3.7517	0.0001	1.3208	0.0026	0.6454	0.0012	5595	15	120.36	0.57	91.82	0.30	91.73	91.67	0.27	155.99	0.75
8410	MD08-3231-345	345	5	4.2382	0.0002	0.1574	0.0005	0.6724	0.0015	55255	221	112.52	0.89	99.13	0.37	99.12	99.05	0.38	148.90	1.20
7507*	GeoB 18141-01-P1-17	17	3	4.9793	0.0001	5.6168	0.0151	0.0412	0.0002	112	1	145.31	0.62	4.00	0.02	3.72	3.66	0.14	146.84	0.63
7507	GeoB 18141-01-P1-17	17	3	5.0221	0.0004	1.4263	0.0127	0.0363	0.0004	391	6	145.56	2.43	3.52	0.04	3.44	3.38	0.05	146.99	2.45
7545	GeoB 18141-01-P1-66	66	3	2.5577	0.0002	0.7119	0.0028	0.1743	0.0009	1943	12	137.55	1.85	18.10	0.10	18.03	17.97	0.10	144.74	1.95
7508	GeoB 18141-01-P1-70	70	3	3.0729	0.0001	3.0301	0.0106	0.1894	0.0008	590	3	138.45	0.73	19.80	0.09	19.55	19.48	0.15	146.31	0.78
7546	GeoB 18141-01-P1-83	83	3	2.7492	0.0003	1.6330	0.0125	0.1913	0.0015	1001	11	138.84	4.10	20.00	0.20	19.85	19.79	0.20	146.86	4.34
7546	GeoB 18141-01-P1-83A 1. Stk	83	3	2.8496	0.0004	0.3725	0.0053	0.1909	0.0017	4459	74	139.57	2.67	19.94	0.20	19.91	19.84	0.21	147.65	2.83
7547	GeoB 18141-01-P1-83B 2. Stk	83	3	2.9477	0.0004	0.5178	0.0053	0.1890	0.0016	3330	44	137.46	3.02	19.77	0.19	19.73	19.66	0.18	145.34	3.20
7509	GeoB 18141-01-P1-95	95	3	2.9694	0.0001	1.3621	0.0083	0.2006	0.0016	1342	13	138.50	2.32	21.09	0.19	20.97	20.91	0.20	146.96	2.47
7548	GeoB 18141-01-P1-107A 1. Stk	107	3	2.6116	0.0003	0.4959	0.0041	0.1988	0.0018	3246	40	140.51	3.33	20.83	0.23	20.78	20.72	0.22	149.01	3.53
7549	GeoB 18141-01-P1-107A 2. Stk	107	3	2.2851	0.0003	0.3158	0.0030	0.1942	0.0021	4355	63	141.90	3.77	20.27	0.25	20.24	20.17	0.25	150.25	3.99
7550	GeoB 18141-01-P1-107B 1. Stk	107	3	2.7349	0.0004	0.3545	0.0038	0.1900	0.0020	4582	68	139.90	3.97	19.84	0.24	19.81	19.74	0.23	147.96	4.20
7510	GeoB 18141-01-P1-127	127	3	3.0731	0.0001	1.8269	0.0078	0.2002	0.0009	1034	7	136.53	0.85	21.08	0.11	20.93	20.86	0.13	144.85	0.90
7551	GeoB 18141-01-P1-138	138	3	2.5699	0.0002	0.4081	0.0022	0.2005	0.0013	3916	33	136.86	2.36	21.11	0.15	21.07	21.00	0.15	145.26	2.51
7511*	GeoB 18141-01-P1-144	144	3	2.7194	0.0026	0.3932	0.0034	0.2123	0.0152	4510	325	169.38	44.48	21.77	1.98	21.73	21.67	1.96	180.11	47.31
7552	GeoB 18141-01-P1-156	156	3	2.6273	0.0002	0.2183	0.0016	0.2000	0.0015	7476	78	135.18	2.18	21.08	0.17	21.06	21.00	0.18	143.47	2.31
7512	GeoB 18141-01-P1-184	184	3	3.1864	0.0001	0.6724	0.0020	0.2070	0.0007	3017	13	135.88	0.71	21.88	0.08	21.83	21.76	0.08	144.52	0.76
7553	GeoB 18141-01-P1-184 2.Stk	184	3	3.4405	0.0003	0.9007	0.0049	0.2035	0.0012	2415	19	134.91	2.46	21.50	0.15	21.43	21.36	0.16	143.33	2.61
7554	GeoB 18141-01-P2-5 2. Stk	275	3	2.8300	0.0003	0.7460	0.0032	0.1999	0.0011	2350	16	136.72	1.53	21.04	0.13	20.98	20.91	0.13	145.07	1.62
7514	GeoB 18141-01-P2-12	282	3	3.5057	0.0002	2.4332	0.0064	0.2118	0.0007	937	4	135.02	0.54	22.46	0.08	22.28	22.22	0.12	143.80	0.58
7555*	GeoB 18141-01-P2-12 2. Stk	282	3	3.3322	0.0003	22.3407	0.0869	0.2055	0.0010	95	1	133.95	1.92	21.75	0.13	20.06	19.99	0.88	141.76	2.07
7556	GeoB 18141-01-PP2-21	291	3	3.3902	0.0003	1.1051	0.0063	0.2076	0.0011	1976	15	134.14	2.10	21.99	0.14	21.91	21.84	0.14	142.71	2.23
7515	GeoB 18141-01-P2-40	310	3	3.8943	0.0001	0.8064	0.0231	0.2123	0.0019	3152	95	137.06	5.32	22.47	0.25	22.42	22.36	0.25	146.03	5.67
7513	GeoB 18141-01-P2-CC 1. Stk	328	3	3.6974	0.0002	0.8475	0.0033	0.2163	0.0010	2901	17	134.87	2.15	22.99	0.12	22.94	22.87	0.13	143.90	2.29
7516	GeoB 18141-01-P3-13	518	3	2.4221	0.0004	0.1005	0.0028	0.2173	0.0019	16014	469	139.30	3.81	23.01	0.24	23.00	22.94	0.25	148.66	4.07
7557	GeoB 18141-01-P3-30	535	3	2.5428	0.0002	0.8828	0.0041	0.2175	0.0010	1944	13	137.02	1.73	23.08	0.12	22.99	22.93	0.13	146.22	1.85
7517	GeoB 18141-01-P3-44	549	3	2.6160	0.0001	0.3663	0.0008	0.2216	0.0006	4851	18	135.95	0.92	23.59	0.08	23.55	23.49	0.08	145.30	0.98
7558	GeoB 18141-01-P3-44 2. Stk	549	3	2.6118	0.0002	3.6557	0.0203	0.2177	0.0013	484	4	136.53	2.14	23.12	0.16	22.77	22.70	0.24	145.60	2.29
7559	GeoB 18141-01-P3-56	561	3	2.7352	0.0002	0.7806	0.0034	0.2196	0.0011	2383	16	134.51	2.08	23.39	0.14	23.32	23.25	0.14	143.67	2.23
7518	GeoB 18141-01-P3-63	568	3	3.3670	0.0002	2.5810	0.0113	0.2298	0.0012	919	6	134.14	0.84	24.61	0.14	24.42	24.36	0.18	143.73	0.90
7560	GeoB 18141-01-P3-63 2. Stk	568	3	4.2911	0.0003	0.6676	0.0031	0.2290	0.0013	4551	33	131.29	1.52	24.59	0.16	24.55	24.49	0.16	140.73	1.63
7562	GeoB 18141-01-P3-73 1. Stk	578	3	2.9354	0.0003	1.1273	0.0065	0.2327	0.0015	1878	16	135.76	2.11	24.93	0.18	24.83	24.76	0.19	145.63	2.26
7519	GeoB 18141-01-P3-79	584	3	2.7366	0.0002	0.4053	0.0024	0.2358	0.0013	4875	39	137.07	1.75	25.25	0.16	25.22	25.15	0.16	147.19	1.88
6991	GeoB 18141-01-P3-87	592	3	3.5731	0.0217	0.3881	0.0031	0.2445	0.0028	6910	88	130.77	6.87	26.47	0.38	26.44	26.38	0.39	140.92	7.41
7563	GeoB 18141-01-P3-CC 3. Stk	593	3	3.9895	0.0003	0.2176	0.0016	0.2783	0.0019	15872	157	129.98	2.17	30.70	0.26	30.69	30.62	0.24	141.76	2.37
7521*	GeoB 18141-01-P4-8	748	3	5.2383	0.0002	28.9220	0.0572	0.2975	0.0007	165	0	127.69	0.43	33.24	0.09	31.85	31.78	0.71	139.71	0.54
7564*	GeoB 18141-01-P4-44	784	3	4.1764	0.0005	10.3875	0.0584	0.2995	0.0019	375	3	129.20	1.86	33.45	0.26	32.83	32.76	0.41	141.76	2.05
7565*	GeoB 18141-01-P4-59	799	3	3.9918	0.0003	8.7109	0.0513	0.3054	0.0021	432	4	125.53	2.15	34.36	0.27	33.81	33.74	0.40	138.11	2.37
7565	GeoB 18141-01-P4-59	799	3	4.2760	0.0004	3.1443	0.0247	0.3126	0.0024	1296	14	128.90	2.57	35.17	0.32	34.98	34.92	0.34	142.30	2.84
7522	GeoB 18141-01-P4-65	805	3	3.2159	0.0001	1.2707	0.0022	0.3085	0.0007	2396	7	127.39	0.57	34.69	0.10	34.59	34.53	0.11	140.47	0.63
7523	GeoB 18141-01-P4-70	810	3	4.2787	0.0002	0.3301	0.0007	0.3099	0.0007	12326	41	126.52	0.56	34.91	0.10	34.89	34.82	0.10	139.63	0.62
7566	GeoB 18141-01-P4-70 2. Stk	810	3	4.4491	0.0004	0.3213	0.0028	0.3044	0.0026	13059	159	125.52	3.12	34.22	0.35	34.21	34.14	0.37	138.26	3.44
7524*	GeoB 18141-01-P4-93	833	3	3.7623	0.0001	0.7307	0.0015	0.3262	0.0009	5151	18	125.75	0.64	37.11	0.12	37.06	37.00	0.13	139.63	0.72
7520*	GeoB 18141-01-P4-CCT	860	3	4.4947	0.0002	7.3113	0.0137	0.3461	0.0009	650	2	123.56	0.61	39.92	0.12	39.51	39.44	0.24	138.16	0.69
7567	GeoB 18141-01-P4-CCB 1. Stk	870	3	3.8650	0.0003	0.1405	0.0012	0.3463	0.0025	29571	331	122.85	3.67	39.98	0.36	39.97	39.90	0.39	137.54	4.12
7568	GeoB 18141-01-P5-13 2. Stk	988	3	3.0817	0.0004	5.0670	0.0408	0.3787	0.0029	718	8	124.28	3.08	44.48	0.45	44.07	44.01	0.49	140.77	3.50
7525	GeoB 18141-01-P5-39	1014	3	3.7584	0.0001	1.1362	0.0023	0.4083	0.0009	4142	13	121.77	0.47	48.97	0.14	48.90	48.83	0.15	139.82	0.55
7569	GeoB 18141-01-P5-39 2.Stk	1014	3	3.4628	0.0004	4.3604	0.0376	0.3989	0.0034	987	12	124.20	3.56	47.44	0.57	47.12	47.05	0.55	141.89	4.08
7570*	GeoB 18141-01-P5-50 1. Stk	1025	3	4.1682	0.0003	74.7882	0.1857	0.4582	0.0015	77	0	131.98	1.32	56.00	0.26	51.46	51.39	2.36	152.65	1.84
7571	GeoB 18141-01-P5- 60	1035	3	3.8890	0.0002	4.1885	0.0068	0.4484	0.0008	1276	3	118.94	0.50	55.34	0.12	55.07	55.00	0.19	138.96	0.59
7572	GeoB 18141-01-P5-65 1. Stk	1040	3	2.7408	0.0001	0.2378	0.0005	0.4584	0.0009	16181	46	122.18	0.72	56.72	0.15	56.70	56.63	0.15	143.42	0.85
7526*	GeoB 18141-01-P5-70	1045	3	3.2687	0.0001	13.6585	0.0201	0.4511	0.0009	331	1	122.36	0.49	55.53	0.14	54.48	54.41	0.55	142.73	0.61
7573	GeoB 18141-01-P5-80	1055	3	2.8634	0.0002	3.1294	0.0055	0.4415	0.0008	1237	3	125.57	0.70	53.81	0.14	53.54	53.47	0.19	146.09	0.82

Lab No (HD)	label	depth (cm)	σ (cm)	^{238}U (µg/g)	2σ (µg/g)	^{232}Th (ng/g)	2σ (ng/g)	^{230}Th/^{238}U AR	2σ AR	^{230}Th/^{232}Th AR	2σ AR	δ^{234}U (‰)	2σ (‰)	Age uncor. (ka)	2σ (ka)	U/Th Age (ka)	U/Th Age (ka BP)	2σ (ka)	$\delta^{234}U_i$ (‰)	2σ (‰)
7527*	GeoB 18141-01-P5-100	1075	3	2.8972	0.0001	35.4699	0.0608	0.4742	0.0008	119	0	124.64	0.54	59.10	0.14	56.00	55.93	1.57	146.01	0.91
6992	GeoB 18141-01-P5-107	1082	3	2.7258	0.0073	1.9716	0.0064	0.5254	0.0034	2236	15	124.61	3.31	67.79	0.67	67.61	67.54	0.68	150.84	4.01
7574	GeoB 18141-01-P5-CCT	1083	3	3.2616	0.0001	0.3556	0.0007	0.4760	0.0009	13378	36	120.69	0.59	59.68	0.15	59.65	59.58	0.15	142.86	0.70
7528	GeoB 18141-01-P5-CCB 1. Stk	1092	3	3.0144	0.0001	1.0691	0.0046	0.4713	0.0021	4074	25	123.06	0.73	58.74	0.34	58.65	58.59	0.35	145.25	0.87
7575	GeoB 18141-01-PP6-11	1221	3	2.7156	0.0002	0.2662	0.0007	0.5137	0.0013	16047	57	119.65	0.95	66.17	0.24	66.15	66.08	0.24	144.24	1.15
7105	GeoB 18141-01-P6-23	1233	3	3.1008	0.0001	2.3517	0.0135	0.5024	0.0029	2030	17	117.35	0.43	64.41	0.51	64.22	64.15	0.52	140.70	0.56
7576	GeoB 18141-01-P6-30 1. Stk	1240	3	2.6720	0.0002	0.3752	0.0007	0.5180	0.0013	11283	35	119.51	0.94	66.94	0.24	66.90	66.84	0.24	144.39	1.14
7111	GeoB 18141-01-P6-36	1246	3	3.0373	0.0001	1.7529	0.0046	0.5080	0.0013	2701	10	118.05	0.48	65.31	0.24	65.17	65.10	0.25	141.92	0.59
7577	GeoB 18141-01-P6-44 1. Stk	1254	3	3.0446	0.0002	0.4682	0.0009	0.5123	0.0012	10184	32	119.75	0.79	65.93	0.23	65.89	65.82	0.23	144.26	0.96
7115*	GeoB 18141-01-P6-57	1267	3	3.3617	0.0001	38.4833	0.3058	0.5211	0.0037	141	2	120.48	0.81	67.40	0.67	64.50	64.44	1.61	144.58	1.17
7115*	GeoB 18141-01-P6-57	1267	3	2.6360	0.0001	86.9969	0.2713	0.5567	0.0018	52	0	125.94	0.84	73.33	0.34	64.83	64.76	4.47	151.26	2.16
7578*	GeoB 18141-01-PP6-89 1. Stk	1299	3	3.0468	0.0002	5.2361	0.0138	0.5820	0.0017	1036	4	113.27	0.93	79.51	0.34	79.08	79.01	0.42	141.64	1.17

Table A.4: Li/Mg temperature results from both coral-bearing cores MD08-3231 and GeoB-18141-01
Samples denoted with * did not pass the U-series quality control, †samples exhibited $\Delta\Delta^{14}C > 0$ suggesting U-series open system behaviour. CWCs from MD08-3231 were analysed in the course of this PhD, and one Bachelor's projects (Rieger, 2015) denoted by [2], all CWCs from GeoB-18141-01 were dated during this project.

Lab No (HD)	[Li] (pg/ml)	σ (pg/ml)	[Mg] (ng/ml)	σ (ng/ml)	Li/Mg uncor. (mg/g)	σ (mg/g)	Li/Mg uncor. (mmol/mol)	σ (mmol/mol)	Li/Mg (mmol/mol)	σ (mmol/mol)	T (°C)	int. 2σ (°C)	ext. 2σ (°C)
8400	23.55	0.30	15.08	0.02	1.56	0.02	5.47	0.07	5.18	0.07	0.87	0.26	1.00
6446 [2]	27.17	0.57	16.27	0.03	1.67	0.04	5.85	0.12	5.20	0.11	0.80	0.43	1.00
6532 †[2]	31.95	1.05	18.20	0.05	1.76	0.06	6.15	0.20	5.47	0.18	-0.22	0.67	1.35
8401 †	25.04	0.23	15.99	0.01	1.57	0.01	5.48	0.05	5.20	0.05	0.81	0.19	1.00
6576 *[2]	26.30	0.22	16.27	0.05	1.62	0.01	5.66	0.05	4.99	0.04	1.65	0.19	1.00
6447 [2]	37.54	0.88	22.00	0.07	1.71	0.04	5.98	0.14	5.22	0.12	0.72	0.48	1.00
6533 [2]	21.37	0.20	13.29	0.03	1.61	0.02	5.63	0.06	4.97	0.05	1.74	0.21	1.00
6577 [2]	30.76	0.56	16.76	0.05	1.84	0.03	6.43	0.12	5.67	0.10	-0.95	0.38	1.00
6578 [2]	27.77	0.68	17.84	0.05	1.56	0.04	5.45	0.13	4.85	0.12	2.24	0.51	1.01
6534 [2]	21.15	0.77	13.27	0.03	1.59	0.06	5.58	0.20	4.97	0.18	1.75	0.75	1.49
6534 [2]	38.80	0.95	23.96	0.07	1.62	0.04	5.67	0.14	4.91	0.12	1.97	0.51	1.02
8402	21.69	0.33	16.06	0.01	1.35	0.02	4.73	0.07	4.49	0.07	3.83	0.35	1.00
6448 [2]	21.76	0.19	14.69	0.02	1.48	0.01	5.19	0.05	4.57	0.04	3.42	0.23	1.00
6579 [2]	24.94	0.76	16.37	0.06	1.52	0.05	5.34	0.16	4.75	0.15	2.67	0.63	1.27
6535 [2]	32.60	0.26	20.64	0.10	1.58	0.01	5.53	0.05	4.88	0.04	2.11	0.20	1.00
8403	22.49	0.13	16.69	0.01	1.35	0.01	4.72	0.03	4.47	0.03	3.88	0.20	1.00
6580 [2]	26.84	0.43	16.44	0.04	1.63	0.03	5.72	0.09	5.04	0.08	1.43	0.33	1.00
6581 [2]	37.87	0.31	21.98	0.05	1.72	0.01	6.03	0.05	5.27	0.04	0.52	0.17	1.00
6581 [2]	22.39	0.40	13.45	0.02	1.67	0.03	5.83	0.10	5.14	0.09	1.03	0.37	1.00
6536 [2]	29.06	0.76	15.63	0.03	1.86	0.05	6.51	0.17	5.79	0.15	-1.39	0.54	1.07
8404	23.61	0.15	14.48	0.01	1.63	0.01	5.71	0.04	5.42	0.03	-0.02	0.13	1.00
6450 †[2]	28.47	0.30	18.33	0.06	1.55	0.02	5.44	0.06	4.80	0.05	2.45	0.24	1.00
8405	21.68	0.22	14.99	0.01	1.45	0.01	5.06	0.05	4.80	0.05	2.44	0.23	1.00
8406	29.07	0.28	18.52	0.01	1.57	0.02	5.50	0.05	5.21	0.05	0.76	0.20	1.00
6583 [2]	24.63	0.82	14.28	0.03	1.73	0.06	6.04	0.20	5.37	0.18	0.14	0.68	1.36
6451 [2]	23.25	0.95	14.26	0.04	1.63	0.07	5.71	0.24	5.08	0.21	1.29	0.84	1.68
6451 [2]	33.21	0.89	19.65	0.05	1.69	0.05	5.92	0.16	5.13	0.14	1.09	0.55	1.10

Lab No (HD)	[Li] (pg/ml)	σ (pg/ml)	[Mg] (ng/ml)	σ (ng/ml)	Li/Mg uncor. (mg/g)	σ (mg/g)	Li/Mg uncor. (mmol/mol)	σ (mmol/mol)	Li/Mg (mmol/mol)	σ (mmol/mol)	T (°C)	int. 2σ (°C)	ext. 2σ (°C)
6453 [2]	34.51	0.85	21.56	0.05	1.60	0.04	5.60	0.14	4.85	0.12	2.22	0.51	1.02
6584 †[2]	30.00	0.85	16.41	0.06	1.83	0.05	6.40	0.18	5.70	0.16	-1.05	0.58	1.16
6459 [2]	27.47	0.41	18.18	0.05	1.51	0.02	5.29	0.08	4.67	0.07	3.02	0.33	1.00
7009 [2]	31.69	0.54	20.01	0.07	1.58	0.03	5.54	0.10	4.89	0.09	2.06	0.37	1.00
8407	21.42	0.08	14.50	0.02	1.48	0.01	5.17	0.02	4.91	0.02	1.99	0.12	1.00
8306	23.26	0.30	14.54	0.01	1.60	0.02	5.60	0.07	5.31	0.07	0.37	0.27	1.00
7020 [2]	27.33	0.16	17.36	0.05	1.57	0.01	5.51	0.04	4.86	0.03	2.18	0.16	1.00
7019 [2]	22.46	0.45	15.50	0.04	1.45	0.03	5.07	0.10	4.51	0.09	3.70	0.44	1.00
7018 [2]	20.77	0.93	15.40	0.05	1.35	0.06	4.72	0.21	4.20	0.19	5.17	0.94	1.89
7017 *[2]	52.66	4.77	32.55	0.14	1.62	0.15	5.66	0.51	5.04	0.46	1.45	1.85	3.70
7017 *[2]	21.29	0.37	11.58	0.01	1.84	0.03	6.44	0.11	5.58	0.10	-0.62	0.35	1.00
7016 *[2]	25.00	0.62	19.37	0.07	1.29	0.03	4.52	0.11	3.99	0.10	6.23	0.57	1.14
8408	24.68	0.39	16.47	0.00	1.50	0.02	5.25	0.08	4.98	0.08	1.71	0.33	1.00
7015 [2]	22.67	0.15	16.92	0.06	1.34	0.01	4.69	0.03	4.14	0.03	5.46	0.27	1.00
7014 †[2]	22.91	0.24	15.62	0.03	1.47	0.02	5.14	0.06	4.53	0.05	3.62	0.26	1.00
7012 †[2]	30.51	1.69	23.52	0.05	1.30	0.07	4.54	0.25	4.04	0.22	5.96	1.16	2.32
7012 †[2]	19.02	0.42	12.87	0.02	1.48	0.03	5.17	0.11	4.48	0.10	3.85	0.47	1.00
7021 [2]	24.18	0.37	17.91	0.06	1.35	0.02	4.73	0.07	4.17	0.07	5.31	0.39	1.00
7022 [2]	16.35	0.11	12.16	0.02	1.34	0.01	4.71	0.03	4.15	0.03	5.40	0.26	1.00
7022 [2]	39.91	0.87	29.52	0.13	1.35	0.03	4.73	0.10	4.14	0.12	5.47	0.61	1.23
7023 [2]	19.10	0.54	16.45	0.05	1.16	0.03	4.07	0.12	3.62	0.10	8.22	0.67	1.35
7024 *[2]	25.78	0.80	20.15	0.07	1.28	0.04	4.48	0.14	3.99	0.12	6.24	0.69	1.37
8410	13.19	0.11	13.16	0.02	1.00	0.01	3.51	0.03	3.33	0.03	9.92	0.44	1.00
7507	16.17	0.47	17.15	0.03	0.94	0.03	3.30	0.10	3.63	0.11	8.12	1.37	1.37
7545	25.56	0.35	17.32	0.09	1.48	0.02	5.17	0.08	5.51	0.08	-0.38	0.60	1.00
7508	29.93	0.82	22.34	0.03	1.34	0.04	4.69	0.13	5.16	0.14	0.95	1.12	1.12
7546	29.23	0.28	22.20	0.06	1.32	0.01	4.61	0.05	4.92	0.05	1.95	0.43	1.00
7547	30.88	0.32	23.10	0.12	1.34	0.02	4.68	0.05	4.99	0.06	1.64	0.49	1.00
7509	26.19	0.67	18.44	0.08	1.42	0.04	4.97	0.13	5.47	0.14	-0.23	1.06	1.06
7548	30.54	0.28	20.80	0.31	1.47	0.03	5.14	0.09	5.59	0.10	-0.67	0.71	1.00
7549	29.16	0.46	20.53	0.29	1.42	0.03	4.97	0.11	5.41	0.12	0.01	0.86	1.00
7550	28.67	0.21	18.85	0.26	1.52	0.02	5.33	0.08	5.79	0.09	-1.39	0.63	1.00
7510	26.49	0.62	19.15	0.05	1.38	0.03	4.84	0.12	5.33	0.13	0.31	0.97	1.00

Lab No (HD)	[Li] (pg/ml)	σ (pg/ml)	[Mg] (ng/ml)	σ (ng/ml)	Li/Mg uncor. (mg/g)	σ (mg/g)	Li/Mg uncor. (mmol/mol)	σ (mmol/mol)	Li/Mg (mmol/mol)	σ (mmol/mol)	T (°C)	int. 2σ (°C)	ext. 2σ (°C)
7551	29.96	0.19	22.10	0.02	1.36	0.01	4.75	0.03	5.06	0.03	1.36	0.29	1.00
7511 *	30.58	0.50	22.56	0.01	1.36	0.02	4.75	0.08	5.22	0.09	0.73	0.67	1.00
7552	30.19	0.20	19.67	0.28	1.54	0.02	5.37	0.09	5.84	0.09	-1.57	0.65	1.00
7512	28.73	0.74	20.13	0.04	1.43	0.04	5.00	0.13	5.50	0.14	-0.34	1.05	1.05
7553	29.01	0.41	20.43	0.28	1.42	0.03	4.97	0.10	5.41	0.11	0.01	0.80	1.00
7554	25.52	0.30	18.14	0.04	1.41	0.02	4.93	0.06	5.25	0.06	0.60	0.49	1.00
7514	25.73	0.55	18.26	0.06	1.41	0.03	4.93	0.11	5.43	0.12	-0.07	0.88	1.00
7555 *	24.01	0.28	16.58	0.08	1.45	0.02	5.07	0.06	5.41	0.07	0.00	0.51	1.00
7556	20.82	0.18	14.81	0.10	1.41	0.02	4.92	0.05	5.25	0.06	0.61	0.45	1.00
7515	24.86	0.51	17.92	0.03	1.39	0.03	4.86	0.10	5.34	0.11	0.25	0.84	1.00
7513	23.32	0.35	17.63	0.01	1.32	0.02	4.63	0.07	5.10	0.08	1.22	0.63	1.00
7516	29.93	0.76	23.39	0.12	1.28	0.03	4.48	0.12	4.93	0.13	1.90	1.07	1.07
7557	27.02	0.27	20.26	0.03	1.33	0.01	4.67	0.05	4.98	0.05	1.68	0.43	1.00
7517	29.60	0.42	22.22	0.04	1.33	0.02	4.67	0.07	5.13	0.07	1.07	0.59	1.00
7558	27.75	0.30	18.31	0.32	1.52	0.03	5.31	0.11	5.77	0.12	-1.32	0.85	1.00
7559	27.33	0.21	20.70	0.08	1.32	0.01	4.62	0.04	4.93	0.04	1.90	0.39	1.00
7518	23.93	0.89	16.95	0.08	1.41	0.05	4.94	0.19	5.44	0.20	-0.10	1.53	1.53
7560	22.87	0.20	15.15	0.30	1.51	0.03	5.29	0.12	5.75	0.13	-1.24	0.89	1.00
7562	28.91	0.38	19.65	0.00	1.47	0.02	5.15	0.07	5.49	0.07	-0.31	0.54	1.00
7519	29.46	0.59	20.25	0.00	1.46	0.03	5.10	0.10	5.61	0.11	-0.73	0.83	1.00
7563	25.01	0.17	19.11	0.02	1.31	0.01	4.58	0.03	4.89	0.03	2.08	0.33	1.00
7521 *	28.14	0.50	18.12	0.02	1.55	0.03	5.44	0.10	5.98	0.11	-2.06	0.75	1.00
7564 *	27.19	0.23	18.19	0.02	1.49	0.01	5.23	0.05	5.58	0.05	-0.64	0.36	1.00
7565 *	21.15	0.18	17.82	0.01	1.19	0.01	4.16	0.04	4.43	0.04	4.07	0.48	1.00
7522	21.50	0.90	17.25	0.05	1.25	0.05	4.36	0.18	4.80	0.20	2.43	1.72	1.72
7523	21.84	0.73	18.36	0.00	1.19	0.04	4.17	0.14	4.58	0.15	3.39	1.39	1.39
7566	97.96	0.98	65.12	2.89	1.50	0.07	5.27	0.24	5.73	0.26	-1.17	1.86	1.86
7524 *	19.99	0.45	18.27	0.02	1.09	0.02	3.83	0.09	4.21	0.09	5.10	1.01	1.01
7520 *	23.19	0.77	16.89	0.03	1.37	0.05	4.81	0.16	5.29	0.18	0.45	1.36	1.36
7567	19.96	0.28	15.07	0.05	1.32	0.02	4.64	0.07	4.95	0.07	1.83	0.61	1.00
7568	18.37	0.34	16.98	0.09	1.08	0.02	3.79	0.07	4.04	0.08	5.96	0.93	1.00
7525	26.30	0.44	21.84	0.08	1.20	0.02	4.22	0.07	4.64	0.08	3.13	0.75	1.00
7570 *	24.26	0.35	17.32	0.08	1.40	0.02	4.90	0.07	5.23	0.08	0.69	0.62	1.00
7571	17.54	0.13	15.38	0.02	1.14	0.01	3.99	0.03	4.26	0.03	4.88	0.50	1.00
7572	19.79	0.27	17.53	0.06	1.13	0.02	3.95	0.06	4.21	0.06	5.10	0.70	1.00

Lab No (HD)	[Li] (pg/ml)	σ (pg/ml)	[Mg] (ng/ml)	σ (ng/ml)	Li/Mg uncor. (mg/g)	σ (mg/g)	Li/Mg uncor. (mmol/mol)	σ (mmol/mol)	Li/Mg (mmol/mol)	σ (mmol/mol)	T (°C)	int. 2σ (°C)	ext. 2σ (°C)
7526 *	23.62	0.22	19.42	0.14	1.22	0.01	4.26	0.05	4.54	0.05	3.57	0.56	1.00
7573	19.99	0.26	17.33	0.07	1.15	0.02	4.04	0.05	4.31	0.06	4.65	0.67	1.00
7527 *	26.13	0.32	25.56	0.07	1.02	0.01	3.58	0.05	3.94	0.05	6.48	0.74	1.00
7574	21.43	0.21	16.29	0.13	1.32	0.02	4.61	0.06	4.91	0.06	1.97	0.53	1.00
7528	20.97	1.15	20.69	0.00	1.01	0.06	3.55	0.19	3.90	0.21	6.66	2.30	2.30
7575	21.34	0.34	18.65	0.08	1.14	0.02	4.01	0.07	4.27	0.07	4.81	0.79	1.00
7105	22.80	0.63	18.88	0.02	1.21	0.03	4.23	0.12	4.65	0.13	3.08	1.16	1.16
7576	22.15	0.20	17.42	0.07	1.27	0.01	4.45	0.04	4.75	0.05	2.66	0.46	1.00
7111	25.14	0.66	23.92	0.03	1.05	0.03	3.68	0.10	4.05	0.11	5.92	1.18	1.18
7577	20.10	0.21	16.79	0.14	1.20	0.02	4.19	0.05	4.47	0.06	3.89	0.62	1.00
7115 *	25.50	0.51	19.21	0.02	1.33	0.03	4.65	0.09	5.11	0.10	1.15	0.82	1.00
7578 *	15.23	0.23	16.45	0.06	0.93	0.01	3.24	0.05	3.46	0.05	9.14	0.99	1.00

Table A.5: ^{14}C dating results from both coral-bearing cores MD08-3231 and GeoB-18141-01
Samples denoted with * did not pass the U-series quality control, †samples exhibited $\Delta\Delta^{14}C > 0$ suggesting U-series open system behaviour. CWCs from MD08-3231 were analysed in the course of this PhD three Bachelor's projects (Beisel, 2017)[3], (Rieger, 2015)[2], (Wefing, 2014)[1]), [4] samples were carried out as first dating of the core. CWCs from GeoB-18141-01 were analysed during this project and (Beisel, 2017)[3].

Lab No (HD)	Lab No (KTL)	U/Th Age (ka BP)	2σ (ka)	pmc (%)	int. σ (%)	ext. σ (%)	^{14}C Age (ka)	int. σ (ka)	ext. σ (ka)	$\delta^{13}C$ (‰)	$\Delta^{14}C$ (‰)	2σ (‰)	$\Delta\Delta^{14}C$ (‰)	2σ (‰)	R Age (ka)	2σ (ka)
MD08-3231																
7008 *[2]	24542	18.88	0.08	12.69	0.07	0.12	16.58	0.05	0.08	-4.2	-	-	-	-	-	-
8400 [3]	31379	18.67	0.06	12.82	0.07	0.07	16.50	0.05	0.05	6.7	228	17	-180	20	1.23	0.14
6446 [4]	18851	20.38	0.19	11.09	0.09	0.09	17.67	0.06	0.06	-	306	37	-130	35	0.98	0.27
6532 †[1]	21735	17.06	0.30	11.28	0.07	0.09	17.53	0.05	0.06	-5.8	-111	35	-482	25	4.11	0.35
8401 †[3]	31376	22.04	0.09	11.17	0.07	0.07	17.60	0.05	0.05	-0.1	607	26	115	27	-0.76	0.18
6576 *[1]	21743	18.65	0.73	11.22	0.07	0.07	17.57	0.05	0.05	-	-	-	-	-	-	-
8411 [3]	31369	20.05	0.07	11.07	0.07	0.07	17.68	0.05	0.05	-8.7	252	19	-177	23	1.34	0.17
6447 [4]	19159	21.63	0.29	10.03	0.10	0.10	18.47	0.08	0.08	4.0	375	55	-107	48	0.72	0.33
6533 [1]	21736	23.22	0.31	8.54	0.06	0.09	19.77	0.06	0.08	-	417	60	-88	55	0.58	0.36
6577 [1]	21744	23.52	0.60	8.53	0.06	0.06	19.77	0.06	0.06	-6.7	472	109	-40	98	0.29	0.62
6578 [1]	21745	23.40	0.44	8.37	0.06	0.06	19.92	0.06	0.06	-7.8	422	78	-88	70	0.58	0.46
6534 [1]	21737	23.07	0.42	8.38	0.06	0.06	19.92	0.06	0.06	-4.2	366	72	-136	66	0.91	0.44
8402 [3]	31368	23.39	0.09	8.43	0.06	0.06	19.87	0.05	0.06	-1.3	428	26	-86	30	0.53	0.17
6448 [4]	19162	23.28	0.28	8.22	0.10	0.10	20.07	0.10	0.10	3.6	376	56	-132	52	0.85	0.35
6449 [1]	21741	23.53	0.26	8.25	0.06	0.10	20.04	0.06	0.10	-	423	56	-92	54	0.57	0.34
6579 [1]	21746	23.27	0.35	8.31	0.06	0.06	19.99	0.06	0.06	-2.2	388	62	-119	56	0.78	0.38
6535 [1]	21738	23.41	0.63	8.41	0.06	0.06	19.89	0.06	0.06	-6.0	433	110	-78	99	0.52	0.64
8403 [3]	31377	23.56	0.07	8.40	0.06	0.06	19.89	0.06	0.06	-6.7	454	25	-62	30	0.38	0.16
6580 [1]	21748	25.05	0.34	7.44	0.05	0.05	20.87	0.06	0.06	0.8	489	133	-70	128	0.39	0.77
6580 *[1]	24540	25.05	0.34	6.88	0.05	0.05	21.50	0.06	0.06	-6.3	-	-	-	-	-	-
6581 [1]	21749	24.79	0.45	7.24	0.05	0.06	21.09	0.06	0.06	1.3	414	118	-132	109	0.83	0.68
6581 [1]	24541	24.79	0.45	6.81	0.06	0.06	21.58	0.07	0.07	-7.1	-	-	-	-	-	-
6536 *[1]	21739	26.14	0.54	5.82	0.05	0.05	22.85	0.07	0.07	-5.1	378	93	-174	101	1.07	0.56
6450 †[4]	19165	27.64	0.47	5.92	0.10	0.10	22.71	0.13	0.13	-4.5	680	110	153	135	-0.60	0.56
8405 [3]	3375	26.80	0.09	5.70	0.05	0.09	23.02	0.07	0.13	-	459	49	-97	50	0.53	0.23
6582 †[1]	21747	27.58	0.56	5.56	0.05	0.05	23.21	0.07	0.07	2.9	568	109	38	136	-0.10	0.57

Lab No (HD)	Lab No (KTL)	U/Th Age (ka BP)	2σ (ka)	pmc (%)	int. σ (%)	ext. σ (%)	^{14}C Age (ka)	int. σ (ka)	ext. σ (ka)	δ^{13}C (‰)	Δ^{14}C (‰)	2σ (‰)	$\Delta\Delta^{14}$C (‰)	2σ (‰)	R Age (ka)	2σ (ka)
6583 [1]	21740	26.63	0.59	5.72	0.05	0.05	22.98	0.07	0.07	-2.8	437	106	-113	111	0.70	0.61
6451 [4]	19167	27.33	0.37	5.44	0.10	0.10	23.39	0.14	0.14	-6.6	486	85	-62	105	0.26	0.42
6452 †[1]	21742	27.75	0.43	5.92	0.05	0.10	22.71	0.07	0.14	-	705	108	184	133	-0.73	0.54
6453 [1]	19168	26.94	0.30	5.66	0.10	0.10	23.07	0.14	0.14	-9.9	476	73	-83	73	0.42	0.37
6584 †[1]	21750	27.69	0.54	5.73	0.05	0.10	22.98	0.07	0.14	-	637	121	113	147	-0.40	0.60
7035 *[2]	24549	24.37	0.35	5.08	0.05	0.05	23.94	0.08	0.08	-9.9	-	-	-	-	-	-
6454 [4]	-	27.93	0.36	4.90	0.08	0.08	24.23	0.14	0.14	-3.0	439	80	-69	97	0.34	0.46
7009 [2]	24543	27.42	0.17	4.88	0.05	0.08	24.26	0.08	0.14	-5.4	290	46	-282	51	1.23	0.30
7014 †[2]	24548	35.94	0.26	2.03	0.03	0.03	31.30	0.12	0.12	1.4	573	52	136	56	-0.78	0.28
7012 †[2]	24546	36.78	0.22	1.72	0.03	0.03	32.65	0.14	0.14	-1.9	470	55	44	57	-0.23	0.36
GeoB-18141-01																
7507	32093	3.38	0.05	63.11	0.16	0.60	3.70	0.02	0.08	9.5	-50	19	-66	20	0.66	0.22
7545	32100	17.97	0.10	13.14	0.09	0.09	16.30	0.05	0.05	2.4	155	21	-242	25	1.70	0.17
7508 [3]	31371	19.48	0.15	12.58	0.07	0.08	16.65	0.04	0.05	-2.4	329	30	-86	29	0.60	0.20
7509	32092	20.91	0.20	11.37	0.08	0.08	17.47	0.06	0.06	5	426	40	-24	36	0.17	0.26
7510 [3]	31373	20.86	0.13	11.01	0.06	0.08	17.72	0.05	0.06	-2.7	374	29	-73	28	0.58	0.21
7512 [3]	31370	21.76	0.08	10.20	0.06	0.06	18.34	0.05	0.05	-2.5	420	22	-69	25	0.46	0.16
7514 [3]	31367	22.22	0.12	9.80	0.06	0.06	18.66	0.05	0.05	-0.1	442	27	-61	28	0.28	0.15
7513	32095	22.87	0.13	8.74	0.08	0.08	19.58	0.07	0.07	3.5	390	32	-105	34	0.72	0.22
7517 [3]	31374	23.49	0.08	8.53	0.06	0.07	19.77	0.06	0.07	-4.9	463	29	-52	34	0.31	0.19
7518 [3]	31372	24.36	0.18	6.64	0.05	0.05	21.79	0.06	0.06	-5.3	265	33	-260	35	1.65	0.20
7519	32096	25.15	0.16	6.82	0.08	0.08	21.57	0.09	0.09	-8.4	430	43	-139	44	0.71	0.21
7523	32099	34.82	0.10	2.07	0.07	0.07	31.16	0.25	0.25	1.7	399	89	-36	93	0.23	0.49
7567	32098	39.90	0.39	1.06	0.06	0.06	36.52	0.47	0.47	9.7	332	170	-203	170	1.18	0.95

A.1.2 Additional information

Information about cores

Table A.6: Core sites for paleoceanographic reconstructions in the southern Gulf of Cádiz and seawater stations (Hebbeln et al., 2015; Van Rooij et al., 2013; Rooij et al., 2008; Turon et al., 2004)

Core	Cruise	Lat N	Long E	Water depth (m)	Drill (m)	Recovery (m; %)	Type
GeoB-18141-01	MoccoMeBo	35°7.15'	07°7.74'	944	52.05	41.63 (78)	CWC
MD08-3231	MiCROSYSTEMS	35°18.90'	6°48.19'	550	5.75	3.78 (66)	CWC
MD04-2805-CQ	Privilege	34°30.99'	07°00.99'	859	8	7.72 (97)	hemipelagic
MD08-3227	MiCROSYSTEMS	35°16.28'	6°47.89'	642	42	33.2 (79)	hemipelagic
Seawater station (εNd)							
Beta-1	GATEWAY	35°17.46'	06°47.16'	510			
MOW1	GATEWAY	35°39.04'	06°55.10'	988			
MOW2	GATEWAY	35°13.11'	07°10.56'	1025			
Seawater station (temperature, salinity, oxygen)							
GeoB-18136-1	MoccoMeBo	35°6.210'	7°7.920'	990			
GeoB-18152-1	MoccoMeBo	35°24.994'	7°0.024'	890			
GeoB-18153-1	MoccoMeBo	35°20.009'	7°2.521'	950			
GeoB-18154-1	MoccoMeBo	35°14.985'	7°5.028'	900			
GeoB-18155-1	MoccoMeBo	35°9.976'	7°7.568'	890			
GeoB-18156-1	MoccoMeBo	35°4.971'	7°10.025'	1005			
GeoB-18157-1	MoccoMeBo	35°4.991'	7°5.032'	925			
GeoB-18158-1	MoccoMeBo	35°4.979'	7°0.028'	860			
GeoB-18159-1	MoccoMeBo	35°10.010'	7°0.020'	840			
GeoB-18160-1	MoccoMeBo	35°15.012'	7°0.037'	860			

Table A.7: Recovery of MeBo drilling core GeoB-18141-01 (Hebbeln et al., 2015)

Barrel (cm)	Start of drilling (cm)	Drilled length (cm)	Cored length (cm)	Section 1 (cm)	Section 2 (cm)	CC	Recovery per section %
1	0	270	260	120	52	13	71.15
2	270	235	235	46	0	15	25.96
3	505	235	235	86	0	16	43.4
4	740	235	235	119	0	13	56.17
5	975	235	235	106	0	14	51.06
6	1210	235	235	102	0	15	49.79
7	1565	235	235	120	91	14	95.74
8	1800	235	235	120	103	14	100.85
9	2035	235	235	120	57	12	80.43
10	2270	235	235	120	60	14	82.55
11	2505	235	235	120	92	14	96.17
12	2740	235	235	120	103	16	101.7
13	2975	235	235	102	0	17	50.64
14	3210	235	235	40	0	10	21.28
15	3445	235	235	122	0	11	56.6
16	3680	235	235	120	76	12	88.51
17	3915	235	235	120	58	16	82.55
18	4150	235	235	120	104	15	101.7
19	4385	235	235	120	59	11	80.85

Table A.8: Depth-age model of hemipelagic sediment cores MD04-2805-CQ and MD08-3227 (Delivet, 2017; Penaud et al., 2010).

MD04-2805-CQ		**MD08-3231**	
Depth (cm)	Ages BP (ka)	Depth (cm)	Ages BP (ka)
10	5.89	5	0.82
90	11.67	135	7.52
100	12.21	259	11.72
110	12.51	500	17.63
130	14.51	525	18.77
160	15.06	529	18.95
180	15.09	550	32.91
240	15.22	631	33.59
250	15.91	650	33.82
290	16.06	770	35.24
300	17.31	861	35.88
350	19.7	1088	38.52
360	20.26	1202	39.38
370	21.1	1359	41.63
400	21.46	1490	42.8
430	22.27	1685	46.16
500	23.44		
530	23.8		
550	24.19		
570	24.74		
640	25.43		
670	25.83		
680	26.35		
690	26.52		
720	27.3		
750	27.71		
760	27.73		

Python script to calculate $\Delta^{14}C$, $\Delta\Delta^{14}C$ and reservoir age R

Reservoir_age.py

```
import numpy as np
import matplotlib.pyplot as plot
from scipy import interpolate
from scipy import optimize


def Reservoir(intCal, decay):

    #Difference function
    def diff(UTh):
        return intCal(UTh) - decay(UTh)

    #Find intersection by finding root of difference
    UTh_intersection = optimize.brentq(diff,2.,49.)

    return UTh_intersection
```

Uncertainty_IntCal.py

```
import numpy as np
from math import fabs

def intCalUncertainty(slopeDecay, slopeIntCal, delta14CSE):
    return fabs(delta14CSE/(slopeDecay-slopeIntCal))
```

Radiocarbon_script

```
import numpy as np
import matplotlib.pylab as plt
import math
import pandas as pd
from matplotlib import rc
from matplotlib.patches import Ellipse
from scipy.interpolate import interp1d
from scipy import misc
import Reservoir_age
import Uncertainty_IntCal

from Plot_styles import * #style includes colors and markers for used data sets

rc('font', family='Times')
rc('text', usetex=True)

#import data
GeoB = pd.read_excel('/GeoB-18141.xlsx', sheetname='GeoB-18141-1', parsecols="A:N", header=0,
    skiprows=[1])
IntCal = pd.read_excel('/IntCal13.xlsx', sheetname='IntCal13', parsecols="A:G", header=0,
    skiprows=[1])

#figure for Delta14C
fig = plt.figure(1, figsize=(14/2.54, 7/2.54))
ax = fig.add_subplot(111)
ax.set_position(pos = [0.15, 0.14, 0.8, 0.8])

#figure for Delta R
fig1=plt.figure(figsize=(14/2.54, 7/2.54))
ax1=fig1.add_subplot(111)

```

```
#figure for DeltaDelta14C
fig2=plt.figure(figsize=(14/2.54, 7/2.54))
ax2=fig2.add_subplot(111)

#allocate and adjust data
GeoBUTh = GeoB['U/Th Age BP']
GeoBUTh2SD = GeoB['U/Th Age 2SE']
GeoB14C = GeoB['14C Age']
GeoB14CSD = GeoB['14C Age SE']

CalAge = IntCal['CAL BP']
deltaC14theo = IntCal['Delta 14C']
sigma_deltaC14theo = IntCal['D14C SD']

GeoBUTh=1000.*GeoBUTh
GeoB14C=1000.*GeoB14C
GeoBUTh2SD=1000.*GeoBUTh2SD
GeoB14C2SD=2*1000.*GeoB14CSD

CalAge=CalAge/1000.

#calculate Delta14C
GeoBdeltaC14_ohne=(math.e**(-GeoB14C/8033.)*math.e**(GeoBUTh/8266.)-1.)*1000.

#number aleatory variable
number = 10000
np.random.seed(3457625575)

#for U-series age  random variable
x = np.linspace(0,45)
GeoBy_list = np.zeros(shape=(len(GeoBUTh),len(x)))

#lists for intersection
GeoBintersectionx_list = np.zeros(len(GeoBUTh))
GeoBintersectiony_list = np.zeros(len(GeoBUTh))
GeoBUncertainty_IntCal_list = np.zeros(len(GeoBUTh))
GeoBintersection_point_list = np.zeros(number)
GeoBUncertainty_cloud_list =np.zeros(len(GeoBUTh))
GeoBDeltaR_list=np.zeros(number)
GeoBDeltaDelta_list=np.zeros(number)

#calculate and plot Delta14C, DeltaDelta14C and R age
for index_UTh, GeoBUThWert in enumerate(GeoBUTh):

    for x_index, x_i in enumerate(x):

        GeoBy_list[index_UTh,x_index]=((math.exp(x_i/8.266)*\
            math.exp(-(GeoB14C[index_UTh]/1000.)/8.033))-1)*1000.

    #interpolate IntCal between data points
    intCal = interp1d(CalAge, deltaC14theo)
    intCalSE = interp1d(CalAge, sigma_deltaC14theo)

    #decay curve through coral data point
    def decay(x):
        return ((math.exp(x/8.266)*math.exp(-(GeoB14C[index_UTh]/1000.)/8.033))-1)*1000.

    def slopeDecay(x):
        return (math.exp(x/8.266)*math.exp(-(GeoB14C[index_UTh]/1000./8.033))*1000./8.266)

    def slopeIntCal(x):
        return misc.derivative(intCal, x, dx=0.01)

    #use function reservoir_age which calculates the intersection
    intersection_x = Reservoir_age.Reservoir(intCal, decay)
    intersection_y = decay(intersection_x)

    GeoBintersectionx_list[index_UTh]=intersection_x
    GeoBintersectiony_list[index_UTh]=intersection_y

```

```
100     #calculate uncertainty resulting from IntCal SE
101     uncertaintyIntCal=Uncertainty_IntCal.intCalUncertainty(slopeDecay(intersection_x),
            slopeIntCal(intersection_x), intCalSE(intersection_x))
102
103     #uncertainty_IntCal in a list
104     GeoBUncertainty_IntCal_list[index_UTh]=uncertaintyIntCal
105
106     xUTh = GeoBUThWert + GeoBUTh2SD[index_UTh] * np.random.randn(number) #make point cloud
107     xC14 = GeoB14C[index_UTh] + GeoB14C2SD[index_UTh] *\
108             np.random.randn(number)
109
110     deltaC14=((math.e**(-xC14/8033.)*math.e**(xUTh/8266.)-1.)*1000**2)
111
112     # for each point of cloud use the decay curve and calculate intersection with IntCal. write
            that into list intersction_point_list and calculate SD over those intersects
113     for index_point in range(number):
114         def decaypoint(x):
115             return ((math.exp(x/8.266)*math.exp(-(xC14[index_point]/1000.)/8.033))-1)*1000.
116         intersection_point = Reservoir_age.Reservoir(intCal, decaypoint) #preliminary
                intersection point wihtout uncertainty of IntCal
117         intersection_point = Reservoir_age.Reservoir(lambda x: intCal(x)+np.random.randn(1)*
                intCalSE(intersection_point), decaypoint) #intersection point wiht uncertainty of
                IntCal
118
119         #R age Calculation
120         GeoBDeltaR_list[index_point]=(intersection_point-xUTh[index_point]/1000)
121
122         #DeltaDelta C Calculation
123         GeoBDeltaDelta_list[index_point] = deltaC14[index_point]/1000.-intCal(xUTh[index_point
                ]/1000.)+np.random.randn(1)*intCalSE(xUTh[index_point]/1000.)
124
125
126     #ellipse for DeltaR
127     xx1 = np.cov(xUTh/1000., GeoBDeltaR_list)
128     cov_delta1 = xx1[0,1]
129
130     DeltaR_list_mean = np.mean(GeoBDeltaR_list)
131     DeltaR_list_std = np.sqrt(xx1[1,1])
132     xUTh_mean1 = np.mean(xUTh)/1000.
133     xUTh_std1 = np.sqrt(xx1[0,0])
134
135     sigma_x_strich1 = np.sqrt( (DeltaR_list_std**2 + xUTh_std1**2)/2 +\
136         np.sqrt((DeltaR_list_std**2 - xUTh_std1**2)**2/4 + cov_delta1**2) )
137     sigma_y_strich1 = np.sqrt( (DeltaR_list_std**2 + xUTh_std1**2)/2 -\
138         np.sqrt((DeltaR_list_std**2 - xUTh_std1**2)**2/4 + cov_delta1**2) )
139
140     theta = 0.5 * np.arctan( 2*cov_delta1 / (xUTh_std1**2 - DeltaR_list_std**2) )
141     theta2 = theta*(180/math.pi)+270
142
143     #plot ellipses
144     e = Ellipse((xUTh_mean1, DeltaR_list_mean),\
145         2*sigma_x_strich1, 2*sigma_y_strich1, theta2,
146         color=color_GeoB18141, alpha=0.3, lw=0.5)
147
148     ax1.add_artist(e)
149     e.set_edgecolor(color_GeoB18141)
150
151     print(DeltaR_list_mean)
152     ax1.scatter(xUTh_mean1, DeltaR_list_mean, color=color_GeoB18141, marker='.')
153
154
155     #ellipses for DeltaDelta14C
156     xx1 = np.cov(xUTh/1000., GeoBDeltaDelta_list)
157     cov_delta1 = xx1[0,1]
158
159     DeltaDelta_list_mean = np.mean(GeoBDeltaDelta_list)
160     DeltaDelta_list_std = np.sqrt(xx1[1,1])
161     xUTh_mean1 = np.mean(xUTh)/1000.
162     xUTh_std1 = np.sqrt(xx1[0,0])
163
```

```
164     sigma_x_strich1 = np.sqrt( (DeltaDelta_list_std**2 + xUTh_std1**2)/2 +\
165         np.sqrt((DeltaDelta_list_std**2 - xUTh_std1**2)**2/4 + cov_delta1**2) )
166     sigma_y_strich1 = np.sqrt( (DeltaDelta_list_std**2 + xUTh_std1**2)/2 -\
167         np.sqrt((DeltaDelta_list_std**2 - xUTh_std1**2)**2/4 + cov_delta1**2) )
168
169     theta = 0.5 * np.arctan( 2*cov_delta1 / (xUTh_std1**2 - DeltaDelta_list_std**2) )
170     theta2 = theta*(180/math.pi)+270
171
172     #plot ellipsen of DeltaDelta14C
173     e = Ellipse((xUTh_mean1, DeltaDelta_list_mean),\
174         2*sigma_x_strich1, 2*sigma_y_strich1, theta2,
175         color=color_GeoB18141, alpha=0.3, lw=0.5)
176
177     ax2.add_artist(e)
178     e.set_edgecolor(color_GeoB18141)
179
180     print(DeltaDelta_list_mean)
181     ax2.scatter(xUTh_mean1, DeltaDelta_list_mean, color=color_GeoB18141, marker='.')
182
183     #calculate ellipses for Delta14C
184     xx = np.cov(xUTh/1000., deltaC14/1000.)
185     cov_delta = xx[0,1]
186
187     deltaC14_mean = np.mean(deltaC14/1000.)
188     deltaC14_std = np.sqrt(xx[1,1])
189     xUTh_mean = np.mean(xUTh/1000.)
190     xUTh_std = np.sqrt(xx[0,0])
191
192     sigma_x_strich = np.sqrt( (deltaC14_std**2 + xUTh_std**2)/2 +\
193         np.sqrt((deltaC14_std**2 - xUTh_std**2)**2/4 + cov_delta**2) )
194     sigma_y_strich = np.sqrt( (deltaC14_std**2 + xUTh_std**2)/2 -\
195         np.sqrt((deltaC14_std**2 - xUTh_std**2)**2/4 + cov_delta**2) )
196
197     theta = 0.5 * np.arctan( 2*cov_delta / (xUTh_std**2 - deltaC14_std**2) )
198     theta2 = theta*(180/math.pi)+270
199
200
201     #plot ellipses of Delta14C
202     e = Ellipse((xUTh_mean, deltaC14_mean),\
203         2*sigma_x_strich, 2*sigma_y_strich, theta2,
204         color=color_GeoB18141, alpha=0.3, lw=0.5)
205
206     ax.add_artist(e)
207     e.set_edgecolor(color_GeoB18141)
208
209
210     print(deltaC14_mean)
211     ax.scatter(xUTh_mean, deltaC14_mean, color=color_GeoB18141, marker='.')
212
213 #1sigma area of Intcal13
214 deltaC14theoplus = deltaC14theo + sigma_deltaC14theo
215 deltaC14theominus = deltaC14theo - sigma_deltaC14theo
216 ax.plot(CalAge,deltaC14theo, 'k', linestyle = '-', \
217 label=r'Atmosphere (Reimer et al.,2013)')
218 ax.plot(CalAge, deltaC14theoplus, 'k:', \
219 label=r'$1\sigma$ Atmosphere')
220 ax.plot(CalAge, deltaC14theominus, 'k:')
221
222 np.set_printoptions(threshold=np.inf)
223
224 #set axis parameters
225 ax.tick_params(axis='y',
226     which='both',
227     right='off',)
228 ax.tick_params(axis='x',
229     which='both',
230     top='off')
231 ax.set_xlim(0,32.5)
232 ax.set_ylim(-150,650)
233 ax.set_xlabel('U/Th Age BP (ka)')
```

```
234 ax.set_ylabel(r'$\Delta ^{14}$C (\textperthousand)')
235 fig.savefig('/GeoB-18141-Delta14C.pdf')
236
237
238 ax1.set_xlim(0,32.5)
239 ax1.set_ylim(-0.5,2)
240 ax1.set_yticks([-0.5,0,0.5,1,1.5,2])
241 ax1.set_xlabel('U/Th Age BP (ka)')
242 ax1.set_ylabel(r'R (ka)')
243 fig1.savefig('/GeoB-18141-Rage.pdf')
244
245
246 ax2.tick_params(axis='y',
247     which='both',
248     right='off',)
249 ax2.tick_params(axis='x',
250     which='both',
251     top='off')
252
253 ax2.set_ylim(-400,50)
254 ax2.set_xlim(0,32.5)
255 ax2.set_yticks([0,-100,-200,-300,-400])
256 ax2.set_xlabel('U/Th Age BP (ka)')
257 ax2.set_ylabel(r'$\Delta\Delta ^{14}$C (\textperthousand)')
258 fig2.savefig('/GeoB-18141-DeltaDelta14C.pdf')
```

A.2 Ba isotopes in cold-water corals

Table A.9: Seawater analysis at co-located stations to CWCs.

Sample name	Cruise	Station	Water depth (m)	[Ba] (nmol/kg) ± 2.5%	Ba/Ca (µmol/mol) ± 2.5%	$\delta^{138/134}$Ba (‰) ± 0.03	n
NBP1103 CTD21 5 m	NBP1103	CTD21	5	55.2	5.4	0.5	2
NBP1103 CTD21 50 m	NBP1103	CTD21	50	57.6	5.6	0.5	2
NBP1103 CTD21 200 m	NBP1103	CTD21	200	58.9	5.7	0.49	2
NBP1103 CTD21 300 m	NBP1103	CTD21	300	60.8	5.9	0.5	2
NBP1103 CTD21 500 m	NBP1103	CTD21	500	63.8	6.2	0.45	2
NBP1103 CTD21 800 m	NBP1103	CTD21	800	71.4	6.9	0.43	2
NBP1103 CTD21 1400 m	NBP1103	CTD21	1400	90.6	8.8	0.32	1
NBP1103 CTD21 1750 m	NBP1103	CTD21	1750	99.2	9.6	0.28	2
NBP1103 CTD21 2250 m	NBP1103	CTD21	2250	102	9.9	0.25	2
ICECTD PL501 PEP6 238 m	ICECTD	PL501 PEP6	238	49.3	4.8	0.51	1
ICECTD PL501 PEP4 300 m	ICECTD	PL501 PEP4	300	51.3	5	0.51	1
ICECTD PL501 PEP8 338 m	ICECTD	PL501 PEP8	338	51.6	5	0.52	1
ICECTD PL498 PEP10 360 m	ICECTD	PL498 PEP10	360	50.3	4.9	0.53	1
ICECTD PL498 PEP2 680 m	ICECTD	PL498 PEP2	680	51.4	5	0.52	1
ICECTD PL498 PEP8 680 m	ICECTD	PL498 PEP8	680	52.9	5.1	0.52	1
ICECTD PL498 PEP5 68 0m	ICECTD	PL498 PEP5	680	51.8	5	0.51	1
NBP1103 CTD100 0 m	NBP1103	CTD100	0	68.8	6.7	0.44	1
NBP1103 CTD100 300 m	NBP1103	CTD100	300	71.7	7	0.41	2
NBP1103 CTD100 650 m	NBP1103	CTD100	650	83.6	8.1	0.34	2
NBP1103 CTD100 800 m	NBP1103	CTD100	800	85	8.3	0.37	1
NBP1103 CTD100 1000 m	NBP1103	CTD100	1000	98.5	9.6	0.32	1
NBP1103 CTD100 1300 m	NBP1103	CTD100	1300	96	9.3	0.29	1
NBP1103 CTD100 1500 m	NBP1103	CTD100	1500	95.8	9.3	0.32	1
from Bates et al., 2017							
JC094 CTD002 11 m (#W0127)	JC094	CTD002	11	36.9 ± 1.1	3.6	0.57 ± 0.04	3
JC094 CTD002 55 m (#W0125)	JC094	CTD002	55	36.0 ± 1.1	3.5	0.57 ± 0.07	2
JC094 CTD002 405 m (#W0124)	JC094	CTD002	405	41.7 ± 1.1	4.1	0.56 ± 0.04	3
JC094 CTD002 705 m (#W0123)	JC094	CTD002	705	48.4 ± 1.1	4.7	0.49 ± 0.04	4
JC094 CTD002 1005 m (#W0122)	JC094	CTD002	1005	55.9 ± 1.2	5.4	0.43 ± 0.03	4
JC094 CTD002 1502 m (#W0121)	JC094	CTD002	1502	54.7 ± 1.2	5.3	0.41 ± 0.03	4
JC094 CTD002 2002 m (#W0120)	JC094	CTD002	2002	58.6 ± 1.2	5.7	0.42 ± 0.04	4
JC094 CTD002 2800 m (#W0119)	JC094	CTD002	2800	66.3 ± 1.4	6.4	0.39 ± 0.04	4
JC094 CTD002 3600 m (#W0118)	JC094	CTD002	3600	72.3 ± 1.5	7	0.37 ± 0.04	4
JC094 CTD002 4299 m (#W0117)	JC094	CTD002	4299	73.6 ± 1.5	7.1	0.31 ± 0.04	4
JC094 CTD002 4512 m (#W0116)	JC094	CTD002	4512	82.3 ± 1.7	8	0.43 ± 0.04	4

Table A.10: Results of Ba isotope measurements in living or young (< 1000 a) CWCs. For abbreviations of species refer to Tab. A.12

Specification	Location	Water depth m	Species	U/Th Age (ka BP)	2σ (ka)	Ba/Ca µmol/mol ± 2.5%	Ba/Ca (SW) µmol/mol ± 2.5%	D_{CWC-SW} ± 3.5%	$\delta^{138/134}$Ba (‰) ± 0.03	$\delta^{138/134}$Ba (SW) (‰) ± 0.03	$\Delta^{138/134}$Ba (‰) (± 0.04)	n
ICE-20-501-6-C3 LP	Reykjanes Ridge	206	Lp	202	0.01	8.1	5.0	1.6	0.35	0.52	-0.17	1
ICE-20-501-6-C8 LPw	Reykjanes Ridge	209	Lp	0	0.00	8.0	5.0	1.6	0.34	0.52	-0.18	2
ICE-20-501-6-C4 LP	Reykjanes Ridge	209	Lp	98	0.02	7.9	5.0	1.6	0.36	0.52	-0.16	1
ICE-17-500-4 GBT DC	Reykjanes Ridge	572	Dd	0	0.00	9.1	5.0	1.8	0.28	0.52	-0.24	2
ICE-17-500-5 GBT LP	Reykjanes Ridge	698	Lp	0	0.00	8.6	5.0	1.7	0.33	0.52	-0.19	2
ICE-17-500-5 GBT DC	Reykjanes Ridge	698	Dd	0	0.00	8.6	5.0	1.7	0.34	0.52	-0.18	1
ICE-17-500-1 GBT DC	Reykjanes Ridge	698	Dd	102	0.004	8.4	5.0	1.7	0.36	0.52	-0.16	1
ICE-17-500-2 GBT DC	Reykjanes Ridge	698	Dd	587	0.01	8.0	5.0	1.6	0.30	0.52	-0.22	1
ICE CTD 12PL4983GBT	Hafadjup	363	Lp	0	0.00	7.8	4.9	1.6	0.33	0.53	-0.20	1
ICE CTD 12PL4983GBT	Hafadjup	363	Dd	0	0.00	7.6	4.9	1.6	0.32	0.53	-0.21	1
ICE CTD 12PL4983A2	Hafadjup	680	Mo	0	0.00	7.5	5.1	1.5	0.32	0.52	-0.20	1
ICE CTD 12PL4983A2	Hafadjup	680	Dd	0	0.00	8.1	5.1	1.6	0.29	0.52	-0.23	1
NBP1103-DH07-BC04	Burdwood Bank	334	Bsp	0	0	12.5	6.0	2.1	0.20	0.49	-0.29	1
NBP1103-DH07-BC14	Burdwood Bank	334	Bsp	0	0	13.9	6.0	2.3	0.24	0.49	-0.25	1
NBP1103-DH14-Fn266	Burdwood Bank	727	Fsp	0	0	15.1	6.8	2.2	0.24	0.43	-0.19	1
NBP1103-DH14-Fn267	Burdwood Bank	727	Fsp	207	206	14.7	6.8	2.2	0.18	0.43	-0.25	1
NBP1103-DH14-Bn282	Burdwood Bank	727	Bsp	0	0	12.9	6.8	1.9	0.20	0.43	-0.23	1
NBP1103-DH14-Bp52	Burdwood Bank	727	Bsp	0	0	13.2	6.8	2.0	0.20	0.43	-0.23	1
NBP1103-DH14-Cn3	Burdwood Bank	727	Csp	358	0	15.3	6.8	2.3	0.21	0.43	-0.22	1
NBP1103-DH14-Cn22	Burdwood Bank	727	Csp	237	0	14.5	6.8	2.2	0.22	0.43	-0.21	1
NBP1103-DH14-Dn01	Burdwood Bank	727	Dd	969	227	15.9	6.8	2.4	0.15	0.43	-0.28	1
NBP1103-TB10-Dp01	Burdwood Bank	728	Dd	0	0	12.7	6.8	1.9	0.15	0.43	-0.28	1
NBP1103-DH16-Bn11	Burdwood Bank	1419	Bsp	391	176	16.3	8.8	1.8	0.07	0.32	-0.24	1
NBP1103-DH22-Dc(f)06	Burdwood Bank	1879	Dd	695	169	17.0	9.7	1.7	0.03	0.27	-0.24	1
JC094-B0424-Dasls/m-002	Carter Seamount	265	Dsp	live	live	8.4	3.8	2.2	0.37± 0.07	0.56	-0.19	1
JC094-B0457-Daslm-001	Carter Seamount	321	Dsp	live	live	9.0	3.9	2.3	0.4± 0.07	0.56	-0.16	1
JC094-B0244-Carls-001	Carter Seamount	621	Csp	live	live	10.4	4.5	2.3	0.24± 0.04	0.51	-0.27	1
JC094-B0045-Carls-001	Carter Seamount	746	Csp	live	live	11.3	4.8	2.4	0.27± 0.04	0.48	-0.21	1
JC094-F0005-Carlm-003	Carter Seamount	994.2	Csp	live	live	10.7	5.4	2.0	0.27± 0.04	0.43	-0.16	1
JC094-F0001-Carls-005	Carter Seamount	1080	Csp	live	live	10.8	5.4	2.0	0.24	0.43	-0.19	1
JC094-B0023-JaAlm-001	Carter Seamount	1351	Ja	live	live	11.7	5.4	2.2	0.26	0.42	-0.16	1
JC094-B0627-JaA?lms-002	Carter Seamount	1364	Ja	live	live	12.8	5.3	2.4	0.24	0.42	-0.18	1
JC094-B0012-JaAlm-001	Carter Seamount	1380	Ja	live	live	10.9	5.3	2.0	0.25	0.41	-0.16	1
JC094-B1584-Carls-001	Carter Seamount	1484	Csp	live	live	10.3	5.3	1.9	0.25	0.41	-0.16	1
JC094-B0712-Carlm-001	Carter Seamount	2260	Csp	live	live	10.8	5.9	1.8	0.18± 0.04	0.41	-0.23	1
JC094-B0015-JaAlm-001	Carter Seamount	2318.3	Ja	live	live	12.7	6.0	2.1	0.25± 0.04	0.41	-0.16	1

Table A.11: Environmental parameters at CWC sites (Spooner et al., 2016; Robinson et al., 2014; Frank et al., 2012; Robinson and Waller, 2011)

Specification	Lat. (dd)	Long. (dd)	Temperature (°C) ± 0.04	Salinity (psu) ± 0.05	pH (tot. Scale) ± 0.04	PO4 (µM) ± 0.02
ICE-20-501-6-C3 LP	-24.544	63.086	7.51	35.16	7.99	n/a
ICE-20-501-6-C8 LPw	-24.542	63.086	7.51	35.16	7.99	n/a
ICE-20-501-6-C4 LP	-24.542	63.086	7.51	35.16	7.99	n/a
ICE-17-500-4 GBT DC	-24.988	62.607	7.31	35.16	7.95	n/a
ICE-17-500-5 GBT LP	-24.988	62.608	7.23	35.16	7.95	n/a
ICE-17-500-5 GBT DC	-24.988	62.608	7.23	35.16	7.95	n/a
ICE-17-500-1 GBT DC	-24.988	62.607	7.23	35.16	7.95	n/a
ICE-17-500-2 GBT DC	-24.988	62.607	7.23	35.16	7.95	n/a
ICE CTD 12PL4983GBT	-19.993	63.570	7.89	35.19	7.98	n/a
ICE CTD 12PL4983GBT	-19.993	63.570	7.89	35.19	7.98	n/a
ICE CTD 12PL4983A2	-19.948	63.467	5.96	35.07	7.96	n/a
ICE CTD 12PL4983A2	-19.948	63.467	5.96	35.07	7.96	n/a
NBP1103-DH07-BC04	-54.504	-62.228	4.40	35.14	8.02	1.42
NBP1103-DH07-BC14	-54.507	-62.228	4.40	35.14	8.02	1.08
NBP1103-DH14-Fn266	-54.713	-62.250	3.60	34.29	7.93	1.42
NBP1103-DH14-Fn267	-54.713	-62.250	3.60	34.29	7.93	1.42
NBP1103-DH14-Bn282	-54.713	-62.250	3.60	34.29	7.93	1.42
NBP1103-DH14-Bp52	-54.713	-62.250	3.60	34.29	7.93	1.42
NBP1103-DH14-Cn3	-54.713	-62.250	3.60	34.29	7.93	1.42
NBP1103-DH14-Cn22	-54.713	-62.250	3.60	34.29	7.93	1.42
NBP1103-DH14-Dn01	-54.713	-62.250	3.60	34.29	7.93	1.42
NBP1103-TB10-Dp01	-54.727	-62.248	3.60	34.29	7.90	1.42
NBP1103-DH16-Bn11	-54.808	-62.119	2.50	34.55	7.85	1.66
NBP1103-DH22-Dc(f)06	-54.839	-62.126	2.20	34.65	7.85	1.60
JC094-B0424-Dasls/m-002	9.243	-21.325	11.20	35.32	7.74	1.70
JC094-B0457-Daslm-001	9.238	-21.322	10.50	35.23	7.74	1.80
JC094-B0244-Carls-001	9.227	-21.317	7.90	34.83	7.79	2.26
JC094-B0045-Carls-001	9.222	-21.313	7.90	34.83	7.79	2.26
JC094-F0005-Carlm-003	9.218	-21.316	5.29	34.78	7.80	2.27
JC094-F0001-Carls-005	9.216	-21.316	6.30	34.80	7.80	2.27
JC094-B0023-JaAlm-001	9.212	-21.301	4.35	34.83	7.89	1.75
JC094-B0627-JaA?lms-002	9.208	-21.301	4.32	34.92	7.89	1.74
JC094-B0012-JaAlm-001	9.206	-21.298	4.26	34.92	7.90	1.73
JC094-B1584-Carls-001	5.611	-26.958	4.18	34.94	7.94	1.63
JC094-B0712-Carlm-001	9.193	-21.281	3.20	34.95	7.98	1.47
JC094-B0015-JaAlm-001	9.190	-21.280	3.20	34.94	8.02	1.36

Table A.12: Ba isotope fractionation for each species

Species	Abbreviation	$\Delta^{138/134}$Ba (‰)	2σ (‰)	2SE (‰)	n
Balanophyllia sp.	Bsp	-0.25	0.05	0.01	5
Caryophyllia sp.	Csp	-0.21	0.07	0.01	8
D. dianthus	Dd	-0.22	0.08	0.01	9
Dasmosmillia sp.	Dsp	-0.18	0.04	0.01	2
Flabellum sp.	Fsp	-0.22	0.06	0.02	2
J. antarctica	Ja	-0.17	0.04	0.004	4
L. pertusa	Lp	-0.18	0.04	0.01	5
M. oculata	Mo	-0.20	0.04	-	1
all		-0.21	0.08	0.01	36

B List of Figures

C List of Tables

D List of Abbreviations

BP	Before Present (before 1950)
DIC	Dissolved Inorganic Carbon
DO	Dansgaard Oeschger (cycle)
HS, HE	Heinrich Stadial, Event
LGM	Last Glacial Maximum
MIS	Marine Isotope Stage
YD	Younger Dryas
AABW	Antarctic Bottom Water
(E/W) AAIW	(Eastern/Western) Antarctic Intermediate Water
AMOC	Atlantic Meridional Overturning Circulation
LSW	Labrador Sea Water
MOW	Mediterranean Outflow Water
MSW	Mediterranean Sea Water
MSL/MWU	Mediterranean Lower/Upper Water
(E/W) NACW	(Eastern/Western) North Atlantic Central Water
NADW	North Atlantic Deep Water
SAW	Surface Atlantic Water
SPG	Subpolar Gyre
STG	Subtropical Gyre
THC	Thermohaline Circulation
AM	Angolan Margin
BM	Brazilian Margin
(s/n) GoC	(Southern/Northern) Gulf of Cádiz
GoM	Gulf of Mexico
MA	Mauritania
(shal./deep) MACP	(shallow/deep) Moroccan Atlantic CWC Province
MCP	Melilla Coral Province
MR	Mingulay Reef
NCM	North Carolina Margin
PDE	Pen Duick Escarpment
PS	Porcupine Seabight
RB	Rockall Bank
SMLCP	Santa Maria di Leuca Coral Province
SoS	Strait of Silicy
STJ	Stjernsund
TRD	Trænadjupet

MAR	Mound Aggregation Rate
MAR_{max}	Maximal MAR found in core
MAR_{min}	Minimal MAR found in core
MAR_{av})	Average MAR over core recovery
MAR_{ana}	Average MAR over analysed part of core
AMS	Accelerator Mass Spectrometer
ICP-QMS	Inductively Coupled Plasma Quadrupole Mass Spectrometer
MICADAS-System	MIni CArbon DAting SYstem
MC-ICP-MS	Multi Collector Inductively Coupled Plasma Mass Spectrometer
TIMS	Thermal Ionisation Mass Spectrometer
AR	Activity Ratio
CTD station	Conductivity, Temperature, Depth Station
CWC	Cold-Water Coral
NGRIP	North Greenland Ice Core Project
pmc	percent modern carbon
R	Reservoir Age
SST	Sea Surface Temperature
IUP	Institute for Environmental Physics, Heidelberg, Germany
LSCE	Laboratoire des Sciences du Climat et de L'Environment, Gif sur-Yvette, France
EPOC	Environments et Paéoenvironments Océanique et Continenteaux, Bordeaux, France
MARUM	Helmholtz Centre for Ocean Research MARUM, Kiel, Germany
KTL	Klaus-Tschira-Labor at the Curt-Engelhorn-Centre Archaeometry, Mannheim, Germany

Bibliography

Spooner, P. T., Robinson, L. F., and Hemsing, F. (submitted). "Ba/Ca Ratio in Cold-Water Coral Skeletons Records Seawater Dissolved Ba Concentration". In: *Chemical Geology*.

Bridgestock, L., Hsieh, Y.-T., Porcelli, D., Homoky, W., Bryan, A., and Henderson, G. M. (in review). "Controls on the Barium Isotope Compositions of Marine Sediments". In:

Wienberg, C. and Titschack, J. (in press). "Framework-Forming Scleractinian Cold-Water Corals Through Space and Time: A Late Quaternary North Atlantic Perspective". In: *Marine Animal Forests*. Ed. by S. Rossi, L. Bramanti, A. Gori, and C. Orejas Saco del Valle. Cham: Springer International Publishing, pp. 1–34. DOI: 10.1007/978-3-319-17001-5_16-1.

Arps, J. (2017). "Towards ε-Precision of U-Series Age Determinations of Secondary Carbonates". Heidelberg, Germany: Heidelberg University. 140 pp.

Bates, S. L., Hendry, K. R., Pryer, H. V., Kinsley, C. W., Pyle, K. M., Woodward, E. M. S., and Horner, T. J. (2017). "Barium Isotopes Reveal Role of Ocean Circulation on Barium Cycling in the Atlantic". In: *Geochimica et Cosmochimica Acta* 204, pp. 286–299. DOI: 10.1016/j.gca.2017.01.043.

Beisel, E. (2017). "Radiokohlenstoff-Alter von Eiszeitlichem Zwischenwasser Im NO-Atlantik". Bachelor's Thesis. Heidelberg, Germany: Heidelberg University, 56 pp.

Blaser, P. (2017). "The Application of Radiogenic Neodymium Isotopes as a Palaeo Water Mass Tracer in the Subpolar North Atlantic". Heidelberg, Germany: Heidelberg University. 163 pp.

Deaney, E. L., Barker, S., and van de Flierdt, T. (2017). "Timing and Nature of AMOC Recovery across Termination 2 and Magnitude of Deglacial CO2 Change". In: *Nature Communications* 8. DOI: 10.1038/ncomms14595. pmid: 28239149.

Delivet, S. (2017). "Sedimentary Expression of Internal Waves on Quaternary Contouritic Processes along the Irish and Moroccan Atlantic Margins". Dissertation. Ghent University.

Dubois-Dauphin, Q., Colin, C., Bonneau, L., Montagna, P., Wu, Q., Van Rooij, D., Reverdin, G., Douville, E., Thil, F., Waldner, A., and Frank, N. (2017a). "Fingerprinting Northeast Atlantic Water Masses Using Neodymium Isotopes". In: *Geochimica et Cosmochimica Acta* 210, pp. 267–288. DOI: 10.1016/j.gca.2017.04.002.

Dubois-Dauphin, Q., Montagna, P., Siani, G., Douville, E., Wienberg, C., Hebbeln, D., Liu, Z., Kallel, N., Dapoigny, A., Revel, M., Pons-Branchu, E., Taviani, M., and Colin, C. (2017b). "Hydrological Variations of the Intermediate Water Masses of the Western Mediterranean Sea during the Past 20 Ka Inferred from Neodymium Isotopic Composition in Foraminifera and Cold-Water Corals". In: *Climate of the Past* 13.1, pp. 17–37. DOI: 10.5194/cp-13-17-2017.

Freiwald, A., Rogers, A., Hall-Spencer, J., Guinotte, J. M., Davies, A. J., Yesson, C., Martin, C. S., and Weatherdon, L. V. (2017). "Global Distribution of Cold-Water Corals (Version 3.0). Second Update to the Dataset in Freiwald et Al. (2004) by UNEP-WCMC". In: *UNEP World Conservation Monitoring Centre*.

Hsieh, Y.-T. and Henderson, G. M. (2017). "Barium Stable Isotopes in the Global Ocean: Tracer of Ba Inputs and Utilization". In: *Earth and Planetary Science Letters*. DOI: 10.1016/j.epsl.2017.06.024.

Jansen, M. F. (2017). "Glacial Ocean Circulation and Stratification Explained by Reduced Atmospheric Temperature". In: *Proceedings of the National Academy of Sciences* 114.1, pp. 45–50. DOI: 10.1073/pnas.1610438113. pmid: 27994158.

Matos, L., Wienberg, C., Titschack, J., Schmiedl, G., Frank, N., Abrantes, F., Cunha, M. R., and Hebbeln, D. (2017). "Coral Mound Development at the Campeche Cold-Water Coral Province, Southern Gulf of Mexico: Implications of Antarctic Intermediate Water Increased Influence during Interglacials". In: *Marine Geology* 392, pp. 53–65. DOI: 10.1016/j.margeo.2017.08.012.

Roesch, C. (2017). "Tiefseekorallen vor Angola: Archive der tropischen Zwischenwasserdynamik seit der letzten Eiszeit". Bachelor's Thesis. Heidelberg, Germany: Heidelberg University. 63 pp.

Skinner, L. C., Primeau, F., Freeman, E., Fuente, M. de la, Goodwin, P. A., Gottschalk, J., Huang, E., McCave, I. N., Noble, T. L., and Scrivner, A. E. (2017). "Radiocarbon Constraints on the Glacial Ocean Circulation and Its Impact on Atmospheric CO_2". In: *Nature Communications* 8, ncomms16010. DOI: 10.1038/ncomms16010.

Struve, T., van de Flierdt, T., Burke, A., Robinson, L. F., Hammond, S. J., Crocket, K. C., Bradtmiller, L. I., Auro, M. E., Mohamed, K. J., and White, N. J. (2017). "Neodymium Isotopes and Concentrations in Aragonitic Scleractinian Cold-Water Coral Skeletons - Modern Calibration and Evaluation of Palaeo-Applications". In: *Chemical Geology*. DOI: 10.1016/j.chemgeo.2017.01.022.

Tachikawa, K., Arsouze, T., Bayon, G., Bory, A., Colin, C., Dutay, J.-C., Frank, N., Giraud, X., Gourlan, A. T., Jeandel, C., Lacan, F., Meynadier, L., Montagna, P., Piotrowski, A. M., Plancherel, Y., Pucéat, E., Roy-Barman, M., and Waelbroeck, C. (2017). "The Large-Scale Evolution of Neodymium Isotopic Composition in the Global Modern and Holocene Ocean Revealed from Seawater and Archive Data". In: *Chemical Geology* 457, pp. 131–148. DOI: 10.1016/j.chemgeo.2017.03.018.

Abbott, A. N., Haley, B. A., and McManus, J. (2016). "The Impact of Sedimentary Coatings on the Diagenetic Nd Flux". In: *Earth and Planetary Science Letters* 449, pp. 217–227. DOI: 10.1016/j.epsl.2016.06.001.

Blaser, P., Lippold, J., Gutjahr, M., Frank, N., Link, J. M., and Frank, M. (2016). "Extracting Foraminiferal Seawater Nd Isotope Signatures from Bulk Deep Sea Sediment by Chemical Leaching". In: *Chemical Geology* 439, pp. 189–204. DOI: 10.1016/j.chemgeo.2016.06.024.

Border, E. (2016). "Tracing Sub-Decadal Iceland Basin Water-Mass Changes Using Desmophyllum Dianthus". Master's Thesis. Heidelberg, Germany: Heidelberg University. 63 pp.

Bullen, T. and Chadwick, O. (2016). "Ca, Sr and Ba Stable Isotopes Reveal the Fate of Soil Nutrients along a Tropical Climosequence in Hawaii". In: *Chemical Geology* 422, pp. 25–45. DOI: 10.1016/j.chemgeo.2015.12.008.

Cao, Z., Siebert, C., Hathorne, E. C., Dai, M., and Frank, M. (2016). "Constraining the Oceanic Barium Cycle with Stable Barium Isotopes". In: *Earth and Planetary Science Letters* 434, pp. 1–9. DOI: 10.1016/j.epsl.2015.11.017.

Chen, T., Robinson, L. F., Beasley, M. P., Claxton, L. M., Andersen, M. B., Gregoire, L. J., Wadham, J., Fornari, D. J., and Harpp, K. S. (2016). "Ocean Mixing and Ice-Sheet Con-

trol of Seawater 234U/238U during the Last Deglaciation". In: *Science*. DOI: 10.1126/science.aag1015.

Douarin, M., Elliot, M., Noble, S. R., Moreton, S. G., Long, D., Sinclair, D., Henry, L.-A., and Roberts, J. M. (2016). "North Atlantic Ecosystem Sensitivity to Holocene Shifts in Meridional Overturning Circulation: VULNERABILITY OF COLD-WATER CORAL REEFS". In: *Geophysical Research Letters* 43.1, pp. 291–298. DOI: 10.1002/2015GL065999.

Du, J., Haley, B. A., and Mix, A. C. (2016). "Neodymium Isotopes in Authigenic Phases, Bottom Waters and Detrital Sediments in the Gulf of Alaska and Their Implications for Paleo-Circulation Reconstruction". In: *Geochimica et Cosmochimica Acta* 193, pp. 14–35. DOI: 10.1016/j.gca.2016.08.005.

Dubois-Dauphin, Q., Bonneau, L., Colin, C., Montero-Serrano, J.-C., Montagna, P., Blamart, D., Hebbeln, D., Van Rooij, D., Pons-Branchu, E., Hemsing, F., Wefing, A.-M., and Frank, N. (2016). "South Atlantic Intermediate Water Advances into the North-East Atlantic with Reduced Atlantic Meridional Overturning Circulation during the Last Glacial Period: HYDROLOGY OF THE NORTH ATLANTIC". In: *Geochemistry, Geophysics, Geosystems* 17.6, pp. 2336–2353. DOI: 10.1002/2016GC006281.

Flierdt, T. van de, Griffiths, A. M., Lambelet, M., Little, S. H., Stichel, T., and Wilson, D. J. (2016). "Neodymium in the Oceans: A Global Database, a Regional Comparison and Implications for Palaeoceanographic Research". In: *Phil. Trans. R. Soc. A* 374.2081, p. 20150293. DOI: 10.1098/rsta.2015.0293.

Hebbeln, D., Van Rooij, D., and Wienberg, C. (2016a). "Good Neighbours Shaped by Vigorous Currents: Cold-Water Coral Mounds and Contourites in the North Atlantic". In: *Marine Geology* 378, pp. 171–185. DOI: 10.1016/j.margeo.2016.01.014.

Hebbeln, D., Wienberg, C., Bender, M., Bergmann, F., Dehning, K., Dullo, W.-C., Eichstädter, R., Flöter, S., Freiwald, A., Gori, A., Haberkern, J., Hoffmann, L., Mendes Joao, F., Lavaleye, M., Leymann, T., Matsuyama, K., Meyer-SChack, B., Mienis, F., Mocambique, I. B., Nowald, N., Orejas Saco del Valle, C., Ramos Cordova, C., Saturov, D., Seiter, C., Titschack, J., Vittori, V., Wefing, A.-M., Wilsenack, M., and Wintersteller, P. (2016b). *ANNA: Cold-Water Coral Ecosystems off Angola and Namibia*. Cruise Report.

Howe, J. N. W., Piotrowski, A. M., and Rennie, V. C. F. (2016). "Abyssal Origin for the Early Holocene Pulse of Unradiogenic Neodymium Isotopes in Atlantic Seawater". In: *Geology* 44.10, pp. 831–834. DOI: 10.1130/G38155.1.

Jeandel, C. (2016). "Overview of the Mechanisms That Could Explain the 'Boundary Exchange' at the Land–ocean Contact". In: *Phil. Trans. R. Soc. A* 374.2081, p. 20150287. DOI: 10.1098/rsta.2015.0287.

Krengel, T. (2016). "Temporal and Spatial Cold-Water Coral Occurrence in the Alboran Sea and the Gulf of Cádiz during Previous Glacial-Interglacial Cycles". Master's Thesis. Heidelberg, Germany: Heidelberg University. 75 pp.

LaVigne, M., Grottoli, A. G., Palardy, J. E., and Sherrell, R. M. (2016). "Multi-Colony Calibrations of Coral Ba/Ca with a Contemporaneous in Situ Seawater Barium Record". In: *Geochimica et Cosmochimica Acta* 179, pp. 203–216. DOI: 10.1016/j.gca.2015.12.038.

Lippold, J., Gutjahr, M., Blaser, P., Christner, E., de Carvalho Ferreira, M. L., Mulitza, S., Christl, M., Wombacher, F., Böhm, E., Antz, B., Cartapanis, O., Vogel, H., and Jaccard, S. L. (2016). "Deep Water Provenance and Dynamics of the (de)Glacial Atlantic Meridional Overturning

Circulation". In: *Earth and Planetary Science Letters* 445, pp. 68–78. DOI: 10.1016/j.epsl.2016.04.013.

Pöppelmeier, F. (2016). "Investigations of Authigenic Neodymium Sediment-Pore Water Interaction and Reconstruction of Deep Water Mass Sourcing in the North-East Atlantic". Master's Thesis. Heidelberg, Germany: Heidelberg University.

Pretet, C., van Zuilen, K., Nägler, T. F., Reynaud, S., Böttcher, M. E., and Samankassou, E. (2016). "Constraints on Barium Isotope Fractionation during Aragonite Precipitation by Corals". In: *The Depositional Record* 1.2, pp. 118–129. DOI: 10.1002/dep2.8.

Raddatz, J., Liebetrau, V., Trotter, J., Rüggeberg, A., Flögel, S., Dullo, W.-C., Eisenhauer, A., Voigt, S., and McCulloch, M. (2016). "Environmental Constraints on Holocene Cold-Water Coral Reef Growth off Norway: Insights from a Multiproxy Approach". In: *Paleoceanography* 31.10, 2016PA002974. DOI: 10.1002/2016PA002974.

Spooner, P. T. (2016). "Investigating the Use of Cold-Water Corals as Archives of Past Ocean Water Properties". Bristol, UK: University of Bristol. 315 pp.

Spooner, P. T., Guo, W., Robinson, L. F., Thiagarajan, N., Hendry, K. R., Rosenheim, B. E., and Leng, M. J. (2016). "Clumped Isotope Composition of Cold-Water Corals: A Role for Vital Effects?" In: *Geochimica et Cosmochimica Acta* 179, pp. 123–141. DOI: 10.1016/j.gca.2016.01.023.

Spratt, R. M. and Lisiecki, L. E. (2016). "A Late Pleistocene Sea Level Stack". In: *Clim. Past* 12.4, pp. 1079–1092. DOI: 10.5194/cp-12-1079-2016.

Taviani, M., Angeletti, L., Beuck, L., Campiani, E., Canese, S., Foglini, F., Freiwald, A., Montagna, P., and Trincardi, F. (2016). "Reprint of 'On and off the Beaten Track: Megafaunal Sessile Life and Adriatic Cascading Processes'". In: *Marine Geology*. Cascading Dense water Flow and its Impact on the Sea Floor in the Adriatic and Aegean Sea, Eastern Mediterranean 375, pp. 146–160. DOI: 10.1016/j.margeo.2015.10.003.

Therre, S. (2016). "Climate Variations in the Arabian Sea from LGM to Holocene - A Stalagmite Radiocarbon Record from Socotra Island". Master's Thesis. Heidelberg University.

Van Zuilen, K., Müller, T., Nägler, T. F., Dietzel, M., and Küsters, T. (2016). "Experimental Determination of Barium Isotope Fractionation during Diffusion and Adsorption Processes at Low Temperatures". In: *Geochimica et Cosmochimica Acta* 186, pp. 226–241. DOI: 10.1016/j.gca.2016.04.049.

Wefing, A.-M. (2016). "Fully Automated Chromatographic Extraction of Th and U: Performance of the prepFAST-MC and Its Application to Cold-Water Corals from the Angolan Margin". Master's Thesis. Heidelberg, Germany: Heidelberg University. 95 pp.

Abbott, A. N., Haley, B. A., and McManus, J. (2015a). "Bottoms up: Sedimentary Control of the Deep North Pacific Ocean's εNd Signature". In: *Geology* 43.11, pp. 1035–1035. DOI: 10.1130/G37114.1.

Abbott, A. N., Haley, B. A., McManus, J., and Reimers, C. E. (2015b). "The Sedimentary Flux of Dissolved Rare Earth Elements to the Ocean". In: *Geochimica et Cosmochimica Acta* 154, pp. 186–200. DOI: 10.1016/j.gca.2015.01.010.

Bahr, A., Kaboth, S., Jiménez-Espejo, F. J., Sierro, F. J., Voelker, A. H. L., Lourens, L., Röhl, U., Reichart, G. J., Escutia, C., Hernández-Molina, F. J., Pross, J., and Friedrich, O. (2015). "Persistent Monsoonal Forcing of Mediterranean Outflow Water Dynamics during the Late Pleistocene". In: *Geology* 43.11, pp. 951–954. DOI: 10.1130/G37013.1.

Böhm, E., Lippold, J., Gutjahr, M., Frank, M., Blaser, P., Antz, B., Fohlmeister, J., Frank, N., Andersen, M. B., and Deininger, M. (2015). "Strong and Deep Atlantic Meridional Over-

turning Circulation during the Last Glacial Cycle". In: *Nature* 517.7532, pp. 73–76. DOI: 10.1038/nature14059.

Chen, T., Robinson, L. F., Burke, A., Southon, J., Spooner, P., Morris, P. J., and Ng, H. C. (2015). "Synchronous Centennial Abrupt Events in the Ocean and Atmosphere during the Last Deglaciation". In: *Science* 349.6255, pp. 1537–1541.

Fink, H. G., Wienberg, C., De Pol-Holz, R., and Hebbeln, D. (2015). "Spatio-Temporal Distribution Patterns of Mediterranean Cold-Water Corals (Lophelia Pertusa and Madrepora Oculata) during the Past 14,000 Years". In: *Deep Sea Research Part I: Oceanographic Research Papers* 103, pp. 37–48. DOI: 10.1016/j.dsr.2015.05.006.

Glogowski, S., Dullo, W.-C., Feldens, P., Liebetrau, V., Reumont, J. von, Hühnerbach, V., Krastel, S., Wynn, R. B., and Flögel, S. (2015). "The Eugen Seibold Coral Mounds Offshore Western Morocco: Oceanographic and Bathymetric Boundary Conditions of a Newly Discovered Cold-Water Coral Province". In: *Geo-Marine Letters* 35.4, pp. 257–269. DOI: 10.1007/s00367-015-0405-7.

Hebbeln, D., Wienberg, C., Bartels, M., Bergenthal, Frank, N., Gaide, S., Henriet, J.-P., Kaszemeik, K., Klar, S., Krengel, T., Kuhnert, M., Meyer-Schack, B., Noorlander, Reuter, M., Rosaik, U., Schmidt, W., Seeba, H., Seiter, C., Stange, N., Terhzaz, C., and Van Rooij, David (2015). *MoccoMeBo: Climate-Driven Development of Moroccan Cold-Water Coral Mounds Revealed by MeBo-Drilling - Atlantic vs. Mediterranean Settings, Cruise MSM36 – February 18 – March 17, 2014 – Malaga (Spain) – Las Palmas (Spain). MARIA S. MERIAN-Berichte, MSM36. DFGSenatskommission Fuer Ozeanographie,* Cruise Report, p. 47.

Hines, S. K., Southon, J. R., and Adkins, J. F. (2015). "A High-Resolution Record of Southern Ocean Intermediate Water Radiocarbon over the Past 30,000 Years". In: *Earth and Planetary Science Letters* 432, pp. 46–58. DOI: 10.1016/j.epsl.2015.09.038.

Horner, T. J., Kinsley, C. W., and Nielsen, S. G. (2015). "Barium-Isotopic Fractionation in Seawater Mediated by Barite Cycling and Oceanic Circulation". In: *Earth and Planetary Science Letters* 430, pp. 511–522. DOI: 10.1016/j.epsl.2015.07.027.

Lausecker, M. (2015). "Das Lithium- Magnesium -Verhältnis als Temperaturproxy in Tiefseekorallen -Temperaturkalibration und Temperaturrekonstruktion -". Bachelor's Thesis. Heidelberg, Germany: Heidelberg University. 67 pp.

Matos, L., Mienis, F., Wienberg, C., Frank, N., Kwiatkowski, C., Groeneveld, J., Thil, F., Abrantes, F., Cunha, M. R., and Hebbeln, D. (2015). "Interglacial Occurrence of Cold-Water Corals off Cape Lookout (NW Atlantic): First Evidence of the Gulf Stream Influence". In: *Deep Sea Research Part I: Oceanographic Research Papers* 105, pp. 158–170. DOI: 10.1016/j.dsr.2015.09.003.

Nan, X., Wu, F., Zhang, Z., Hou, Z., Huang, F., and Yu, H. (2015). "High-Precision Barium Isotope Measurements by MC-ICP-MS". In: *J. Anal. At. Spectrom.* 30.11, pp. 2307–2315. DOI: 10.1039/C5JA00166H.

Rieger, N. (2015). "Cold Water Coral Ecosystem Changes in the Southern Gulf of Cádiz Induced by Ocean Dynamic Variances from 20 to 40 Ka BP". Bachelor's Thesis. Heidelberg, Germany: Heidelberg University. 98 pp.

Roberts, N. L. and Piotrowski, A. M. (2015). "Radiogenic Nd Isotope Labeling of the Northern NE Atlantic during MIS 2". In: *Earth and Planetary Science Letters* 423, pp. 125–133. DOI: 10.1016/j.epsl.2015.05.011.

Stalder, C., Vertino, A., Rosso, A., Rüggeberg, A., Pirkenseer, C., Spangenberg, J. E., Spezzaferri, S., Camozzi, O., Rappo, S., and Hajdas, I. (2015). "Microfossils, a Key to Unravel

Cold-Water Carbonate Mound Evolution through Time: Evidence from the Eastern Alboran Sea". In: *PLOS ONE* 10.10, e0140223. DOI: 10.1371/journal.pone.0140223.

Stichel, T., Hartman, A. E., Duggan, B., Goldstein, S. L., Scher, H., and Pahnke, K. (2015). "Separating Biogeochemical Cycling of Neodymium from Water Mass Mixing in the Eastern North Atlantic". In: *Earth and Planetary Science Letters* 412, pp. 245–260. DOI: 10.1016/j.epsl.2014.12.008.

Thornalley, D. J. R., Bauch, H. A., Gebbie, G., Guo, W., Ziegler, M., Bernasconi, S. M., Barker, S., Skinner, L. C., and Yu, J. (2015). "A Warm and Poorly Ventilated Deep Arctic Mediterranean during the Last Glacial Period". In: *Science* 349.6249, pp. 706–710. DOI: 10.1126/science.aaa9554. pmid: 26273049.

Titschack, J., Baum, D., De Pol-Holz, R., López Correa, M., Forster, N., Flögel, S., Hebbeln, D., and Freiwald, A. (2015). "Aggradation and Carbonate Accumulation of Holocene Norwegian Cold-Water Coral Reefs". In: *Sedimentology* 62.7, pp. 1873–1898. DOI: 10.1111/sed.12206.

Aagaard-Sørensen, S., Husum, K., Hald, M., Marchitto, T., and Godtliebsen, F. (2014). "Sub Sea Surface Temperatures in the Polar North Atlantic during the Holocene: Planktic Foraminiferal Mg/Ca Temperature Reconstructions". In: *The Holocene* 24.1, pp. 93–103. DOI: 10.1177/0959683613515730.

Flögel, S., Dullo, W. .-.-C., Pfannkuche, O., Kiriakoulakis, K., and Rüggeberg, A. (2014). "Geochemical and Physical Constraints for the Occurrence of Living Cold-Water Corals". In: *Deep Sea Research Part II: Topical Studies in Oceanography*. Biology and Geology of Deep-Sea Coral Ecosystems: Proceedings of the Fifth International Symposium on Deep Sea Corals 99, pp. 19–26. DOI: 10.1016/j.dsr2.2013.06.006.

Förstel, J. (2014). "Messung von Lithium-Magnesium-Verhältnissen an einem iCAP Q™ Quadrupol-Massenspektrometer mit induktiv gekoppelter Plasmaionenquelle". Bachelor's Thesis. Heidelberg, Germany: Heidelberg University. 83 pp.

Hebbeln, D., Wienberg, C., Wintersteller, P., Freiwald, A., Becker, M., Beuck, L., Dullo, C., Eberli, G. P., Glogowski, S., Matos, L., Forster, N., Reyes-Bonilla, H., and Taviani, M. (2014). "Environmental Forcing of the Campeche Cold-Water Coral Province, Southern Gulf of Mexico". In: *Biogeosciences* 11.7, pp. 1799–1815. DOI: 10.5194/bg-11-1799-2014.

Henry, L.-A., Frank, N., Hebbeln, D., Wienberg, C., Robinson, L., van de Flierdt, T., Dahl, M., Douarin, M., Morrison, C. L., Correa, M. L., Rogers, A. D., Ruckelshausen, M., and Roberts, J. M. (2014). "Global Ocean Conveyor Lowers Extinction Risk in the Deep Sea". In: *Deep Sea Research Part I: Oceanographic Research Papers* 88, pp. 8–16. DOI: 10.1016/j.dsr.2014.03.004.

Hernandez-Molina, F. J., Llave, E., Preu, B., Ercilla, G., Fontan, A., Bruno, M., Serra, N., Gomiz, J. J., Brackenridge, R. E., Sierro, F. J., Stow, D. A. V., Garcia, M., Juan, C., Sandoval, N., and Arnaiz, A. (2014). "Contourite Processes Associated with the Mediterranean Outflow Water after Its Exit from the Strait of Gibraltar: Global and Conceptual Implications". In: *Geology* 42.3, pp. 227–230. DOI: 10.1130/G35083.1.

Lambeck, K., Rouby, H., Purcell, A., Sun, Y., and Sambridge, M. (2014). "Sea Level and Global Ice Volumes from the Last Glacial Maximum to the Holocene". In: *Proceedings of the National Academy of Sciences* 111.43, pp. 15296–15303. DOI: 10.1073/pnas.1411762111. pmid: 25313072.

Margolin, A. R., Robinson, L. F., Burke, A., Waller, R. G., Scanlon, K. M., Roberts, M. L., Auro, M. E., and van de Flierdt, T. (2014). "Temporal and Spatial Distributions of Cold-Water Corals in the Drake Passage: Insights from the Last 35,000 Years". In: *Deep Sea Research Part II: Topical Studies in Oceanography* 99, pp. 237–248. DOI: 10.1016/j.dsr2.2013.06.008.

Miyazaki, T., Kimura, J.-I., and Chang, Q. (2014). "Analysis of Stable Isotope Ratios of Ba by Double-Spike Standard-Sample Bracketing Using Multiple-Collector Inductively Coupled Plasma Mass Spectrometry". In: *Journal of Analytical Atomic Spectrometry* 29.3, p. 483. DOI: 10.1039/c3ja50311a.

Montagna, P., McCulloch, M., Douville, E., López Correa, M., Trotter, J., Rodolfo-Metalpa, R., Dissard, D., Ferrier-Pagès, C., Frank, N., Freiwald, A., Goldstein, S., Mazzoli, C., Reynaud, S., Rüggeberg, A., Russo, S., and Taviani, M. (2014). "Li/Mg Systematics in Scleractinian Corals: Calibration of the Thermometer". In: *Geochimica et Cosmochimica Acta* 132, pp. 288–310. DOI: 10.1016/j.gca.2014.02.005.

Navas, J. M., Miller, P. L., Henry, L.-A., Hennige, S. J., and Roberts, J. M. (2014). "Ecohydrodynamics of Cold-Water Coral Reefs: A Case Study of the Mingulay Reef Complex (Western Scotland)". In: *PLOS ONE* 9.5, e98218. DOI: 10.1371/journal.pone.0098218.

Raddatz, J., Rüggeberg, A., Liebetrau, V., Foubert, A., Hathorne, E. C., Fietzke, J., Eisenhauer, A., and Dullo, W.-C. (2014). "Environmental Boundary Conditions of Cold-Water Coral Mound Growth over the Last 3 Million Years in the Porcupine Seabight, Northeast Atlantic". In: *Deep Sea Research Part II: Topical Studies in Oceanography* 99, pp. 227–236. DOI: 10.1016/j.dsr2.2013.06.009.

Robinson, L. F. (2014). *RRS James Cook Cruise JC094, October 13–November 30 2013, Tenerife-Trinidad. TROPICS, Tracing Oceanic Processes Using Corals and Sediments. Reconstructing Abrupt Changes in Chemistry and Circulation of the Equatorial Atlantic Ocean: Implications for Global Climate and Deep-Water Habitats.* Cruise Report.

Robinson, L. F., Adkins, J. F., Frank, N., Gagnon, A. C., Prouty, N. G., Brendan Roark, E., and van de Flierdt, T. (2014). "The Geochemistry of Deep-Sea Coral Skeletons: A Review of Vital Effects and Applications for Palaeoceanography". In: *Deep Sea Research Part II: Topical Studies in Oceanography* 99, pp. 184–198. DOI: 10.1016/j.dsr2.2013.06.005.

Thiagarajan, N., Subhas, A. V., Southon, J. R., Eiler, J. M., and Adkins, J. F. (2014). "Abrupt Pre-Bølling–Allerød Warming and Circulation Changes in the Deep Ocean". In: *Nature* 511.7507, pp. 75–78. DOI: 10.1038/nature13472.

Wefing, A.-M. (2014). "Eiszeitliche Ozeandynamik im Golf von Cádiz: datierte Tiefseekorallen als Archive". Bachelor's Thesis. Heidelberg, Germany: Heidelberg University. 67 pp.

Wilson, D. J., Crocket, K. C., van de Flierdt, T., Robinson, L. F., and Adkins, J. F. (2014). "Dynamic Intermediate Ocean Circulation in the North Atlantic during Heinrich Stadial 1: A Radiocarbon and Neodymium Isotope Perspective: Atlantic Circulation Heinrich Stadial 1". In: *Paleoceanography* 29.11, pp. 1072–1093. DOI: 10.1002/2014PA002674.

Zhang, X., Lohmann, G., Knorr, G., and Purcell, C. (2014). "Abrupt Glacial Climate Shifts Controlled by Ice Sheet Changes". In: *Nature* 512.7514, pp. 290–294. DOI: 10.1038/nature13592.

Adkins, J. F. (2013). "The Role of Deep Ocean Circulation in Setting Glacial Climates: DEEP CIRCULATION REVIEW". In: *Paleoceanography* 28.3, pp. 539–561. DOI: 10.1002/palo.20046.

Cheng, H., Lawrence Edwards, R., Shen, C.-C., Polyak, V. J., Asmerom, Y., Woodhead, J., Hellstrom, J., Wang, Y., Kong, X., Spötl, C., Wang, X., and Calvin Alexander, E. (2013). "Improvements in 230Th Dating, 230Th and 234U Half-Life Values, and U–Th Isotopic Measurements by Multi-Collector Inductively Coupled Plasma Mass Spectrometry". In: *Earth and Planetary Science Letters* 371-372, pp. 82–91. DOI: 10.1016/j.epsl.2013.04.006.

Douarin, M., Elliot, M., Noble, S. R., Sinclair, D., Henry, L.-A., Long, D., Moreton, S. G., and Murray Roberts, J. (2013). "Growth of North-East Atlantic Cold-Water Coral Reefs and Mounds during the Holocene: A High Resolution U-Series and 14C Chronology". In: *Earth and Planetary Science Letters* 375, pp. 176–187. DOI: 10.1016/j.epsl.2013.05.023.

Fedorov, A. V., Brierley, C. M., Lawrence, K. T., Liu, Z., Dekens, P. S., and Ravelo, A. C. (2013). "Patterns and Mechanisms of Early Pliocene Warmth". In: *Nature* 496.7443, pp. 43–49. DOI: 10.1038/nature12003.

Fink, H. G., Wienberg, C., De Pol-Holz, R., Wintersteller, P., and Hebbeln, D. (2013). "Cold-Water Coral Growth in the Alboran Sea Related to High Productivity during the Late Pleistocene and Holocene". In: *Marine Geology* 339, pp. 71–82. DOI: 10.1016/j.margeo.2013.04.009.

Flato, G., Marotzke, J., Abiodun, B., Braconnot, P., Chou, S. C., Collins, W. J., Cox, P., Driouech, F., Emori, S., Eyring, V., et al. (2013). "Evaluation of Climate Models. In: Climate Change 2013: The Physical Science Basis. Contribution of Working Group I to the Fifth Assessment Report of the Intergovernmental Panel on Climate Change". In: *Climate Change 2013* 5, pp. 741–866.

Garcia, H., Locarnini, R., Boyer, T., Antonov, J., Baranova, O., Zweng, M., Reagan, J., and Johnson, D. (2013). *Dissolved Inorganic Nutrients (Phosphate, Nitrate, Silicate)*. Technical Report 4.

Hathorne, E. C., Felis, T., Suzuki, A., Kawahata, H., and Cabioch, G. (2013a). "Lithium in the Aragonite Skeletons of Massive Porites Corals: A New Tool to Reconstruct Tropical Sea Surface Temperatures". In: *Paleoceanography* 28.1, pp. 143–152. DOI: 10.1029/2012PA002311.

Hathorne, E. C., Gagnon, A., Felis, T., Adkins, J., Asami, R., Boer, W., Caillon, N., Case, D., Cobb, K. M., Douville, E., deMenocal, P., Eisenhauer, A., Garbe-Schönberg, D., Geibert, W., Goldstein, S., Hughen, K., Inoue, M., Kawahata, H., Kölling, M., Cornec, F. L., Linsley, B. K., McGregor, H. V., Montagna, P., Nurhati, I. S., Quinn, T. M., Raddatz, J., Rebaubier, H., Robinson, L., Sadekov, A., Sherrell, R., Sinclair, D., Tudhope, A. W., Wei, G., Wong, H., Wu, H. C., and You, C.-F. (2013b). "Interlaboratory Study for Coral Sr/Ca and Other Element/Ca Ratio Measurements: INTERLABORATORY STUDY FOR CORAL SR/CA". In: *Geochemistry, Geophysics, Geosystems* 14.9, pp. 3730–3750. DOI: 10.1002/ggge.20230.

Kromer, B., Lindauer, S., Synal, H.-A., and Wacker, L. (2013). "MAMS – A New AMS Facility at the Curt-Engelhorn-Centre for Achaeometry, Mannheim, Germany". In: *Nuclear Instruments and Methods in Physics Research Section B: Beam Interactions with Materials and Atoms*. Proceedings of the Twelfth International Conference on Accelerator Mass Spectrometry, Wellington, New Zealand, 20-25 March 2011 294, pp. 11–13. DOI: 10.1016/j.nimb.2012.01.015.

Montero-Serrano, J.-C., Frank, N., Tisnérat-Laborde, N., Colin, C., Wu, C.-C., Lin, K., Shen, C.-C., Copard, K., Orejas, C., Gori, A., De Mol, L., Van Rooij, D., Reverdin, G., and Douville, E. (2013). "Decadal Changes in the Mid-Depth Water Mass Dynamic of the Northeastern Atlantic Margin (Bay of Biscay)". In: *Earth and Planetary Science Letters* 364, pp. 134–144. DOI: 10.1016/j.epsl.2013.01.012.

Raddatz, J., Liebetrau, V., Rüggeberg, A., Hathorne, E., Krabbenhöft, A., Eisenhauer, A., Böhm, F., Vollstaedt, H., Fietzke, J., López Correa, M., Freiwald, A., and Dullo, W.-C. (2013). "Stable Sr-Isotope, Sr/Ca, Mg/Ca, Li/Ca and Mg/Li Ratios in the Scleractinian Cold-Water Coral Lophelia Pertusa". In: *Chemical Geology* 352, pp. 143–152. DOI: 10.1016/j.chemgeo.2013.06.013.

Reimer, P. J., Bard, E., Bayliss, A., Beck, J. W., Blackwell, P. G., Ramsey, C. B., Buck, C. E., Cheng, H., Edwards, R. L., Friedrich, M., Grootes, P. M., Guilderson, T. P., Haflidason, H., Hajdas, I., Hatté, C., Heaton, T. J., Hoffmann, D. L., Hogg, A. G., Hughen, K. A., Kaiser, K. F., Kromer, B., Manning, S. W., Niu, M., Reimer, R. W., Richards, D. A., Scott, E. M., Southon, J. R., Staff, R. A., Turney, C. S. M., and Plicht, J. van der (2013). "IntCal13 and Marine13 Radiocarbon Age Calibration Curves 0–50,000 Years Cal BP". In: *Radiocarbon* 55.4, pp. 1869–1887. DOI: 10.2458/azu_js_rc.55.16947.

Ruckelshausen, M. (2013). "PhD2013_Ruckelshausen.Pdf". Heidelberg, Germany: Heidelberg University. 215 pp.

Thiagarajan, N., Gerlach, D., Roberts, M. L., Burke, A., McNichol, A., Jenkins, W. J., Subhas, A. V., Thresher, R. E., and Adkins, J. F. (2013). "Movement of Deep-Sea Coral Populations on Climatic Timescales: CORAL POPULATIONS AND CLIMATE". In: *Paleoceanography* 28.2, pp. 227–236. DOI: 10.1002/palo.20023.

Thierens, M., Browning, E., Pirlet, H., Loutre, M. .-.-F., Dorschel, B., Huvenne, V. A. I., Titschack, J., Colin, C., Foubert, A., and Wheeler, A. J. (2013). "Cold-Water Coral Carbonate Mounds as Unique Palaeo-Archives: The Plio-Pleistocene Challenger Mound Record (NE Atlantic)". In: *Quaternary Science Reviews* 73, pp. 14–30. DOI: 10.1016/j.quascirev.2013.05.006.

Van Rooij, D., Hebbeln, D., Cormas, M., Vandorpe, T., Delivet, S., and MD194 shipboard scientists,
bibinitperiod the (2013). *EuroFLEETS Cruise Summary Report "MD194 GATEWAY"*. Cruise Report. Cádiz (ES) - Lissabon (PT): Ghent University, Belgium, p. 214.

Wilson, D. J., Piotrowski, A. M., Galy, A., and Clegg, J. A. (2013). "Reactivity of Neodymium Carriers in Deep Sea Sediments: Implications for Boundary Exchange and Paleoceanography". In: *Geochimica et Cosmochimica Acta* 109, pp. 197–221. DOI: 10.1016/j.gca.2013.01.042.

Böttcher, M. E., Geprägs, P., Neubert, N., von Allmen, K., Pretet, C., Samankassou, E., and Nägler, T. F. (2012). "Barium Isotope Fractionation during Experimental Formation of the Double Carbonate BaMn[CO $_3$] $_2$ at Ambient Temperature". In: *Isotopes in Environmental and Health Studies* 48.3, pp. 457–463. DOI: 10.1080/10256016.2012.673489.

Burke, A. and Robinson, L. F. (2012). "The Southern Ocean's Role in Carbon Exchange During the Last Deglaciation". In: *Science* 335.6068, pp. 557–561. DOI: 10.1126/science.1208163. pmid: 22174131.

Copard, K., Colin, C., Henderson, G., Scholten, J., Douville, E., Sicre, M.-A., and Frank, N. (2012). "Late Holocene Intermediate Water Variability in the Northeastern Atlantic as Recorded

by Deep-Sea Corals". In: *Earth and Planetary Science Letters* 313-314, pp. 34–44. DOI: 10.1016/j.epsl.2011.09.047.

Fink, H. G., Wienberg, C., Hebbeln, D., McGregor, H. V., Schmiedl, G., Taviani, M., and Freiwald, A. (2012). "Oxygen Control on Holocene Cold-Water Coral Development in the Eastern Mediterranean Sea". In: *Deep Sea Research Part I: Oceanographic Research Papers* 62, pp. 89–96. DOI: 10.1016/j.dsr.2011.12.013.

Frank, N., Montagna, P., Arnaud-Haond, and & the ICECTD shipboard scientists (2012). *Cruise Report ICECTD, Brest (FR) – Reykjavik (IS) – Ponta Delgada (PO), 11 June – 07 July 2012*. Cruise Report, p. 68.

Lacan, F., Tachikawa, K., and Jeandel, C. (2012). "Neodymium Isotopic Composition of the Oceans: A Compilation of Seawater Data". In: *Chemical Geology* 300-301, pp. 177–184. DOI: 10.1016/j.chemgeo.2012.01.019.

López Correa, M., Montagna, P., Joseph, N., Rüggeberg, A., Fietzke, J., Flögel, S., Dorschel, B., Goldstein, S., Wheeler, A., and Freiwald, A. (2012). "Preboreal Onset of Cold-Water Coral Growth beyond the Arctic Circle Revealed by Coupled Radiocarbon and U-Series Dating and Neodymium Isotopes". In: *Quaternary Science Reviews* 34, pp. 24–43. DOI: 10.1016/j.quascirev.2011.12.005.

Mienis, F., De Stigter, H., De Haas, H., Van der Land, C., and Van Weering, T. (2012). "Hydrodynamic Conditions in a Cold-Water Coral Mound Area on the Renard Ridge, Southern Gulf of Cadiz". In: *Journal of Marine Systems* 96-97, pp. 61–71. DOI: 10.1016/j.jmarsys.2012.02.002.

Robinson, L. F. and Siddall, M. (2012). "Palaeoceanography: Motivations and Challenges for the Future". In: *Philosophical Transactions of the Royal Society A: Mathematical, Physical and Engineering Sciences* 370.1980, pp. 5540–5566. DOI: 10.1098/rsta.2012.0396.

Sabatier, P., Reyss, J.-L., Hall-Spencer, J. M., Colin, C., Frank, N., Tisnérat-Laborde, N., Bordier, L., and Douville, E. (2012). "210Pb-226Ra Chronology Reveals Rapid Growth Rate of Madrepora Oculata and Lophelia Pertusa on World's Largest Cold-Water Coral Reef". In: *Biogeosciences* 9.3, pp. 1253–1265. DOI: 10.5194/bg-9-1253-2012.

Stichel, T., Frank, M., Rickli, J., and Haley, B. A. (2012). "The Hafnium and Neodymium Isotope Composition of Seawater in the Atlantic Sector of the Southern Ocean". In: *Earth and Planetary Science Letters* 317–318, pp. 282–294. DOI: 10.1016/j.epsl.2011.11.025.

Wilson, D. J., Piotrowski, A. M., Galy, A., and McCave, I. N. (2012). "A Boundary Exchange Influence on Deglacial Neodymium Isotope Records from the Deep Western Indian Ocean". In: *Earth and Planetary Science Letters* 341, pp. 35–47. DOI: 10.1016/j.epsl.2012.06.009.

Anagnostou, E., Sherrell, R. M., Gagnon, A., LaVigne, M., Field, M. P., and McDonough, W. F. (2011). "Seawater Nutrient and Carbonate Ion Concentrations Recorded as P/Ca, Ba/Ca, and U/Ca in the Deep-Sea Coral Desmophyllum Dianthus". In: *Geochimica et Cosmochimica Acta* 75.9, pp. 2529–2543. DOI: 10.1016/j.gca.2011.02.019.

Chen, T. and Yu, K. (2011). "P/Ca in Coral Skeleton as a Geochemical Proxy for Seawater Phosphorus Variation in Daya Bay, Northern South China Sea". In: *Marine Pollution Bulletin* 62.10, pp. 2114–2121. DOI: 10.1016/j.marpolbul.2011.07.014.

Copard, K., Colin, C., Frank, N., Jeandel, C., Montero-Serrano, J.-C., Reverdin, G., and Ferron, B. (2011). "Nd Isotopic Composition of Water Masses and Dilution of the Mediterranean Outflow along the Southwest European Margin: ND ISOTOPIC COMPOSITION OF WA-

TER MASSES". In: *Geochemistry, Geophysics, Geosystems* 12.6, n/a–n/a. DOI: 10.1029/2011GC003529.

Davies, A. J. and Guinotte, J. M. (2011). "Global Habitat Suitability for Framework-Forming Cold-Water Corals". In: *PLOS ONE* 6.4, e18483. DOI: 10.1371/journal.pone.0018483.

Eisele, M., Frank, N., Wienberg, C., Hebbeln, D., López Correa, M., Douville, E., and Freiwald, A. (2011). "Productivity Controlled Cold-Water Coral Growth Periods during the Last Glacial off Mauritania". In: *Marine Geology* 280 (1-4), pp. 143–149. DOI: 10.1016/j.margeo.2010.12.007.

Elmore, A. C., Piotrowski, A. M., Wright, J. D., and Scrivner, A. E. (2011). "Testing the Extraction of Past Seawater Nd Isotopic Composition from North Atlantic Deep Sea Sediments and Foraminifera: N. ATLANTIC SEDIMENT AND FORAMINIFERAL εNd". In: *Geochemistry, Geophysics, Geosystems* 12.9, n/a–n/a. DOI: 10.1029/2011GC003741.

Frank, N., Freiwald, A., Correa, M. L., Wienberg, C., Eisele, M., Hebbeln, D., Van Rooij, D., Henriet, J.-P., Colin, C., van Weering, T., et al. (2011). "Northeastern Atlantic Cold-Water Coral Reefs and Climate". In: *Geology* 39.8, pp. 743–746.

Horikawa, K., Martin, E. E., Asahara, Y., and Sagawa, T. (2011). "Limits on Conservative Behavior of Nd Isotopes in Seawater Assessed from Analysis of Fish Teeth from Pacific Core Tops". In: *Earth and Planetary Science Letters* 310.1, pp. 119–130. DOI: 10.1016/j.epsl.2011.07.018.

LaVigne, M., Hill, T. M., Spero, H. J., and Guilderson, T. P. (2011). "Bamboo Coral Ba/Ca: Calibration of a New Deep Ocean Refractory Nutrient Proxy". In: *Earth and Planetary Science Letters* 312 (3-4), pp. 506–515. DOI: 10.1016/j.epsl.2011.10.013.

Louarn, E. and Morin, P. (2011). "Antarctic Intermediate Water Influence on Mediterranean Sea Water Outflow". In: *Deep Sea Research Part I: Oceanographic Research Papers* 58.9, pp. 932–942. DOI: 10.1016/j.dsr.2011.05.009.

Mason, H. E., Montagna, P., Kubista, L., Taviani, M., McCulloch, M., and Phillips, B. L. (2011). "Phosphate Defects and Apatite Inclusions in Coral Skeletal Aragonite Revealed by Solid-State NMR Spectroscopy". In: *Geochimica et Cosmochimica Acta* 75.23, pp. 7446–7457. DOI: 10.1016/j.gca.2011.10.002.

McIntyre, C. P., Roberts, M. L., Burton, J. R., McNichol, A. P., Burke, A., Robinson, L. F., von Reden, K. F., and Jenkins, W. J. (2011). "Rapid Radiocarbon (14C) Analysis of Coral and Carbonate Samples Using a Continuous-Flow Accelerator Mass Spectrometry (CFAMS) System". In: *Paleoceanography* 26.4, PA4212. DOI: 10.1029/2011PA002174.

Montero-Serrano, J.-C., Frank, N., Colin, C., Wienberg, C., and Eisele, M. (2011). "The Climate Influence on the Mid-Depth Northeast Atlantic Gyres Viewed by Cold-Water Corals: THE MID-DEPTH NORTHEAST ATLANTIC GYRES". In: *Geophysical Research Letters* 38.19, n/a–n/a. DOI: 10.1029/2011GL048733.

Penaud, A., Eynaud, F., Sánchez-Goñi, M., Malaizé, B., Turon, J., and Rossignol, L. (2011). "Contrasting Sea-Surface Responses between the Western Mediterranean Sea and Eastern Subtropical Latitudes of the North Atlantic during Abrupt Climatic Events of MIS 3". In: *Marine Micropaleontology* 80 (1-2), pp. 1–17. DOI: 10.1016/j.marmicro.2011.03.002.

Raddatz, J., Rüggeberg, A., Margreth, S., and Dullo, W.-C. (2011). "Paleoenvironmental Reconstruction of Challenger Mound Initiation in the Porcupine Seabight, NE Atlantic". In: *Marine*

Geology. Special Issue on COld-water CArbonate Reservoir systems in Deep Environments - COCARDE 282.1, pp. 79–90. DOI: 10.1016/j.margeo.2010.10.019.

Rempfer, J., Stocker, T. F., Joos, F., Dutay, J.-C., and Siddall, M. (2011). "Modelling Nd-Isotopes with a Coarse Resolution Ocean Circulation Model: Sensitivities to Model Parameters and Source/Sink Distributions". In: *Geochimica et Cosmochimica Acta* 75.20, pp. 5927–5950. DOI: 10.1016/j.gca.2011.07.044.

Robinson, L. F. and Waller, R. G. (2011). *Historic Perspectives on Climate and Biogeography from Deep-Sea Corals in the Drake Passage.' Cruise Report RVIB Nathaniel B Palmer Cruise 11–03, May 09–June 2011*. Cruise Report.

Sherwood, O. A., Lehmann, M. F., Schubert, C. J., Scott, D. B., and McCarthy, M. D. (2011). "Nutrient Regime Shift in the Western North Atlantic Indicated by Compound-Specific δ15N of Deep-Sea Gorgonian Corals". In: *Proceedings of the National Academy of Sciences* 108.3, pp. 1011–1015. DOI: 10.1073/pnas.1004904108. pmid: 21199952.

Thiagarajan, N., Adkins, J., and Eiler, J. (2011). "Carbonate Clumped Isotope Thermometry of Deep-Sea Corals and Implications for Vital Effects". In: *Geochimica et Cosmochimica Acta* 75.16, pp. 4416–4425. DOI: 10.1016/j.gca.2011.05.004.

Thompson, W. G., Allen Curran, H., Wilson, M. A., and White, B. (2011). "Sea-Level Oscillations during the Last Interglacial Highstand Recorded by Bahamas Corals". In: *Nature Geoscience* 4.10, pp. 684–687. DOI: 10.1038/ngeo1253.

Yoshimura, T., Tanimizu, M., Inoue, M., Suzuki, A., Iwasaki, N., and Kawahata, H. (2011). "Mg Isotope Fractionation in Biogenic Carbonates of Deep-Sea Coral, Benthic Foraminifera, and Hermatypic Coral". In: *Analytical and Bioanalytical Chemistry* 401.9, pp. 2755–2769. DOI: 10.1007/s00216-011-5264-0.

Andersen, M. B., Stirling, C. H., Zimmermann, B., and Halliday, A. N. (2010). "Precise Determination of the Open Ocean ^{234} U/ ^{238} U Composition: DATA BRIEF". In: *Geochemistry, Geophysics, Geosystems* 11.12, n/a–n/a. DOI: 10.1029/2010GC003318.

Burke, A., Robinson, L. F., McNichol, A. P., Jenkins, W. J., Scanlon, K. M., and Gerlach, D. S. (2010). "Reconnaissance Dating: A New Radiocarbon Method Applied to Assessing the Temporal Distribution of Southern Ocean Deep-Sea Corals". In: *Deep Sea Research Part I: Oceanographic Research Papers* 57.11, pp. 1510–1520. DOI: 10.1016/j.dsr.2010.07.010.

Case, D. H., Robinson, L. F., Auro, M. E., and Gagnon, A. C. (2010). "Environmental and Biological Controls on Mg and Li in Deep-Sea Scleractinian Corals". In: *Earth and Planetary Science Letters* 300 (3-4), pp. 215–225. DOI: 10.1016/j.epsl.2010.09.029.

Colin, C., Frank, N., Copard, K., and Douville, E. (2010). "Neodymium Isotopic Composition of Deep-Sea Corals from the NE Atlantic: Implications for Past Hydrological Changes during the Holocene". In: *Quaternary Science Reviews* 29 (19-20), pp. 2509–2517. DOI: 10.1016/j.quascirev.2010.05.012.

Copard, K., Colin, C., Douville, E., Freiwald, A., Gudmundsson, G., De Mol, B., and Frank, N. (2010). "Nd Isotopes in Deep-Sea Corals in the North-Eastern Atlantic". In: *Quaternary Science Reviews* 29 (19-20), pp. 2499–2508. DOI: 10.1016/j.quascirev.2010.05.025.

Douville, E., Sallé, E., Frank, N., Eisele, M., Pons-Branchu, E., and Ayrault, S. (2010). "Rapid and Accurate U–Th Dating of Ancient Carbonates Using Inductively Coupled Plasma-Quadrupole Mass Spectrometry". In: *Chemical Geology* 272 (1-4), pp. 1–11. DOI: 10.1016/j.chemgeo.2010.01.007.

Esat, T. M. and Yokoyama, Y. (2010). "Coupled Uranium Isotope and Sea-Level Variations in the Oceans". In: *Geochimica et Cosmochimica Acta* 74.24, pp. 7008–7020. DOI: 10.1016/j.gca.2010.09.007.

Houlbrèque, F., McCulloch, M., Roark, B., Guilderson, T., Meibom, A., Kimball, J., Mortimer, G., Cuif, J.-P., and Dunbar, R. (2010). "Uranium-Series Dating and Growth Characteristics of the Deep-Sea Scleractinian Coral: Enallopsammia Rostrata from the Equatorial Pacific". In: *Geochimica et Cosmochimica Acta* 74.8, pp. 2380–2395. DOI: 10.1016/j.gca.2010.01.017.

Mangini, A., Godoy, J. M., Godoy, M. L., Kowsmann, R., Santos, G. M., Ruckelshausen, M., Schroeder-Ritzrau, A., and Wacker, L. (2010). "Deep Sea Corals off Brazil Verify a Poorly Ventilated Southern Pacific Ocean during H2, H1 and the Younger Dryas". In: *Earth and Planetary Science Letters* 293.3, pp. 269–276. DOI: 10.1016/j.epsl.2010.02.041.

McCulloch, M., Taviani, M., Montagna, P., López Correa, M., Remia, A., and Mortimer, G. (2010). "Proliferation and Demise of Deep-Sea Corals in the Mediterranean during the Younger Dryas". In: *Earth and Planetary Science Letters* 298 (1-2), pp. 143–152. DOI: 10.1016/j.epsl.2010.07.036.

Penaud, A., Eynaud, F., Turon, J., Blamart, D., Rossignol, L., Marret, F., Lopez-Martinez, C., Grimalt, J., Malaizé, B., and Charlier, K. (2010). "Contrasting Paleoceanographic Conditions off Morocco during Heinrich Events (1 and 2) and the Last Glacial Maximum". In: *Quaternary Science Reviews* 29 (15-16), pp. 1923–1939. DOI: 10.1016/j.quascirev.2010.04.011.

Roberts, N. L., Piotrowski, A. M., McManus, J. F., and Keigwin, L. D. (2010). "Synchronous Deglacial Overturning and Water Mass Source Changes". In: *Science* 327.5961, pp. 75–78. DOI: 10.1126/science.1178068. pmid: 20044573.

Rollion-Bard, C., Blamart, D., Cuif, J.-P., and Dauphin, Y. (2010). "In Situ Measurements of Oxygen Isotopic Composition in Deep-Sea Coral, Lophelia Pertusa: Re-Examination of the Current Geochemical Models of Biomineralization". In: *Geochimica et Cosmochimica Acta* 74.4, pp. 1338–1349. DOI: 10.1016/j.gca.2009.11.011.

Van de Flierdt, T., Robinson, L. F., and Adkins, J. F. (2010). "Deep-Sea Coral Aragonite as a Recorder for the Neodymium Isotopic Composition of Seawater". In: *Geochimica et Cosmochimica Acta* 74.21, pp. 6014–6032. DOI: 10.1016/j.gca.2010.08.001.

Van der Land, C., Mienis, F., De Haas, H., Frank, N., Swennen, R., and Van Weering, T. C. E. (2010). "Diagenetic Processes in Carbonate Mound Sediments at the South-West Rockall Trough Margin". In: *Sedimentology* 57.3, pp. 912–931. DOI: 10.1111/j.1365-3091.2009.01125.x.

Von Allmen, K., Böttcher, M. E., Samankassou, E., and Nägler, T. F. (2010). "Barium Isotope Fractionation in the Global Barium Cycle: First Evidence from Barium Minerals and Precipitation Experiments". In: *Chemical Geology* 277 (1-2), pp. 70–77. DOI: 10.1016/j.chemgeo.2010.07.011.

Wacker, L., Bonani, G., Friedrich, M., Hajdas, I., Kromer, B., Němec, M., Ruff, M., Suter, M., Synal, H.-A., and Vockenhuber, C. (2010). "MICADAS: Routine and High-Precision Radiocarbon Dating". In: *Radiocarbon* 52.2, pp. 252–262. DOI: 10.1017/S0033822200045288.

Wienberg, C., Frank, N., Mertens, K. N., Stuut, J.-B., Marchant, M., Fietzke, J., Mienis, F., and Hebbeln, D. (2010). "Glacial Cold-Water Coral Growth in the Gulf of Cádiz: Implications of Increased Palaeo-Productivity". In: *Earth and Planetary Science Letters* 298 (3-4), pp. 405–416. DOI: 10.1016/j.epsl.2010.08.017.

Bower, A. S., Lozier, M. S., Gary, S. F., and Böning, C. W. (2009). "Interior Pathways of the North Atlantic Meridional Overturning Circulation". In: *Nature* 459.7244, pp. 243–247. DOI: 10.1038/nature07979.

Clark, P. U., Dyke, A. S., Shakun, J. D., Carlson, A. E., Clark, J., Wohlfarth, B., Mitrovica, J. X., Hostetler, S. W., and McCabe, A. M. (2009). "The Last Glacial Maximum". In: *Science* 325.5941, pp. 710–714. DOI: 10.1126/science.1172873. pmid: 19661421.

Davies, A. J., Duineveld, G. C. A., Lavaleye, M. S. S., Bergman, M. J. N., van Haren, H., and Roberts, J. M. (2009). "Downwelling and Deep-Water Bottom Currents as Food Supply Mechanisms to the Cold-Water Coral Lophelia Pertusa (Scleractinia) at the Mingulay Reef Complex". In: *Limnology and Oceanography* 54.2, pp. 620–629. DOI: 10.4319/lo.2009.54.2.0620.

Eynaud, F., de Abreu, L., Voelker, A., Schönfeld, J., Salgueiro, E., Turon, J.-L., Penaud, A., Toucanne, S., Naughton, F., Sánchez Goñi, M. F., Malaizé, B., and Cacho, I. (2009). "Position of the Polar Front along the Western Iberian Margin during Key Cold Episodes of the Last 45 Ka: TRACKING THE PF ALONG THE WESTERN IBERIAN MARGIN". In: *Geochemistry, Geophysics, Geosystems* 10.7, n/a–n/a. DOI: 10.1029/2009GC002398.

Frank, N., Ricard, E., Lutringer-Paquet, A., van der Land, C., Colin, C., Blamart, D., Foubert, A., Van Rooij, D., Henriet, J.-P., de Haas, H., and van Weering, T. (2009). "The Holocene Occurrence of Cold Water Corals in the NE Atlantic: Implications for Coral Carbonate Mound Evolution". In: *Marine Geology* 266 (1-4), pp. 129–142. DOI: 10.1016/j.margeo.2009.08.007.

García, M., Hernández-Molina, F., Llave, E., Stow, D., León, R., Fernández-Puga, M., Diaz del Río, V., and Somoza, L. (2009). "Contourite Erosive Features Caused by the Mediterranean Outflow Water in the Gulf of Cadiz: Quaternary Tectonic and Oceanographic Implications". In: *Marine Geology* 257 (1-4), pp. 24–40. DOI: 10.1016/j.margeo.2008.10.009.

Henderson, P. and Henderson, Gideon M. (2009). *The Cambridge Handbook of Earth Science Data*. New York: Cambridge University Press.

Mienis, F., van der Land, C., de Stigter, H., van de Vorstenbosch, M., de Haas, H., Richter, T., and van Weering, T. (2009). "Sediment Accumulation on a Cold-Water Carbonate Mound at the Southwest Rockall Trough Margin". In: *Marine Geology* 265 (1-2), pp. 40–50. DOI: 10.1016/j.margeo.2009.06.014.

Rickli, J., Frank, M., and Halliday, A. N. (2009). "The Hafnium–neodymium Isotopic Composition of Atlantic Seawater". In: *Earth and Planetary Science Letters* 280 (1-4), pp. 118–127. DOI: 10.1016/j.epsl.2009.01.026.

Roberts, J. M., Wheeler, A. J., Freiwald, A., and Cairns, S. D. (2009). *Cold-Water Corals – The Biology and Geology of Deep-Sea Coral Habitats*. Cambridge University Press.

Robinson, L. F. and Flierdt, T. van de (2009). "Southern Ocean Evidence for Reduced Export of North Atlantic Deep Water during Heinrich Event 1". In: *Geology* 37.3, pp. 195–198. DOI: 10.1130/G25363A.1.

Rollion-Bard, C., Vigier, N., Meibom, A., Blamart, D., Reynaud, S., Rodolfo-Metalpa, R., Martin, S., and Gattuso, J.-P. (2009). "Effect of Environmental Conditions and Skeletal Ultrastructure on the Li Isotopic Composition of Scleractinian Corals". In: *Earth and Planetary Science Letters* 286 (1–2), pp. 63–70. DOI: 10.1016/j.epsl.2009.06.015.

Titschack, J., Thierens, M., Dorschel, B., Schulbert, C., Freiwald, A., Kano, A., Takashima, C., Kawagoe, N., and Li, X. (2009). "Carbonate Budget of a Cold-Water Coral Mound (Chal-

lenger Mound, IODP Exp. 307)". In: *Marine Geology* 259.1, pp. 36–46. DOI: 10.1016/j.margeo.2008.12.007.

Waelbroeck, C., Paul, A., Kucera, M., Rosell-Melé, A., Weinelt, M., Schneider, R., Mix, A. C., Abelmann, A., Armand, L., Bard, E., Barker, S., Barrows, T. T., Benway, H., Cacho, I., Chen, M.-T., Cortijo, E., Crosta, X., de Vernal, A., Dokken, T., Duprat, J., Elderfield, H., Eynaud, F., Gersonde, R., Hayes, A., Henry, M., Hillaire-Marcel, C., Huang, C.-C., Jansen, E., Juggins, S., Kallel, N., Kiefer, T., Kienast, M., Labeyrie, L., Leclaire, H., Londeix, L., Mangin, S., Matthiessen, J., Marret, F., Meland, M., Morey, A. E., Mulitza, S., Pflaumann, U., Pisias, N. G., Radi, T., Rochon, A., Rohling, E. J., Sbaffi, L., Schäfer-Neth, C., Solignac, S., Spero, H., Tachikawa, K., and Turon, J.-L. (2009). "Constraints on the Magnitude and Patterns of Ocean Cooling at the Last Glacial Maximum". In: *Nature Geoscience* 2.2, pp. 127–132. DOI: 10.1038/ngeo411.

Walker, M., Johnsen, S., Rasmussen, S. O., Popp, T., Steffensen, J.-P., Gibbard, P., Hoek, W., Lowe, J., Andrews, J., Björck, S., Cwynar, L. C., Hughen, K., Kershaw, P., Kromer, B., Litt, T., Lowe, D. J., Nakagawa, T., Newnham, R., and Schwander, J. (2009). "Formal Definition and Dating of the GSSP (Global Stratotype Section and Point) for the Base of the Holocene Using the Greenland NGRIP Ice Core, and Selected Auxiliary Records". In: *Journal of Quaternary Science* 24.1, pp. 3–17. DOI: 10.1002/jqs.1227.

Wienberg, C., Hebbeln, D., Fink, H. G., Mienis, F., Dorschel, B., Vertino, A., Correa, M. L., and Freiwald, A. (2009). "Scleractinian Cold-Water Corals in the Gulf of Cádiz—First Clues about Their Spatial and Temporal Distribution". In: *Deep Sea Research Part I: Oceanographic Research Papers* 56.10, pp. 1873–1893. DOI: 10.1016/j.dsr.2009.05.016.

Bryan, S. P. and Marchitto, T. M. (2008). "Mg/Ca–temperature Proxy in Benthic Foraminifera: New Calibrations from the Florida Straits and a Hypothesis Regarding Mg/Li". In: *Paleoceanography* 23.2, PA2220. DOI: 10.1029/2007PA001553.

Davies, A. J., Wisshak, M., Orr, J. C., and Murray Roberts, J. (2008). "Predicting Suitable Habitat for the Cold-Water Coral Lophelia Pertusa (Scleractinia)". In: *Deep Sea Research Part I: Oceanographic Research Papers* 55.8, pp. 1048–1062. DOI: 10.1016/j.dsr.2008.04.010.

Eisele, M., Hebbeln, D., and Wienberg, C. (2008). "Growth History of a Cold-Water Coral Covered Carbonate Mound — Galway Mound, Porcupine Seabight, NE-Atlantic". In: *Marine Geology* 253 (3-4), pp. 160–169. DOI: 10.1016/j.margeo.2008.05.006.

Foubert, A., Depreiter, D., Beck, T., Maignien, L., Pannemans, B., Frank, N., Blamart, D., and Henriet, J.-P. (2008). "Carbonate Mounds in a Mud Volcano Province off North-West Morocco: Key to Processes and Controls". In: *Marine Geology* 248.1, pp. 74–96. DOI: 10.1016/j.margeo.2007.10.012.

Landais, A., Barkan, E., and Luz, B. (2008). "Record of δ^{18} O and ^{17} O-Excess in Ice from Vostok Antarctica during the Last 150,000 Years". In: *Geophysical Research Letters* 35.2. DOI: 10.1029/2007GL032096.

LaVigne, M., Field, M. P., Anagnostou, E., Grottoli, A. G., Wellington, G. M., and Sherrell, R. M. (2008). "Skeletal P/Ca Tracks Upwelling in Gulf of Panamá Coral: Evidence for a New Seawater Phosphate Proxy". In: *Geophysical Research Letters* 35.5, p. L05604. DOI: 10.1029/2007GL031926.

Lozier, M. S. and Stewart, N. M. (2008). "On the Temporally Varying Northward Penetration of Mediterranean Overflow Water and Eastward Penetration of Labrador Sea Water". In:

Journal of Physical Oceanography 38.9, pp. 2097–2103. DOI: 10.1175/2008JPO3908.1.

Orejas, C., Gori, A., and Gili, J. M. (2008). "Growth Rates of Live Lophelia Pertusa and Madrepora Oculata from the Mediterranean Sea Maintained in Aquaria". In: *Coral Reefs* 27.2, pp. 255–255. DOI: 10.1007/s00338-007-0350-7.

Pahnke, K., Goldstein, S. L., and Hemming, S. R. (2008). "Abrupt Changes in Antarctic Intermediate Water Circulation over the Past 25,000 Years". In: *Nature Geoscience* 1.12, pp. 870–874. DOI: 10.1038/ngeo360.

Rooij, D. V., Blamart, D., and & the MiCROSYSTEMS shipboard scientists (2008). *Cruise Report MD169 MiCROSYSTEMS, Brest (FR)-Algeciras (ES), 15-25 July 2008. ESF EuroDIVERSITY MiCROSYSTEMS Internal Report*. Cruise Report, p. 86.

Sherwood, O. A., Edinger, E. N., Guilderson, T. P., Ghaleb, B., Risk, M. J., and Scott, D. B. (2008). "Late Holocene Radiocarbon Variability in Northwest Atlantic Slope Waters". In: *Earth and Planetary Science Letters* 275.1, pp. 146–153. DOI: 10.1016/j.epsl.2008.08.019.

Siddall, M., Rohling, E. J., Thompson, W. G., and Waelbroeck, C. (2008). "Marine Isotope Stage 3 Sea Level Fluctuations: Data Synthesis and New Outlook". In: *Reviews of Geophysics* 46.4, RG4003. DOI: 10.1029/2007RG000226.

Stramma, L., Johnson, G. C., Sprintall, J., and Mohrholz, V. (2008). "Expanding Oxygen-Minimum Zones in the Tropical Oceans". In: *Science* 320.5876, pp. 655–658. DOI: 10.1126/science.1153847. pmid: 18451300.

Allison, N., Finch, A. A., Webster, J. M., and Clague, D. A. (2007). "Palaeoenvironmental Records from Fossil Corals: The Effects of Submarine Diagenesis on Temperature and Climate Estimates". In: *Geochimica et Cosmochimica Acta* 71.19, pp. 4693–4703. DOI: 10.1016/j.gca.2007.07.026.

Cairns, S. D. (2007). "Deep-Water Corals: An Overview with Special Reference to Diversity and Distribution of Deep-Water Scleractinian Corals". In: *Bulletin of Marine Science* 81.3, pp. 311–322.

Dorschel, B., Hebbeln, D., Rüggeberg, A., and Dullo, C. (2007). "Carbonate Budget of a Cold-Water Coral Carbonate Mound: Propeller Mound, Porcupine Seabight". In: *International Journal of Earth Sciences* 96.1, pp. 73–83. DOI: 10.1007/s00531-005-0493-0.

Fantle, M. S. and DePaolo, D. J. (2007). "Ca Isotopes in Carbonate Sediment and Pore Fluid from ODP Site 807A: The Ca2+(Aq)–calcite Equilibrium Fractionation Factor and Calcite Recrystallization Rates in Pleistocene Sediments". In: *Geochimica et Cosmochimica Acta* 71.10, pp. 2524–2546. DOI: 10.1016/j.gca.2007.03.006.

Fedorov, A., Barreiro, M., Boccaletti, G., Pacanowski, R., and Philander, S. G. (2007). "The Freshening of Surface Waters in High Latitudes: Effects on the Thermohaline and Wind-Driven Circulations". In: *Journal of Physical Oceanography* 37.4, pp. 896–907. DOI: 10.1175/JPO3033.1.

Gagnon, A. C., Adkins, J. F., Fernandez, D. P., and Robinson, L. F. (2007). "Sr/Ca and Mg/Ca Vital Effects Correlated with Skeletal Architecture in a Scleractinian Deep-Sea Coral and the Role of Rayleigh Fractionation". In: *Earth and Planetary Science Letters* 261 (1-2), pp. 280–295. DOI: 10.1016/j.epsl.2007.07.013.

Gutjahr, M., Frank, M., Stirling, C. H., Klemm, V., van de Flierdt, T., and Halliday, A. N. (2007). "Reliable Extraction of a Deepwater Trace Metal Isotope Signal from Fe–Mn Oxyhydroxide

Coatings of Marine Sediments". In: *Chemical Geology* 242.3, pp. 351–370. DOI: 10.1016/j.chemgeo.2007.03.021.

Jeandel, C., Arsouze, T., Lacan, F., Téchiné, P., and Dutay, J.-C. (2007). "Isotopic Nd Compositions and Concentrations of the Lithogenic Inputs into the Ocean: A Compilation, with an Emphasis on the Margins". In: *Chemical Geology* 239 (1-2), pp. 156–164. DOI: 10.1016/j.chemgeo.2006.11.013.

Kano, A., Ferdelman, T. G., Williams, T., Henriet, J.-P., Ishikawa, T., Kawagoe, N., Takashima, C., Kakizaki, Y., Abe, K., Sakai, S., Browning, E. L., and Li, X. (2007). "Age Constraints on the Origin and Growth History of a Deep-Water Coral Mound in the Northeast Atlantic Drilled during Integrated Ocean Drilling Program Expedition 307". In: *Geology* 35.11, pp. 1051–1054. DOI: 10.1130/G23917A.1.

Mienis, F., de Stigter, H. C., White, M., Duineveld, G., de Haas, H., and van Weering, T. C. E. (2007). "Hydrodynamic Controls on Cold-Water Coral Growth and Carbonate-Mound Development at the SW and SE Rockall Trough Margin, NE Atlantic Ocean". In: *Deep Sea Research Part I: Oceanographic Research Papers* 54.9, pp. 1655–1674. DOI: 10.1016/j.dsr.2007.05.013.

Paytan, A. and Griffith, E. M. (2007). "Marine Barite: Recorder of Variations in Ocean Export Productivity". In: *Deep Sea Research Part II: Topical Studies in Oceanography* 54 (5-7), pp. 687–705. DOI: 10.1016/j.dsr2.2007.01.007.

Robinson, L. F., Adkins, J. F., Scheirer, D. S., Fernandez, D. P., Gagnon, A., and Waller, R. G. (2007). "Deep-Sea Scleractinian Coral Age and Depth Distributions in the Northwest Atlantic for the Last 225,000 Years". In: *Bulletin of Marine Science* 81.3, pp. 371–391.

Rüggeberg, A., Dullo, C., Dorschel, B., and Hebbeln, D. (2007). "Environmental Changes and Growth History of a Cold-Water Carbonate Mound (Propeller Mound, Porcupine Seabight)". In: *International Journal of Earth Sciences* 96.1, pp. 57–72. DOI: 10.1007/s00531-005-0504-1.

SCOR Working Group, . (2007). "GEOTRACES – An International Study of the Global Marine Biogeochemical Cycles of Trace Elements and Their Isotopes". In: *Chemie der Erde - Geochemistry* 67.2, pp. 85–131. DOI: 10.1016/j.chemer.2007.02.001.

Synal, H.-A., Stocker, M., and Suter, M. (2007). "MICADAS: A New Compact Radiocarbon AMS System". In: *Nuclear Instruments and Methods in Physics Research Section B: Beam Interactions with Materials and Atoms*. Accelerator Mass Spectrometry 259.1, pp. 7–13. DOI: 10.1016/j.nimb.2007.01.138.

Wheeler, A. J., Beyer, A., Freiwald, A., Haas, H. de, Huvenne, V. a. I., Kozachenko, M., Roy, K. O.-L., and Opderbecke, J. (2007). "Morphology and Environment of Cold-Water Coral Carbonate Mounds on the NW European Margin". In: *International Journal of Earth Sciences* 96.1, pp. 37–56. DOI: 10.1007/s00531-006-0130-6.

White, M. (2007). "Benthic Dynamics at the Carbonate Mound Regions of the Porcupine Sea Bight Continental Margin". In: *International Journal of Earth Sciences* 96.1, p. 1. DOI: 10.1007/s00531-006-0099-1.

Böhm, F., Gussone, N., Eisenhauer, A., Dullo, W.-C., Reynaud, S., and Paytan, A. (2006). "Calcium Isotope Fractionation in Modern Scleractinian Corals". In: *Geochimica et Cosmochimica Acta* 70.17, pp. 4452–4462. DOI: 10.1016/j.gca.2006.06.1546.

Cacho, I., Shackleton, N., Elderfield, H., Sierro, F. J., and Grimalt, J. O. (2006). "Glacial Rapid Variability in Deep-Water Temperature and δ18O from the Western Mediterranean Sea". In:

Quaternary Science Reviews. Critical Quaternary Stratigraphy 25.23, pp. 3294–3311. DOI: 10.1016/j.quascirev.2006.10.004.

Cohen, A. L., Gaetani, G. A., Lundälv, T., Corliss, B. H., and George, R. Y. (2006). "Compositional Variability in a Cold-Water Scleractinian, Lophelia Pertusa: New Insights into "Vital Effects"". In: *Geochemistry, Geophysics, Geosystems* 7.12, Q12004. DOI: 10.1029/2006GC001354.

Criado-Aldeanueva, F., García-Lafuente, J., Vargas, J. M., Del Río, J., Vázquez, A., Reul, A., and Sánchez, A. (2006). "Distribution and Circulation of Water Masses in the Gulf of Cadiz from in Situ Observations". In: *Deep Sea Research Part II: Topical Studies in Oceanography*. The Gulf of Cadiz Oceanography: A Multidisciplinary View 53.11, pp. 1144–1160. DOI: 10.1016/j.dsr2.2006.04.012.

Eltgroth, S. F., Adkins, J. F., Robinson, L. F., Southon, J., and Kashgarian, M. (2006). "A Deep-Sea Coral Record of North Atlantic Radiocarbon through the Younger Dryas: Evidence for Intermediate Water/Deepwater Reorganization". In: *Paleoceanography* 21.4, PA4207. DOI: 10.1029/2005PA001192.

Fietzke, J. and Eisenhauer, A. (2006). "Determination of Temperature-Dependent Stable Strontium Isotope (^{88} Sr/ ^{86} Sr) Fractionation via Bracketing Standard MC-ICP-MS: SR ISOTOPE FRACTIONATION". In: *Geochemistry, Geophysics, Geosystems* 7.8, n/a–n/a. DOI: 10.1029/2006GC001243.

Gass, S. E. and Roberts, J. M. (2006). "The Occurrence of the Cold-Water Coral Lophelia Pertusa (Scleractinia) on Oil and Gas Platforms in the North Sea: Colony Growth, Recruitment and Environmental Controls on Distribution". In: *Marine Pollution Bulletin* 52.5, pp. 549–559. DOI: 10.1016/j.marpolbul.2005.10.002.

Ghosh, P., Adkins, J., Affek, H., Balta, B., Guo, W., Schauble, E. A., Schrag, D., and Eiler, J. M. (2006). "13C–18O Bonds in Carbonate Minerals: A New Kind of Paleothermometer". In: *Geochimica et Cosmochimica Acta* 70.6, pp. 1439–1456. DOI: 10.1016/j.gca.2005.11.014.

Hernández-Molina, F., Llave, E., Stow, D., García, M., Somoza, L., Vázquez, J., Lobo, F., Maestro, A., Díaz del Río, V., León, R., Medialdea, T., and Gardner, J. (2006). "The Contourite Depositional System of the Gulf of Cádiz: A Sedimentary Model Related to the Bottom Current Activity of the Mediterranean Outflow Water and Its Interaction with the Continental Margin". In: *Deep Sea Research Part II: Topical Studies in Oceanography* 53 (11-13), pp. 1420–1463. DOI: 10.1016/j.dsr2.2006.04.016.

Montagna, P., McCulloch, M., Taviani, M., Mazzoli, C., and Vendrell, B. (2006). "Phosphorus in Cold-Water Corals as a Proxy for Seawater Nutrient Chemistry". In: *Science* 312.5781, pp. 1788–1791. DOI: 10.1126/science.1125781. pmid: 16794077.

Rahmstorf, S. (2006). *Thermohaline Ocean Circulation*. In: *Encyclopedia of Quaternary Sciences*. Ed. by S. Elias. 2nd ed. Amsterdam: Elsevier.

Roberts, J. M. (2006). "Reefs of the Deep: The Biology and Geology of Cold-Water Coral Ecosystems". In: *Science* 312.5773, pp. 543–547. DOI: 10.1126/science.1119861.

Robinson, L. F., Adkins, J. F., Fernandez, D. P., Burnett, D. S., Wang, S.-L., Gagnon, A. C., and Krakauer, N. (2006). "Primary U Distribution in Scleractinian Corals and Its Implications for U Series Dating". In: *Geochemistry, Geophysics, Geosystems* 7.5, Q05022. DOI: 10.1029/2005GC001138.

Sinclair, D. J., Williams, B., and Risk, M. (2006). "A Biological Origin for Climate Signals in Corals—Trace Element "Vital Effects" Are Ubiquitous in Scleractinian Coral Skeletons". In: *Geophysical Research Letters* 33.17. DOI: 10.1029/2006GL027183.

Van de Flierdt, T., Robinson, L. F., Adkins, J. F., Hemming, S. R., and Goldstein, S. L. (2006). "Temporal Stability of the Neodymium Isotope Signature of the Holocene to Glacial North Atlantic: Nd ISOTOPES IN ATLANTIC DEEP-SEA CORALS". In: *Paleoceanography* 21.4, n/a–n/a. DOI: 10.1029/2006PA001294.

Voelker, A. H. L., Lebreiro, S. M., Schönfeld, J., Cacho, I., Erlenkeuser, H., and Abrantes, F. (2006). "Mediterranean Outflow Strengthening during Northern Hemisphere Coolings: A Salt Source for the Glacial Atlantic?" In: *Earth and Planetary Science Letters* 245 (1–2), pp. 39–55. DOI: 10.1016/j.epsl.2006.03.014.

Colman, J. G., Gordon, D. M., Lane, A. P., Forde, M. J., and Fitzpatrick, J. J. (2005). "Carbonate Mounds off Mauritania, Northwest Africa: Status of Deep-Water Corals and Implications for Management of Fishing and Oil Exploration Activities". In: *Cold-Water Corals and Ecosystems*. Erlangen Earth Conference Series. Springer, Berlin, Heidelberg, pp. 417–441. DOI: 10.1007/3-540-27673-4_21.

Dorschel, B., Hebbeln, D., Ruggeberg, A., Dullo, W., and Freiwald, A. (2005). "Growth and Erosion of a Cold-Water Coral Covered Carbonate Mound in the Northeast Atlantic during the Late Pleistocene and Holocene". In: *Earth and Planetary Science Letters* 233 (1-2), pp. 33–44. DOI: 10.1016/j.epsl.2005.01.035.

Foss, J. H., Lindberg, B., Christensen, O., Lundälv, T., Svellingen, I., Mortensen, P. B., and Alvsvg, J. (2005). "Mapping of Lophelia Reefs in Norway: Experiences and Survey Methods". In: *Cold-Water Corals and Ecosystems*. Erlangen Earth Conference Series. Springer, Berlin, Heidelberg, pp. 359–391. DOI: 10.1007/3-540-27673-4_18.

Lacan, F. and Jeandel, C. (2005a). "Acquisition of the Neodymium Isotopic Composition of the North Atlantic Deep Water". In: *Geochemistry, Geophysics, Geosystems* 6.12, Q12008. DOI: 10.1029/2005GC000956.

— (2005b). "Neodymium Isotopes as a New Tool for Quantifying Exchange Fluxes at the Continent–ocean Interface". In: *Earth and Planetary Science Letters* 232 (3-4), pp. 245–257. DOI: 10.1016/j.epsl.2005.01.004.

Potter, E.-K., Stirling, C. H., Wiechert, U. H., Halliday, A. N., and Spötl, C. (2005). "Uranium-Series Dating of Corals in Situ Using Laser-Ablation MC-ICPMS". In: *International Journal of Mass Spectrometry* 240.1, pp. 27–35. DOI: 10.1016/j.ijms.2004.10.007.

Robinson, L. F., Adkins, J. F., Keigwin, L. D., Southon, J., Fernandez, D. P., Wang, S. L., and Scheirer, D. S. (2005). "Radiocarbon Variability in the Western North Atlantic during the Last Deglaciation". In: *Science* 310.5753, pp. 1469–1473.

Rogerson, M., Rohling, E. J., Weaver, P. P. E., and Murray, J. W. (2005). "Glacial to Interglacial Changes in the Settling Depth of the Mediterranean Outflow Plume: CHANGES IN THE MEDITERRANEAN OUTFLOW". In: *Paleoceanography* 20.3, n/a–n/a. DOI: 10.1029/2004PA001106.

White, M., Mohn, C., Stigter, H. de, and Mottram, G. (2005). "Deep-Water Coral Development as a Function of Hydrodynamics and Surface Productivity around the Submarine Banks of the Rockall Trough, NE Atlantic". In: *Cold-Water Corals and Ecosystems*. Erlangen Earth Conference Series. Springer, Berlin, Heidelberg, pp. 503–514. DOI: 10.1007/3-540-27673-4_25.

Adkins, J., Henderson, G., Wang, S.-L., O'Shea, S., and Mokadem, F. (2004). "Growth Rates of the Deep-Sea Scleractinia Desmophyllum Cristagalli and Enallopsammia Rostrata". In: *Earth and Planetary Science Letters* 227 (3-4), pp. 481–490. DOI: 10.1016/j.epsl.2004.08.022.

Andersen, K. K., Azuma, N., Barnola, J.-M., Bigler, M., Biscaye, P., Caillon, N., Chappellaz, J., Clausen, H. B., Dahl-Jensen, D., Fischer, H., Flückiger, J., Fritzsche, D., Fujii, Y., Goto-Azuma, K., Grønvold, K., Gundestrup, N. S., Hansson, M., Huber, C., Hvidberg, C. S., Johnsen, S. J., Jonsell, U., Jouzel, J., Kipfstuhl, S., Landais, A., Leuenberger, M., Lorrain, R., Masson-Delmotte, V., Miller, H., Motoyama, H., Narita, H., Popp, T., Rasmussen, S. O., Raynaud, D., Rothlisberger, R., Ruth, U., Samyn, D., Schwander, J., Shoji, H., Siggard-Andersen, M.-L., Steffensen, J. P., Stocker, T., Sveinbjörnsdóttir, A. E., Svensson, A., Takata, M., Tison, J.-L., Thorsteinsson, T., Watanabe, O., Wilhelms, F., and White, J. W. C. (2004). "High-Resolution Record of Northern Hemisphere Climate Extending into the Last Interglacial Period". In: *Nature* 431.7005, pp. 147–151. DOI: 10.1038/nature02805.

Bayon, G., German, C. R., Burton, K. W., Nesbitt, R. W., and Rogers, N. (2004). "Sedimentary Fe–Mn Oxyhydroxides as Paleoceanographic Archives and the Role of Aeolian Flux in Regulating Oceanic Dissolved REE". In: *Earth and Planetary Science Letters* 224.3, pp. 477–492. DOI: 10.1016/j.epsl.2004.05.033.

Currie, L. A. (2004). "The Remarkable Metrological History of Radiocarbon Dating [II]". In: *Journal of Research of the National Institute of Standards and Technology* 109.2, pp. 185–217. DOI: 10.6028/jres.109.013. pmid: 27366605.

DePaolo, D. J. (2004). "Calcium Isotopic Variations Produced by Biological, Kinetic, Radiogenic and Nucleosynthetic Processes". In: *Chapter in REVIEWS in MINERALOGY and GEOCHEMISTRY* 55, pp. 255–288.

Feely, R. A., Sabine, C. L., Lee, K., Berelson, W., Kleypas, J., Fabry, V. J., and Millero, F. J. (2004). "Impact of Anthropogenic CO2 on the CaCO3 System in the Oceans". In: *Science* 305.5682, pp. 362–366. DOI: 10.1126/science.1097329. pmid: 15256664.

Foster, D. A., Staubwasser, M., and Henderson, G. M. (2004). "226Ra and Ba Concentrations in the Ross Sea Measured with Multicollector ICP Mass Spectrometry". In: *Marine Chemistry* 87 (1–2), pp. 59–71. DOI: 10.1016/j.marchem.2004.02.003.

Frank, N., Paterne, M., Ayliffe, L., van Weering, T., Henriet, J.-P., and Blamart, D. (2004). "Eastern North Atlantic Deep-Sea Corals: Tracing Upper Intermediate Water Δ14C during the Holocene". In: *Earth and Planetary Science Letters* 219 (3-4), pp. 297–309. DOI: 10.1016/S0012-821X(03)00721-0.

Freiwald, A., Fossa, J. H., Grehan, A., Koslow, T., and Roberts, J. M. (2004). "Cold Water Coral Reefs: Out of Sight-No Longer out of Mind". In:

Hemming, S. R. (2004). "Heinrich Events: Massive Late Pleistocene Detritus Layers of the North Atlantic and Their Global Climate Imprint". In: *Reviews of Geophysics* 42.1. DOI: 10.1029/2003RG000128.

Marriott, C. S., Henderson, G. M., Belshaw, N. S., and Tudhope, A. W. (2004). "Temperature Dependence of δ7Li, δ44Ca and Li/Ca during Growth of Calcium Carbonate". In: *Earth and Planetary Science Letters* 222.2, pp. 615–624. DOI: 10.1016/j.epsl.2004.02.031.

Martin, E. E. and Scher, H. D. (2004). "Preservation of Seawater Sr and Nd Isotopes in Fossil Fish Teeth: Bad News and Good News". In: *Earth and Planetary Science Letters* 220 (1–2), pp. 25–39. DOI: 10.1016/S0012-821X(04)00030-5.

McManus, J. F., Francois, R., Gherardi, J.-M., Keigwin, L. D., and Brown-Leger, S. (2004). "Collapse and Rapid Resumption of Atlantic Meridional Circulation Linked to Deglacial Climate Changes". In: *Nature* 428.6985, pp. 834–837. DOI: 10.1038/nature02494.

Piotrowski, A. M., Goldstein, S. L., Hemming, S. R., and Fairbanks, R. G. (2004). "Intensification and Variability of Ocean Thermohaline Circulation through the Last Deglaciation". In: *Earth and Planetary Science Letters* 225 (1-2), pp. 205–220. DOI: 10.1016/j.epsl.2004.06.002.

Robinson, L. F., Henderson, G. M., Hall, L., and Matthews, I. (2004). "Climatic Control of Riverine and Seawater Uranium-Isotope Ratios". In: *Science* 305.5685, pp. 851–854. DOI: 10.1126/science.1099673. pmid: 15297670.

Rogerson, M., Rohling, E. J., Weaver, P. P. E., and Murray, J. W. (2004). "The Azores Front since the Last Glacial Maximum". In: *Earth and Planetary Science Letters* 222.3, pp. 779–789. DOI: 10.1016/j.epsl.2004.03.039.

Tachikawa, K., Roy-Barman, M., Michard, A., Thouron, D., Yeghicheyan, D., and Jeandel, C. (2004). "Neodymium Isotopes in the Mediterranean Sea: Comparison between Seawater and Sediment Signals1 1Associate Editor: S. J. G. Galer". In: *Geochimica et Cosmochimica Acta* 68.14, pp. 3095–3106. DOI: 10.1016/j.gca.2004.01.024.

Turon, J.-L., Mellet, M., Sultan, N., and Blamart, D. (2004). *Cruise Report MD140 Privilege, Gulf of Cadiz, IPEV, May-June 2004*. Cruise Report, p. 151.

Vance, D., Scrivner, A. E., Beney, P., Staubwasser, M., Henderson, G. M., and Slowey, N. C. (2004). "The Use of Foraminifera as a Record of the Past Neodymium Isotope Composition of Seawater". In: *Paleoceanography* 19.2, PA2009. DOI: 10.1029/2003PA000957.

Adkins, J. F., Boyle, E. A., Curry, W. B., and Lutringer, A. (2003). "Stable Isotopes in Deep-Sea Corals and a New Mechanism for "Vital Effects"". In: *Geochimica et Cosmochimica Acta* 67.6, pp. 1129–1143.

Edwards, R. L., Gallup, C. D., and Cheng, H. (2003). "Uranium-Series Dating of Marine and Lacustrine Carbonates". In: *Reviews in Mineralogy and Geochemistry* 52.1, pp. 363–405. DOI: 10.2113/0520363.

Goldstein, S. and Hemming, S. R. (2003). *Long-Lived Isotopic Tracers in Oceanography Paleoceanography, and Ice-Sheet Dynamics*. In: *Treatise on Geochemistry*. Ed. by H. Elderfield. Vol. 6. New York: Elsevier, pp. 453–489.

Pérez-Folgado, M., Sierro, F. J., Flores, J. A., Cacho, I., Grimalt, J. O., Zahn, R., and Shackleton, N. (2003). "Western Mediterranean Planktonic Foraminifera Events and Millennial Climatic Variability during the Last 70 Kyr". In: *Marine Micropaleontology* 48 (1–2), pp. 49–70. DOI: 10.1016/S0377-8398(02)00160-3.

Rahmstorf, S. (2003). "Timing of Abrupt Climate Change: A Precise Clock: TIMING OF ABRUPT CLIMATE CHANGE". In: *Geophysical Research Letters* 30.10, n/a–n/a. DOI: 10.1029/2003GL017115.

Sarnthein, M., Van Kreveld, S., Erlenkeuser, H., Grootes, P. M., Kucera, M., Pflaumann, U., and Schulz, M. (2003). "Centennial-to-Millennial-Scale Periodicities of Holocene Climate and Sediment Injections off the Western Barents Shelf, 75°N". In: *Boreas* 32.3, pp. 447–461. DOI: 10.1111/j.1502-3885.2003.tb01227.x.

Schröder-Ritzrau, A., Mangini, A., and Lomitschka, M. (2003). "Deep-Sea Corals Evidence Periodic Reduced Ventilation in the North Atlantic during the LGM/Holocene Transition". In: *Earth and Planetary Science Letters* 216.3, pp. 399–410. DOI: 10.1016/S0012-821X(03)00511-9.

Stocker, T. F. and Johnsen, S. J. (2003). "A Minimum Thermodynamic Model for the Bipolar Seesaw". In: *Paleoceanography* 18.4, p. 1087. DOI: 10.1029/2003PA000920.

Tachikawa, K. (2003). "Neodymium Budget in the Modern Ocean and Paleo-Oceanographic Implications". In: *Journal of Geophysical Research* 108 (C8). DOI: 10.1029/1999JC000285.

Adkins, J. F., Griffin, S., Kashgarian, M., Cheng, H., Druffel, E. R. M., Boyle, E. A., Edwards, R. L., and Shen, C.-C. (2002). "Radiocarbon Dating of Deep-Sea Corals". In: *Radiocarbon* 44.2, pp. 567–580.

Bower, A. S., Le Cann, B., Rossby, T., Zenk, W., Gould, J., Speer, K., Richardson, P. L., Prater, M. D., and Zhang, H.-M. (2002). "Directly Measured Mid-Depth Circulation in the Northeastern North Atlantic Ocean". In: *Nature* 419.6907, pp. 603–607. DOI: 10.1038/nature01078.

Cabeçadas, G., José Brogueira, M., and Gonçalves, C. (2002). "The Chemistry of Mediterranean Outflow and Its Interactions with Surrounding Waters". In: *Deep Sea Research Part II: Topical Studies in Oceanography*. Canary Islands, Azores, Gibraltar Observations (Canigo) Volume II : Studies of the Azores and Gibraltar regions 49.19, pp. 4263–4270. DOI: 10.1016/S0967-0645(02)00154-6.

De Mol, B., Van Rensbergen, P., Pillen, S., Van Herreweghe, K., Van Rooij, D., McDonnell, A., Huvenne, V., Ivanov, M., Swennen, R., and Henriet, J. P. (2002). "Large Deep-Water Coral Banks in the Porcupine Basin, Southwest of Ireland". In: *Marine Geology* 188.1, pp. 193–231. DOI: 10.1016/S0025-3227(02)00281-5.

Frank, M. (2002). "Radiogenic Isotopes: Tracers of Past Ocean Circulation and Erosional Input". In: *Reviews of Geophysics* 40.1. DOI: 10.1029/2000RG000094.

Henderson, G. M. (2002). "New Oceanic Proxies for Paleoclimate". In: *Earth and Planetary Science Letters* 203.1, pp. 1–13.

Risk, M. J., Heikoop, J. M., Snow, M. G., and Beukens, R. (2002). "Lifespans and Growth Patterns of Two Deep-Sea Corals: Primnoa Resedaeformis and Desmophyllum Cristagalli". In: *Hydrobiologia* 471 (1-3), pp. 125–131. DOI: 10.1023/A:1016557405185.

Schiebel, R., Waniek, J., Zeltner, A., and Alves, M. (2002). "Impact of the Azores Front on the Distribution of Planktic Foraminifers, Shelled Gastropods, and Coccolithophorids". In: *Deep Sea Research Part II: Topical Studies in Oceanography*. Canary Islands, Azores, Gibraltar Observations (Canigo) Volume II : Studies of the Azores and Gibraltar regions 49.19, pp. 4035–4050. DOI: 10.1016/S0967-0645(02)00141-8.

Smith, J. E., Schwarcz, H. P., and Risk, M. J. (2002). "Patterns of Isotopic Disequilibria in Azooxanthellate Coral Skeletons". In: *Hydrobiologia* 471 (1-3), pp. 111–115. DOI: 10.1023/A:1016553304276.

Waelbroeck, C., Labeyrie, L., Michel, E., Duplessy, J. C., McManus, J. F., Lambeck, K., Balbon, E., and Labracherie, M. (2002). "Sea-Level and Deep Water Temperature Changes Derived from Benthic Foraminifera Isotopic Records". In: *Quaternary Science Reviews* 21.1, pp. 295–305.

Goldstein, S. J., Lea, D. W., Chakraborty, S., Kashgarian, M., and Murrell, M. T. (2001). "Uranium-Series and Radiocarbon Geochronology of Deep-Sea Corals: Implications for Southern Ocean Ventilation Rates and the Oceanic Carbon Cycle". In: *Earth and Planetary Science Letters* 193.1, pp. 167–182. DOI: 10.1016/S0012-821X(01)00494-0.

Mortensen, P. B., Hovland, T., Foss, J. H., and Furevik, D. M. (2001). "Distribution, Abundance and Size of Lophelia Pertusa Coral Reefs in Mid-Norway in Relation to Seabed Characteristics". In: *Journal of the Marine Biological Association of the UK* 81 (04), pp. 581–597. DOI: 10.1017/S002531540100426X.

Mortensen, P. B. (2001). "Aquarium Observations on the Deep-Water Coral Lophelia Pertusa (L., 1758) (Scleractinia) and Selected Associated Invertebrates". In: *Ophelia*. DOI: 10.1080/00785236.2001.10409457.

Roemmich, D., Boebel, O., Desaubies, Y., Freeland, H., Kim, K., King, B., Le Traon, P.-Y., Molinari, R., Owens, B. W., Riser, S., Send, U., Takeuchi, K., and Wijffels, S. (2001). "Argo: The Global Array of Profiling Floats". In:

Waelbroeck, C., Duplessy, J.-C., Michel, E., Labeyrie, L., Paillard, D., and Duprat, J. (2001). "The Timing of the Last Deglaciation in North Atlantic Climate Records". In: *Nature* 412.6848, pp. 724–727. DOI: 10.1038/35089060.

Cheng, H., Adkins, J., Edwards, R. L., and Boyle, E. A. (2000). "U-Th Dating of Deep-Sea Corals". In: *Geochimica et Cosmochimica Acta* 64.14, pp. 2401–2416. DOI: 10.1016/S0016-7037(99)00422-6.

Lear, C. H., Elderfield, H., and Wilson, P. A. (2000). "Cenozoic Deep-Sea Temperatures and Global Ice Volumes from Mg/Ca in Benthic Foraminiferal Calcite". In: *Science* 287.5451, pp. 269–272. DOI: 10.1126/science.287.5451.269. pmid: 10634774.

Rutberg, R. L., Hemming, S. R., and Goldstein, S. L. (2000). "Reduced North Atlantic Deep Water Flux to the Glacial Southern Ocean Inferred from Neodymium Isotope Ratios". In: *Nature* 405.6789, pp. 935–938. DOI: 10.1038/35016049.

Tanaka, T., Togashi, S., Kamioka, H., Amakawa, H., Kagami, H., Hamamoto, T., Yuhara, M., Orihashi, Y., Yoneda, S., Shimizu, H., Kunimaru, T., Takahashi, K., Yanagi, T., Nakano, T., Fujimaki, H., Shinjo, R., Asahara, Y., Tanimizu, M., and Dragusanu, C. (2000). "JNdi-1: A Neodymium Isotopic Reference in Consistency with LaJolla Neodymium". In: *Chemical Geology* 168.3, pp. 279–281. DOI: 10.1016/S0009-2541(00)00198-4.

Blanckenburg, F. von (1999). "Tracing Past Ocean Circulation?" In: *Science* 286.5446, pp. 1862–1863. DOI: 10.1126/science.286.5446.1862b.

Frank, M., Gersonde, R., and Mangini, A. (1999). "Sediment Redistribution, 230Thex- Normalization and Implications for the Reconstruction of Particle Flux and Export Paleoproductivity". In: *Use of Proxies in Paleoceanography*. Springer, Berlin, Heidelberg, pp. 409–426. DOI: 10.1007/978-3-642-58646-0_16.

Lomitschka, M. and Mangini, A. (1999). "Precise Th/U-Dating of Small and Heavily Coated Samples of Deep Sea Corals". In: *Earth and Planetary Science Letters* 170.4, pp. 391–401. DOI: 10.1016/S0012-821X(99)00117-X.

Monnin, C., Jeandel, C., Cattaldo, T., and Dehairs, F. (1999). "The Marine Barite Saturation State of the World's Oceans". In: *Marine Chemistry* 65 (3–4), pp. 253–261. DOI: 10.1016/S0304-4203(99)00016-X.

Stoll, H. M., Schrag, D. P., and Clemens, S. C. (1999). "Are Seawater Sr/Ca Variations Preserved in Quaternary Foraminifera?" In: *Geochimica et Cosmochimica Acta* 63.21, pp. 3535–3547. DOI: 10.1016/S0016-7037(99)00129-5.

Stosch, H.-G. (1999). *Einführung in Die Isotopenchemie*.

Vance, D. and Burton, K. (1999). "Neodymium Isotopes in Planktonic Foraminifera: A Record of the Response of Continental Weathering and Ocean Circulation Rates to Climate Change". In: *Earth and Planetary Science Letters* 173.4, pp. 365–379. DOI: 10.1016/S0012-821X(99)00244-7.

Wefer, G., Berger, W. H., Bijma, J., and Fischer, G. (1999). "Clues to Ocean History: A Brief Overview of Proxies". In: *Use of Proxies in Paleoceanography*. Springer, Berlin, Heidelberg, pp. 1–68. DOI: 10.1007/978-3-642-58646-0_1.

Adkins, J. F., Cheng, H., Boyle, E. A., Druffel, E. R., and Edwards, R. L. (1998). "Deep-Sea Coral Evidence for Rapid Change in Ventilation of the Deep North Atlantic 15,400 Years Ago". In: *Science* 280.5364, pp. 725–728.

Gagan, M. K., Ayliffe, L. K., Hopley, D., Cali, J. A., Mortimer, G. E., Chappell, J., McCulloch, M. T., and Head, M. J. (1998). "Temperature and Surface-Ocean Water Balance of the Mid-Holocene Tropical Western Pacific". In: *Science* 279.5353, pp. 1014–1018. DOI: 10.1126/science.279.5353.1014. pmid: 9461430.

Mangini, A., Lomitschka, M., Eichstädter, R., Frank, N., Vogler, S., Bonani, G., Hajdas, I., and Patzold, J. (1998). "Coral Provides Way to Age Deep Water". In: *Nature* 392.6674, pp. 347–348. DOI: 10.1038/32804.

Mortensen, P. B., Rapp, H. T., and Bmstedt, U. (1998). "Oxygen and Carbon Isotope Ratios Related to Growth Line Patterns in Skeletons of Lophelia Pertusa (L) (Anthozoa, Scleractinia): Implications for Determination of Linear Extension Rate". In: *Sarsia* 83.5, pp. 433–446. DOI: 10.1080/00364827.1998.10413702.

Adkins, J. F. and Boyle, E. A. (1997). "Changing Atmospheric Δ14C and the Record of Deep Water Paleoventilation Ages". In: *Paleoceanography* 12.3, pp. 337–344. DOI: 10.1029/97PA00379.

Schiller, A., Mikolajewicz, U., and Voss, R. (1997). "The Stability of the North Atlantic Thermohaline Circulation in a Coupled Ocean-Atmosphere General Circulation Model". In: *Climate Dynamics* 13.5, pp. 325–347. DOI: 10.1007/s003820050169.

Mitsuguchi, T., Matsumoto, E., Abe, O., Uchida, T., Isdale, P. J., et al. (1996). "Mg/Ca Thermometry in Coral Skeletons". In: *Science* 274.5289, pp. 961–963. JSTOR: pdf/2891294.pdf.

Paillard, D., Labeyrie, L., and Yiou, P. (1996). "Macintosh Program Performs Time-Series Analysis". In: *Eos, Transactions American Geophysical Union* 77.39, pp. 379–379. DOI: 10.1029/96EO00259.

Pollard, R. T., Griffttths, M. J., Cunningham, S. A., Read, J. F., Pérez, F. F., and Ríos, A. F. (1996). "Vivaldi 1991 - A Study of the Formation, Circulation and Ventilation of Eastern North Atlantic Central Water". In: *Progress in Oceanography* 37.2, pp. 167–192. DOI: 10.1016/S0079-6611(96)00008-0.

Manighetti, B., McCave, I. N., Maslin, M., and Shackleton, N. J. (1995). "Chronology for Climate Change: Developing Age Models for the Biogeochemical Ocean Flux Study Cores". In: *Paleoceanography* 10.3, pp. 513–525.

Min, G. R., Edwards, R. L., Taylor, F. W., Recy, J., Gallup, C. D., and Beck, J. W. (1995). "Annual Cycles of UCa in Coral Skeletons and UCa Thermometry". In: *Geochimica et Cosmochimica Acta* 59.10, pp. 2025–2042.

Rosenthal, Y., Lam, P., Boyle, E. A., and Thomson, J. (1995). "Authigenic Cadmium Enrichments in Suboxic Sediments: Precipitation and Postdepositional Mobility". In: *Earth and Planetary Science Letters* 132.1, pp. 99–111. DOI: 10.1016/0012-821X(95)00056-I.

Shen, G. T. and Dunbar, R. B. (1995). "Environmental Controls on Uranium in Reef Corals". In: *Geochimica et Cosmochimica Acta* 59.10, pp. 2009–2024.

Ivanovich, M. (1994). *Uranium Series Disequilibrium: Concepts and Applications : Radiochimica Acta*. URL: https://www.degruyter.com/view/j/ract.1994.64.issue-2/ract.1994.64.2.81/ract.1994.64.2.81.xml (visited on 08/07/2017).

Dansgaard, W., Johnsen, S. J., Clausen, H. B., Dahl-Jensen, D., Gundestrup, N. S., Hammer, C. U., Hvidberg, C. S., Steffensen, J. P., Sveinbjörnsdottir, A. E., Jouzel, J., and Bond, G.

(1993). “Evidence for General Instability of Past Climate from a 250-Kyr Ice-Core Record”. In: *Nature* 364.6434, pp. 218–220. DOI: 10.1038/364218a0.

Henderson, G. M., Cohen, A. S., and O’Nions, R. K. (1993). “234U/238U Ratios and230Th Ages for Hateruma Atoll Corals: Implications for Coral Diagenesis and seawater234U/238U Ratios”. In: *Earth and Planetary Science Letters* 115.1, pp. 65–73. DOI: 10.1016/0012-821X(93)90213-S.

Jeandel, C. (1993). “Concentration and Isotopic Composition of Nd in the South Atlantic Ocean”. In: *Earth and Planetary Science Letters* 117.3, pp. 581–591. DOI: 10.1016/0012-821X(93)90104-H.

Lea, D. W. and Boyle, E. A. (1993). “Determination of Carbonate-Bound Barium in Foraminifera and Corals by Isotope Dilution Plasma-Mass Spectrometry”. In: *Chemical Geology* 103.1, pp. 73–84. DOI: 10.1016/0009-2541(93)90292-Q.

Rhein, M. and Hinrichsen, H. H. (1993). “Modification of Mediterranean Water in the Gulf of Cadiz, Studied with Hydrographic, Nutrient and Chlorofluoromethane Data”. In: *Deep Sea Research Part I: Oceanographic Research Papers* 40.2, pp. 267–291. DOI: 10.1016/0967-0637(93)90004-M.

Beck, J. W., Edwards, R. L., Ito, E., Taylor, F. W., Recy, J., Rougerie, F., Joannot, P., and Henin, C. (1992). “Sea-Surface Temperature from Coral Skeletal Strontium Calcium Ratios”. In: *Science* 257.5070, pp. 644–647.

Johnsen, S. J., Clausen, H. B., Dansgaard, W., Fuhrer, K., Gundestrup, N., Hammer, C. U., Iversen, P., Jouzel, J., Stauffer, B., and Steffensen, J. P. (1992). “Irregular Glacial Interstadials Recorded in a New Greenland Ice Core”. In: *Nature* 359.6393, pp. 311–313. DOI: 10.1038/359311a0.

Stocker, T. F., Mysak, L. A., and Wright, D. G. (1992). “A Zonally Averaged, Coupled Ocean-Atmosphere Model for Paleoclimate Studies”. In: *Journal of Climate* 5.8, pp. 773–797. DOI: 10.1175/1520-0442(1992)005<0773:AZACOA>2.0.CO;2.

Broecker, W. S. (1991). “The Great Ocean Conveyor”. In: *Oceanography* 4.2, pp. 79–89. JSTOR: 43924572.

Broecker, W. S., Klas, M., Clark, E., Trumbore, S., Bonani, G., Wölfli, W., and Ivy, S. (1990a). “Accelerator Mass Spectrometric Radiocarbon Measurements on Foraminifera Shells from Deep-Sea Cores”. In: *Radiocarbon* 32.2, pp. 119–133. DOI: 10.1017/S003382220004011X.

Broecker, W. S., Peng, T.-H., Trumbore, S., Bonani, G., and Wolfli, W. (1990b). “The Distribution of Radiocarbon in the Glacial Ocean”. In: *Global Biogeochemical Cycles* 4.1, pp. 103–117. DOI: 10.1029/GB004i001p00103.

Lea, D. W. and Boyle, E. A. (1990). “Foraminiferal Reconstruction of Barium Distributions in Water Masses of the Glacial Oceans”. In: *Paleoceanography* 5.5, pp. 719–742. DOI: 10.1029/PA005i005p00719.

Altabet, M. A. and Curry, W. B. (1989). “Testing Models of Past Ocean Chemistry Using Foraminifera 15N/14N”. In: *Global Biogeochemical Cycles* 3.2, pp. 107–119. DOI: 10.1029/GB003i002p00107.

Dansgaard, W., White, J. W. C., and Johnsen, S. J. (1989). “The Abrupt Termination of the Younger Dryas Climate Event”. In: *Nature* 339.6225, pp. 532–534.

Keigwin, L. D. and Boyle, E. A. (1989). “Late Quaternary Paleochemistry of High-Latitude Surface Waters”. In: *Palaeogeography, Palaeoclimatology, Palaeoecology* 73.1, pp. 85–106. DOI: 10.1016/0031-0182(89)90047-3.

Lea, D. W., Shen, G. T., and Boyle, E. A. (1989). "Coralline Barium Records Temporal Variability in Equatorial Pacific Upwelling". In: *Nature* 340.6232, pp. 373–376. DOI: 10.1038/340373a0.

Tsuchiya, M. (1989). "Circulation of the Antarctic Intermediate Water in the North Atlantic Ocean". In: *Journal of Marine Research* 47.4, pp. 747–755.

Bishop, J. K. B. (1988). "The Barite-Opal-Organic Carbon Association in Oceanic Particulate Matter". In: *Nature* 332.6162, pp. 341–343. DOI: 10.1038/332341a0.

Grousset, F. E., Biscaye, P. E., Zindler, A., Prospero, J., and Chester, R. (1988). "Neodymium Isotopes as Tracers in Marine Sediments and Aerosols: North Atlantic". In: *Earth and Planetary Science Letters* 87.4, pp. 367–378. DOI: 10.1016/0012-821X(88)90001-5.

Heinrich, H. (1988). "Origin and Consequences of Cyclic Ice Rafting in the Northeast Atlantic Ocean during the Past 130,000 Years". In: *Quaternary research* 29.2, pp. 142–152.

Martinson, D. G., Pisias, N. G., Hays, J. D., Imbrie, J., Moore, T. C., and Shackleton, N. J. (1987). "Age Dating and the Orbital Theory of the Ice Ages: Development of a High-Resolution 0 to 300,000-Year Chronostratigraphy". In: *Quaternary Research* 27.1, pp. 1–29. DOI: 10.1016/0033-5894(87)90046-9.

Piepgras, D. J. and Wasserburg, G. J. (1987). "Rare Earth Element Transport in the Western North Atlantic Inferred from Nd Isotopic Observations". In: *Geochimica et Cosmochimica Acta* 51.5, pp. 1257–1271. DOI: 10.1016/0016-7037(87)90217-1.

Emery, W. J. and Meincke, J. (1986). "Global Water Masses-Summary and Review". In: *Oceanologica acta* 9.4, pp. 383–391.

Genin, A., Dayton, P. K., Lonsdale, P. F., and Spiess, F. N. (1986). "Corals on Seamount Peaks Provide Evidence of Current Acceleration over Deep-Sea Topography". In: *Nature* 322, pp. 59–61.

Prell, W. L., Imbrie, J., Martinson, D. G., Morley, J. J., Pisias, N. G., Shackleton, N. J., and Streeter, H. F. (1986). "Graphic Correlation of Oxygen Isotope Stratigraphy Application to the Late Quaternary". In: *Paleoceanography* 1.2, pp. 137–162. DOI: 10.1029/PA001i002p00137.

Delaney, M. L., W.H.Bé, A., and Boyle, E. A. (1985). "Li, Sr, Mg, and Na in Foraminiferal Calcite Shells from Laboratory Culture, Sediment Traps, and Sediment Cores". In: *Geochimica et Cosmochimica Acta* 49.6, pp. 1327–1341. DOI: 10.1016/0016-7037(85)90284-4.

Falkowski, P. G., Dubinsky, Z., Muscatine, L., and Porter, J. W. (1984). "Light and the Bioenergetics of a Symbiotic Coral". In: *BioScience* 34.11, pp. 705–709. DOI: 10.2307/1309663.

Fiúza, A. F. G. (1984). "Hidrologia e Dinaˆmica Das A´ Guas Costeiras de Portugal (Hydrology and Dynamics of the Portuguese Coastal Waters)". Universidade de Lisboa. 294 pp.

Imbrie, J., Hays, J. D., Martinson, D. G., McIntyre, A., Mix, A. C., Morley, J. J., Pisias, N. G., Prell, W. L., and Shackleton, N. J. (1984). "The Orbital Theory of Pleistocene Climate: Support from a Revised Chronology of the Marine d18O Record". In:

Porter, J. W., Muscatine, L., Dubinsky, Z., and Falkowski, P. G. (1984). "Primary Production and Photoadaptation in Light- and Shade-Adapted Colonies of the Symbiotic Coral, Stylophora Pistillata". In: *Proceedings of the Royal Society of London B: Biological Sciences* 222.1227, pp. 161–180. DOI: 10.1098/rspb.1984.0057.

Shackleton, N. J., Backman, J., Zimmerman, H., Kent, D. V., Hall, M. A., Roberts, D. G., Schnitker, D., Baldauf, J. G., Desprairies, A., Homrighausen, R., Huddlestun, P., Keene, J. B., Kaltenback, A. J., Krumsiek, K. a. O., Morton, A. C., Murray, J. W., and Westberg-Smith, J. (1984). "Oxygen Isotope Calibration of the Onset of Ice-Rafting and History of

Glaciation in the North Atlantic Region". In: *Nature* 307.5952, pp. 620–623. DOI: 10.1038/307620a0.

Lugmair, G. W., Shimamura, T., Lewis, R. S., and Anders, E. (1983). "Samarium-146 in the Early Solar System: Evidence from Neodymium in the Allende Meteorite". In: *Science* 222.4627, pp. 1015–1018. DOI: 10.1126/science.222.4627.1015. pmid: 17776245.

Broecker, W. S. and Peng, T.-H. (1982). *Tracers in the Sea*. Lamont-Doherty Geological Observatory. 690 pp.

Friedman, I., O'Neil, J., and Cebula, G. (1982). "Two New Carbonate Stable-Isotope Standards". In: *Geostandards and Geoanalytical Research*.

McCartney, M. S. and Talley, L. D. (1982). "The Subpolar Mode Water of the North Atlantic Ocean". In: *Journal of Physical Oceanography* 12.11, pp. 1169–1188. DOI: 10.1175/1520-0485(1982)012<1169:TSMWOT>2.0.CO;2.

Goldstein, S. and O'nions, R. K. (1981). "Nd and Sr Isotopic Realtionships in Pleagic Clays and Ferromanganese Deposits". In: *Nature* 292, pp. 324–327.

Dehairs, F., Chesselet, R., and Jedwab, J. (1980). "Discrete Suspended Particles of Barite and the Barium Cycle in the Open Ocean". In: *Earth and Planetary Science Letters* 49.2, pp. 528–550. DOI: 10.1016/0012-821X(80)90094-1.

Jacobsen, S. B. and Wasserburg, G. J. (1980). "Sm-Nd Isotopic Evolution of Chondrites". In: *Earth and Planetary Science Letters* 50.1, pp. 139–155. DOI: 10.1016/0012-821X(80)90125-9.

Ambar, I. and Howe, M. R. (1979). "Observations of the Mediterranean Outflow—I Mixing in the Mediterranean Outflow". In: *Deep Sea Research Part A. Oceanographic Research Papers* 26.5, pp. 535–554.

Piepgras, D. J., Wasserburg, G. J., and Dasch, E. J. (1979). "The Isotopic Composition of Nd in Different Ocean Masses". In: *Earth and Planetary Science Letters* 45.2, pp. 223–236. DOI: 10.1016/0012-821X(79)90125-0.

Smith, S. V., Buddemeier, R. W., Redalje, R. C., and Houck, J. E. (1979). "Strontium-Calcium Thermometry in Coral Skeletons". In: *Science* 204, pp. 404–407. DOI: 10.1126/science.204.4391.404.

Weber, J. N. (1973). "Deep-Sea Ahermatypic Scleractinian Corals: Isotopic Composition of the Skeleton". In: *Deep Sea Research and Oceanographic Abstracts* 20.10, pp. 901–909. DOI: 10.1016/0011-7471(73)90108-3.

Wolgemuth, K. and Broecker, W. S. (1970). "Barium in Sea Water". In: *Earth and Planetary Science Letters* 8.5, pp. 372–378. DOI: 10.1016/0012-821X(70)90110-X.

Godwin, H. (1962). "Half-Life of Radiocarbon". In: *Nature* 195.4845, pp. 984–984. DOI: 10.1038/195984a0.

Chow, T. J. and Goldberg, E. D. (1960). "On the Marine Geochemistry of Barium". In: *Geochimica et Cosmochimica Acta* 20.3, pp. 192–198. DOI: 10.1016/0016-7037(60)90073-9.

Libby, W. F. (1952). "Chicago Radiocarbon Dates, III". In: *Science* 116.3025, pp. 673–681. JSTOR: 1680807.

Anderson, E. C. and Libby, W. F. (1951). "World-Wide Distribution of Natural Radiocarbon". In: *Physical Review* 81.1, pp. 64–69. DOI: 10.1103/PhysRev.81.64.

Iselin, C. O. (1936). *A Study of the Circulation of the Western North Atlantic*. Massachusetts Institute of Technology and Woods Hole Oceanographic Institution.

/

Acknowledgements

Ganz besonders möchte ich Nobert Frank danken, der mich während der gesamten Promotion immer unterstützt hat. Norbert Frank ermöglichte es mir selbständig mein Promotionsprojekt zu gestalten und gab gleichzeitig immer die Hilfestellung, die ich brauchte. Seine Begeisterung für Paläoozeanographie und Korallen war immer ansteckend und hat mich motiviert und auf viele neue Ideen gebracht. Mit Norberts Hilfe konnte ich ein Jahr meiner Promotion als Teil von Gideon Hendersons Gruppe verbringen und an Konferenzen teilnehmen wo ich viele Bekanntschaften mit anderen Wissenschaftlern machen konnte.

A special thanks goes to my second supervisor Gideon Henderson for the great support during my year of research with his group at the University of Oxford. Working with Gideon, I left the paleoceanographic world and for the first time jumped into the 'modern world'. His guidance during my stay with his research group and his support throughout the writing period of the paper on Ba isotopes in corals was a great help. I am really happy that Gideon also agreed to be my examiner in the defence of my thesis.

Ich möchte mich auch herzlich bei Monica Dunford bedanken, die sich bereiterklärt hat, in die Welt der Paläoozeanographie einzutauchen und Gutachterin für meine Arbeit zu sein. Auch Manfred Salmhofer möchte ich danken, dass er als Prüfer in meiner Verteidigung teilnimmt.

Die Proben, die ich in meiner Promotion bearbeitet habe, wurden während verschieder Forschungsfahrten geborgen. Diese Fahrten wurden von Laura Robinson, Dierk Hebbeln, Claudia Wienberg, David van Rooij und Norbert Frank organisiert. Ich möchte mich bei allen bedanken, dass sie ihre Proben so bereitwillig zur Verfügung gestellt haben. Claudia Wienberg, Fréderique Eynaud, Dominique Blamart und Jolene Cook gebührt ein großer Dank für die Hilfe während der Beprobung der verschiedenen Kerne und Korallen vor Ort. Ohne Marleen Lausecker, Patrick Blaser und Thomas Krengel hätte ich wohl keinen der Sediment- und Korallenkerne in Bordeaux, Gif-sur Yvette und Bremen in Rekordzeit beprobt und sicher nach Heidelberg gebacht.

Dieses Projekt wäre ohne die Hilfe von ganz vielen Menschen in meinem Umfeld nicht möglich gewesen. Ein riesiger Dank gilt allen, die mich bei Laborarbeiten und Messungen an den Massenspektrometern unterstützt haben. Niclas Rieger, Marleen Lausecker, Anne-Marie Wefing, Patrick Blaser, René Eichstädter, Frerk Pöppelmeier, Steffen Therre, Nils Schorndorf, Elvira Beisel, Alan Hsieh, Luke Bridgestock, Marcus Gutjahr, Ronny Friedrich, und Lucile Bonneau haben alle zu der erfolgreichen Probenaufbereitung und -analyse beigetragen. Besonders Marleen Lausecker, meine gute Fee, ist mir immer wieder im Labor beigesprungen.
Vielen Dank an alle, die mir all das beigebracht haben, was ich für die erfolgreiche Durchführung meiner Promotion brauchte. Norbert Frank, Gideon Henderson, Patrick Blaser, Lucile Bonneau, Alan Hsieh, Luke Bridgstock haben neben vielen anderen besonders dazu beigetragen. Augusto Mangini gebührt ein besonderer Dank, da mit ihm meine Reise in die Paläoozeanographie be-

gann.

My time in Oxford would not have been the same without Alan Hsieh and Luke Bridgestock. I will always remember our chemistry crisis as well as the evenings in a pub. Thank you for the great support and the answers to all the thousand questions I had about lab stuff, TIMS measurements, paper manuscript and whatever else came to my mind.
Special thanks also go to Peter Spooner and Laura Robinson for the productive and fun work on our barium projects.

Puas, es macht unglaublich Spaß mit euch und ich freu mich, dass ich noch eine Weile die schöne Arbeitsatmosphäre mit euch genießen kann. Vielen Dank, dass ihr alle in den letzten Wochen für alle Fragen und Korrekturlesearbeiten und zu haben wart.
Jenny und Patrick, ich hatte ne super Zeit mit euch, bei Diskussionen im Büro, auf der Neckarwiese, beim Gärtnern und beim Feiern oder U-Channel nehmen ;-)
Und dann gibts da noch meine Bürofamilie. Benny, Michi, Tine und Julian haben viele Höhen und Tiefen mitbekommen und mich wo sie konnten unterstützt. Unseren Süßigkeitenberg werden wir wohl aber nie in den Griff kriegen. Der wächst und wächst und wächst... dabei hab ich mich in den letzten Wochen echt angestrengt...
Lucile, Moritz und besonders Thomas, Danke für unser schönes WG-Leben, die leckeren Abendessen und die schönen langen Abende auf dem Balkon.
Meiner Familie, die mich immer unterstützt hat gilt ein ganz besonderer Dank. Besonders meine kleine Schwester und ihre Lebensfreude sind aus meinem Leben nicht wegzudenken. Auch meiner Tante Lulu möchte ich besonders danken. Besuche bei ihr und Markus und besonders bei meinen Cousins Julius, Titus und meiner Cousine Mara waren immer eine spaßige Abwechslung.
Max, Danke dass du die letzten 3,5 Jahre mit mir geteilt hast und immer für mich da bist. Die vielen Diskussionen und kritischen Fragen, deine unermüdlichen Vorschläge zur Verbesserung meiner Arbeit und deine Tips für die Python-Skripte waren eine unglaubliche Hilfe. Ohne dich wäre es wohl ziemlich unmöglich gewesen die großen Korallenpuzzle zu lösen.